الجمهورية الجزائرية الديمقراطية الشعبية

République Algérienne Démocratique et Populaire

Ministère de L'Enseignement Supérieur et de la Recherche Scientifique



UNIVERSITÉ FERHAT ABBAS - SETIF1 FACULTÉ DE TECHNOLOGIE

THÈSE

Présentée au Département de d'Electrotechnique

Pour l'obtention du diplôme de

DOCTORAT

Domaine: Sciences et Technologie

Filière: Electrotechnique Option: Commande Electrique

Par

DEGHFEL Nassir

THÈME

Développement d'une stratégie intelligente de contrôle et de gestion d'un système hybride connecté au réseau

Soutenue le 13/07/2025 devant le Jury:

| RAHMANI Lazhar | Professeur | Univ. Ferhat Abbas Sétif 1 | Président |
|------------------------|------------|-----------------------------|--------------------|
| BADOUD Abd Essalam | Professeur | Univ. Ferhat Abbas Sétif 1 | Directeur de thèse |
| OULD BOUAMAMA Belkacem | Professeur | Univ. Lille, France | Examinateur |
| BAHI Tahar | Professeur | Univ. Badji Mokhtar, Annaba | Examinateur |
| MERAHI Farid | MCA | Univ. Ferhat Abbas Sétif 1 | Examinateur |

| To the sun that lights my path, the shelter that protects me, and the endless source of love |
|--|
| and strength My mother. |
| To the foundation of my courage and the pillar of my strength, My Father |
| To those who selflessly placed me before themselves my dear brothers and sisters |
| |
| |
| |
| |

Acknowledgement

Praise be to Allah • Who enabled me to complete this dissertation, and peace be upon His final Messenger, Muhammad, .

I would like to express my deepest gratitude and sincere appreciation to my esteemed supervisor, Professor BADOUD Abd Essalam, for his invaluable guidance, continuous support, and insightful advice throughout the course of this research. His expertise, patience, and encouragement have been instrumental in shaping my work and refining my understanding of the subject matter.

I also thank my colleagues, both Doctors and future Doctors. I am grateful for their wonderful companionship throughout our time together.

I would like to express my gratitude to my parents for their encouragement and support through all the years of my life. I am also grateful to my brothers and sisters for their support during the previous years of my studies.

Abstract

This thesis focusses on the development and implementation of advanced intelligent control and management strategies for a grid-connected hybrid renewable energy system, integrating photovoltaic (PV) arrays, proton exchange membrane fuel cells (PEMFCs), and wind energy conversion systems (WECS). Unfortunately, the mentioned sources face several challenges, including low conversion efficiency, particularly under fluctuating weather conditions, and the nonlinear characteristics of their output power and current. Therefore, the primary objective is to optimize power extraction, enhance grid integration, and ensure system stability under dynamic operating conditions. Novel maximum power point tracking (MPPT) algorithms are proposed for PV systems, including a high-order sliding mode Super-Twisting (STA) technique to mitigate chattering effects, a two-level artificial neural network-based model reference adaptive control (ANN-MRAC), and a double-stage ANN-finite control set model predictive control (ANN-FSC-MPC). Moreover, this research also focuses on the modeling and control design of variable-speed wind turbines. The aim is to optimize energy extraction from the wind below the rated power range, while controlling electrical power output above the rated power range, all while reducing mechanical transient disturbances. As matter of fact, the first control scheme is designed using classical regulators, specifically employing a PI controller. However, given the strong non-linearity and uncertainty of the wind turbine aerodynamics, a robust controller based high order sliding mode algorithms has been proposed. Additionally, a grid-side control strategy employing a finite control set model predictive controller (FCS-MPC) for a multilevel neutral-point clamped (NPC) inverter is introduced. This approach ensures DC-link voltage stability, minimizes switching frequency, reduces total harmonic distortion (THD), and maintains high-quality power injection into the grid, even during variable power generation from hybrid sources. To guarantee that the hybrid system can reliably meet power demands while respecting the operational limits of each energy source, an energy management strategy has been incorporated and critically discussed. The latter approach aims to balance energy distribution efficiently, ensuring uninterrupted power supply without exceeding the capabilities of individual components. Simulation results validate the superiority of the proposed methods, demonstrating enhanced efficiency, robustness, and dynamic response compared to traditional techniques. The developed strategies collectively address critical challenges in renewable energy integration, offering a scalable framework for reliable, sustainable, and intelligent hybrid energy systems.

Résumé:

Cette thèse porte sur le développement et la mise en œuvre de stratégies avancées de contrôle et de gestion intelligentes pour un système hybride renouvelable connecté au réseau, intégrant des panneaux photovoltaïques (PV), des piles à combustible à membrane échangeuse de protons (PEMFC) et des systèmes de conversion d'énergie éolienne (WECS). Ces sources renouvelables présentent plusieurs défis, notamment un faible rendement de conversion, en particulier sous des conditions météorologiques fluctuantes, ainsi que des caractéristiques non linéaires de leur puissance et de leur courant de sortie. L'objectif principal est d'optimiser l'extraction de puissance, d'améliorer l'intégration au réseau et d'assurer la stabilité du système en conditions dynamiques. Pour un système PV, des algorithmes novateurs de suivi du point de puissance maximale (MPPT) sont proposés : une technique de mode de glissement d'ordre supérieur appelée Super-Twisting Algorithm (STA) pour atténuer les phénomènes de « chattering » ; également, une commande en cascade basée sur la combinaison de la commande adaptative par modèle de référence et des réseaux de neurones artificiels (ANN-MRAC); en outre, le troisième MPPT employant un contrôleur prédictif a été combiné avec les réseaux de neurones (ANN-FSC-MPC). En ce qui concerne les turbines éoliennes à vitesse variable, la modélisation et la conception de contrôle visent à maximiser l'extraction d'énergie en dessous de la puissance nominale et à maîtriser la puissance électrique au-dessus de cette limite, tout en réduisant les perturbations mécaniques transitoires. Dans un premier temps, un régulateur classique PI est utilisé ; toutefois, face à la forte non-linéarité et aux incertitudes aérodynamiques, un contrôleur robuste basé sur des algorithmes de mode de glissement d'ordre supérieur est également proposé afin de faire face au défi susmentionné. Côté réseau, une stratégie de contrôle faisant appel à un contrôleur prédictif (FCS-MPC) est introduite pour un onduleur multiniveau à point neutre (NPC). Cette approche garantit la stabilité de la tension au bus continu (DC-link), minimise la fréquence de commutation, réduit la distorsion harmonique totale (THD) et maintient une injection de puissance de haute qualité, même en cas de génération variable issue des sources hybrides. Pour assurer que le système hybride réponde de manière fiable à la demande tout en respectant les limites opérationnelles de chaque source, des stratégies de gestion d'énergie sont intégrées et analysées. Celles-ci visent à équilibrer efficacement la distribution d'énergie pour garantir une alimentation ininterrompue sans dépasser les capacités des composants. Les résultats de simulation confirment la supériorité des méthodes proposées en termes d'efficacité, de robustesse et de temps de réponse par rapport aux techniques traditionnelles. Les stratégies développées forment un cadre évolutif pour des systèmes hybrides intelligents, fiables et durables.

Mots-clés : Commande intelligente, Super-Twisting Algorithm (STA), Gestion d'énergie, Réseaux de neurones artificiels (ANN), Commande prédictive (FCS-MPC), Systèmes hybrides renouvelables

الملخص:

تركز هذه الرسالة على تطوير وتنفيذ إستراتيجيات متقدمة ذكية للتحكم والإدارة لنظام طاقة متجدد هجين متصل بالشبكة، يجمع بين الألواح الضوئية (PV) ، وخلايا الوقود ذات غشاء التبادل البروتوني (PEMFC)، وأنظمة تحويل طاقة الرياح (WECS) .تواجه هذه المصادر عدة تحديات، من ضمنها الكفاءة المنخفضة للتحويل خاصة في ظل ظروف الطقس المتقلبة، وخصائص خرج القدرة والتيار غير الخطية . الهدف الأساسي هو تحسين إستخلاص الطاقة، وتعزيز التكامل مع الشبكة، وضمان إستقرار النظام في ظل ظروف تشغيل ديناميكية. لزيادة كفاءة إستخراج الطاقة من الأنظمة الكهروضوئية، تم إقتراح خوارزميات مبتكرة لتتبع نقطة القدرة القصوى (MPPT) و تقليل التذبذب بما في ذلك تقنية الإنزلاق من الدرجة الثانية والتي تعرف بخوارزمية الإلتواء الفائق للحد من ظاهرة التموج العالي. في نفس السياق تم تطوير خوارزمية بينما يقوم المتحكم التكيفي بايصال جهد اللوح الضوئي الى الجهد المرجعي باستخدام الشبكات العصبونية بينما يقوم المتحكم التكيفي بايصال جهد اللوح الضوئي الى الجهد المرجعي المطلوب. أخيرا , تم بناء خوارزمية هجينة تجمع بين التحكم التنبؤي مع الشبكات العصبونية.

فيما يخص توليد الطاقة من الرياح، تم تصميم و نمذجة تقنيات للتحكم في توربينات الرياح ذات السرعة المتغيرة بهدف تحسين استخلاص الطاقة اثناء تغيرات الطقس، والسيطرة على القدرة الكهربائية مع تقليل الإضطرابات الميكانيكية العابرة. يستخدم المخطط الأول منظم PI كلاسيكي، لكن نظراً لدرجة اللاخطية العالية والاضطراب في الأداء الأيروديناميكي، فقد تم اقتراح مخطط متين يعتمد بدوره على خوارز مبات الانز لاق من الدرجة الثانية.

على جانب الشبكة، تم تقديم إستراتيجية تحكم تستخدم التحكم التنبؤي لعاكس متعدد المستويات بنقطة محايدة. تضمن هذه الطريقة إستقرار جهد الوصلة المستمرة (DC-link) ، وتقليل تردد التبديل، وخفض التشوه التوافقي الكلي (THD) ، والحفاظ على جودة عالية في القوة الكهربائية المدخلة إلى الشبكة حتى أثناء تغير إنتاج المصادر الهجينة. ولضمان قدرة النظام الهجين على تلبية الطلب على الطاقة بشكل موثوق مع احترام الحدود التشغيلية لكل مصدر، تم دمج ومناقشة استراتيجية لإدارة الطاقة. تهدف هذه الاستراتيجية إلى تحقيق توازن فعّال في توزيع الطاقة، وضمان إمداد مستمر دون تجاوز قدرات المكونات الفردية . تؤكد نتائج المحاكاة تفوق الأساليب المقترحة من حيث الكفاءة، والصلابة، والاستجابة الديناميكية مقارنة بالتقنيات القليدية، مقدمةً إطار عمل قابل للتوسع لأنظمة طاقة هجينة ذكية ومستدامة وموثوقة.

الكلمات المفتاحية: التحكم الذكي، خوارزمية الالتواء الفائق، إدارة الطاقة، الشبكات العصبية الاصطناعية ، التحكم التنبئي، الأنظمة الهجينة المتجددة.

Table of Contents

| CHAPTER 1 : GENERAL INTRODUCTION | 21 |
|--|--------|
| 1.1 Background | 21 |
| 1.2 Hybrid Systems and Grid Integration | 24 |
| 1.3 PROBLEM STATEMENT | 25 |
| 1.3 Thesis Objectives and Contribution | 27 |
| CHAPTER 2 : POWER SOURCES MODELING | 30 |
| 2.1 Introduction | 30 |
| 2.2 MATHEMATICAL MODEL OF A PV SOLAR CELL | 33 |
| 2.2.1 PV Solar Characteristic Curves | 34 |
| 2.2.2 Weather Conditions Effect | 35 |
| 2.3 FUEL CELL | 36 |
| 2.3.1 Modeling and Analysis of PEMFC | 37 |
| 2.3.1.1 PEMFC's Static Model | 38 |
| 2.3.1.2 Dynamic Model | 41 |
| 2.3.2 Pressure and Temperature Effect on PEM Fuel Cell Performan | nce42 |
| 2.4 WIND ENERGY CONVERSION SYSTEMS | 43 |
| 2.4.1 Wind Turbine | 45 |
| 2.4.2 Mathematical Model of Permanent Magnet Synchronous Gen | erator |
| (PMSG) | 49 |
| 2.5 Power Converter | 50 |
| 2.5.1 DC-DC Converters for Photovoltaic Systems | 50 |

| 2.5.2 Fuel-cell's Power Converter | 51 |
|---|-------|
| 2.5.3 WECS Power Converter | 52 |
| 2.5.3.1 Three-Phase PWM Rectifier Model | 53 |
| 2.6 CONCLUSION | 54 |
| CHAPTER 3 : SURVEY ON CONTROL AND ENERGY | |
| MANAGEMENT OF HYBRID POWER SYSTEMS GRID-TIED | 56 |
| 3.1 Introduction | 56 |
| 3.2 MPPT STRATEGIES FOR PV SYSTEMS | 57 |
| 3.2.1 Classical MPPT | 58 |
| 3.2.1.1 Perturb and Observe Method | 58 |
| 3.2.1.2 Open-Circuit Voltage (OCV) | 58 |
| 3.2.1.3 Constant Voltage Method (CV) | 58 |
| 3.2.1.4 Incremental Conductance Method (INC) | 59 |
| 3.2.2 Intelligence Technique Based MPPT | 60 |
| 3.2.2.1 Fuzzy Logic based MPPT | 60 |
| 3.2.2.2 Artificial Neural Network (ANN)-based MPPT | 62 |
| 3.2.3 Optimization Algorithms based-MPPT | 63 |
| 3.2.3.1 Particle Swarm Optimization | 63 |
| 3.2.3.2 Arithmetic Optimization (AO) Algorithm | 65 |
| 3.2.3.3 Coot Optimization Algorithm | 65 |
| 3.2.4 Hybrid MPPT | 66 |
| 3.2.4.1 Hybrid MPPT Based on INC-Integral Backstepping Controll | er 66 |

| 3.2.4.2 Hybrid FLC- Ant Colony Optimization (ACO) | 66 |
|--|----|
| 3.2.4.3 Hybrid PSO-ANN- Flying Squirrel Search Optimization (FSSO) |) |
| | 67 |
| 3.2.4.4 Variable step-size P&O Model Reference Adaptive Control | 67 |
| 3.3 CONTROL STRATEGIES FOR WECS | 68 |
| 3.3.1 MPPT Controller | 68 |
| 3.3.1.1 IPC MPPT Techniques | 69 |
| 3.3.1.2 DPC MPPT Techniques | 69 |
| 3.3.2 Machine Side Control: Case 'PMSG' | 71 |
| 3.4 FC CONTROL | 73 |
| 3.4.1An overview of Output power control of PEMFC | 74 |
| 3.4.1.1 Proportional Integral (PI) controller | 74 |
| 3.4.1.2 Lyapunov- PI controller | 75 |
| 3.4.1.3 GA-Based Robust LQR Controller | 75 |
| 3.5 DC Bus Voltage Regulation | 76 |
| 3.6 GRID CURRENT CONTROL | 77 |
| 3.6.1 Hysteresis Control Technique | 78 |
| 3.6.2 Linear Control Method | 79 |
| 3.6.3 Finite Control Set Model Predictive Control | 80 |
| 3.6.4 Other Control Methods | 81 |
| 3.7 GRID SYNCHRONIZATION | 83 |
| 3.7.1 Zero-Crossing Approach | 84 |
| 3.7.2 Filtering of Grid Voltages | 84 |

| 3.7.3 Phase-Locked-Loop (PLL)84 |
|--|
| 3.8 POWER MANAGEMENT STRATEGIES85 |
| 3.8.1 Rule-Based Algorithms: |
| 3.8.2 Optimization-Based Algorithms |
| 3.9 CONCLUSION |
| CHAPTER 4 INTELLIGENT CONTROL DESIGN OF A GRID |
| CONNECTED HYBRID WIND/PHOTOVOLTAIC/FUEL CELL |
| SYSTEM90 |
| 4.1 Introduction |
| 4.2 MPPT CONTROL DESIGN FOR SOLAR PV SYSTEMS90 |
| 4.2.1 High Order Sliding Mode Control90 |
| 4.2.1.1 Robust MPPT Controller Based on Super-Twisting for PV |
| Systems92 |
| 4.2.2 Double-Stage Control Based MPPT Using Neural Network and Model |
| Reference Adaptive Control95 |
| 4.2.2.1 Neural-Network Approach for Generating Reference Voltage 95 |
| 4.2.2.2 Proposed MRAC Approach |
| 4.2.3 Double-Stage Control-Based MPPT Using NN and Model Predictive |
| Control |
| 4.2.4 Results Evaluation |
| 4.3 CONTROL DESIGN FOR PMSG -BASED-WECS |
| 4.3.1 MPPT Control |

| | 109 |
|--|-------------------------------|
| 4.3.1.2 Super-Twisting Algorithm | 109 |
| 4.3.2 PMSG Control | 110 |
| 4.3.3 Performance Assessment via MATLAB environment | 112 |
| 4.4 PEMFC CONTROL DESIGN | 114 |
| 4.4.1 Performance Assessment | 115 |
| 4.5 FCS-MPC FOR THREE-PHASE GRID-TIED 3-LEVEL NPC INVERTER | 116 |
| 4.5.1 Mathematical Model | 117 |
| 4.5.2 FCS-MPC Design | 118 |
| 4.5.3 Performance Assessment of the Grid Connected Mode | 119 |
| 4.6 CONCLUSION | 127 |
| CHAPTER 5 ENERGY MANAGEMENT AND POWER FLOW | |
| | |
| SCHEMES DESIGN | 128 |
| SCHEMES DESIGN | |
| | 128 |
| 5.1 Introduction | 128 снеѕ 129 |
| 5.1 Introduction | 128 снеѕ 129 129 |
| 5.1 Introduction | 128 снез 129 129 129 |
| 5.1 Introduction | 128 CHES 129 129 129 130 |
| 5.1 Introduction | 128 CHES 129 129 130 131 |
| 5.1 Introduction | 128 CHES 129 129 130 131 |
| 5.1 Introduction | 128 CHES 129 129 130 131 132 |

| 6.1 A SUMMARY OF THE RESEARCH WORK | 138 |
|------------------------------------|-----|
| 6.2 Perspectives and Future Works | 139 |

Table of Figures

| Figure 1.1 : Energy employed per person in Algeria from 1965 till 2023 [1] | 21 |
|---|----|
| Figure 1.2: Installed solar PV capacity worldwide from 2000 to 2022. [7] | 22 |
| Figure 1.3: Wind Power Report: a) New Installed wind capacity. b) Cumulative | ve |
| wind power capacity.[9] | 24 |
| Figure 2.1 : A hybrid energy system structure connected to the grid | 32 |
| Figure 2.2: The schematic representation of the equivalent circuit for a | |
| photovoltaic (PV) cell | 33 |
| Figure 2.3 : P-V & I-V characteristics of a PV panel under STC | 35 |
| Figure 2.4: P-V & I-V characteristics of a PV panel under diverse irradiation | |
| levels | 36 |
| Figure 2.5: P-V & I-V properties of a photovoltaic (PV) panel at various | |
| temperature levels. | 36 |
| Figure 2.6 : The Varying Forms of Fuel Cells. | 37 |
| Figure 2.7 : PEMFC functioning Diagram | 38 |
| Figure 2.8: Equivalent circuit of the PEMFC dynamic behavior | 41 |
| Figure 2.9: PEMFC characteristics under different temperature values | 43 |
| Figure 2.10: PEMFC characteristics under different pressure conditions | 43 |
| Figure 2.11: Horizontal axis wind turbine scheme | 44 |
| Figure 2.12 : Advantages and drawbacks of HAWT. | 45 |
| Figure 2.13 : Wind energy conversion system scheme | 45 |
| Figure 2.14 : Diagram illustrating the energy extraction in a wind turbine | 46 |

| Figure 2.15 : Drive-Train scheme using two-mass model | 49 |
|--|----|
| Figure 2.16: Equivalent Circuits of the PMSG on the d-q axis | 50 |
| Figure 2.18: PEMFC with traditional Boost converter interface | 52 |
| Figure 2.19: A two-level variable source rectifier connected to PMSG-based | 1 |
| WECS | 54 |
| Figure 3.1 : PV MPPT Classification | 57 |
| Figure 3.2 : P&O Flow-chart | 59 |
| Figure 3.3 : INC Flow-Chart. | 60 |
| Figure 3.4 : FLC based- MPPT Scheme. | 61 |
| Figure 3.5 : ANN Scheme. | 63 |
| Figure 3.6 : PSO Flow-Chart | 64 |
| Figure 3.7: Operation Regions of WT | 68 |
| Figure 3.8 : MPPT classification for WECS. | 71 |
| Figure 3.9 : Classification of Machine Drive Control. | 72 |
| Figure 3.10: Control Architecture of a PEMFC Stack. Reprinted with some | |
| modification from Ref.[122]. | 73 |
| Figure 3.11: Control of PEMFC Using PI Controller | 74 |
| Figure 3.12 : Control of PEMFC Using Adaptive PI-based Lyapunov | 75 |
| Figure 3.13 : DC-Link voltage Regulation Scheme. | 76 |
| Figure 3.14: Inverter Control Strategies for grid-tied applications | 78 |
| Figure 3.15 : DPC Bloc Diagram. | 79 |
| Figure 3.16 : Bloc Diagram of VOC method | 80 |
| Figure 3.17 : FCS-MPC Block scheme. | 81 |
| • | |

| Figure 3.18 : SMC control for grid-tied inverter. | 82 |
|---|-----|
| Figure 3.19 : ANN based grid-tied inverter control. | 83 |
| Figure 3.20 : The PLL structure in dq frame. | 85 |
| Figure 3.21: Management Strategies Categories. | 87 |
| Figure 4.1 : phase plane representation of SMC method | 92 |
| Figure 4.2 : phase plane representation of the Super-Twisting algorithm | 93 |
| Figure 4.3: Bloc Diagram of the proposed NN-MRAC MPPT | 95 |
| Figure 4.4 : ANN Scheme for Voltage reference estimation | 96 |
| Figure 4.5: small-signal model of a PV power system[161] | 98 |
| Figure 4.6 : The MRAC architecture. | 99 |
| Figure 4.7: The detailed structure of the proposed MPPT | 102 |
| Figure 4.8: ANN-MPC control-based MPPT. | 102 |
| Figure 4.9: ANN-MPC-based MPPT Flowchart | 103 |
| Figure 4.10: MATLAB Simulation of the Proposed MPPT Schemes | 104 |
| Figure 4.11: Irradiance Profile | 104 |
| Figure 4.12: Dynamic Performance of the PV Power output | 104 |
| Figure 4.13 : Zoom-in of the Power response | 106 |
| Figure 4.14: Graphical representation of the total efficiency. | 107 |
| Figure 4.15: Graphical representation of the power loss. | 107 |
| Figure 4.16: PV Voltage Output. | 107 |
| Figure 4.17 : PV current Output. | 107 |
| Figure 4.18: P-V characteristics under the proposed MPPT control | 108 |
| Figure 4.19 : Mechanical speed control. | 109 |

| Figure 4.20 : Vector Control of PMSG based WECS | 111 |
|--|-----|
| Figure 4.21: Simulink Implementation of the proposed WECS along with the | ·, |
| control scheme1 | 112 |
| Figure 4.22: Wind Velocity | 112 |
| Figure 4.23: Mechanical power response | 112 |
| Figure 4.24 : Electrical Power response | 113 |
| Figure 4.25 : Mechanical speed performance of the WT | 113 |
| Figure 4.26: Power coefficient behavior. | 113 |
| Figure 4.27: Tip Speed Ratio behavior. | 113 |
| Figure 4.28 : The proposed FC system control | 115 |
| Figure 4.29 : Power tracking behavior. | 116 |
| Figure 4.30 : Response of the FC current. | 116 |
| Figure 4.31 : Fuel consumption. | 116 |
| Figure 4.32: Schematic of a grid-tied NPC inverter. | 117 |
| Figure 4.33 : FCS-MPC Flowchart for 3-level inverter | 119 |
| Figure 4.34 : Simulink model of the proposed hybrid system integrated to the | |
| network1 | 120 |
| Figure 4.35 : Solar Irradiance | 121 |
| Figure 4.36 : Power response of the different sources | 122 |
| Figure 4.37: Active and Reactive power injected into the grid | 122 |
| Figure 4.38: DC-Link Voltage performance. | 122 |
| Figure 4.39: Grid Current performance. | 122 |
| Figure 4.40: Zoom-in of the grid current response | 123 |

| Figure 4.41: FFT Analysis for different irradiation states. a) State 1 (500 |
|--|
| w/m^2), b) State 2 2(1000 w/m^2), State 3 (500 w/m^2) |
| Figure 4.42: Wind Velocity |
| Figure 4.43: DC-Link Voltage |
| Figure 4.44: Power Performance of the different sources |
| Figure 4.45: Active and Reactive power injected into the grid |
| Figure 4.46: The Grid Current |
| Figure 4.47: Zoom-in of the grid current |
| Figure 4.48: FFT Analysis for different wind velocity states. a) State 1 (12 m/s), |
| b) State 2 (8 m/s), c) State 3 (15 m/s) |
| Figure 5.1: Power Flow of the proposed hybrid system |
| Figure 5.2 : Energy Management Configurations: a) Classical PI. b) State |
| Machine Control. c) Equivalent Consumption Minimization Strategy. d) |
| External energy maximization strategy. 132 |
| Figure 5.3 : Irradiance and Wind Velocity Behavior |
| Figure 5.4: Load Power |
| Figure 5.5: (PV+WT) Power generation versus power required |
| Figure 5.6 :DC-Bus Voltage |
| (d) Figure 5.7: PEMFC, Battery, and Grid power response using: (a) classical PI |
| (b) STMC (c) ECMS (d) EEMS |
| Figure 5.8: H2 consumption in lpm for the examined EMS techniques 135 |
| Figure 5.9: H2 consumption in gm for the examined EMS techniques |
| Figure 5.10: The SOC response for the examined EMS techniques |

| Figure 5.11: system efficiency for each evaluated method |
|--|
| List of Tables |
| Table I: Operation modes of boost converters |
| Table II: Introducing the specifications of DC-DC converters utilized in Fuel Cell |
| applications45 |
| Table III: The used data set for ANN training. 96 |
| Table IV: In-depth comparative examination |
| Table V:Performance Comparison. 113 |
| Table VI : NPC-Inverter switching states. 118 |
| Table VII : State Machine Decisions 130 |
| Table VIII: Analysis of various management approaches. 137 |

List of Acronyms

ANN Artificial Neural Network

CV Constante Voltage

DC Direct Current

DPC Direct Power Control

ECMS Equivalent Consumption Minimization Strategy

EEMS Extern Energy Maximization Strategy

EMS Energy Management Strategy

FFT Fast Fourier Transform

FLC Fuzzy Logic Control

FSC- MPC Finite Set Control Model Predictive Control

GA Genetic Algorithm

INC Incremental Conductance

IPC Indirect Power Control

LQR Linear Quadratic Regulator

MPPT Maximum Power Point Tracking

MRAC Model Reference Adaptive Control

NPC Neutral Point Converter

OCV Open Circuit Voltage

PEMFC Proton Exchange Membrane Fuel Cell

PI Proportional Integral

PLL Phase Locked Loop

PMSG Permanent Magnet Synchronous Generator

PV Photovoltaic

PWM Pulse Width Modulation

SMC Sliding Mode Control

SOC State of Charge

STA Super Twisting Algorithm

STC Standard Test Condition

STMC State Machine Control

THD Total Harmonic Distortion

VOC Voltage Oriented Control

WECS Wind Energy Conversion System

WT Wind Turbine

Chapter 1 : General Introduction

1.1 Background

The prevailing issue in the public discourse on energy is climate change. A climate crisis poses a threat to the natural environment in our vicinity, not only to our present welfare but also to the welfare of future generations. In 2018, global emissions of carbon dioxide hit 36.6 billion tons, continuing a rapid upward trend. Our contribution to global warming will continue so long as we release greenhouse gases into the air[1]. The consumption of fossil fuels has risen dramatically over the last 50 years, increasing about eight times since 1950 and nearly doubling since 1980[2]. However, fossil fuel is considered the main source of electrical power production in the world, which leads to more pollution spread and global warming. Moreover, the growing demand for power is increasing day after day. For instance, in Algeria, the utilization of energy per person has increased from 2000 kwh in 1996 up to 16000 kwh in 2023 as shown in Figure 1.1. For these reasons, every energy producer and user, including the academia and government, are studying and reconsidering methods to address greenhouse gas emissions and climate change, as well as strategies to enhance power quality without the need to build a costly new system[3]. In the last decade, renewable energy sources have been introduced as a vital solution in order to tackling climatic changing and reducing carbon emissions. Forecasts indicate that the power consumption from renewable energy sources will rise by 66% from 2020 to 2030, representing about 80% of the worldwide electricity demand[4].

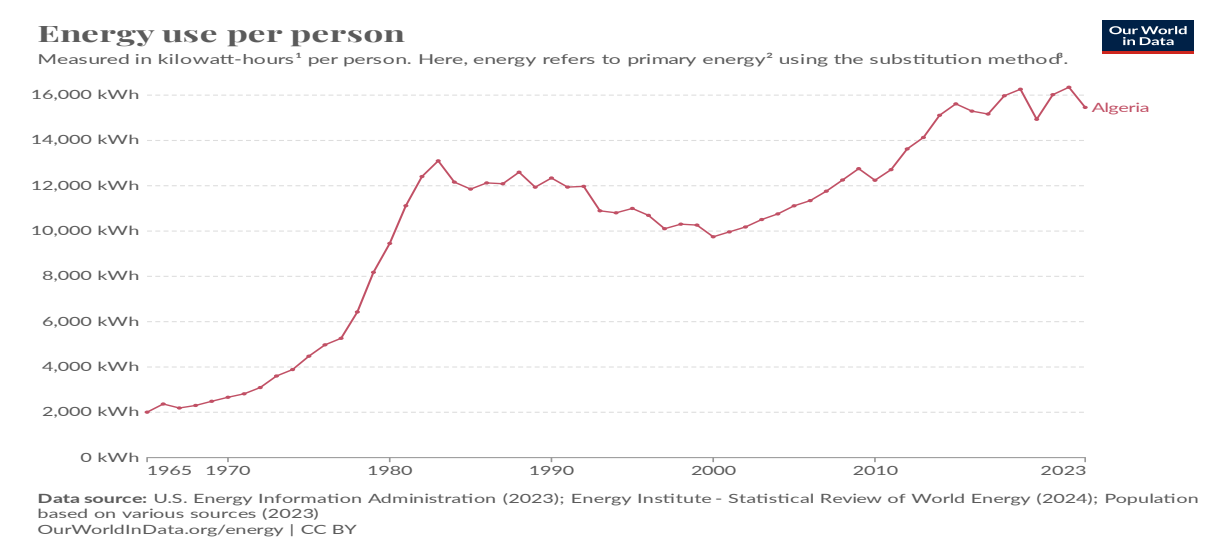


Figure 1.1: Energy employed per person in Algeria from 1965 till 2023 [1].

Solar energy, being one of the most plentiful and pristine forms of renewable energy, has the capacity to greatly promote the goals of sustainability. Due to its outstanding costeffectiveness, solar photovoltaics have experienced a significant surge in their worldwide installed capacity in recent years. Solar energy is becoming increasingly popular due to its adaptability across a range of industrial applications, such as power generation for both residential and commercial purposes, solar drying of fruits in food processing industries, and providing power for vehicles and airplanes, among others [5]. It provides a sustainable means of producing electrical power without any release of greenhouse gases into the surroundings[6]. Figure (1.2) displays the evolution of the global annual installed solar power capacity in the world which shows that the total installed capacity shown exponential growth, rising from 1.23 GW in 2000 to 1053.12 GW by 2022. Moreover, we can conclude that from 2000 to 2022, the solar capacity saw an average annual growth rate of 37% per year. In fact, extensive deployment of solar energy infrastructure, coupled with effective use, holds the potential to enhance energy provision and decrease reliance on fossil fuels. Despite this growth, the current allocation of solar power to the overall energy demand remains at a minimal level and is confronted by multiple financial and environmental obstacles. The environmental consequences linked to the utilization of solar energy encompass the substantial land consumption and the disposal of dangerous substances throughout the production process. Furthermore, the primary techno-economic difficulty remains in the restricted efficiency of solar energy harvesting[6].

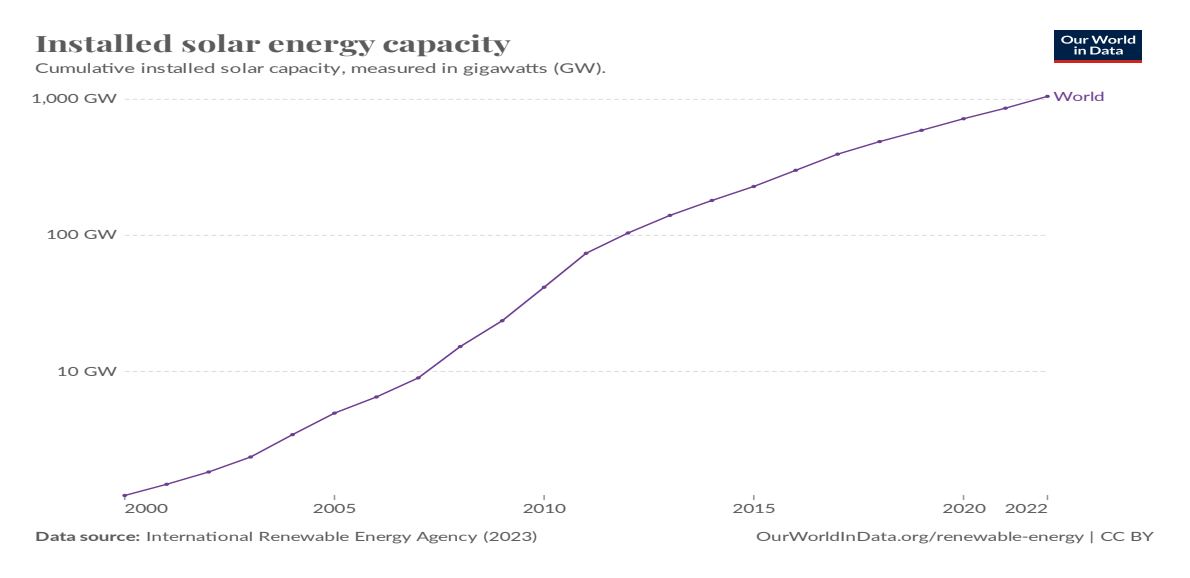
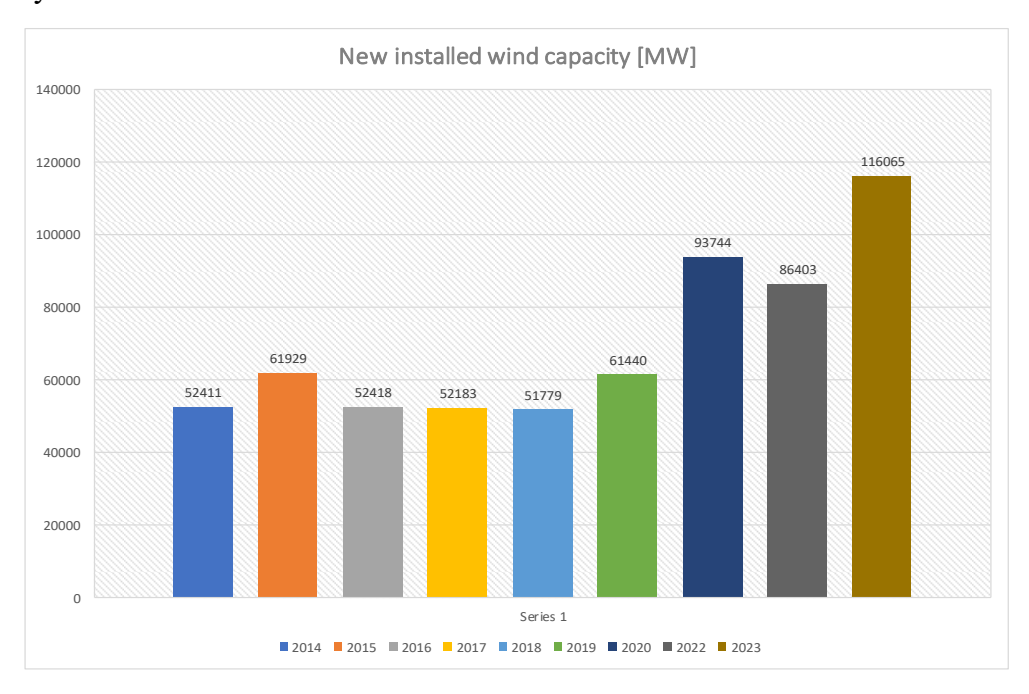


Figure 1.2: Installed solar PV capacity worldwide from 2000 to 2022. [7]

In recent years, Wind Energy has been widely attractive in the world, which globally is the fastest-growing energy resource. Ongoing improvements in wind turbine technological fields, in addition to government support and favorable legislation, have significantly contributed to the expansion of wind energy as a sustainable, clean, and dependable power source. These factors contribute to wind energy becoming widely accepted and strong contenders with traditional energy sources. After 2000, the worldwide wind energy capacity was documented at 17.7 GW, signifying the first phases of the industry's expansion. In the subsequent ten years, wind energy had substantial growth, with its capacity reaching 191 GW by the end of 2010. The expansion rate continued consistently, and by the end of 2018, the worldwide wind energy capacity had increased to around 561 GW. A growth of this magnitude highlights the increasing significance of wind energy in the worldwide transition towards renewable energy sources[8]. As shown in Figure (1.3), 2023 concluded with a new record for the installation of new wind turbines: The global addition of new capacity amounted to 116,065 Megawatts within a single year, surpassing any previous record. A preliminary report released currently via the World Wind Energy Organization reveals that the worldwide wind power capacity has exceeded one million Megawatt, reaching a total of 1,047,288 Megawatts [9]. The exponential expansion of wind energy development has been followed by a commensurate rise in the dimensions of wind turbines with a consistent decline in the prices of generated electricity.



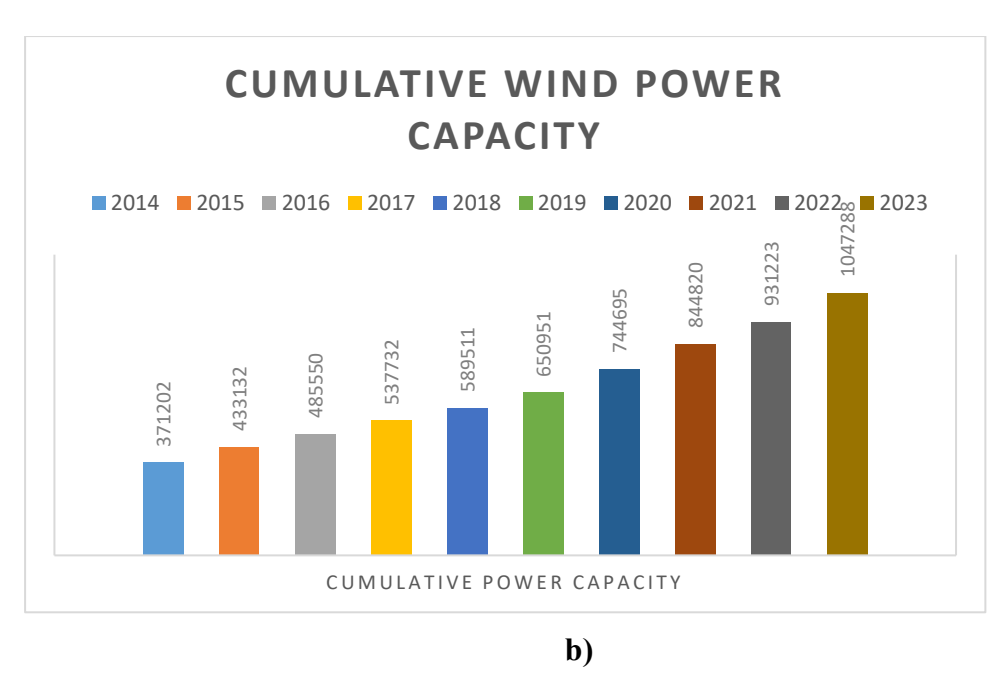


Figure 1.3: Wind Power Report: a) New Installed wind capacity. b) Cumulative wind power capacity.[9].

Regrettably, renewable energy sources including the aforementioned sources are heavily reliant on weather conditions and consequently cannot provide continuous performance for consumers owing to potential interruptions. The maximum production of solar power occurs during daylight hours, although wind power may be used even during times of diminished solar availability. Accordingly, the integration of various sources has the potential to enhance the consistency and reliability of the energy supply.

1.2 Hybrid Systems and Grid Integration

A hybrid energy system combines two or more sustainable energy sources, working in tandem to enhance overall efficiency and bolster the reliability of electrical power to a certain extent[10]. Indeed, one of the most ubiquitous limitations of solar and wind energy is their inherent unpredictability. For a significant period of the year, standalone photovoltaics or wind power systems do not provide useful electricity. This is mostly attributed to the reliance on daylight hours and the comparatively high cut-in wind velocity[11]. Furthermore, the fluctuations in both wind and solar power do not align with the temporal distribution of consumer demand. To address the limitations of a singular energy source, integrating a hybrid solar and wind energy system helps mitigate variations in generated power, substantially decreasing the need for energy storage[11], [12]. However, only the WECS still works at night, which means unproviding the required power in cases of low wind velocity or over-power

demand. These lead us to consider incorporating another RE source independent of meteorological conditions or a backup system that ensures optimal energy flow and supply. Currently, within the realm of small and medium size, energy is mostly stored in batteries and, for some purposes, in supercapacitors. In the immediate term, energy storage systems primarily serve to accommodate surplus or shortage of energy, as well as ensure system security and power delivery during sudden changes in the load. Conversely, over a longer duration, energy storage devices serve the purpose of meeting the demand at times when the production is inadequate to sustain the load. Undoubtedly, Supercapacitors have superior dynamic characteristics compared to batteries, enabling them to promptly react to demand shocks and provide energy effectively. Notwithstanding these benefits, their limited capacity limits its use. By comparison, batteries are components characterized by worse dynamic responsiveness and a finite lifespan determined by the number of charge/discharge operations. Furthermore, batteries may experience degradation and during regular operation might generate hazardous gasses. Lately, the potential of the hydrogen technique has been shown to have significant future worth[13]. Fuel cells (FCs) are a very promising renewable energy source due to their non-intermittent nature, independent of the environment, time, and spatial factors, compared to solar and wind which greatly depend on weather situations. An FC typically functions as a storage device that catalyzes electrochemical reactions to produce power, consequently, fuel cells made a paradigm shift in power systems and storage. Hence, one of the most common types of FCs that has been suggested in the literature and commonly employed in the industry is the proton exchange membrane fuel cell (PEMFC) which usually incorporates a PV hybrid system or Wind-based hybrid system or both [14], [15], [16]. However, in general, the Hybrid Power Systems (HPS) may be used in two distinct modes. The first application known as Offgrid mode which refers to the use of HPS to provide electricity to distant loads that are not linked to the electric grid. On-grid applications, on the other hand, include the use of hybrid systems to offer energy to both local loads and the electric transmission grid. Notably, the gridtied mode can solve two main challenges faced by the studied HPS. In case of excess energy where the power demand is lower than the produced power, this latter can be injected into the grid which helps to stabilize the system in addition to gaining more energy in the national network. Otherwise, if the power demand over than the available power, then it can rely on the grid to bring-in the required power to the local load.

1.3 Problem Statement

Despite the notable benefits of the studied hybrid system, its performance remains exposed to the inherent intermittency of solar and wind energy sources. This can lead to a range of challenges, including fluctuations in power output, grid stability issues, and difficulties in integrating these renewable sources into existing power grids. Furthermore, the complexity of the issue intensifies when irradiance levels or wind velocity experience sudden and sharp changes. To address these challenges and ensure the long-term viability of hybrid power systems, it is essential to develop robust control strategies that can effectively manage the variable nature of solar and wind energy. Indeed, grid-connected hybrid systems commonly employ a three-tier control structure, including MPPT (Maximum Power Point Tracking), DC-link voltage regulation, and grid-side power control. These control approaches have been the subject of considerable research and remain an area of ongoing exploration.

Efforts are underway globally to devise strategies that optimize power generation from sustainable energy resources. Hence, a wide variety of MPPT algorithms have emerged for solar and wind energy applications in recent times. However, choosing the most suitable MPPT algorithm can be challenging, as each method possesses both advantages and disadvantages. Moreover, many of these MPPT techniques suffer from limitations such as tracking direction errors, slow tracking speeds, and excessive oscillations. In addition, it is crucial to consider the appropriate power converter topology when designing MPPT controllers. Based on the abovementioned, the primary objective of this research is to develop an innovative MPPT controller for both PV and wind turbines capable of adapting to rapidly fluctuating environmental and parametric conditions including variations in solar irradiance, temperature, abrupt load demand, boost converter inductance, and capacitance, partial shading, cloudy conditions, and grid-connected operation. While for wind turbine power extraction, the high fluctuation of wind velocity is considered the big impediment in this context in addition to choosing suitable topology.

On the other hand, the widespread adoption of static power converters, such as rectifiers, inverters, and switched-mode power supplies, has led to a significant increase in harmonic current injection into distribution systems. Accordingly, harmonic mitigation is a critical aspect of grid-connected hybrid systems, ensuring compliance with electrical code standards. To comply with international standards, the total harmonic distortion (THD) of the current introduced into the electrical grid must remain below 5%. In order to achieve this condition and overcome impediments related to power quality issues, multi-level inverters have recently been widely used in HPS applications. Nevertheless, classical linear control schemes-

based Pulse Width (PWM) or Space Vector Modulation SVM struggle to provide pure current injection into the grid and high-power quality. Accordingly, this dissertation research also aims to deal with these problems faced in the second stage (inverter control).

After ensuring optimal and effective power extraction from the used power sources and smooth injection of current into the grid, the next challenge that must be dealt with is power management. The system frequently experiences abrupt variations in load demand and sources of power, resulting in significant fluctuations in the DC link voltage, which may impact the performance of the HPS. A well-implemented energy management strategy can enhance system performance by ensuring adequate supply to meet demand, extending the lifespan of components, reducing operating costs, and ultimately providing a technically and economically viable solution. However, in order to design a power management strategy, it is crucial to consider several factors including the energy storage type and its features, sizing, weather variation, and power demand data across a defined period.

1.3 Thesis Objectives and Contribution

This dissertation aims to develop a novel control strategy for a grid-connected hybrid power system. However, the integration and coordination of multiple energy sources within a hybrid system presents significant challenges for control system implementation. In addition, the practical design of control systems for hybrid systems with more than two energy sources remains a formidable challenge. The suggested system involves the integration of photovoltaic and wind energy sources with fuel cells, serving as a storage solution to replace traditional large batteries or supercapacitors.

For the PV systems, the nonlinear voltage/current characteristics of PV modules inherently limit their power conversion efficiency. Accordingly, maximum power point trackers (MPPTs) are essential components in maximizing PV energy generation by ensuring optimal operating conditions. Therefore, the first objective of this research is to develop and simulate an efficient PV system controller capable of rapidly identifying and tracking the maximum power point (MPP) under diverse conditions, while minimizing tracking errors and fluctuations.

The second objective of this research is to design an optimal algorithm that enhances the power output performance and efficiency of the PMSG-based wind energy conversion system WECS despite the uncertainty in the WT characteristics, significant inertia, and abrupt change wind velocity.

Upon integrating hybrid renewable energy sources into the utility grid, a robust inverter control system becomes indispensable. Grid synchronization and the injection of pure sinusoidal currents are critical functions that this system must fulfill. However, traditional algorithms like SVM controllers, hysteresis controllers, and sinusoidal pulse width modulation (SPWM) for inverter control often present challenges due to their complex tuning processes. In light of what has been mentioned, we aim to overcome these demerits and inject high-quality energy into the grid, while minimizing the current THD.

Optimal power management, which optimizes power exchange, guarantees controllable power generation, regulates DC bus voltage, maintains continuous load supply, and subsequently reduces energy production costs, is the final objective of this thesis.

In order to accomplish the aforementioned objectives, this research work offers the following significant contributions:

- Design a novel control strategy based Two-level MPPT farmwork for PV systems via combining artificial neural network (ANN) and model reference adaptive controller. Hence, ANN is employed to identify the ultimate maximum power point and the MRAC to effectively manage the dynamics of the DC-DC converter.
- 2. The second intelligent strategy that has been suggested in this dissertation for PV systems is a hybrid neural network with model predictive control (NN-MPC). Neural networks are utilized to forecast the reference value of the MPP and to enhance both tracking speed and accuracy; an MPC is implemented to regulate photovoltaic power systems for MPP tracking. The suggested approach exhibits commendable dynamic and steady-state performance.
- 3. The PMSG-based WECS exhibits significant uncertainties, rendering the standard control method, which lacks robustness, inadequate for fulfilling performance requirements. This work proposes a robust nonlinear high-order super twisting sliding mode controller (STSMC) to assure the efficiency and stability of the system, facilitating maximum power point tracking for PMSGbased WECS.

- 4. A finite-set model predictive control (FCS-MPC) approach is proposed for controlling the grid-tied centralized three-level NPC inverter. This control method offers a straightforward and versatile solution, capable of managing various converter types and variables without the need for additional modulation techniques or internal cascade control loops. The controller directly generates drive signals for the power switches. FCS-MPC's effectiveness stems from its ability to capitalize on the discrete nature of power converters and microprocessors.
- 5. To guarantee that fuel cell hybrid systems can reliably meet power demands while respecting the operational limits of each energy source, several energy management strategies have been proposed and critically compared each other. These include state machine control, classical proportional-integral (PI) controllers, external energy maximization strategy, and equivalent consumption minimization techniques. Each approach aims to balance energy distribution efficiently, ensuring uninterrupted power supply without exceeding the capabilities of individual components.

Chapter 2 : Power Sources Modeling

2.1 Introduction

In recent times, there has been a growing focus on renewable energy sources due to their ability to mitigate the pollution caused by fossil fuels and address the issue of climate change. The global shift towards dependable and viable hybrid renewable energy systems is primarily driven by two factors: the potential techno-economic benefits of combining different energy sources as well as the fast exhaustion of traditional energy sources[17]. By 2050, renewable energy is projected to make up 95% of the increase in global power capacity [18]. Renewable energy sources, like photovoltaic or wind, cannot generate a consistent amount of power. However, when combined, their complementary nature allows for a continuous flow of electricity[19]. Efficiently integrating solar and wind resources can mitigate their intermittent nature, resulting in a more reliable and less expensive operational system [20]. A hybrid system can include not only energy sources, but also a network for distribution, converters, a storage system, and an energy management or supervision system.

Solar photovoltaic energy generation is increasingly becoming the most cost-effective option for power production in several global locations. This trend is expected to lead to significant investments in the next years [21]. Furthermore, photovoltaic installations have emerged as a crucial element in endeavors to diminish greenhouse gas emissions in addition shift towards a more environmentally friendly future.

Wind energy (WE) is one of the optimal alternatives for decentralized energy production, resulting in lower energy expenses. Wind energy is a renewable and environmentally friendly source of power that is cost-effective and user-friendly. This is achieved by harnessing the power of turbines to convert wind energy into mechanical energy. Electric generators convert the latter into electrical energy, with the quantity of energy produced being closely correlated with wind speed [22], [23].

However, the sporadic nature of the aforementioned renewable sources necessitates the inclusion of a support energy system and/or efficient energy storage to consistently supply the demand. By incorporating a WT, PV panel, and an appropriate storage system into a hybrid system, it becomes possible to leverage their complementary attributes, resulting in improved dependability and efficiency of the overall system[24]. Batteries are inexpensive and increasingly prevalent. However, their limited lifespan and environmental impact have led to

the introduction of hydrogen energy storage devices. The employing of fuel cells as a secondary source or a backup has been suggested by various researchers [25]. Currently, researchers and manufacturers are primarily focusing on the development of Proton-Exchange Membrane Fuel Cell (PEMFC) systems. If clean hydrogen is used, these systems have the ability to produce zero tank emissions and achieve high system productivity.

The power system under investigation in this thesis is a hybrid system that is linked to the grid and consists of a photovoltaic, wind, and proton exchange membrane fuel cell system as illustrated in Figure 2.1. Wind and PV energy sources have been used as primary sources, whilst PEMFC have been employed as a backup or secondary source. This chapter presents a detail modelling of aforementioned power sources, together with their corresponding power conversion systems. Initially, the solar power generator is represented using a single diode model. Subsequently, the FC stack is analyzed by taking into account its specific attributes. Furthermore, the WECS model is thoroughly elucidated. Ultimately, the converter for each source is modeled.

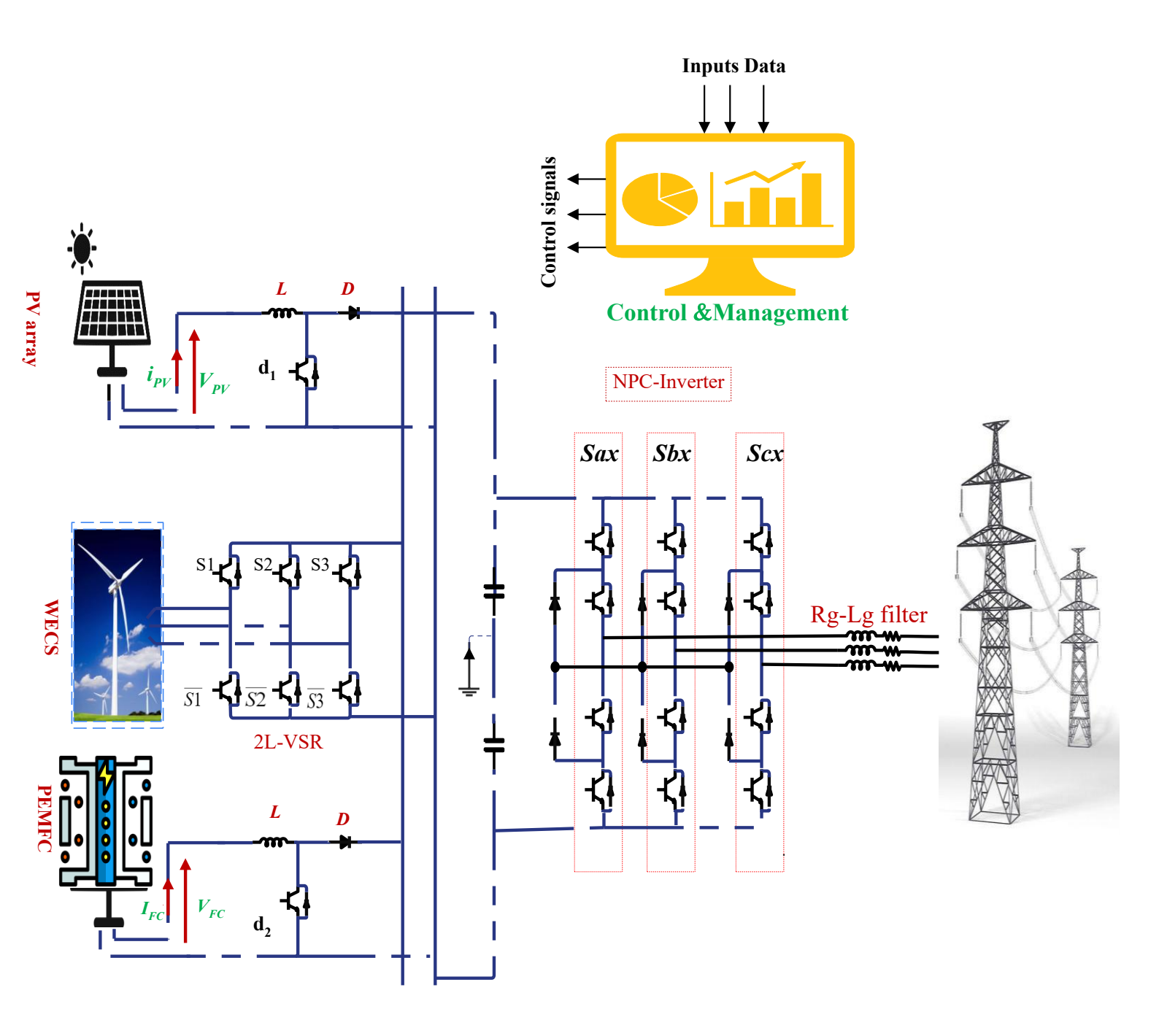


Figure 2.1: A hybrid energy system structure connected to the grid.

2.2 Mathematical Model of A PV Solar Cell

A solar cell is the main component of a PV panel, which can be labeled as an electronic device capable of harnessing the energy of photons and converting it directly into electricity [26]. In fact, there are two famous models used in literature to represent a PV cell: the two-diode model (DDM) and the single-diode model (SDM) [27], [28]. According to the literature [29], [30], the single-diode model is the more prevalent choice because of its ability to be represented by a straightforward and precise simulation model. The equivalent circuit of a PV cell using the mentioned SDM is depicted in Figure 2.2. Accordingly, this model consists of a current source I_{Ph} represents the cell's photocurrent, one parallel diode which signifies the p-n junction, the inner series resistor (R_s) , and a shunt (parallel) resistor (R_p) which refers to the losses caused by the junction's leakage currents. The equivalent circuit of a PV cell.

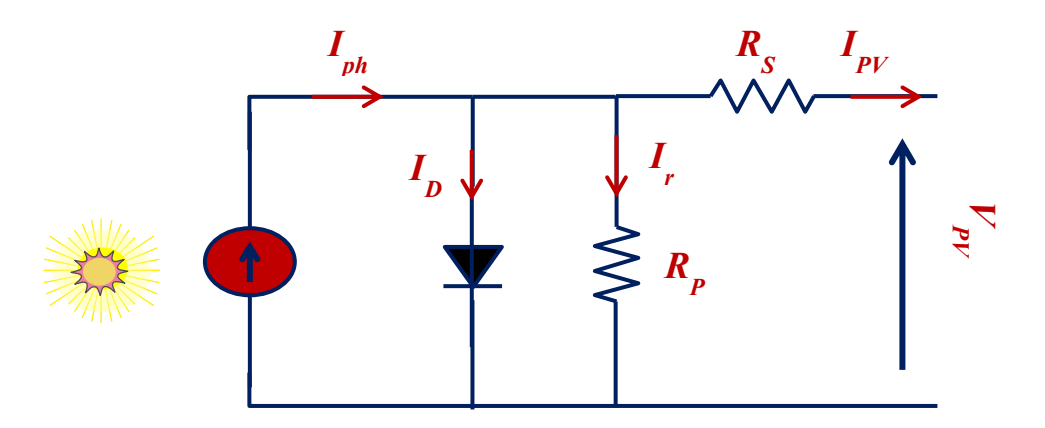


Figure 2.2: The schematic representation of the equivalent circuit for a photovoltaic (PV) cell.

The output current (I_{PV}) derived from the equivalent circuit depicted in Figure 2.1 is specified as follows:

$$I_{PV} = I_{ph} - I_D - I_r (2.1)$$

The expression for the diode current I_D is given in Equation (2.1):

$$I_{D} = I_{s} \left[\exp \left(\frac{V_{PV} + I_{PV} R_{s}}{\eta V_{T}} \right) - 1 \right]$$
(2.2)

 V_T denoted to the thermal voltage, which can be defined as

$$V_T = \frac{KT_c}{q} \tag{2.3}$$

q is the electronic charge; K refers to Boltzmann constant.

 I_{Ph} Is described by the following equation

$$I_{Ph} = \left(\frac{G}{G_n}\right) \left[I_{scr} + K_i \left(T - T_r\right)\right]$$
(2.4)

Where ' G_n ' represents the nominal irradiance, its value is estimated at $1000 \text{ w/}m^2$, in contrast G denotes the actual irradiance, I_{scr} is the short-circuit current, T and T_r are the cell temperature and the reference temperature in kelvin (K) respectively.

The parallel resistance current I_r can be described as

$$I_r = \frac{V_{PV} + I_{PV}R_S}{R_P} \tag{2.5}$$

The calculation of the current produced by a photovoltaic (PV) cell can be determined by substituting the equations provided in (2.2), (2.4), and (2.5) into equation (2.1):

$$I_{PV} = I_{Ph} - I_{s} \left[exp \left(\frac{V_{PV} + I_{PV}R_{s}}{\eta V_{T}} \right) - 1 \right] - \frac{V_{PV} + I_{PV}R_{s}}{R_{P}}$$
 (2.6)

In the context of photovoltaic (PV) systems, a PV panel (module) refers to a collection of PV cells that are interconnected either in series or in parallel, or a combination of both, with the objective of generating the desired output power. When the number of cells connected in series is denoted as NS, and the number of cells connected in parallel is denoted as NP, Equation (2.6) is modified as follows:

$$I_{PV} = N_{P}I_{Ph} - N_{P}I_{s} \left[exp \left(\frac{N_{s}V_{PV} + \frac{N_{s}}{N_{P}}I_{PV}R_{s}}{N_{s}\eta V_{T}} \right) - 1 \right] - \frac{N_{s}V_{PV} + \frac{N_{s}}{N_{P}}I_{PV}R_{s}}{\frac{N_{s}}{N_{P}}R_{P}}$$
(2.7)

2.2.1 PV Solar Characteristic Curves

Typically, the performance assessment of photovoltaic (PV) modules is conducted by considering their maximum output power under standard test conditions (STC). These STC conditions entail an operating temperature of 25 °C for the PV cell and an incident solar irradiance level of 1000 W/m². By establishing these standardized conditions, consistent and comparable assessments of PV module performance can be achieved across various systems and manufacturers[31]. Figure 2.3 illustrates the power-voltage (P-V) curve in addition to the current-voltage (I-V) characteristics curve of a selected PV panel (MSX-60) under the STC test. Throughout these curves, we can figure out three important points of the PV panel the open-circuit voltage (V_{OC}) which agrees with the zero current ($I_{PV} = 0$) furthermore, the shunt resistor is negligible, secondly the short circuit current (I_{SC}) which can be discovered at ($V_{PV}=0$), another significant point can be indicated from these curves is the maximum power point (MPP) which is achieved when the multiplication $V_{PV} * I_{PV}$ is maximal.

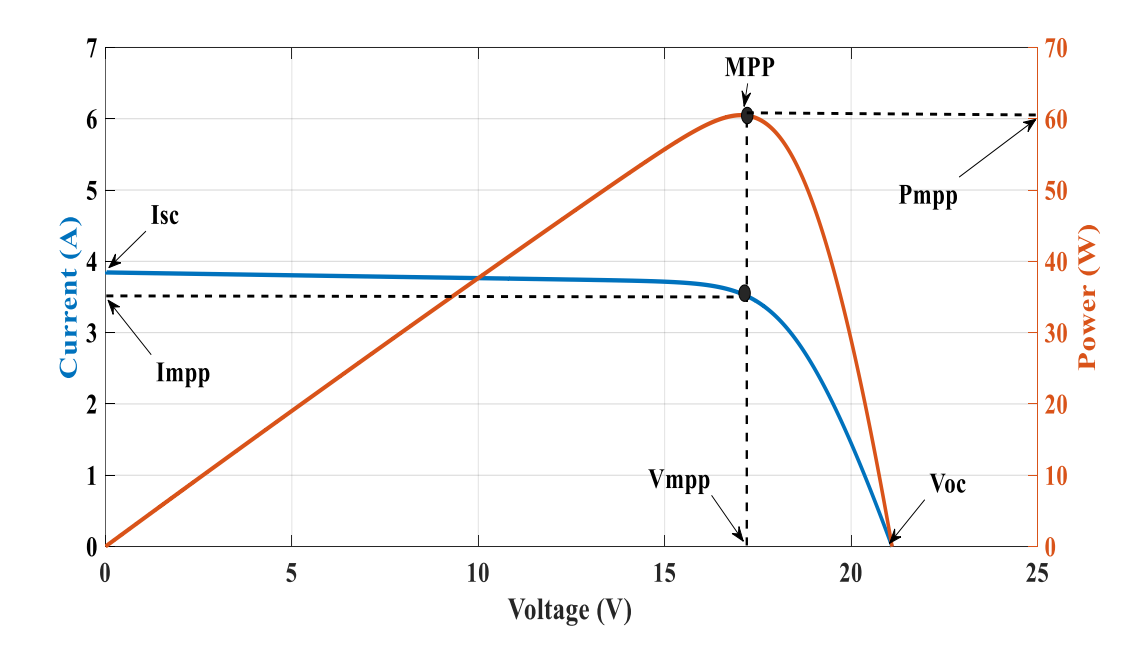


Figure 2.3: P-V & I-V characteristics of a PV panel under STC.

2.2.2 Weather Conditions Effect

Indeed, the efficiency of converting solar energy into electrical energy in photovoltaic (PV) systems is significantly impacted by solar irradiation and temperature conditions. Figures 2.4 and 2.5 clearly demonstrate the substantial correlation between the performance of the PV module and variations in temperature and irradiance level. Figure 2.4 illustrates the I-V and P-V characteristics for different levels of solar radiation. In cases of low solar radiation, there is a considerable reduction in the short circuit current, nonetheless, the change in open circuit

voltage is minimal. This observation confirms that the maximum power output from the module decreases. Likewise, Figure 2.5 displays the I-V and P-V characteristics for various temperature values. It is evident that an increase in temperature leads to a decrease in open circuit voltage, while the short circuit current remains relatively unchanged. Consequently, the maximum power output from the panel decreases[32], [33].

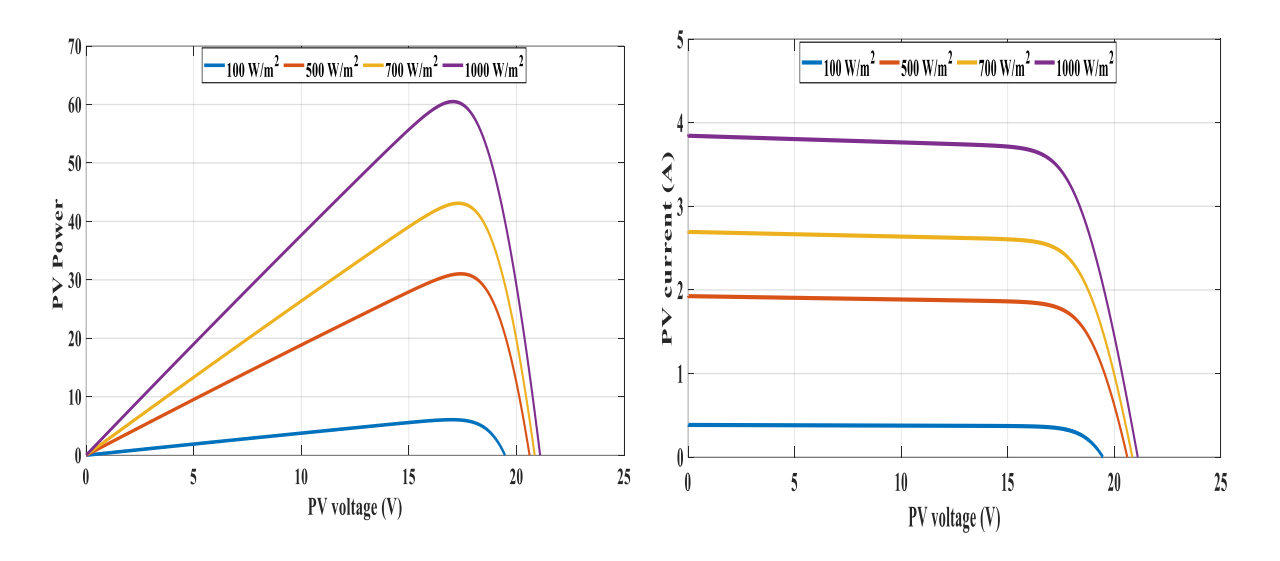


Figure 2.4: P-V & I-V characteristics of a PV panel under diverse irradiation levels.

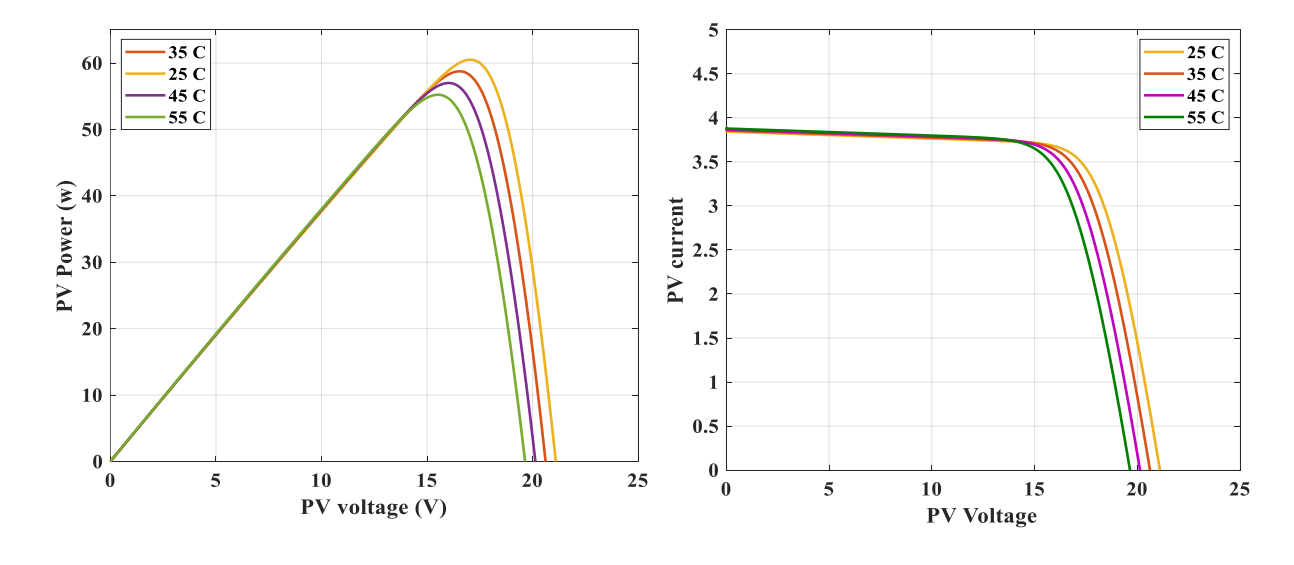


Figure 2.5: P-V & I-V properties of a photovoltaic (PV) panel at various temperature levels.

2.3 Fuel Cell

A fuel cell (FC) is an electrochemical apparatus that generates electrical power using hydrogen and oxygen. Actually, the process involves the catalytic oxidation of hydrogen at the anode and the catalytic reduction of oxygen at the cathode. This leads to creating a voltage

difference between the electrodes, which may be exploited by an external circuit. The electrolyte acts as a barrier between the electrodes, allowing the interchange of ions with mass and charge. In addition to the generation of electricity, the process also yields water and heat as byproducts[34], [35]. The electrochemical processes taking place on the electrodes may be expressed by the following equations:

Anode:
$$H_2 \to 2H^+ + 2e^-$$
 (2.8)

Cathode:
$$2H^+ + \frac{1}{2}O_2 + 2e^- \to H_2O$$
 (2.9)

While the overall electrochemical processes can be described as

$$H_2 + \frac{1}{2}O_2 \rightarrow H_2O + electrical\ energy$$
 (2.10)

According to the literature, several fuel cell unit layouts were suggested, taking into account various electrolyte and electrode materials, catalysts, and operating temperatures. Currently, there exist six primary fuel cell types, as presented in Figure 2.6. Nonetheless, in this study, we will focus only on the proton exchange membrane fuel cell (PEMFC) type because of its advantages and reliability compared with other FC types.

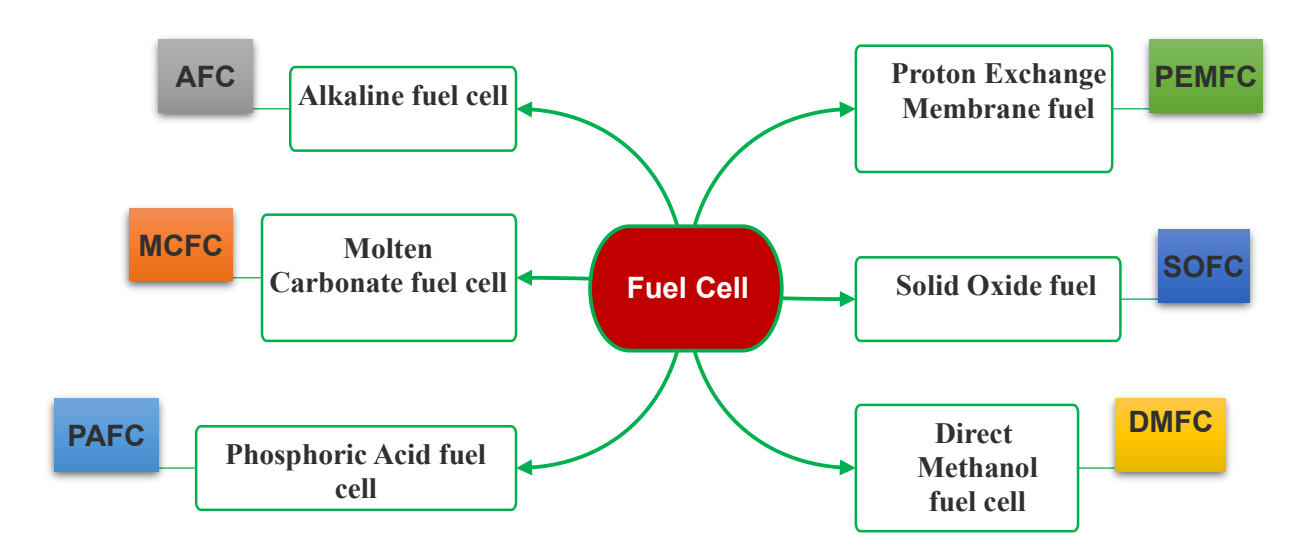


Figure 2.6: The Varying Forms of Fuel Cells.

2.3.1 Modeling and Analysis of PEMFC

PEMFC, also recognized as Polymer Electrolyte fuel cells is a prevalent kind of FC that is widely used in practical applications. The principle of operation of the PEMFC is more like

that mentioned before for the general FC operation process. It utilizes hydrogen (H2) as fuel in addition, it employs oxygen (O2) from the air for the reason of oxidization. Literally, when the hydrogen collides with the electrolyte membrane it leads the protons to pass from the anode toward the cathode; in contrast, the electrons traverse across an external circuit to reach the cathode and provide electricity during this way. Oxygen undergoes a chemical reaction with protons and electrons, resulting in the formation of water and the production of heat at the cathode[11-14]. The typical process of PEMFC functioning is illustrated in Figure 2.7.

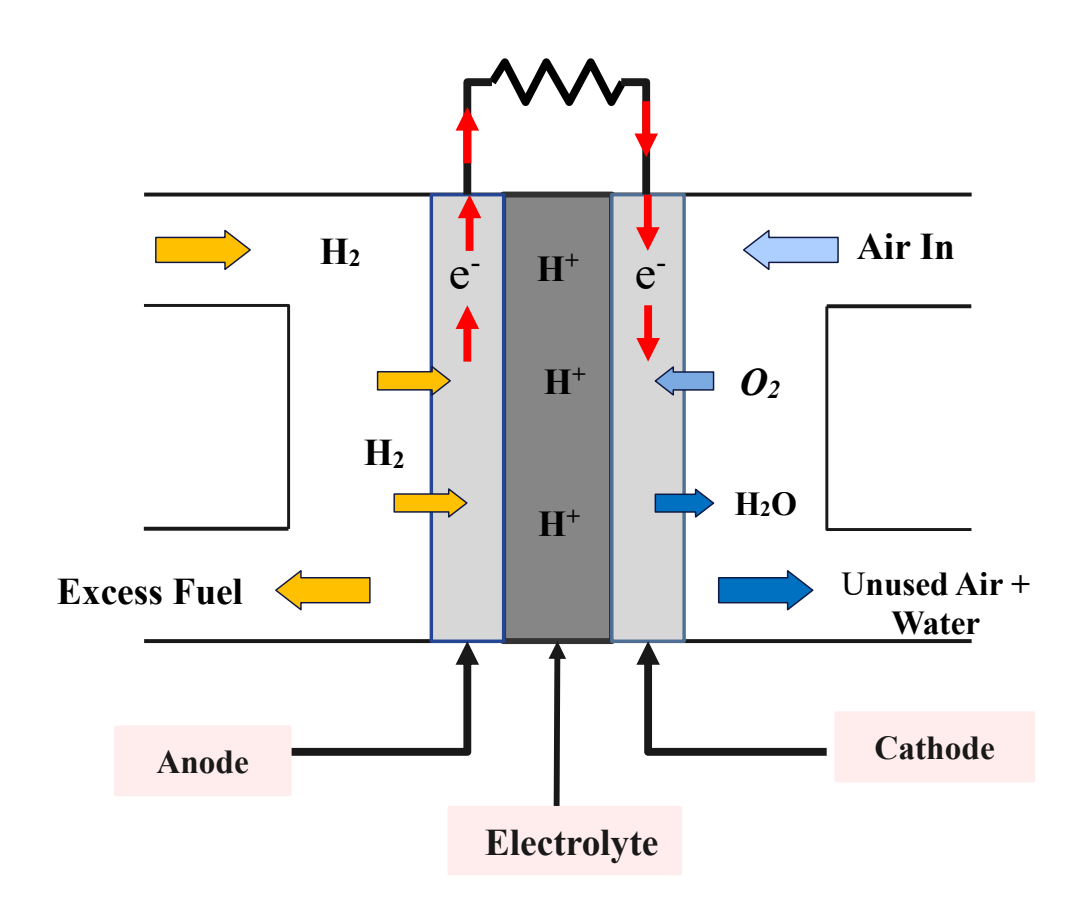


Figure 2.7: PEMFC functioning Diagram.

In fact, the PEMFC model can be categorized into static behavior and dynamic model according to literature [40], [41].

2.3.1.1 PEMFC's Static Model

According to Ref [36], [37], [41], [42], The output voltage for each cell can be represented by the following equation:

$$V_{cell} = E_{Nernst} - E_{act} - E_{ohmic} - E_{conc}$$
 (2.11)

Where: E_{Nernst} represents the equilibrium thermodynamic potential or known also as the electrochemical thermodynamic potential, E_{act} represents the activation loss, E_{conc} denotes the concentration loss, and E_{ohmic} represents the ohmic loss.

The Nernst voltage is determined as follows

$$E_{\textit{Nernst}} = 1.229 - \left(8.5 \times 10^{-4}\right) \left(T - 298.15\right) + \left(4.385 \times 10^{-5}T\right) \left[\ln\left(P_{H2}\right) + 0.5\ln\left(P_{O2}\right)\right] \tag{2.12}$$

Where T represents temperature, P_{H2} denotes hydrogen pressure, and P_{O2} signifies oxygen pressure.

The **activation voltage loss** is influenced by temperature, partial pressures, as well as the catalyst employed on the electrodes. It is calculated using a semi-empirical equation expressed by [43]

$$E_{act} = \xi_1 + \xi_2 \cdot T + \xi_3 \cdot T \cdot \ln(C_{O2}) + \xi_4 \cdot T \cdot \ln(i_{FC})$$

$$\tag{2.13}$$

Where: i_{FC} represents the current of the cell, $\xi_{(1\cdots 4)}$ are parametric coefficients determined based on kinetic, thermodynamic, and electrochemical phenomena for each cell. C_{02} denoted to the concentration of oxygen in (mol / Cm^3) determined based on the oxygen partial pressure as well as cell temperature using Henry's law, given by [44]

$$C_{O2} = \frac{P_{O2}}{5.08 \times 10^6 e^{\left(-\frac{498}{T}\right)}} \tag{2.14}$$

Ohmic polarization loss $E_{\it ohmic}$: The ohmic polarization loss results from two main sources. The first one is from the resistance obtainable by the membrane to the transfer of protons. While the other loss reason is coming from the electrical resistance arise during the transfer of

electrons between the fuel cell's electrodes. The ohmic loss can be expressed as the following equations [44], [45]

$$E_{ohmic} = i_{FC} \cdot (R_m \cdot R_c) \tag{2.15}$$

Where: R_m refers to the electron flow resistance (membrane resistance) that impedes the electrons' exchange within electrodes. R_c denoted to the proton resistance which approximatively taken as constant.

The membrane resistance R_m is expressed as [35]

$$R_{m} = \frac{\rho_{M} \cdot l}{A} \tag{2.16}$$

$$\rho_{M} = \frac{181.6 \left[1 + 0.03 \left(\frac{T}{A} \right) + 0.062 \left(\frac{T}{303} \right)^{2} \cdot \left(\frac{i_{FC}}{A} \right)^{2.5} \right]}{\left[\psi - 0.634 - 3 \cdot \left(\frac{i_{FC}}{A} \right) \right] \cdot \exp^{\left[4.18 (T - 303)/T \right]}}$$
(2.17)

A : is defined as the active area of the membrane.

 Ψ : denotes a variable that can be adjusted within a range up to a maximum value of 23.

l: represents the membrane's thickness in (cm). while the exponential term in the denominator serves as a factor correction of temperature when the cell operates at different value of 30 C°.

Concentration Polarization loss: Concentration loss occurs due to the decrease in the concentration of the reactants, hydrogen and, oxygen as they are consumed in the reaction. Hence, it can be depicted as the absence in the chemical process[38], [46]. It be given as follows.

$$E_{conc} = -\beta \ln \left(1 - \frac{J}{J_{\text{max}}} \right)$$
 (2.18)

Where β refers to a parametric coefficient which is specific to the fuel cell and its functioning conditions. J and J_{max} represent the cell's current density in (A/cm²), and the maximum current density, respectively.

2.3.1.2 Dynamic Model

Understanding the dynamic electrical behavior of fuel cells is crucial, with the charge double layer playing a significant role[47]. As electrons flow from the anode through the external load and reach the cathode in a fuel cell, hydrogen ions also arrive at the cathode simultaneously. This synchronized movement of electrons and hydrogen H^+ ions lead to the formation of two charged layers with opposite polarities across the boundary between the cathode and the membrane. The accumulation of positive hydrogen ions and negative electrons in these respective layers creates an electrical potential difference. This configuration resembles that of an electrical capacitor, as it stores and holds electrical charge and energy[48], [49]. The accumulation of charges produces an electrical voltage that represents the sum of concentration overvoltage and activation overvoltage. Thus, there is a delay before the concentration overvoltage and activation overvoltage adjust to the abrupt change in current. In contrast, the ohmic voltage drop reacts immediately to a current change. FIGURE (2.8) illustrates the dynamic behaviors of PEM fuel cell as discussed above, where the resistances R_{act} , R_{con} and R_{Ohm} represent the activation overvoltage, the concentration loss and the ohmic losses, respectively.

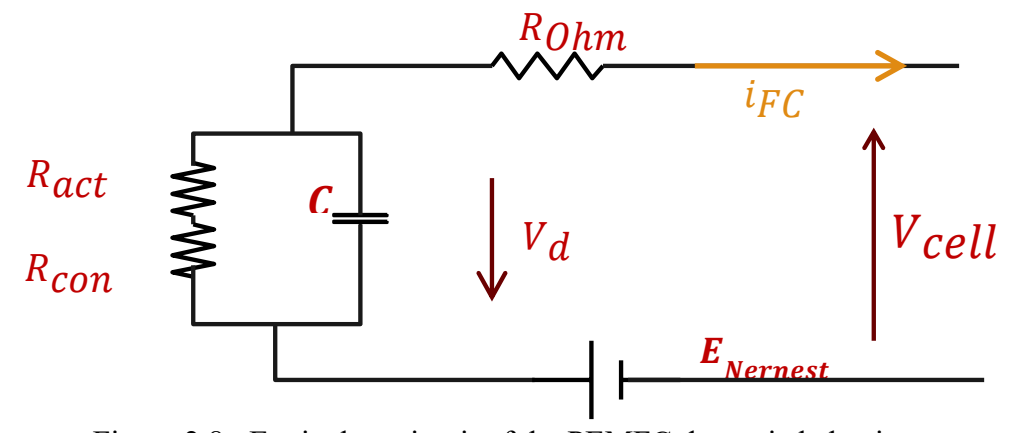


Figure 2.8: Equivalent circuit of the PEMFC dynamic behavior.

The dynamic behavior of the PEMFC according to the above equivalent circuit may be represented as follows.

$$\frac{dV_d}{dt} = \frac{1}{C}i_{FC} - \frac{1}{\tau}V_d \tag{2.19}$$

Where V_d denotes the dynamic voltage across the equivalent capacitor, which is associated with R_{act} and R_{com} . While C represents the equivalent electrical capacitance of the fuel cell. τ represents the fuel cell electrical time constant associated with the cell temperature it can be expressed as

$$\tau = C \cdot \left(R_{act} + R_{Con} \right) \tag{2.20}$$

Therefore, the new representation of the total cell voltage equation may be given as:

$$V_{cell} = E_{Nernst} - E_{act} - E_{ohmic} - E_{conc} - V_d$$
 (2.21)

2.3.2 Pressure and Temperature Effect on PEM Fuel Cell Performance

In fact, fuel cell performance may be influenced through various operating circumstances such as pressure, temperature, and relative humidity. In this section we will only discuss the temperature and pressure effect on the overall performance of PEM fuel cell. Figure (2.9) depicts the variation of FC Voltage & FC Power in term of FC current under different temperature operation values. While Figure (2.10) presents the PEMFC characteristics under different pressure conditions. According to [50], The performance of a fuel cell is influenced by temperature, which impacts its kinetics, open circuit voltage (OCV), membrane conductivity, hydrogen crossover, and mass transfer processes. These temperature-induced effects have a direct impact on the overall efficiency and performance of the fuel cell. Therefore, higher temperatures may enhance performance. In Ref [51], authors discovered that higher temperatures enhance performance and efficiency, power output, voltage, and leakage current, while reducing mass transfer and durability. They concluded that an optimal temperature is necessary for peak performance. Moreover, operating pressure may also influence on the PEMFC performance as studies confirmed. Ref[52], indicates that higher pressure resulted in a more forceful introduction of reactant gases into the fuel cell, leading to increased gas flow into the electrolyte. Thus, the electrochemical reaction rate rises, leading to enhanced cell performance. In[53], it was observed that the higher cell pressures increase cell

performance at low current densities, whereas worsen the cell performance at moderate to high current densities. Thus, it's necessary to optimize the fuel cell operation in order to obtain the desired performance.

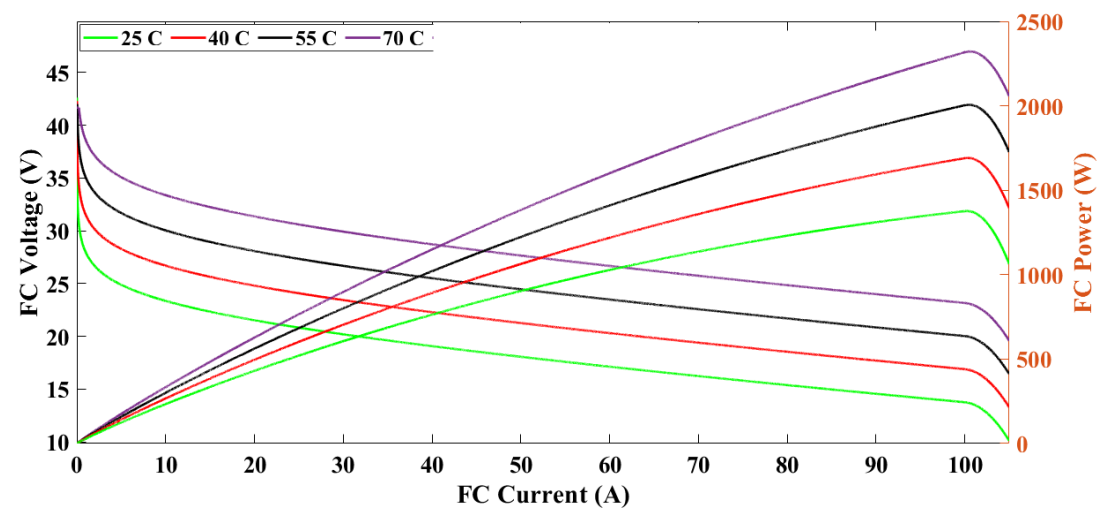


Figure 2.9: PEMFC characteristics under different temperature values.

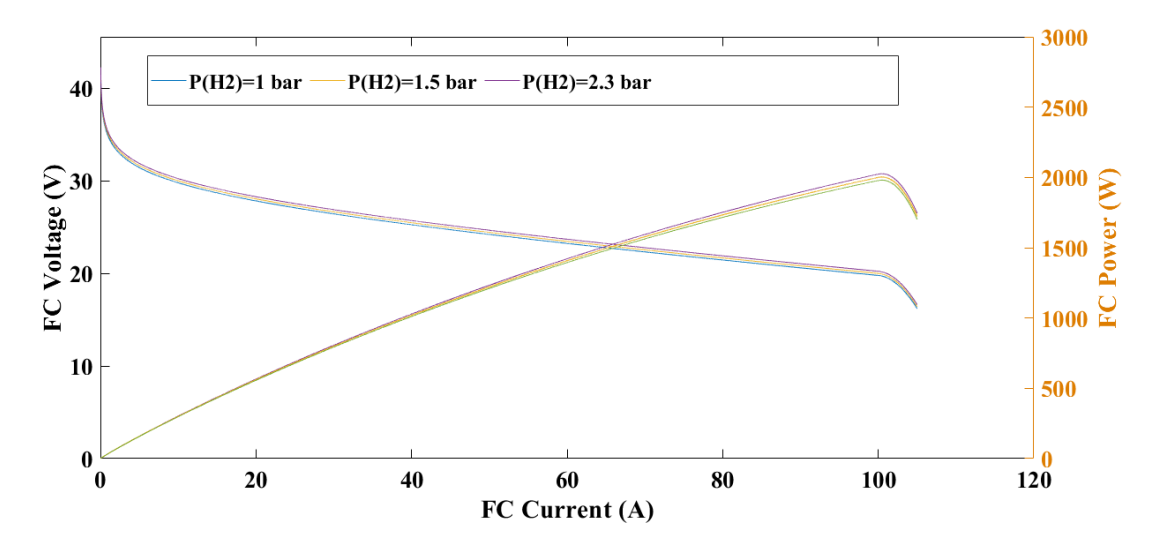


Figure 2.10: PEMFC characteristics under different pressure conditions.

2.4 Wind Energy Conversion Systems

Wind turbines (WT) generate power by converting the kinetic energy of the air into rotational mechanical energy of the turbine rotor blades[32]. Indeed, wind turbines are commonly categorized into two models: vertical-axis type (VAWT) and horizontal-axis type (HAWT). HAWTs are generally preferred over VAWTs in the majority of wind industries because of their higher performance. Figure (2.11) presents the horizontal-axis configuration of wind turbine. Generally, in this configuration used three blades faced the wind, which called the upwind configuration. However, it can be seen also turbines equipped with one, two or over

than three blades [54]. Figure (2.12) shows the main advantages and drawbacks of wind turbines with horizontal axes.

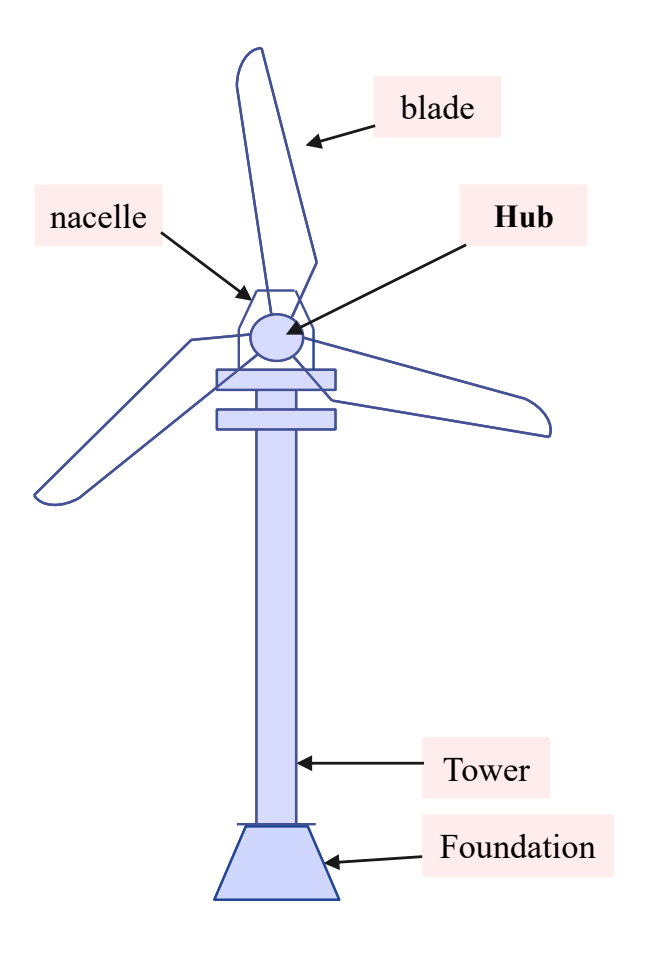


Figure 2.11: Horizontal axis wind turbine scheme

Another way to categorize wind turbines is by their speed, which can be either fixed or variable. The variable-speed wind turbines (VSWTs) provide several benefits in comparison to previous fixed-speed wind turbines[55]. Currently, VSWTs are the most often utilized wind energy conversion systems (WECS). Their ability to operate at varied speeds is made possible by the interface of power electronic converters, which allows for complete or partial separation from the grid [40]. However, the strength of VSWT technology is its ability to achieve the maximum energy conversion across different wind speed conditions.

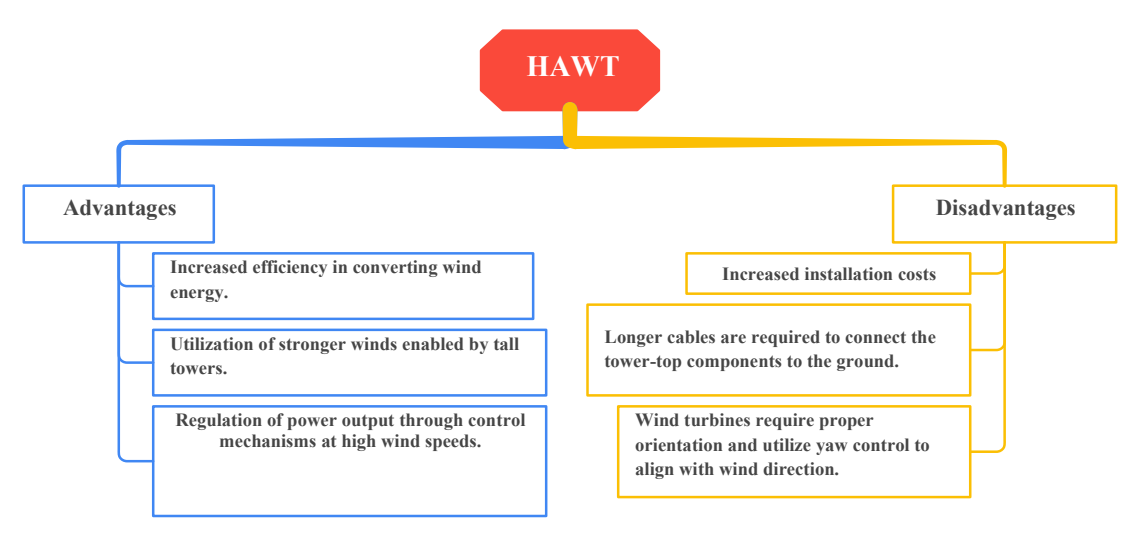


Figure 2.12: Advantages and drawbacks of HAWT.

2.4.1 Wind Turbine

The wind energy conversion system, as shown in Figure (2.13), consists of a wind turbine including three blades of length R, fixed on a drive shaft. However, in order to achieve satisfactory velocity, it's necessary to use an intermediate device called the gearbox. This gearbox drives an electrical generator to produce electrical power. Various generator kinds are employed in WECS over the last decades. It is worth noting that the most commonly used generators are the Doubly Fed Induction Generator (DFIG) as well as the Permanent Magnet Synchronous Generator (PMSG). However, the squirrel cage induction generator (SCIG) is also used in some specific cases.

According to literature, the mathematical modelling of the WECS can be divided into Aerodynamic model and the mechanical part model.

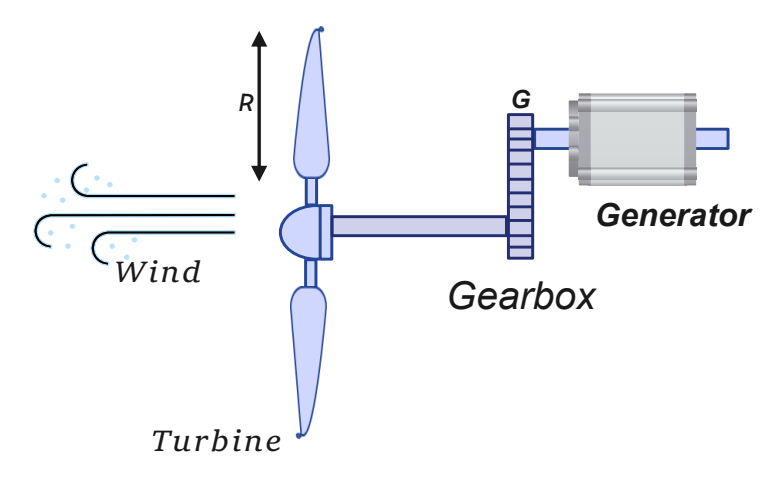


Figure 2.13: Wind energy conversion system scheme.

Aerodynamic Model

The wind turbine rotor engages with the wind flow, giving rise to a phenomenon known as aerodynamics, which is heavily influenced by the shape of the blade. The extraction process of the kinetic energy and the aerodynamic behavior analysis can be explained through the actuator disk theory as shown in Figure (2.14). The rotor wind that captured the kinetic energy is perceived as a disk with a porous structure. Where P_{ν} , V_{ν} and S_1 refer to the pressure, velocity and the surface located anterior to the actuator disc, while S_0 and V_0 denoted to the conditions at the disc, wherein P_2 , S_2 and V_2 denoted to the conditions behind the actuator disc[56], [57].

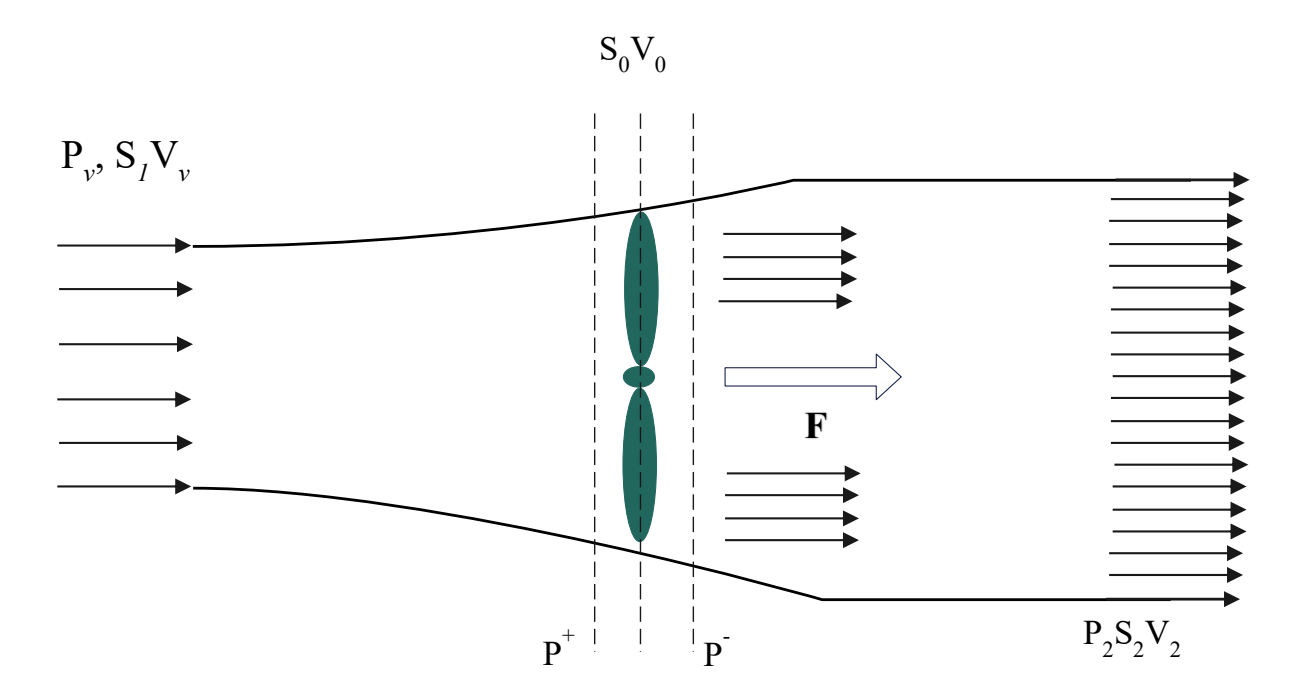


Figure 2.14: Diagram illustrating the energy extraction in a wind turbine.

The kinetic energy of an air mass moving at a velocity V_{ν} across a certain area S_1 may be determined using the following formula:

$$P_{v} = \frac{1}{2} \rho S_{v} V_{v}^{3} \tag{2.22}$$

Where ρ denoted to the air density (Kg/m³), which is dependent on both air pressure and air temperature. Generally, it given approximately 1.225 Kg/m³.

The wind turbine can capture only a part of that power. The aerodynamic power extracted by the rotor wind can be expressed by

$$P_{t} = \frac{1}{2} \rho \pi R^{2} V_{v}^{3} C_{P} \tag{2.23}$$

The parameter C_p is dimensionless which called the power coefficient, it denoted to the capability of a wind turbine to extraction the kinetic energy from the wind. Indeed, according to Betz, the power coefficient does not exceed 0.59 (59%) as a maximum value. For a selected wind turbine, the power coefficient C_P is given in terms of the Tip Speed Ratio (TSR) λ as well as the pitch angle β . One of the most famous expressions of C_p used in the published work is given by

$$C_p = \wp_1 \left(\frac{\wp_2}{\lambda_i} - \wp_3 \cdot \beta - \wp_4 \right) \exp^{\left(-\frac{\wp_5}{\lambda_i} \right)} + \wp_6.\lambda$$
 (2.24)

Where: $\wp_1 = 0.5176, \wp_2 = 116, \wp_3 = 0.4, \wp_4 = 5, \wp_5 = 21, \wp_6 = 0.006795$.

$$\frac{1}{\lambda_i} = \frac{1}{\lambda + 0.08\beta} - \frac{0.035}{\beta^3 + 1} \tag{2.25}$$

The tip speed ratio λ is defined by

$$\lambda = \frac{R\Omega_t}{V_v} \tag{2.26}$$

Where: Ω_t represents the rotor speed, V_v is the wind velocity and R refers to the turbine rotor radius.

The kinetic energy of the wind captured by the aero-turbine is transformed into mechanical energy which results in a motor torque T_t rotating the rotor at a speed Ω_t in terms of power. The following expression defines the torque produced by the rotor:

$$T_{t} = \frac{P_{t}}{\Omega_{t}} = \frac{1}{2} \rho \pi R^{2} C_{P} \frac{V_{v}^{3}}{\Omega_{t}}$$
 (2.27)

a) Drive-Train Model

The drive train system allows to transform the low-speed rotation in the rotor side to high-speed rotation for the generator side[55], [58]. There are many representations are used in literature to model the mechanical behavior and the forces applied to the drive train transmission, including one-mass model[59], two-mass model[60], as well as three-mass model as in [61]. However, the two-mass model is commonly preferred in the scientific papers, thus it has been chosen in this work as shown in Figure (2.15). A two-mass model consists of two rotating inertias linked by a flexible shaft and a gear mechanism. The gear mechanism interconnects the low-speed aerodynamic rotor shaft side with the high-speed generator shaft side[58]. The time domain torque equation that describes the mechanical behavior, can be expressed as follows[62]:

$$T_t - T_{em} = \left(J_m + J_t\right) \frac{d\Omega_t}{dt} + \left(D_m + D_t\right) \Omega_t \tag{2.28}$$

Where: J_t represents the turbine side inertia, while J_m denoted to the machine side inertia. The damping coefficient are denoted by D_t for the turbine side and D_m for the machine side.

In order to simplify Eq. (2.28), let assume the following

$$\begin{cases}
J = (J_m + J_t) \\
D = (D_m + D_t)
\end{cases}$$
(2.29)

Where J is the total inertia, whereas D presents the total stiffness coefficient. In this way, we get:

$$T_t - T_{em} = J \frac{d\Omega_t}{dt} + D\Omega_t \tag{2.30}$$

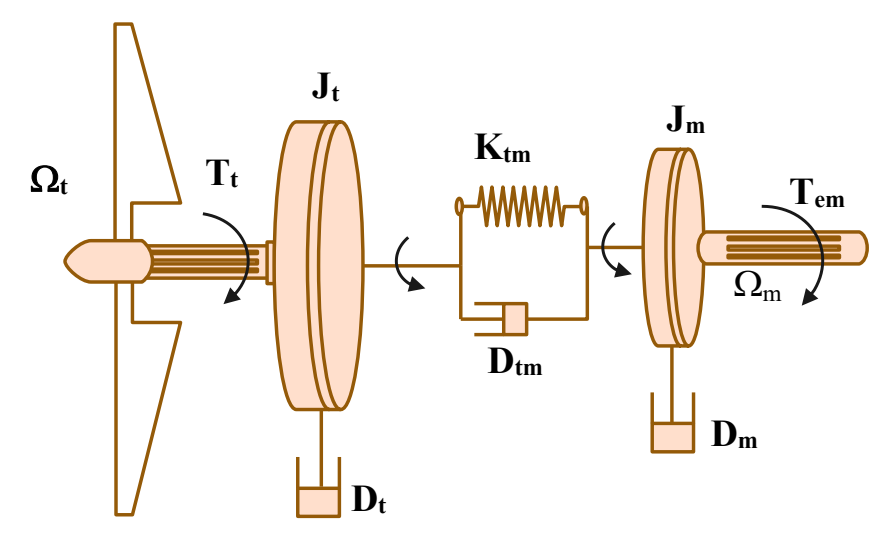


Figure 2.15: Drive-Train scheme using two-mass model.

2.4.2 Mathematical Model of Permanent Magnet Synchronous Generator (PMSG)

Wind energy conversion systems employ several sorts of generators, as mentioned in the previous subsection. In this thesis, the permanent magnet synchronous generator is employed as a wind turbine generator due to its notable attributes, including high efficiency, low losses, compact size, little maintenance requirements, high dependability, and the capability to function without the need for a gearbox[63], [64]. The PMSG may be engineered to accommodate a greater number of poles, making it well-suited for employing direct drive gearless wind turbines. The equation describing the behavior of the permanent magnet synchronous generator (PMSG) in the *dq* coordinate frame is presented below:

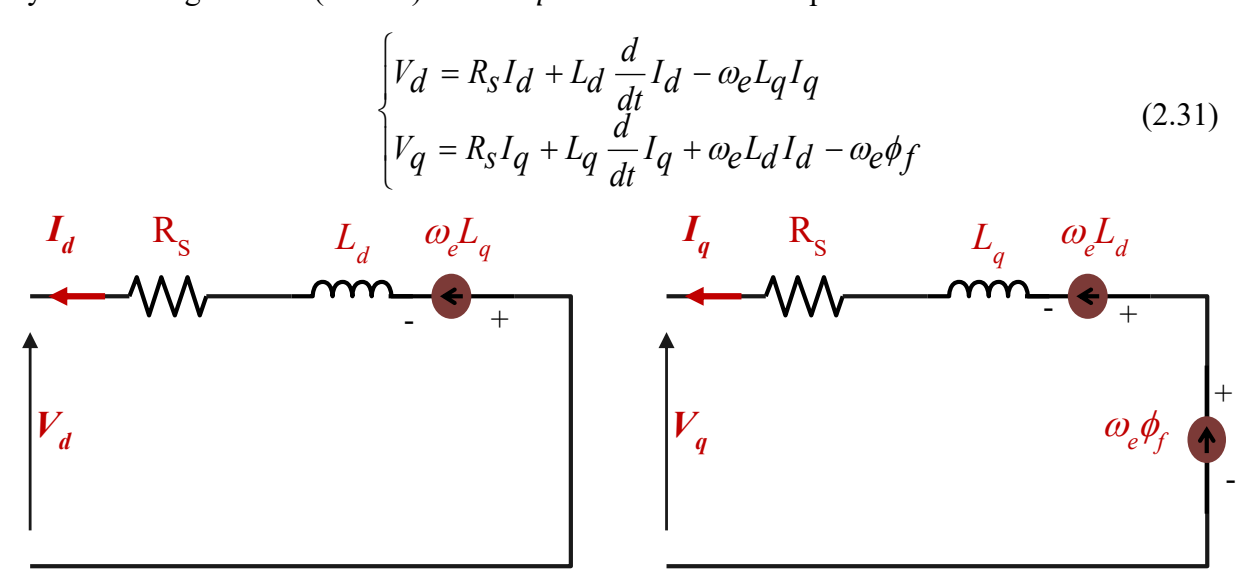


Figure 2.16: Equivalent Circuits of the PMSG on the d-q axis.

Where the variables in the equation are as follows: R represents the stator resistance, Vd and Vq represent the d and q stator voltages, while I_d and I_q are denoted to statoric current in the d-q reference frame, L_d and L_q represent the d-q inductances, and ω_e represents the electric pulsation. Figure (2.16) shows the d-q model of PMSG in a synchronous reference frame. The equation that describes the torque of the PMSG can be written as follows:

$$T_{em} = \frac{3}{2} p \left[\left(L_d - L_q \right) I_d I_q - \phi_f I_q \right]$$
 (2.32)

where P denotes the total number of pole pairs, whereas ϕ_f refers to the permanent magnetic flux.

2.5 Power Converter

2.5.1 DC-DC Converters for Photovoltaic Systems

In this context, various power electronic converters have been used in the literature as well as industry fields including 'Boost, Buck, and Buck-Boost converters in addition to ZETA and SEPIC converters [65]. Nevertheless, among DC-DC converters, boost converters which increase voltage from its input to output are the most common. An inductor (L), a diode (D), and a controlled switch (S') make up the boost converter. If the system was in stand-alone mode, then the load be connected to a capacitor filter (C) at the output side[66]. Hence, to obtain a satisfied voltage in the DC-Bus of the proposed hybrid system, a boost converter has been chosen as illustrated in Figure (2.17).

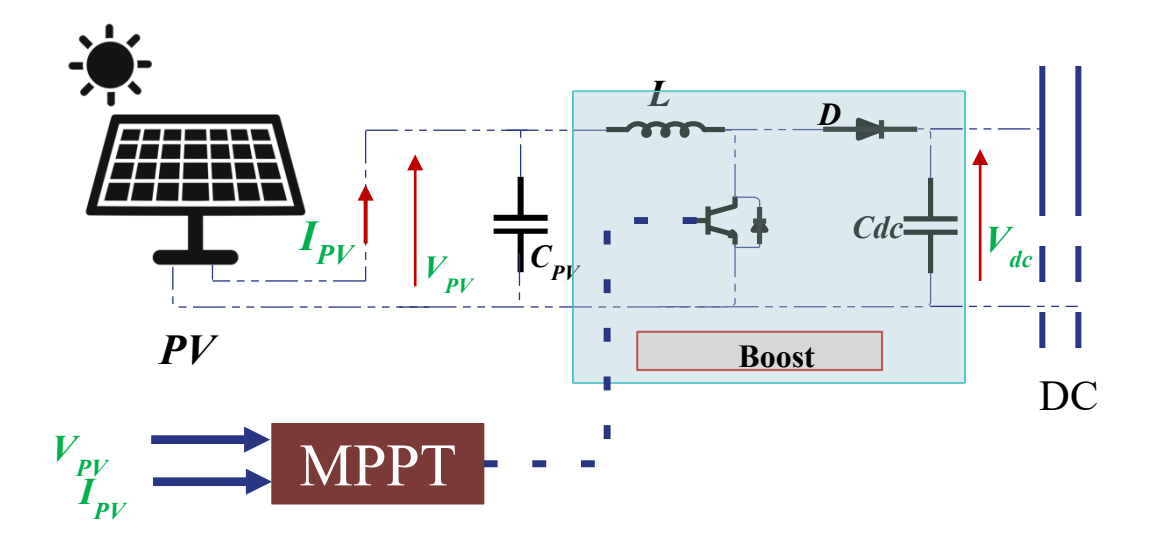


Figure 2.17: Schema illustrates PV system with MPPT controller.

The boost converter may be studied based on two potential states of the switch S', as shown in the table below:

TABLE I: Operation modes of boost converters.

| Switch ON: <i>S'</i> =1 | Switch OFF: S' =0 |
|--------------------------------------|---|
| $\int L \frac{dI_L}{dt} = V_{PV}$ | $\int L \frac{dI_L}{dt} = V_{PV} - V_{dc}$ |
| $C_{dc} \frac{dV_{dc}}{dt} = I_{dc}$ | $C_{dc} \frac{dV_{dc}}{dt} = I_{dc} - I_{PV}$ |

2.5.2 Fuel-cell's Power Converter

The development of units' power-conditioning is of paramount importance in facilitating the integration of fuel cell systems with standalone or grid-connected systems, especially considering the drooping characteristics exhibited by fuel cells[67]. In literature, many studies have attempted to compile a comprehensive list of the most favorable architectural chances which includes FC with Power converters while considering the essential criteria. Undoubtedly, those architectural designs have the potential to enhance reliability, efficiency, and cost-effectiveness[68]. TABLE II summarizes the different converters' topologies used in fuel cell applications. Even though, the boost converter remains the most widespread due to its high advantages as well as its extremely reliable. Accordingly, the conventional boost converter was employed for the proposed system as shown in Figure (2.18).

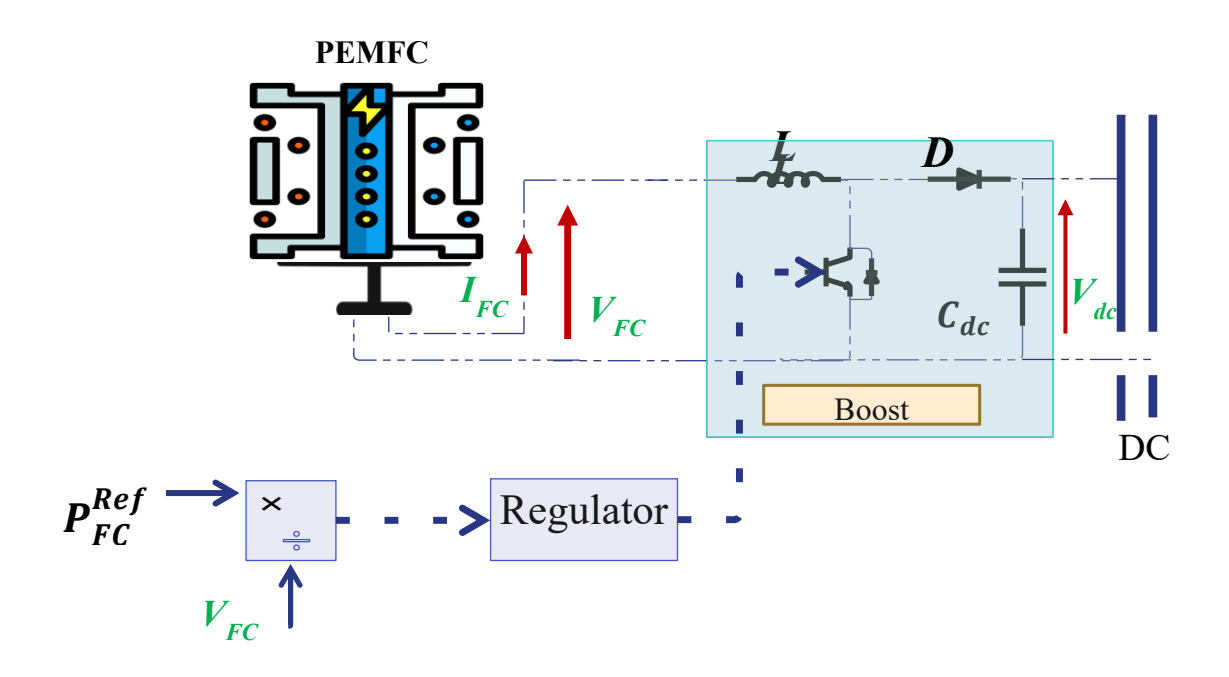


Figure 2.18: PEMFC with traditional Boost converter interface.

TABLE II: Introducing the specifications of DC-DC converters utilized in Fuel Cell applications.

| Topology | Direction | Switch | Isolation | Complexity |
|-----------------------------------|----------------|--------|-----------|------------|
| Boost[69] | Unidirectional | 1 | No | Low |
| Buck-Boost[70] | Bidirectional | 2 | No | Low |
| Interleaved Boost[71] | Unidirectional | 2 | No | Medium |
| Interleaved Buck- Boost[72] | Bidirectional | n | No | Medium |
| Floating-Interleaved Boost[73] | Unidirectional | 2 | No | Complex |
| Z-Source Inverter[74] | Bidirectional | 6 | No | Medium |
| Quasi Z-Source Inverter[75] | Depend | 6 | No | Medium |
| Half- bridge [76] | Unidirectional | 2 | Yes | Low |
| Full-bridge[77] | Unidirectional | 4 | Yes | Low |
| Dual active bridge[78] | Bidirectional | 8 | Yes | Complex |

2.5.3 WECS Power Converter

The use of power electronic converters in wind turbine systems enables variable speed operation, which in turn enhances the overall power extraction capabilities. In a variable-speed operation, a control method is necessary to extract the maximum power from the turbine while also providing a constant grid voltage and frequency[79]. In recent times, numerous power converter configurations have emerged to facilitate the integration of PMSG-based WECS with the electrical grid. A diode rectifier followed by a DC-Link capacitor is one of the most favorable schemes as in Ref. [80]. Another prevalent method involves a dc/dc converter rather than the dc-link capacitor, this configuration allows the voltage variation on the machine side in addition to smoothing power output [81], [82]. However, the most widely spread topology for WECS grid connected Known as the Back-to-Back (BTB) converter, this configuration is divided into two stages where the first one is called the machine side converter whereas the second is the grid side converter[61]. The rectifying mode is used by the first side converter and the inverting mode by the other(grid-side). This architecture provides various benefits, such as the ability to actively and reactively control, a high-power factor on the generator side, and excellent efficiency. Nevertheless, it also exhibits certain disadvantages, including a very limited duration of existence, elevated switching losses, and the production of frequency harmonics[83]. Noteworthy that there are several emerging WT manufacturers have implemented innovative power conversion architectures in order to distinguish themselves from established turbine/converter companies. Hence, the B-T-B topology has been recommended in this work. However, this subsection will focus only on the modeling of the voltage source rectifier (VSR) as depicted in Figure 2.19.

2.5.3.1 Three-Phase PWM Rectifier Model

The AC/DC converter has a very important role in the WECS, not only in the rectification of the AC voltage coming from the PMSG but also it has a great role for the control process. Figure 2.19 depicts the power circuit of the proposed three-phase PWM rectifier.

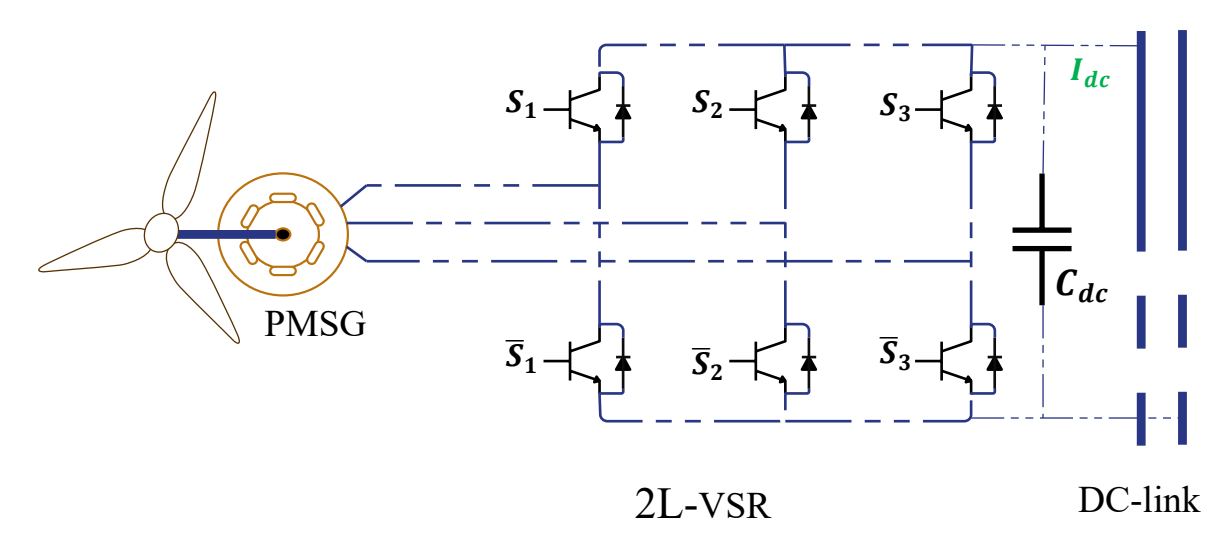


Figure 2.19: A two-level variable source rectifier connected to PMSG-based WECS.

The rectifier connection matrix can be represented as the following

$$\begin{bmatrix} V_{\omega_1} \\ V_{\omega_2} \\ V_{\omega_3} \end{bmatrix} = \frac{V_{dc}}{2} \cdot \begin{bmatrix} -2 & 1 & 1 \\ 1 & -2 & 1 \\ 1 & 1 & -2 \end{bmatrix} \cdot \begin{bmatrix} S_1 \\ S_2 \\ S_3 \end{bmatrix}$$
(2.33)

$$I_{dc} = S_1 i_{\omega 1} + S_2 i_{\omega 2} + S_3 i_{\omega 3}$$
 (2.34)

Where:

 $V_{\omega 1}, V_{\omega 2}, V_{\omega 3}$: denoted to the voltages generated by the WECS.

 $i_{\omega 1}, i_{\omega 2}, i_{\omega 3}$: represent the current generated by the WECS.

 $\begin{bmatrix} S_1 & S_2 & S_3 \end{bmatrix}$: represent logic functions that relate to the state of the switch.

 I_{dc} : Current modulated by the rectifier.

2.6 Conclusion

The hybrid system including its renewable energy sources as well as the power converter of each source have been apparently presented and discussed in this chapter. A single diode model-based PV cell has been mathematically modeled and its propriety adequately discussed. Furthermore, the second DC source that has been presented is a fuel cell device,

specifically a proton exchange membrane FC type. Hence, the chemical characteristics in tandem with electrical characteristics are both clearly presented and illustrated. The wind energy conversion system including the wind turbine, the Driven-train based two mass model as well as the PMSG has been also adequately presented and deeply discussed. Afterward, the power converter that has been preferred for the DC renewable energy sources (PV & FC) is the boost converter which was previously modeled, in contrast, the three-phase PWM rectifier was chosen for the WECS and has been modeled in detail.

Chapter 3 : Survey on Control and Energy Management of Hybrid Power Systems Grid-Tied

3.1 Introduction

Solar and wind energy are significant renewable energy sources as they have the capacity to partially address the energy dilemma. Nevertheless, these sources, when examined individually, are not entirely dependable due to their unexpected characteristics. Hybrid energy systems are considered more reliable and cost-effective due to the complementing nature of these sources. By synergistically incorporating these resources in an optimal configuration, the adverse effects of their fluctuating nature can be mitigated to some extent, resulting in a more dependable and cost-effective overall system[84], [85]. Nevertheless, solar photovoltaic and wind systems are unable to offer a consistent power supply because to their reliance on bright and windy circumstances. Additionally, these systems are very susceptible to the rapid fluctuations in weather conditions. For this reason, Maximum power point tracking (MPPT) control is essential in wind and solar systems either in stand-alone topology or grid-connected mode. Furthermore, in the case of grid-connected hybrid systems, the design and operation of the inverter necessitates substantial attention to attain high efficiency across various power structures. The grid-connected inverter must meet specific requirements, such as low total harmonic distortion of the injected currents, high efficiency, and controlled power injection into the grid[86]. In contrast, for the reliable operation of a grid-connected hybrid power system, the implementation of appropriate energy management strategies is of utmost importance. These energy management schemes determine the output powers and/or voltages of each source, which are then fed as the control tracking references to the interfacing converters' control systems[87].

In this chapter, the focus has been on giving an overview of the grid-tied hybrid configurations comprising wind, photovoltaic (PV), and fuel cell (FC) systems. The typical control requirements for this configuration include maximum power point tracking (MPPT), grid synchronization (i.e. phase-locked loop (PLL)), DC-Bus voltage control, and power management strategies.

3.2 MPPT strategies for PV systems

In photovoltaic (PV) systems, the highest amount of power production is achieved at a specific position known as the maximum power point (MPP). The location of this point is constantly shifting in response to variations in irradiance amount and temperature. In order to maximize the power output of the photovoltaic panel, it is necessary to operate at the MPP. Consequently, it is necessary to constantly monitor MPP using maximum power point tracking (MPPT) controller. This section provides a systematic and succinct overview of MPPT approaches used in PV systems, as documented in literature, including current papers and different design strategies. In fact, multiple MPPT approaches and designs are documented in the literature. Nevertheless, each approach has distinct specifications, limits, as well as its applications. According to [88], their classification can be established as follow: Conventional MPPT algorithms, Intelligent algorithms, Optimal techniques and Hybrid MPPT. In Ref.[89] the author preferred to classified the MPPT algorithms according to irradiance, which may be uniform or partial shading state. Due to the lack of assessment researches that categorize techniques and takes into consideration their suitability for different applications, the authors in [90], have been categorified MPPT approaches into five main groups. MPPT with constant parameters, with measurement and comparison, with trial-and-error method, with mathematical calculation, and eventually methods with intelligent prediction. Indeed, in this work, the classification mentioned in [88] will be approved due to its comprehensiveness as depicted in Figure 3.1.

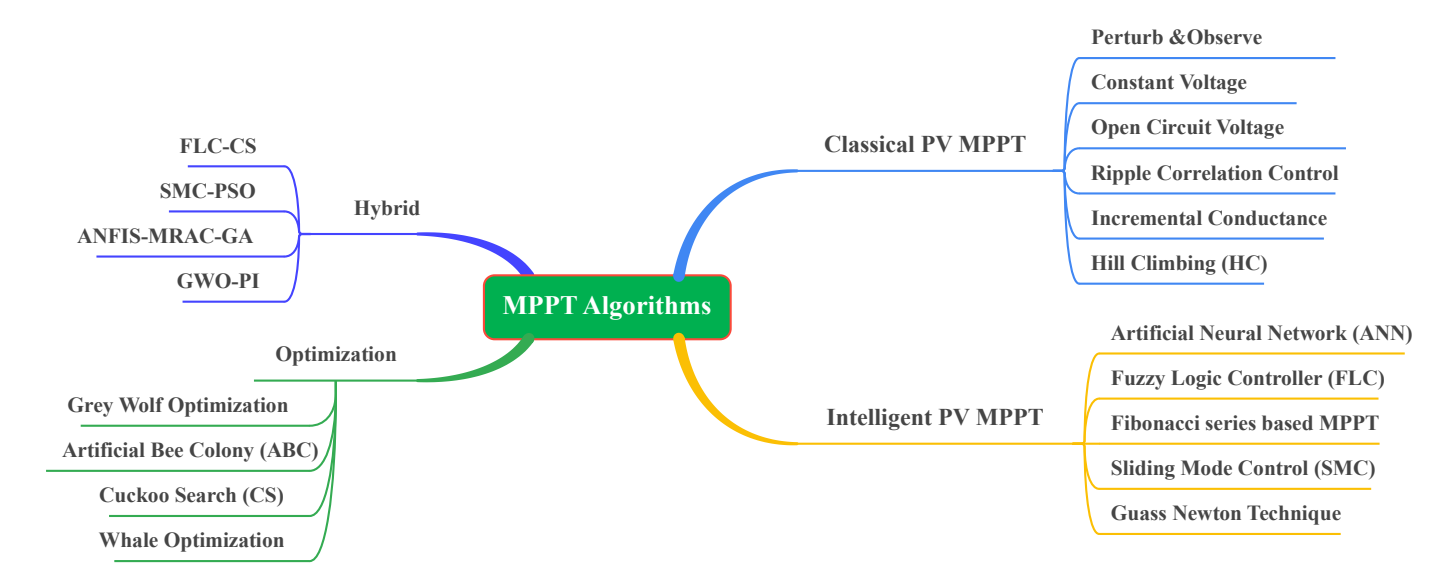


Figure 3.1 : PV MPPT Classification.

3.2.1 Classical MPPT

3.2.1.1 Perturb and Observe Method

The P & O approach is commonly employed in practice and favored by most writers. This approach relies on the iterative process of trial and error to locate and monitor the maximum power point (MPP). During every loop, the tracking controller obtains the PV voltage and current measurements and calculates the real PV power. It then adjusts the operating point by systematically changing the actual voltage and observing the resulting changes in power. If the power level rises, the subsequent disturbance in the voltage must also occur in the same direction. Nevertheless, in the event of a drop in power, the operating voltage is disturbed in the reverse direction. This scenario is iterated till the point of achieving the Maximum Power Point (MPP). The maximum point is attained when the derivative of P_{pv} with respect to V_{pv} is equal to zero. Figure 3.2 displays the fundamental flowchart of the P & O technique[90], [91].

3.2.1.2 Open-Circuit Voltage (OCV)

The OCV MPPT algorithm is a method utilized in solar energy systems to enhance the efficiency of electrical power production. The OCV approach entails intermittently halting the functioning of the PV module to gauge its open-circuit voltage, which is subsequently utilized to approximate the maximum power point (MPP). This calculation is derived from the empirical observation that the MPP voltage is often a constant proportion of the open-circuit voltage. The algorithm optimizes the operating point of the PV module to the predicted MPP, hence assuring efficient power conversion. Although the OCV MPPT method is simple and easy to implement, it may have drawbacks in dynamic situations since it periodically interrupts power generation to monitor voltage[92]. The relationship of the above-mentioned approach is given by

$$V_{MPP} = K_{OC} * V_{OC} (K_{OC} < 1) (3.1)$$

3.2.1.3 Constant Voltage Method (CV)

This approach involves the operation of the PV system at a constant voltage, usually set at the MPP voltage measured under standard test circumstances. The selection of this constant voltage is based on empirical evidence, which serves as a trade-off to achieve nearly ideal power output in different situations[93]. The CV approach is preferred because to its

simplicity and cheap cost of implementation, since it does not need intricate calculations or frequent measurements like the open-circuit voltage (OCV) method. Nevertheless, its efficiency may be less than optimum when faced with swiftly changing environmental circumstances, since it lacks the ability to adapt in real-time to the MPP. Nonetheless, the CV approach continues to be used in applications that stress simplicity and cost-effectiveness.

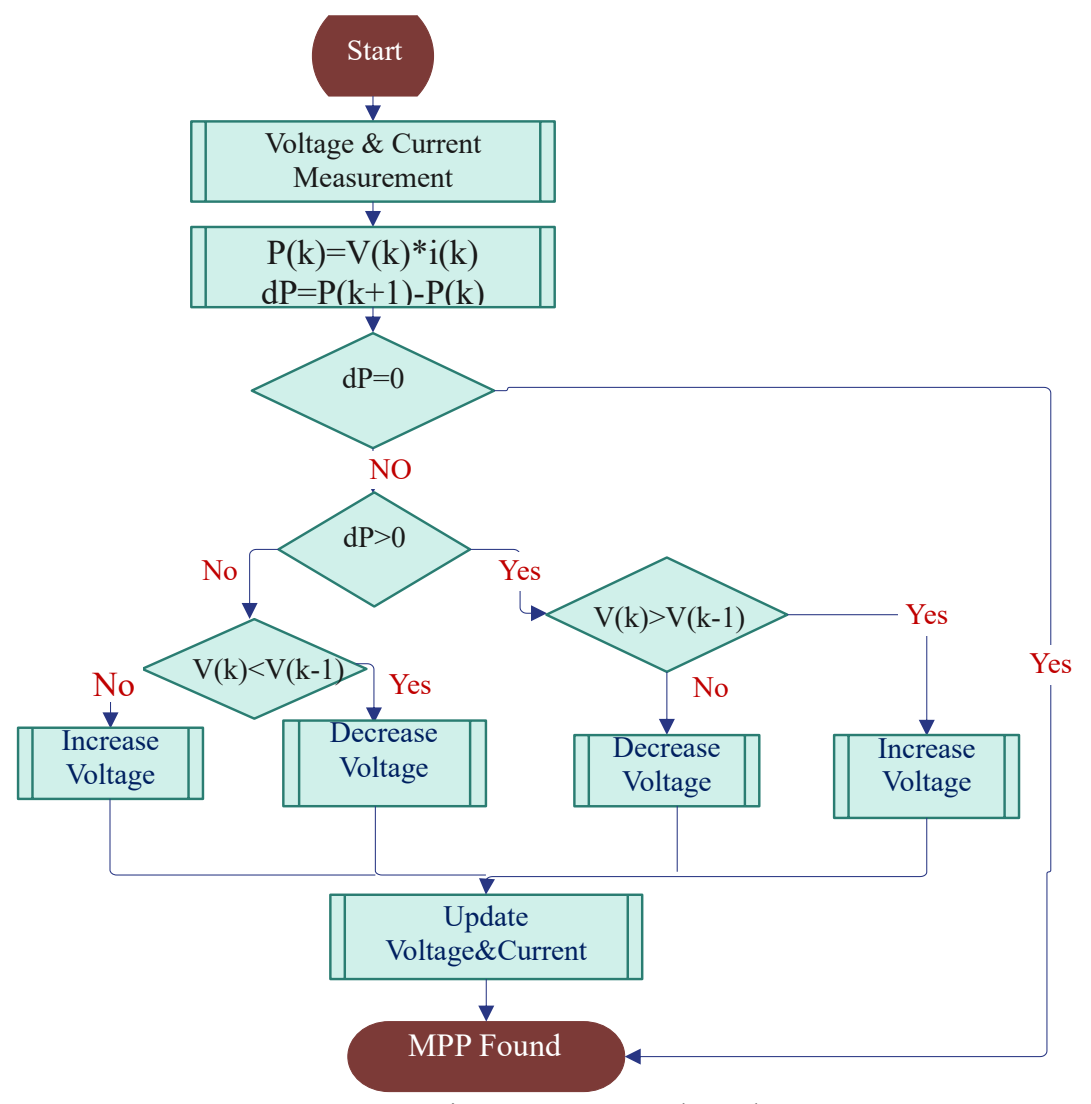


Figure 3.2 : P&O Flow-chart.

3.2.1.4 Incremental Conductance Method (INC)

This technique is an advanced MPPT method employed generally in PV systems to optimize the power output. Unlike simpler methods, INC continuously adjusts the operating point of the PV system by comparing the incremental conductance $(\frac{dI}{dV})$ to the instantaneous conductance $(\frac{I}{V})$. The fundamental idea is that at the MPP, the derivative of power with respect to voltage $(\frac{dP}{dV})$ is zero, leading to the condition that $(\frac{dI}{dV} = -\frac{I}{V})$. By tracking these changes,

the INC algorithm can accurately identify and maintain the MPP even under rapidly changing environmental conditions. The process of this algorithm is illustrated in Figure 3.3. This dynamic adjustment makes INC more efficient and responsive compared to methods like constant voltage or open-circuit voltage (OCV) techniques. However, the complexity and computational requirements of the INC algorithm are higher, necessitating more sophisticated hardware and software to implement effectively [43], [94], [95].

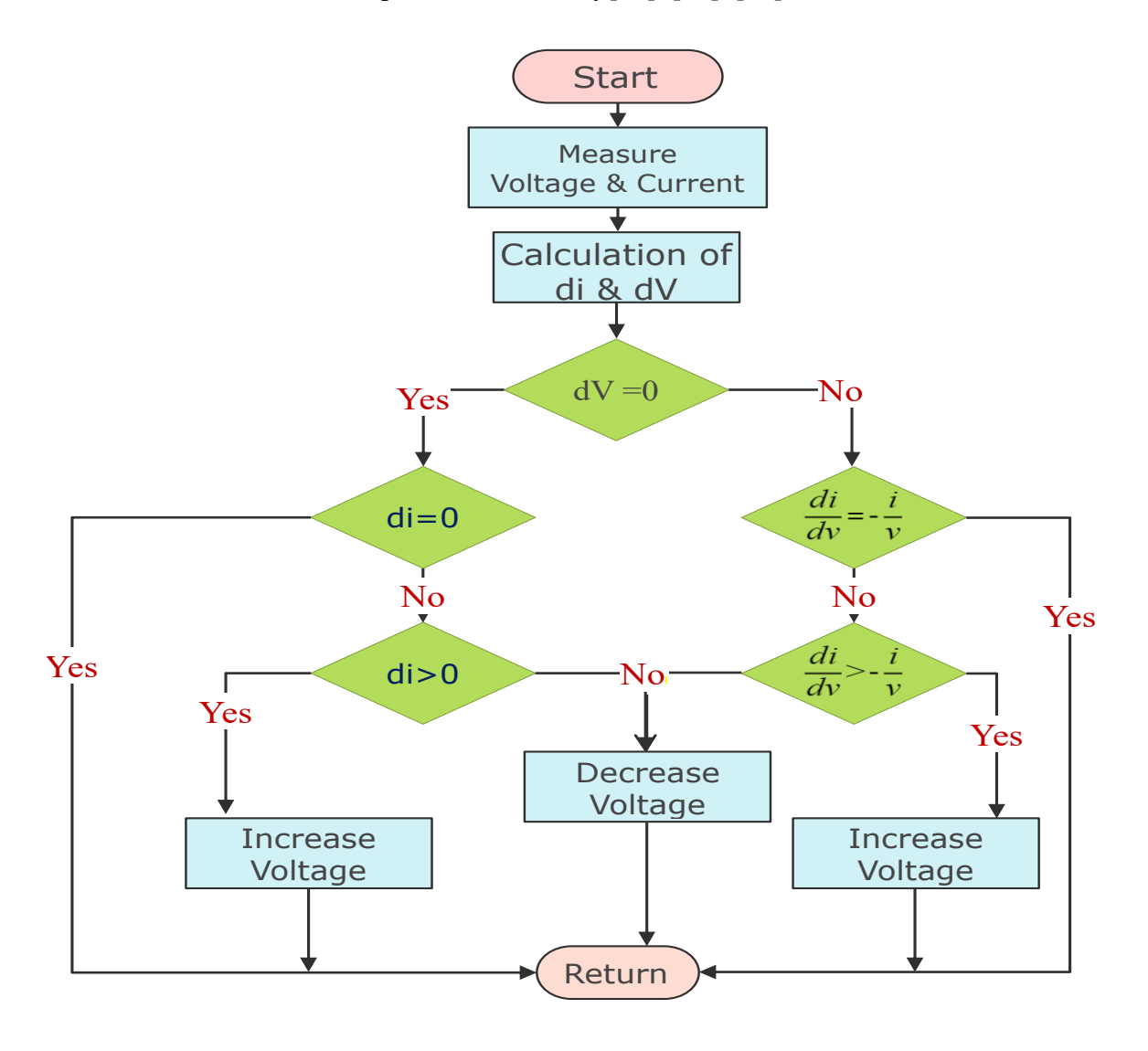


Figure 3.3 : INC Flow-Chart.

3.2.2 Intelligence Technique Based MPPT

3.2.2.1 Fuzzy Logic based MPPT

Fuzzy Logic Control (FLC)- based MPPT is one of the intelligent techniques used in a photovoltaic system to enhance the extraction of electrical power from the solar panel [96]. FLC is fundamentally different from most of the conventional MPPT techniques that work on more

accurate mathematical models and fixed algorithms, while FLC applies the concepts of fuzzy logic to capture the uncertainties and fluctuations of PV systems, for instance, changes in the intensity and temperature of sunlight[97]. This methodology enables higher elasticity and adaptability to be accomplished since this kind of control can counteract dynamic and unpredictable surroundings, thereby enhancing the general interpersonal performance and energy conversion competence. This is because the FLC-based MPPT algorithm incorporates qualitative reasoning decision-making in the same way as a human being; hence, it is well appropriate for the kind of uncertain conditions likely to be experienced in real life PV systems. The FLC-based MPPT algorithm includes three key steps: namely, fuzzification, rule base, and defuzzification processes[98].

- Fuzzification: This step scales the input variables, change in power (ΔP) and change in voltage (ΔV), and transforms them into fuzzy sets with linguistic terms including Positive Large, Positive Small, Zero, Negative Small, and Negative Large.
- ➤ Rule Base: It employs a group of fuzzy rules which could be derived either from experts' opinion or statistical evidence to define control actions. These rules bind the fuzzy inputs to appropriate outputs, which might be the change in the duty cycle of the DC-DC converter.
- ➤ **Defuzzification:** This process converts the fuzzy outputs back into a specific control signal in order change the PV system's operating point.

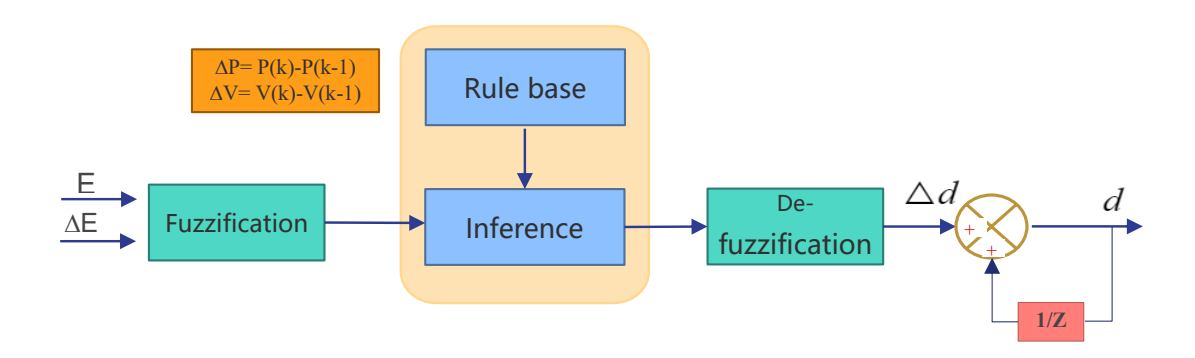


Figure 3.4: FLC based- MPPT Scheme.

3.2.2.2 Artificial Neural Network (ANN)-based MPPT

ANN-based MPPT is an elite method developed and employed in the PV system to extract the maximum power using Artificial Neural Network. ANNs are modeled after the brain, which is made up of neurons and their interconnections for the transfer of info and data. These networks have the ability to train on data, find out features of the input data and arrive at decision based on available variables. Used in MPPT, ANNs are used to estimate the time of MPP of the PV system based on inputs like irradiation, temperature and voltage. Thus, the ANN-based MPPT approach takes advantage of such a network's capacity to respond to nonlinear correlation between the input and output data and adapt to different conditions thus making it a reliable approach to improving the yield of energy from solar panels[99], [100].

In the case of ANN-based MPPT, it entails the utilization of a neural network having prior data of diverse environmental conditions and the corresponding MPPs to train the model. This training process helps in enabling the ANN discover the relationship between various inputs and the point of optimum operation. Therefore, after training the ANN, it is possible to obtain real-time data concerning MPP and the PV system may efficiently regulate its function. This became useful especially in the natural conditions where there are variations in days or temperatures whereby cloudy days for instance affect the efficiency of the normal MPPT techniques. The ANN-based MPPT method does also rise the efficiency of power conversion alongside to the improvement of the reliability and dynamism of PV systems[101].

The general processes of the ANN-based MPPT process are as follows:

- ➤ Training: The ANN is fed with previous records of the environmental parameters and MPPs, known to be related to such conditions. This training enables the network to identify function, which defines the relationship between the input variables and the best operating point in the system.
- ➤ Input Layer: The trained ANN receives the real time input data of the PV system such as irradiance and temperature which is entered at the input layer of the ANN.
- ➤ **Hidden Layers**: The input data goes through one or many layers through the network where higher order calculations are performed in a concealed manner. These hidden layers help ANN in defining the relations and patterns of the data sets that are prevailing.

- ➤ Output Layer: The processed data is then sent to the output layer of the ANN that produces an approximate of the operating point or duty cycle for the PV system.
- ➤ **Adjustment:** Therefore, the overall operation of the PV system relies within the ANN to optimize the system's use at or around the MPP to effectively conduct power conversion.

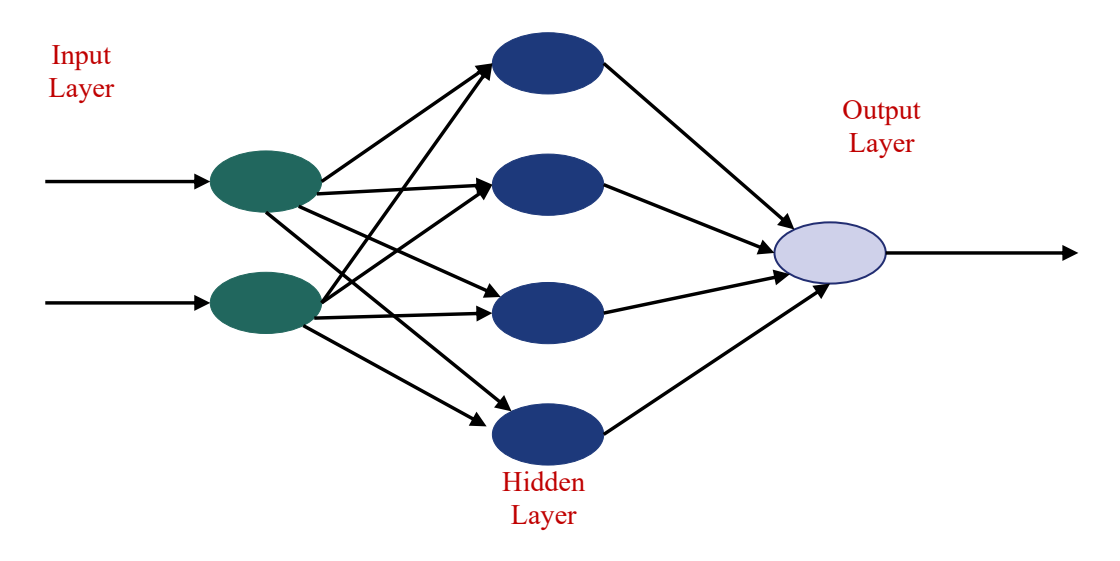


Figure 3.5 : ANN Scheme.

3.2.3 Optimization Algorithms based-MPPT

3.2.3.1 Particle Swarm Optimization

The particle swarm optimization technique may be defined as a process in which particles simulate the behavior of fish schooling or bird flocking to hunt for food in a given region. This algorithm utilizes the velocity vector, the individual experience of each particle, and the collective experience of neighboring particles to produce a random position vector within the space[102]. The fundamental steps of this method are outlined as follows.

a) Initialization:

- Place particles of a swarm randomly and assign random velocity for each particle in the search space.
- Initialize (x_i) and (v_i) with some values of their initial conditions.
- **b)** Evaluation: Assess the quality of each particle's position by calculating fitness using the objective function.

c) Update Personal Best:

- To do this, take the current fitness value of the particle in question and then compare it to the current best solution value for that particle known as P_{Best} .
- If the current position is better, update the personal best position of that particle P_{Best_i} .

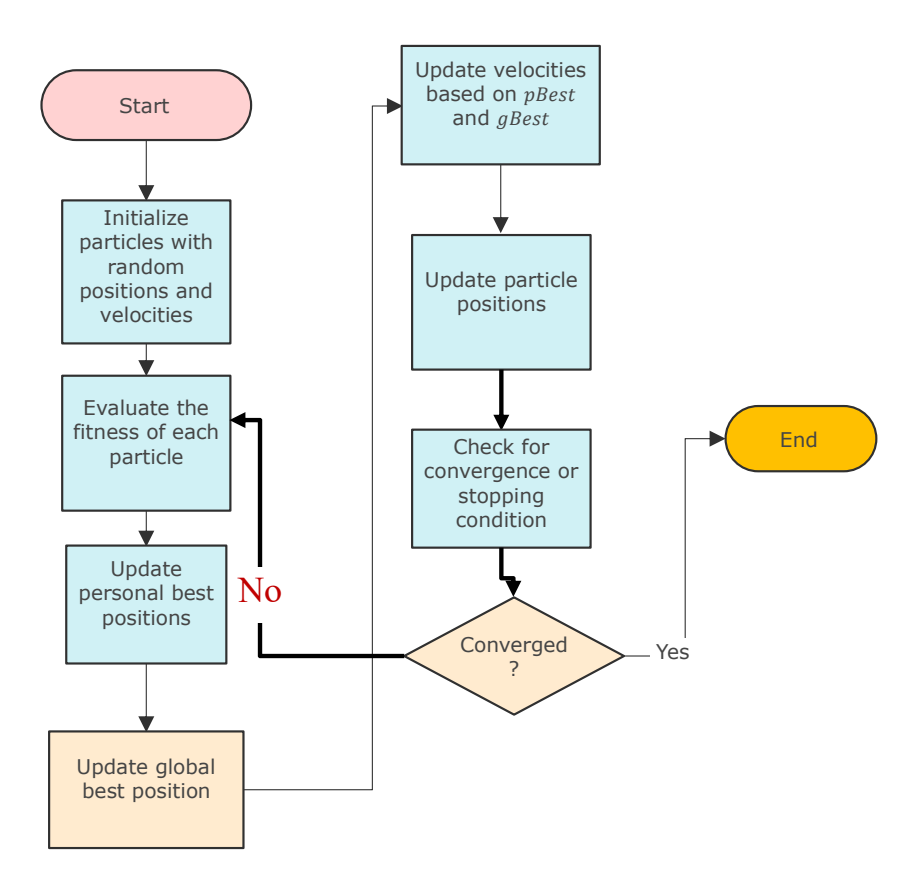


Figure 3.6: PSO Flow-Chart.

- d) Update Global Best: Find the particle of the best fitness in the whole of the swarm. This position is referred to as the global best, abbreviated as g_{Best} .
- e) Velocity Update: Update the velocity of each particle using the formula

$$v_i(t+1) = \omega v_i(t) + c_1 r_1 (pBest_i - x_i(t)) + c_2 r_2 (gBest - x_i(t))$$
 (3.2)

where

- Typically, the inertia weight ω is kept positive to allow the particle to explore the search space.
- Instead, the coefficients c_1 and c_2 are cognitive and social coefficients.

- r_1 and r_2 are two random numbers between 0 and 1.
- f) Position Update: Update the position of each particle using the new velocity:

$$x_i(t+1) = x_i(t) + v_i(t+1)$$
(3.3)

- **g) Termination**: Perform steps 2 to 6 iteratively until the termination condition occurs, it may be either a maximum number of iterations or if and only if the fitness level comes closer to the optimal level.
- **h) Output**: The position that puts each controlling swarm in the best position as identified by the coding is taken as the optimal solution to the problem.

The flow chart that summarizes the aforementioned process is illustrated in Figure 3.6.

3.2.3.2 Arithmetic Optimization (AO) Algorithm

Arithmetic Optimization (AO) is a metaheuristic optimization algorithm as explained in[103], which is based on distributive properties of arithmetic operators in mathematics. It utilizes a hierarchical structure of four main operators: addend, factor, sum, and difference, subtraction, division, and multiplication. These operators are used to manipulate a population of candidate solutions which are hypothetical duty cycle values in this quest. Thus, the transformation of these solutions throughout the search process is represented with the help of operators' dominance at different iterations of the algorithm. First, the decision is made in the direction of exploration over the division and multiplication, which allows determining the search of the space of solutions widely enough. At this stage, exploitation is carried out through addition and subtraction with the aim of moving the solutions towards locating the global optimal solution which in this case is the duty cycle corresponding to the MPP of the PV array.

3.2.3.3 Coot Optimization Algorithm

Coot Optimization Algorithm (COA) is a fairly new metaheuristic algorithm based on the movement patterns of coots, a type of waterfowl. Developed by Naruei in 2021 [104], this algorithm imitates the manner in which the coots are portrayed in groups while in the process of foraging for their food. Thus, COA uses the exploration and exploitation phases combined together, like coots that switch between searching for new territories and using the best feeding areas. Cooperatively foraging birds like coots exhibit a sit-and-probe pattern in which during exploration, the bird moves in a random fashion but during exploitation, it move towards the

best discovered food location. This balance, alongside its population-based characteristic, enables COA to search through difficult search spaces and possibly discover the best solutions to various global optimization issues.

3.2.4 Hybrid MPPT

Hybrid MPPT approaches excel in their performance by enhancing tracking accuracy and reducing the computational load on hardware. Tracking the Global MPP out of several Local MPPs accurately is not effectively accomplished by either intelligence or optimization strategies alone. For this reason, combining two or more MPPT strategies may be considered a good option in several cases.

3.2.4.1 Hybrid MPPT Based on INC-Integral Backstepping Controller

A novel method to enhance power extraction from PV systems has been presented by [105]. This work's main contribution is the creation of a hybrid MPPT system that combines the advantages of two different approaches: the Incremental Conductance (INC) algorithm and the Integral Backstepping Controller (IBSC). The suggested hybrid approach is based on the INC algorithm, which is renowned for its simplicity and efficacy in monitoring the MPP under generally steady circumstances. However, acknowledging the inherent constraints of INC in managing fast swings, the authors combine it with an IBSC. To accommodate the fluctuating environmental conditions, which are dynamic in nature, the concept of the IBSC, a nonlinear control strategy, is introduced to improve the overall system's stability. This work elaborates on the process of designing the IBSC for tuning the parameters of the given functions through mathematical modeling that ensures that the resulting system is stable in accordance with Lyapunov stability analysis and is guaranteed to converge to the MPP. One of the major strengths of this two-mode system is that it also does not require expensive solar irradiance sensors that are normally needed by most of the nonlinear MPPT controllers.

3.2.4.2 Hybrid FLC- Ant Colony Optimization (ACO)

An innovative approach to improving Maximum Power Point Tracking in solar PV systems, particularly under the challenging conditions of partial shading has been presented in [106]. The authors suggest a hybrid approach called Ant-Fuzzy Optimization (AFO), which combines the advantages of Ant Colony Optimization (ACO) and Fuzzy Logic (FL). The suggested AFO's strength resides in its two-stage strategy. ACO, initially used for its extensive search capacity, is implemented to efficiently limit the search area to a region that encompasses

the global maximum power point (GMPP). FL, with its intrinsic capacity for precise adjustment and operation near the desired value with minimum fluctuations, subsequently narrows down the search within this narrower area to properly locate the GMPP. This combination aims to achieve a compromise between the need for worldwide exploration and local exploitation, which is essential for effective MPPT in the presence of partial shade.

3.2.4.3 Hybrid PSO-ANN- Flying Squirrel Search Optimization (FSSO)

A novel hybrid MPPT was suggested in [107]. The authors proposed a hybrid algorithm combining Particle Swarm Optimization (PSO) trained machine learning and Flying Squirrel Search Optimization (FSSO), termed PSO-ML-FSSO. This hybrid approach aims to leverage the strengths of both machine learning, which excels at pattern recognition from data, and bioinspired optimization algorithms like FSSO, known for their global search capabilities. According to the obtained results, the proposed PSO-ML-FSSO algorithm outperforms several existing MPPT methods, including conventional techniques such as P&O, and INC, as well as other optimization algorithms.

3.2.4.4 Variable step-size P&O Model Reference Adaptive Control

Maximizing the efficiency of photovoltaic (PV) systems, especially in the face of fluctuating environmental conditions like cloud cover and partial shading considered a hard challenge faced by PV systems applications. For this reason, the authors in [108], propose a novel approach called adjustable variable step-based MRAC MPPT. The limitations of traditional P&O often struggle to balance tracking speed and accuracy. Noteworthily selecting an optimal size is considered extremely difficult. Hence a large one it may cause oscillations around the MPP. Conversely, a smaller step size enhances accuracy but slows down the tracking process. To overcome this, the authors introduce a two-level hybrid approach. The first level employs an adjustable VS-PO algorithm. This algorithm dynamically adjusts the step size based on the system's operating point on the power-voltage (P-V) curve. During transient conditions, the step size increases for faster tracking, while it decreases near the MPP to minimize oscillations and improve accuracy. The second level incorporates an MRAC controller to further enhance robustness and tracking precision. MRAC continuously compares the PV system's performance to a reference model and adjusts the controller parameters accordingly. This ensures optimal system response even under varying atmospheric conditions.

3.3 Control Strategies for WECS

3.3.1 MPPT Controller

The erratic velocity of wind and the fluctuating environment significantly impact the reliability of wind energy[109]. The power output from a wind turbine can be effectively managed within a designated range of wind speeds, defined by the cut-in speed (Vw_{in}) and cut-out speed (Vw_{out}) . Outside this range, the turbine should not operate to ensure the safety of both the turbine and the generator. Rated power (P_{rated}) is achieved at a specific wind speed (V_{rated}) . Accordingly, four main operating regions are identified, as shown in Figure 3.7.

The first and fourth regions are below Vw_{in} and above Vw_{out} , respectively, where the turbine should be halted and disconnected from the grid to prevent it from being driven by the generator. The second region, which lies between Vw_{in} and V_{rated} , involves the activation of the wind turbine controller to maximize energy extraction using the maximum power point tracking (MPPT) algorithm[100]. In the third region, between V_{rated} and Vw_{out} , it is crucial to limit mechanical power generation to the rated power to protect the turbine from damage. Therefore, the MPPT algorithm primarily focuses on the second region.

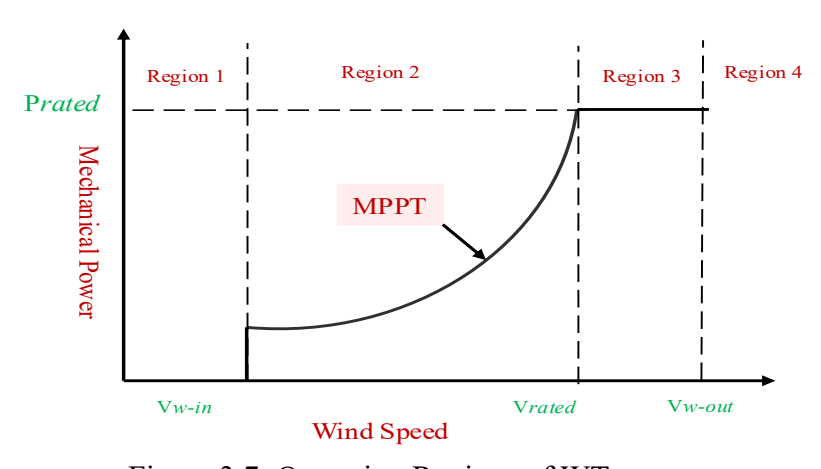


Figure 3.7: Operation Regions of WT.

Generally, MPPT algorithms in WT may be categorized into two methods: direct power control (DPC) and indirect power control (IPC). Indeed, IPC method increases output power by adjusting mechanical power based on predefined power-speed curves. In contrast, DPC algorithms monitor changes in output electrical power to identify the MPP.

3.3.1.1 IPC MPPT Techniques

- a) Tip speed ratio (TSR): In this method, output power is maximized by adjusting the generator's speed to maintain an optimal TSR value. Additionally, the error between the actual rotational speed and the optimal speed for a given condition is used to track maximum mechanical power[110].
- b) Optimal torque (OT) method: This method establishes a particular relationship between electromagnetic torque and rotational speed based on the "rotor speed-maximum aerodynamic power" curve, guiding the rotational speed toward its optimal value[111]. When the wind turbine operates at the optimal tip speed ratio (λ_{opt}), the wind energy utilization coefficient reaches its maximum value (Cp_{max}). Consequently, the optimal power can be determined as follows:

$$P_{opt} = 0.5 \frac{\rho \pi R^5 C_{P \text{ max}}}{\lambda_{opt}^3} \Omega_t^3 = K_{opt} \cdot \Omega_t^3$$
(3.4)

An additional calculation of equation (3.4) can be obtained as follows:

$$T_{opt} = K_{opt} \cdot \Omega_t^2 \tag{3.5}$$

c) Power signal feedback (PSF): This algorithm executes mechanical tracking based on the power-speed curve, utilizing the characteristic data of the wind turbine to gain insights into its maximum power curve for effective tracking. Noteworthily that either the OT or PSF algorithms exhibit the same limitations when it comes to tracking the MPP at low-speed winds for large-inertia wind turbines. Nevertheless, these algorithms are known for their robustness and cost-effectiveness[112].

3.3.1.2 DPC MPPT Techniques

a) Perturb&Observe: P&O technique is renowned for its straightforward deployment and cost-effectiveness. This algorithm quantifies the present output from the previous cycle, calculates the accurate phase for the subsequent cycle, and modifies the different duty cycle or voltage parameters. Nevertheless, when there are fast wind variations, the system becomes slow and the algorithm fails to accurately determine the correct direction to reach the MPP. Various modified P&O have been presented in literature to overcome this demerit.

b) Incremental Conductance: This algorithm operates independently of sensor requirements and the specifications of the turbine and generator, enhancing system reliability and reducing costs. The turbine output power can be expressed as a function of the DC link voltage. Furthermore, there is an optimal DC link voltage that maximizes the generator's output power, which can be analyzed in real-time using the Incremental Conductance (INC) algorithm[113].

c) Smart MPPT:

An artificial neural network (ANN) can effectively track maximum power in both stationary and dynamic conditions, along with providing a wind speed tracking system that operates more quickly than an anemometer. This strategy has shown a reduction in generator speed fluctuations, enhancing the safety of the wind turbine (WT) system while also increasing its capacity to generate more electricity from changing wind speeds.[109].

Fuzzy logic control also has been introduced in literature. The primary advantage of this controller is its ability to rapidly adjust controller parameters in response to changes in system dynamics without the need for parameter estimation. When climatic conditions shift, a fuzzy-based MPPT algorithm demonstrates strong performance, offering fast convergence, insensitivity to parameter variations, and the capacity to handle noisy and imprecise signals[111].

d) Hybrid MPPT:

In order to efficiently optimize the power extracted from WT and minimize mechanical stress on the turbine components, a novel control strategy has been innovated in [114]. The authors specifically investigate the use of fuzzy backstepping sliding mode control, optimized by a multi-objective particle swarm optimization (MOPSO) algorithm, for variable speed wind turbines operating below their rated wind speed. A combination between Integral sliding mode control and artificial neural network strategy for a Doubly-Fed Induction Generator (DFIG) based Wind Energy Conversion System (WECS) has been presented by [115]. The authors aim to address the challenge of maximizing energy production and ensuring grid integration in the face of system nonlinearities and parameter variations. The authors in [116], have been introduced a hybrid approach combining the conventional Perturb and Observe (P&O) method with an Artificial Neural Network (ANN). Due to the limitations of conventional methods such as oscillations around the MPP and slow response times. This paper tackles these limitations

by combining an artificial neural network (ANN) with the traditional P&O technique. The ANN is trained offline using the operational principles of the P&O method, allowing it to learn the relationship between changes in power output and the corresponding adjustments to generator speed. After training, the ANN is deployed online to predict optimal generator speed adjustments for dynamic tracking of the maximum power point. A combination between the TSR method and a highly efficient robust control technique called the super twisting algorithm was introduced in [117] to address the uncertainty challenge and improve the system performance in the presence of wind fluctuation conditions. Accordingly, the findings obtained exhibit exceptional performance in comparison to conventional controllers.

The aforementioned and discussed MPPT algorithms are summarized in figure 3.8.

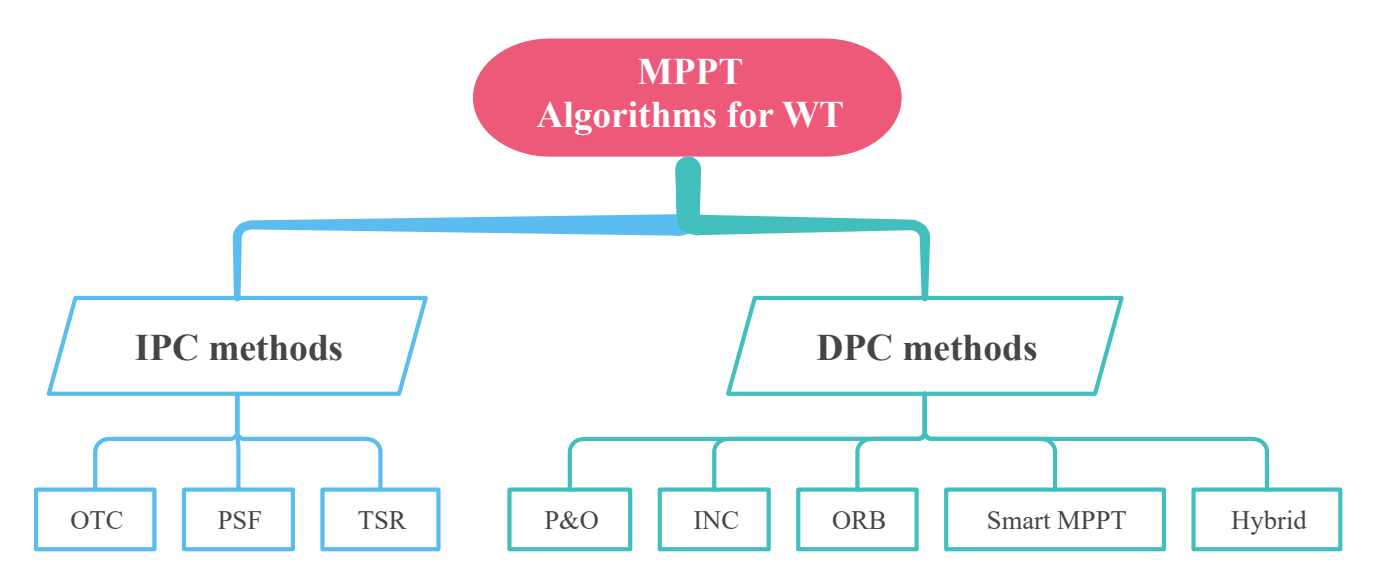


Figure 3.8: MPPT classification for WECS.

3.3.2 Machine Side Control: Case 'PMSG'

The MSC regulates variable speed functionality to optimize power capture. By adjusting the rotor speed, it ensures system stability and maximizes power output. Direct torque control (DTC) and field-oriented control (FOC) represent two principal categories of control strategies employed in machine-side converters (MSC). Notably, the dynamic performance and characteristics of FOC and DTC exhibit minimal differences. FOC utilizes a dual-loop control system to regulate generator speed, encompassing both an outer and an inner loop. The outer loop requires rotor speed and position to generate three-phase reference currents. Typically, the inner loop control operates within natural or synchronous reference frames. To maximize electromagnetic torque while minimizing stator current, the d-axis component of the stator

current is maintained at zero, while the generated electromagnetic torque is regulated through the q-axis component. This direct current control in FOC facilitates optimal torque production, enhancing the overall efficiency of the machine. Conversely, DTC offers a more direct approach to torque and power management, resulting in a more responsive system with reduced complexity. The DTC methodology eliminates the necessity for a dual-loop configuration, as it does not require transformations between reference frames, thereby simplifying the inner control loop. This streamlined approach contributes to an effective and efficient control mechanism for modern electric drives[118], [119].

Scalar control is a straightforward technique employed to manage the speed of machine drives exhibiting complex and nonlinear behavior, relying solely on the magnitude and frequency of the applied voltages. This method is based on a per-phase steady-state equivalent circuit of the AC machine, aiming to keep the magnetizing current constant by adjusting the voltage magnitude in proportion to the applied frequency[120].

In recent years, the FCS-MPC has been implemented in power converters as a straightforward and potent control strategy. In contrast to conventional control methods, this technique obviates the requirement for PI regulators as well as the modulation bloc, and presents a conceptually distinct approach to controlling power converters[121]. The FCS-MPC technique has been demonstrated to be one of the most effective approaches for addressing all of the challenges and conditions in machine drive control.

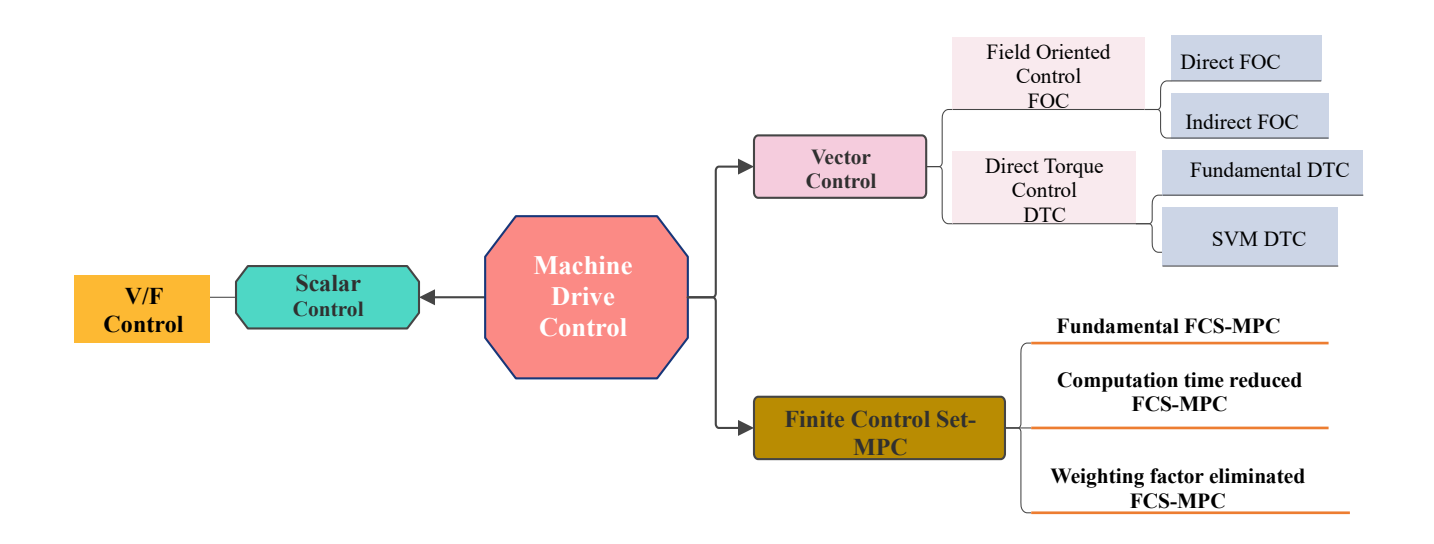


Figure 3.9 : Classification of Machine Drive Control.

3.4 FC Control

Generally, PEM fuel cells are considered a Multi-input Multi-output (MIMO) system from a control systems perspective. In fact, the PEMFC might be partitioned according to its structure into 5 subsystems: fuel cell stacks, air supply and hydrogen supply subsystems, humidification, and heat management subsystems[122]. Consequently, the PEMFC control is subordinate to this division. Figure 3.10 illustrates the above-mentioned control architecture.

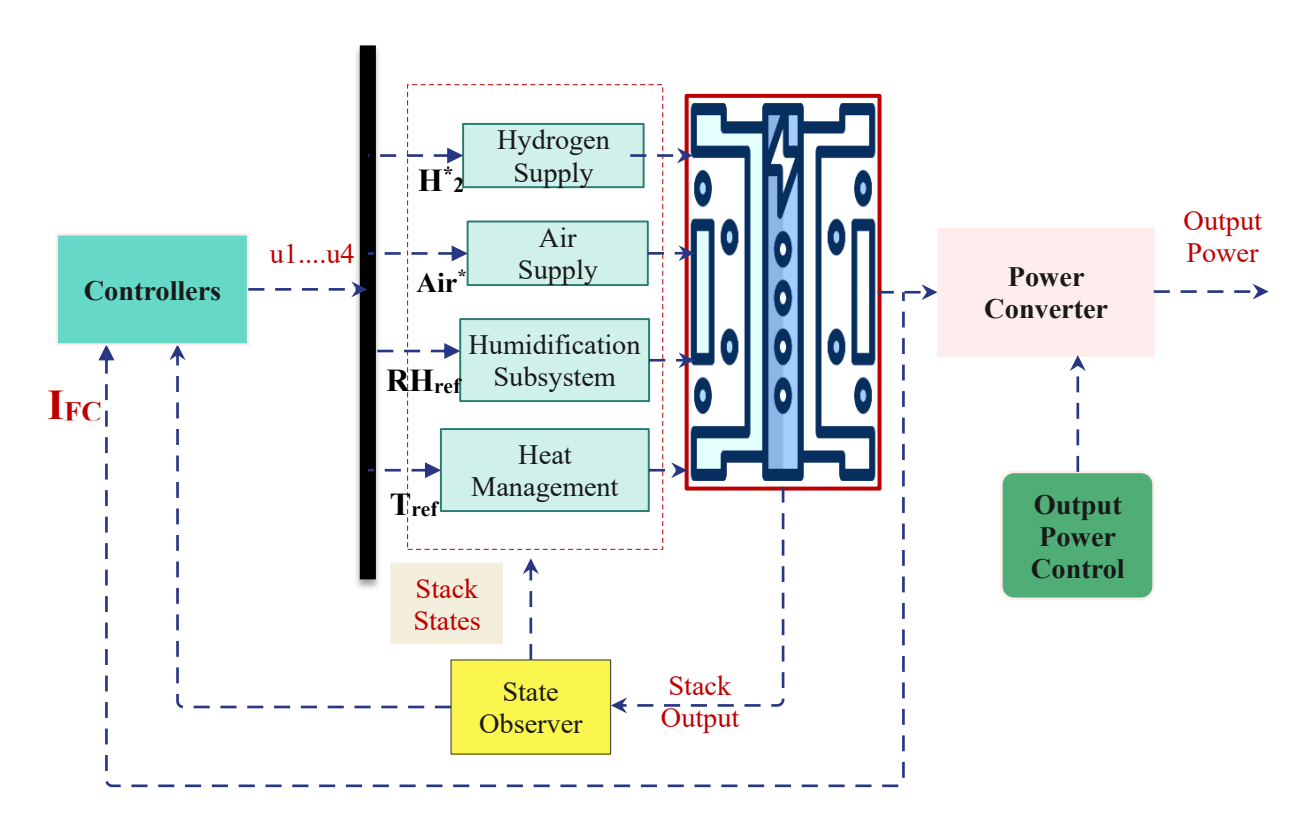


Figure 3.10: Control Architecture of a PEMFC Stack. Reprinted with some modification from Ref.[122].

The authors in [122] have pointed out that the control approaches for PEMFC stacks can be categorized into:

- Start-Up and Shut-Down Control
- Load Following Control
- Maximum Power Point Tracking
- Fuel Starvation Control
- Operation Optimization Control: Enhances operational efficiency and prolongs the lifespan of the fuel cells.

However, this study primarily focuses on the use of PEMFC in microgrid and hybrid systems. Thus, in this work, we will focus only on the control features used in power-generating applications. Significantly, the control target may vary depending on whether the FC is used as a main or supplementary source. When used as the main source, the control purpose is to provide electricity to the grid or load at a consistent voltage and frequency. However, when used as an auxiliary source, the goal is to regulate the power flow in order to meet the system's power needs [123]. In this thesis the PEMFC has been employed as a secondary source, furthermore, it maintains consistent output power according to a desired reference. In this context, several control methods have been utilized in literature which shall be discussed in the following subsection.

3.4.1An overview of Output power control of PEMFC

3.4.1.1 Proportional Integral (PI) controller

PEMFCs are renowned for their high efficiency and ability to generate clean energy. However, they have notable difficulties in maintaining a steady voltage output when faced with fluctuating load and input conditions. In order to ensure that the fuel cell operates efficiently and reliably, incorporating a control technique strategy to address these challenges is crucial. The traditional proportional-integral (PI) controller is considered to be the most basic and straightforward type of controller[124]. It was commonly employed in literature to regulate the FC based on the generated power reference. The transfer function of the controller can be expressed as

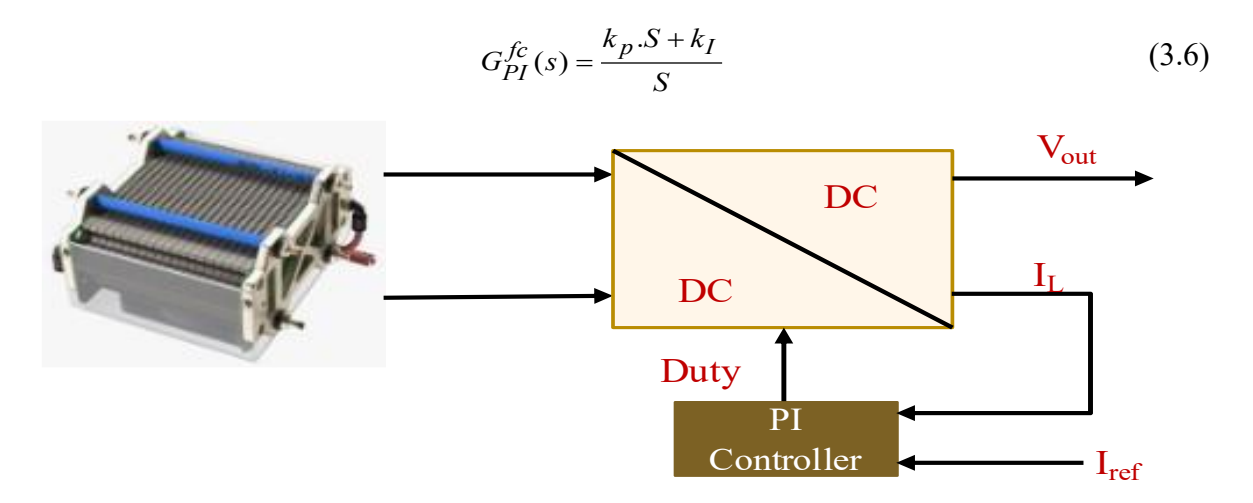


Figure 3.11 : Control of PEMFC Using PI Controller.

3.4.1.2 Lyapunov- PI controller.

Generally, conventional PI controllers, struggle to provide stability and optimal performance under varying loads or dynamic environments. For this reason, there is a significant requirement for more robust control strategies that can deal with those challenges, in addition to ensuring that the output voltage remains stable and within desired limits despite fluctuations in load and environmental factors. Accordingly, Ref.[125] presents a Lyapunov-based PI controller that dynamically adjusts the arbitrary gains (KP and Ki) of the PI controller, hence enhancing the stability of the system across various operating situations (Figure 3.12). The achieved results show better stability and adaptability compared to the classical PI controller. Furthermore, the settling time has been decreased, along with the reduction of overshoot and ripple in the output voltage. These factors are crucial for achieving efficient and dependable power conversion.

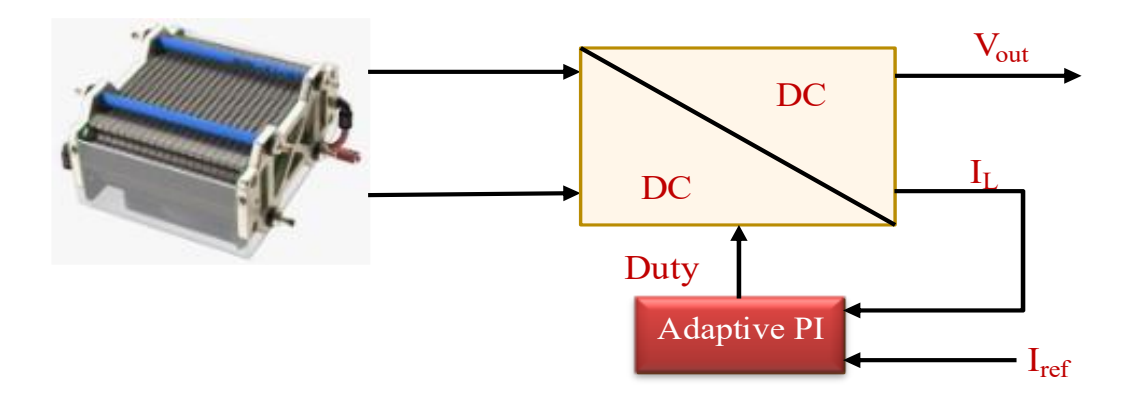


Figure 3.12: Control of PEMFC Using Adaptive PI-based Lyapunov.

3.4.1.3 GA-Based Robust LQR Controller

A new control technique has been devised in [126] to enhance voltage regulation in fuel cells, which is essential given their high current production and susceptibility to load fluctuations. The authors propose a study on the construction and improvement of a robust linear quadratic regulator (LQR) controller, which is improved with the use of genetic algorithms (GA). This controller is designed for an interleaved boost DC-DC converter that is used in the PEMFC system. The results indicate that the GA-LQR controller outperforms traditional PI controllers concerning overshoot, settling time, and ripple reduction.

3.5 DC Bus Voltage Regulation

Regulating the DC-Link voltage of the Inverter input is a crucial step in guaranteeing optimal performance of the entire system. DC side regulation loop is required to maintain a steady voltage and determine the grid current reference value(I_g^*). Furthermore, to ensure appropriate power injection, the minimum needed DC-link voltage reference must be at least double the magnitude of the phase's maximum voltage[127]. The voltage regulation loop is developed using a transfer function that connects the DC bus voltage output (v_{dc}) to the amplitude of the injected grid current (I_g). The bloc diagram of the above-mentioned loop illustrated in Figure 3.13. Notably, conventionally PI controller is the most used in this application. Accordingly, the transfer function of the studied closed loop can be expressed as follows:

$$\frac{V_{dc}}{V_{dc}^*} = \frac{1}{1 - \frac{K_p . S + K_i}{\Theta . S^2}}$$
(3.7)

Where: $\Theta = \frac{\sqrt{2}C_{dc}V_{dc}^*}{3V_{gm}}$, V_{dc} : the dc-link voltage, V_{gm} : the grid voltage maximum value.

In this way we get

$$\frac{V_{dc}}{V_{dc}^*} = \frac{\Theta.S^2}{\Theta.S^2 - K_p.S + K_i}$$
 (3.8)

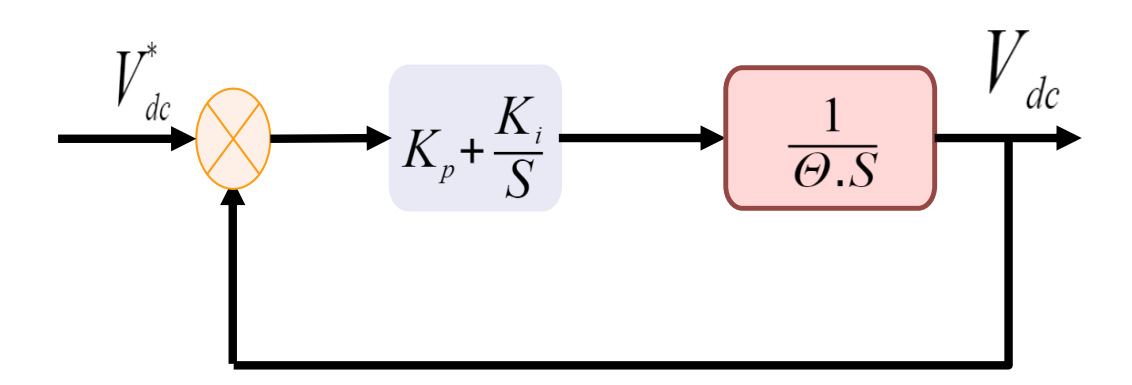


Figure 3.13: DC-Link voltage Regulation Scheme.

Nevertheless, the conventional PI controller exhibits drawbacks such as a long response time, large overshoot, and significant voltage ripples during steady-state operation. For this reason, the authors in [128] have been developed a new adaptive fuzzy controller applied to

adjust the DC link voltage. The proposed controller aims to adapt the output gain of the controller for every system condition, as a function of the voltage error and its variation. In Ref.[129], the conventional PI regulator has been replaced by a non-linear robust SMC controller, due to its exceptional dynamic performance and the control law designed according to the system model. The results demonstrate that the SMC technique achieves a faster dynamic response and eliminates steady-state error in the DC-link voltage, as compared to the conventional control scheme. In [130], the authors proposed the use of machine learning-based controllers to address the drawbacks of the traditional controller. Furthermore, the results obtained demonstrate that the proposed neural network (NN) controller demonstrated improved robustness and superior transient as well as steady-state performance compared to the traditional controller.

3.6 Grid Current Control

For hybrid power systems, an inverter is necessary as a power interface to connect DC sources like PV arrays or fuel cells to an AC grid or AC loads. Connecting an inverter to the grid might impact the power quality on the grid due to the use of pulse width modulation techniques in operating the inverters. The primary issue in achieving improved power quality, reduced cost and output filter size, simplified control, enhanced dependability, and increased availability lies in selecting the appropriate inverter architecture. However, the development of control techniques for power inverter interface in grid-tied applications remains an active and ongoing research area. Many control algorithms have been suggested and discussed in literatures. Generally, we can classify the inverter control techniques for grid-connected field into classical or conventional methods and advanced control methods. The control structures that included under conventional methods are Hysteresis control and linear control techniques, while advanced methods include robust control techniques, Intelligent control and model predictive control (MPC) technique [131]. The aforementioned classification is summarized in Figure 3.14. The following subsections will provide a brief description of each control method.

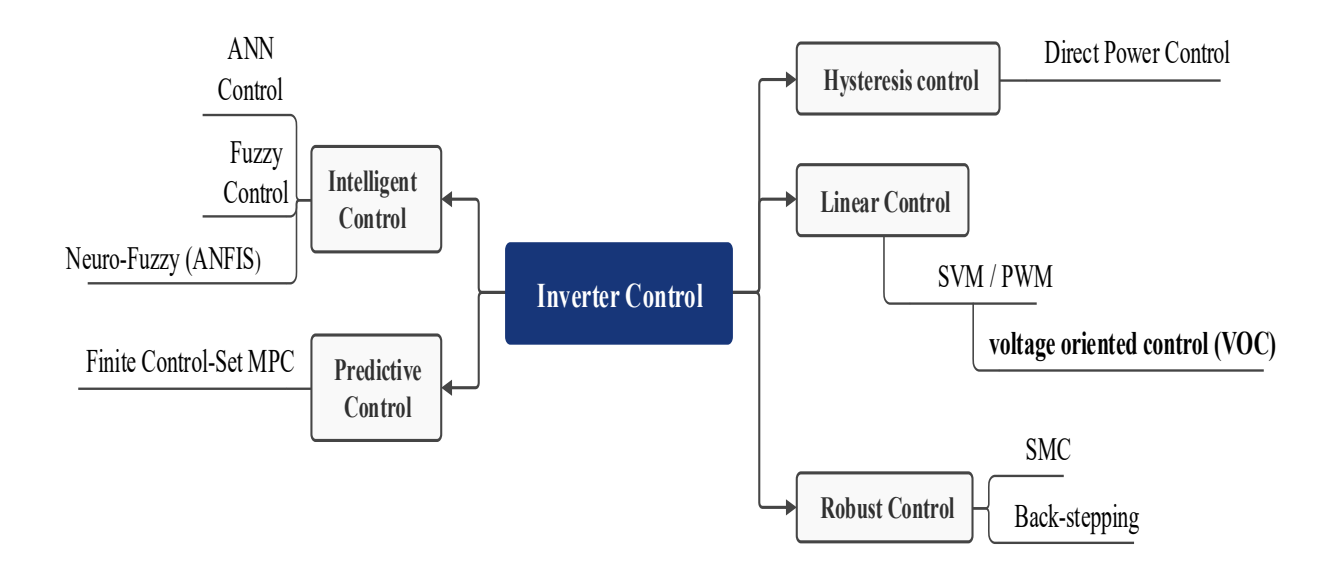


Figure 3.14: Inverter Control Strategies for grid-tied applications.

3.6.1 Hysteresis Control Technique

This controller is identified as a nonlinear approach. The actual currents are compared to the reference currents using hysteresis (bang-bang) controllers, and the gating signals are generated based on the reference tracking. The error in reference tracking can be minimized by narrowing the hysteresis band [121]. This method does not necessitate a modulator, so the switching frequency of the inverter is dependent on the hysteresis bandwidth, operating conditions, and filter parameters[132].

An enhanced variant of this approach is the Direct Power Control (DPC) method. This approach has its origins in the initial and primary Direct Torque Control (DTC) method used for AC machines. The switching states are determined using a switching table. Moreover, the instantaneous active and reactive power values are compared against their respective references. The active power reference is derived from the output of the DC bus voltage regulator V_{dc} , while the reactive power reference is set to zero to ensure a unity power factor. Furthermore, the DPC method does not necessitate any internal control loops or coordinate transformations, thereby avoiding coupling effects between the transformed variables. The bloc diagram of this approach is illustrated in Figure 3.15.

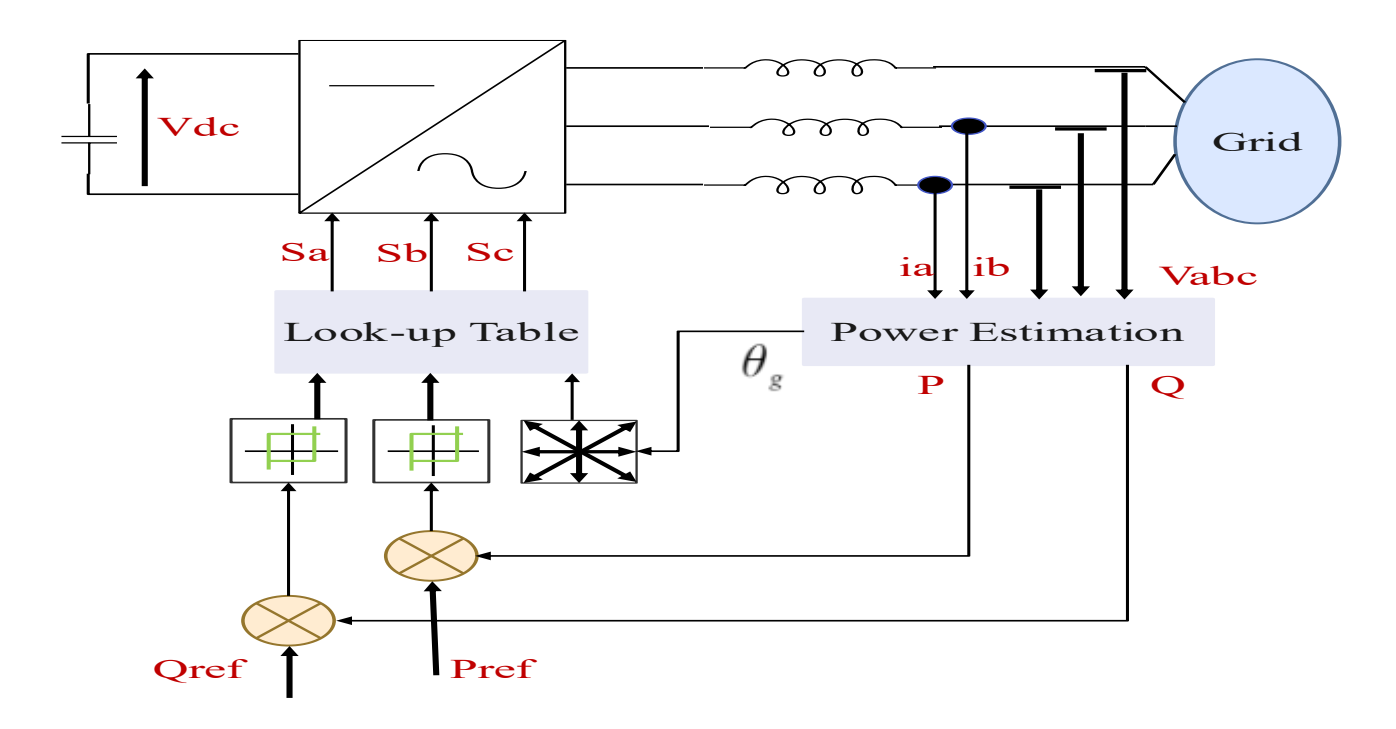


Figure 3.15 : DPC Bloc Diagram.

However, the primary drawback of the DPC approach is the inherent variable switching frequency, which is generally not bounded and is influenced by the sampling time, lookup table structure, load parameters, and system conditions. This can lead to a scattered harmonic spectrum, posing difficulties in designing an effective line filter to avoid possible grid resonances[133].

3.6.2 Linear Control Method

In an effort to address the key limitations of the hysteresis controller, researchers have proposed linear control techniques that aim to linearize the inherent nonlinearity of the power converter. In order to obtain this, a combination between linear (PI) controllers and a modulation stage have to been designed. Noteworthily that the usually utilized modulation technique are the space vector modulation (SVM) as well as pulse width modulation (PWM).

The linear control approaches for VSI have been preferred widely either in machines drive control or power systems integration. Field oriented control (FOC) was developed in drives industry application, in contrast Voltage Oriented Control (VOC) have been used for grid-tied application. The VOC approach shares similarities with FOC technique, as it utilizes a dual control loop structure as shown in Figure 3.16. VOC comprises an outer loop regulating the DC link voltage and an inner loop controlling the current. By setting the current in the q-

axis to zero, the system can achieve unity power factor operation. The VOC strategy exhibits high steady-state performance and faster dynamic response, attributed to its direct measurement of the DC link voltage. Additionally, the power quality of the system is enhanced, which is a crucial factor for grid integration. Nevertheless, the primary drawback of VOC is the stability challenges associated with the active and reactive components of the system, along with the necessary reference frame transformation[131].

Furthermore, for both the hysteresis and linear control methods, the incorporation of system constraints and technical specifications, including maximum current, switching losses reduction, load voltage spectrum shaping, and total harmonic distortion (THD) minimization, cannot be easily achieved in the design of the control scheme. This leads researchers to develop advanced control approaches to overcome the pre-mentioned challenges.

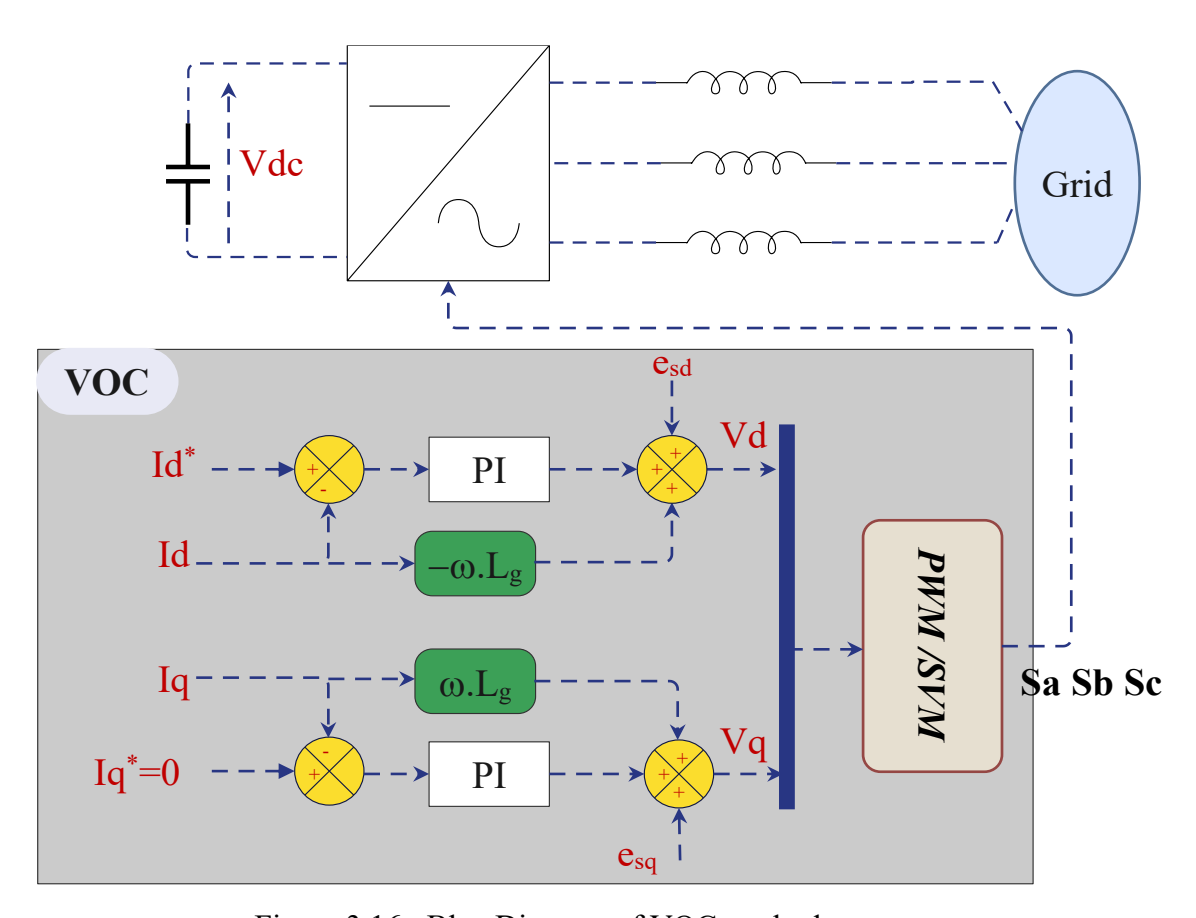


Figure 3.16: Bloc Diagram of VOC method.

3.6.3 Finite Control Set Model Predictive Control

Model predictive control (MPC) is a promising option for controlling a power converter due to its adaptable control philosophy that enables the seamless integration of system restrictions and nonlinearities. A system model is employed in this control to forecast the behavior of the system based on the current states and the control strategy. Furthermore, a cost function is used as a criterion to choose the most advantageous switching states. The primary feature of predictive control is its reliance on a system model to forecast the future behavior of the controlled variables. This information is utilized by the controller to achieve optimal actuation based on a specified optimization criterion. However, the control objectives of Model Predictive Control (MPC) might significantly differ depending on the specific application[134].

In this context, Finite control set MPC (FCS-MPC) is a form of predictive control that employs a discrete representation of the system model. Its minimized cost function determines the state to be utilized based on the potential states of the converter. In contrast to classical control techniques, this scheme removes the requirement for linear PI regulators and the modulation stage, providing a fundamentally different approach to managing power converters[121], [134]. Nevertheless, regarding drawbacks, the task of deriving the control law is more intricate in comparison to traditional controllers like PI. Additionally, the process time significantly increases when taking into account the constraints. Lastly, the performance of the controller can be influenced by the modeling of the plant. Figure 3.17 presents the simplified bloc diagram of inverter grid connected system controlled via FCS-MPC.

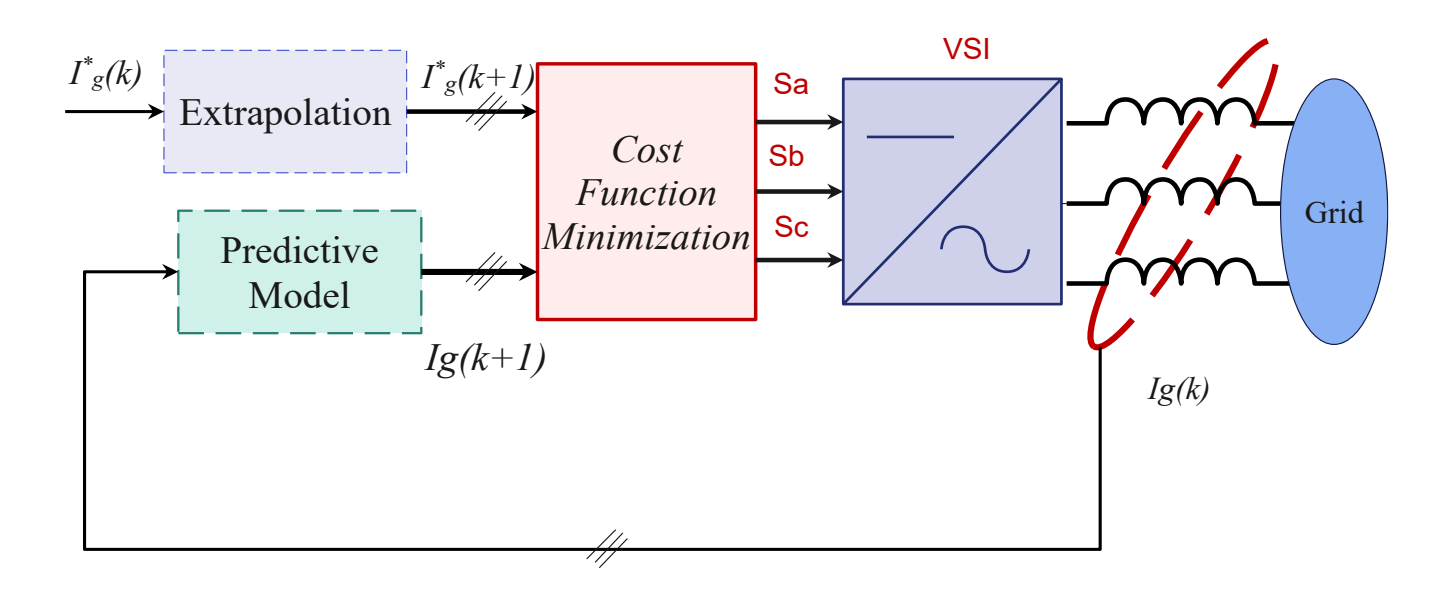


Figure 3.17: FCS-MPC Block scheme.

3.6.4 Other Control Methods

Sliding mode control is a sophisticated method for controlling power converters that is part of the family of control systems that use variable structures. Any system, linear or

otherwise, may be controlled using this nonlinear approach. Sliding controllers are used to force control variables to follow predetermined trajectories by generating voltage references in converters that provide drive signals. The control scheme of this approach is presented in Figure 3.18. Regardless of changes in system parameters or disruptions caused by the load, the reaction remains constant and strong as a consequence[121]. Sliding mode control is more resilient and can get rid of steady-state mistakes than classical controllers. Nevertheless, there are a few downsides to using this technology. For instance, it's too hard to select the best sliding surface, and the sampling rate constraint can reduce the performance of the sliding mode control. Another issue with the sliding mode control approach is the chattering phenomena, which can decrease the overall efficiency of the system while monitoring a changeable reference[132].

Another sophisticated technique usually employed for this issue is fuzzy logic control[135].

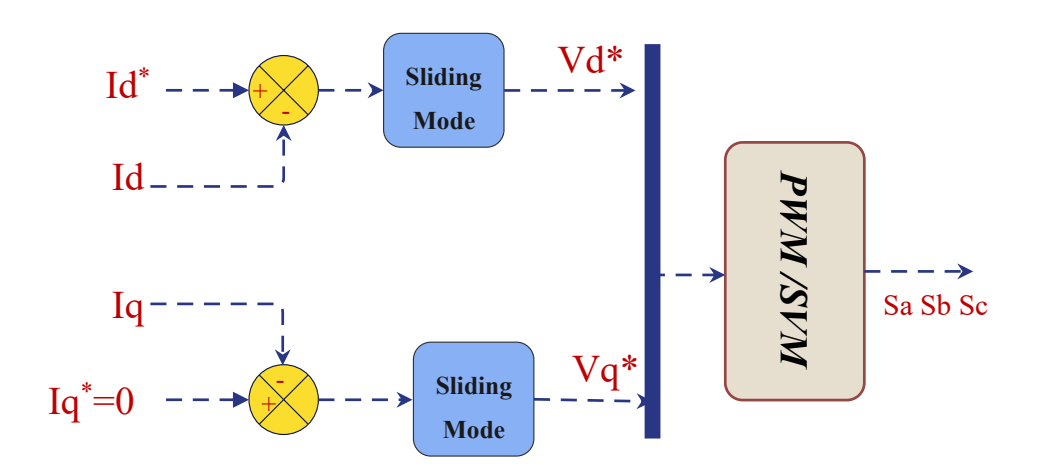


Figure 3.18: SMC control for grid-tied inverter.

This control approach is classified as a member of the intelligent control systems family. This approach substitutes the PI controller with a fuzzy logic controller. The input to the fuzzy controller is the load current reference tracking error and its derivative. This controller encapsulates the experience, knowledge, and intuition of the converter operator or designer in the form of membership functions. Given the inherent nonlinearity of power converters, the fuzzy controller can enhance the system robustness during parameter variations, without requiring the exact converter model. Furthermore, the fuzzy control approach is a category of nonlinear control techniques, and is considered one of the most effective among the adaptive controllers.

The grid connected systems controlled via Artificial Neural Network (ANN) was also proposed and discussed in the literature. Alternative to traditional controllers, utilizing ANN controllers is an ingenious approach to decrease the intricacy and expenses of real-time system installation. Hence the signals of tracking error serve as inputs to the ANN, which then generates switching signals for the power converter as shown in Figure 3.19. This method allows for operation at a constant switching frequency. According to [136], the neural network control exhibits quicker response, effectiveness in suppressing the circulating current, and maintenance of sufficient power quality.

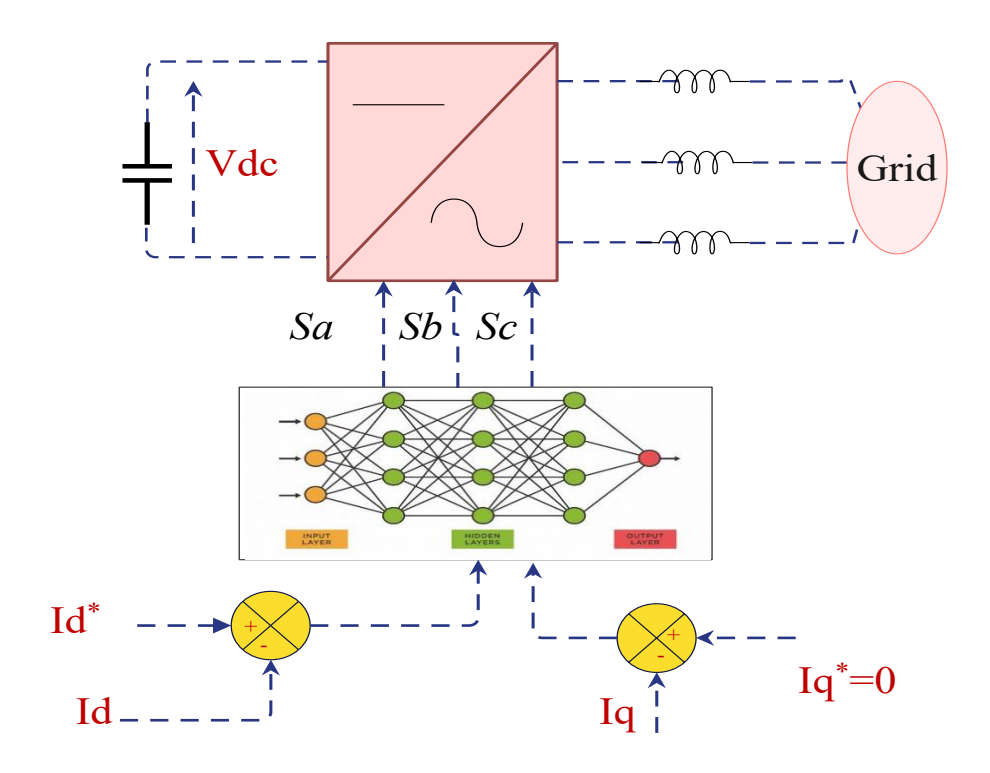


Figure 3.19: ANN based grid-tied inverter control.

3.7 Grid Synchronization

In the synchronous frame control approach, knowledge of the grid voltage's amplitude and phase is required for the control system. This data is critical for the stabilization of the current and voltage control loops. The synchronization algorithm is primarily employed to determine the phase angle of the grid voltage. This grid angle is utilized as a feedback variable to transform into an appropriate reference frame. Therefore, accurate and rapid detection of the grid angle is crucial for the control techniques of grid-connected inverters[137]. An optimal synchronization method should include the following desirable attributes:

- Proficiency in accurately detecting the phase angle of the utility signal.
- Ability to effectively monitor changes in frequency and phase.
- Robustness in rejecting noise and higher-order harmonics.
- Rapid responsiveness to fluctuations in the utility grid.

To gather this essential information, a synchronization technique should be utilized to align the inverter output with the utility grid. Various methods are available for extracting phase details from a signal, and several of these techniques will be discussed in the following subsections.

3.7.1 Zero-Crossing Approach

Zero Crossing Detection (ZCD) is the most straightforward synchronization technique. This method involves a circuit that identifies when an AC voltage transitions from one polarity to another, generating a corresponding pulse. However, its low dynamic response, susceptibility to noise, and sensitivity to higher-order harmonics make it inadequate for utility grids that demand precise phase angle measurements. The voltage zero-crossing technique has been somewhat enhanced through the application of various digital approaches [137].

3.7.2 Filtering of Grid Voltages

Filtering of grid voltages is possible in both the dq frame and the $\alpha\beta$ reference frame. Implementing voltage filtering enhances the efficacy of the zero-crossing technique. However, the filtering methodology still faces challenges in accurately extracting the phase angle when grid fluctuations or faults arise in the utility network. In order to determine the phase angle of the utility voltage, the arctangent function is necessary under this approach. The induction of a delay in the processed signal is a widely recognized consequence of filtering. For the purpose of obtaining the grid voltage angle, this is deemed unsatisfactory. Therefore, an appropriate filter design is essential. Where the current controller is applied in the stationary reference frame, the calculation of the arctangent function is unnecessary as the knowledge of the grid voltage angle θ is not required. Indeed, the filtered $\alpha\beta$ components can serve as a direct template for synchronizing the reference current signal[138].

3.7.3 Phase-Locked-Loop (PLL)

The Phase-Locked Loop (PLL) operates as a negative feedback closed-loop system, effectively synchronizing the power converter with the grid. PLLs are frequently utilized for grid synchronization in both single-phase and three-phase systems due to their ease of implementation and resilience under diverse grid conditions[139]. Noteworthily, despite the existence of higher order harmonics or noise in the grid, the PLL performs effectively. The primary components of a Phase-Locked Loop (PLL) are:

- **Phase Detector**: This component generates an error signal by comparing the input/reference signal with the output signal.
- Loop Filter: This filter eliminates unwanted harmonic components from the error signal.
- Voltage Controlled Oscillator (VCO): The VCO produces the output signal, with its frequency varying around a central frequency based on the output from the loop filter.

Generally, the implementation of the PLL establish in the d-q reference frame. The overall diagram of the PLL approach is shown in Figure 3.20.

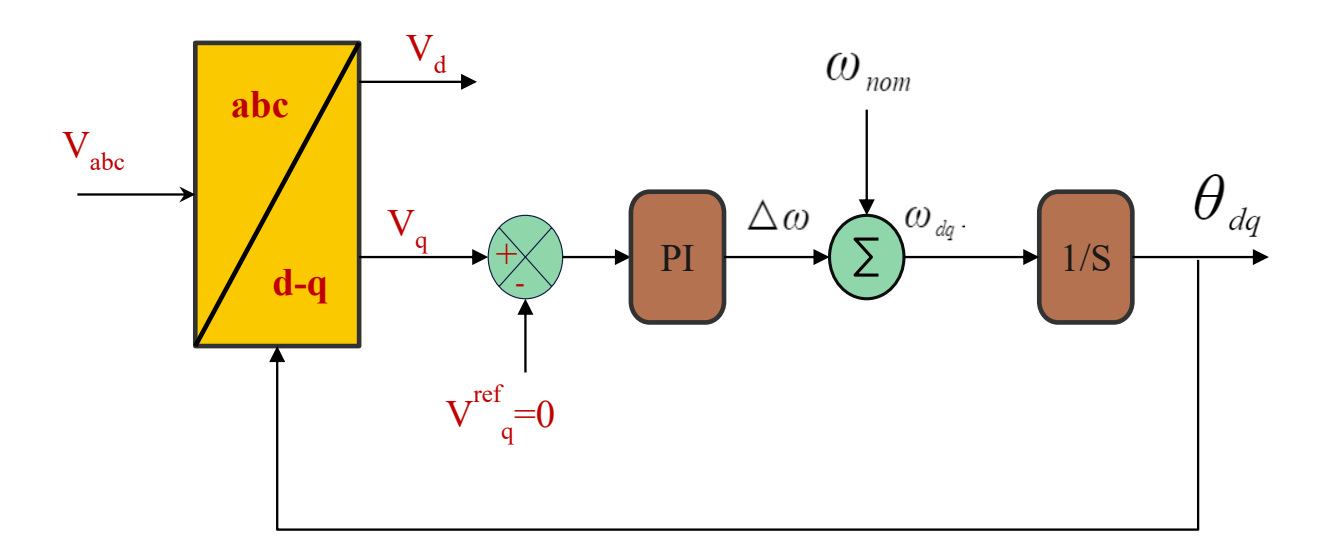


Figure 3.20: The PLL structure in dq frame.

3.8 Power Management Strategies

The existence of two or more power sources bring attention to the requirement of developing an energy management (EM) approach to distribute power among them. The main

objective of Power Management Control is to coordinate the various sources within a hybrid system, particularly regarding their power exchange. This coordination aims to make the generated power manageable, maintain the DC bus stable, ensure a continuous supply to the load side, and optimize energy production costs. However, the power management strategy is influenced by the specific type of energy system and its constituent components[19]. Several energy management algorithms have been extensively studied and applied in the literature. Currently, the prevailing approaches for energy management in hybrid power systems described in Figure 3.21 can be classified into two main groups are Rule-Based algorithms and Optimization-Based algorithms [140].

3.8.1 Rule-Based Algorithms:

Rule-based management techniques are classic control systems that rely on the specific mode of operation. These systems can be readily integrated with real-time supervisory control to effectively regulate the power flow in a hybrid power facility. Generally, the rules are established by considering human intellect, heuristics, or mathematical models. The two main forms of rule-based mechanisms are the Fuzzy Logic Rule-Based Control Strategy and the Deterministic Rule-Based (DRB). Indeed, DRB also known as static logic threshold techniques. Further, these rules are formulated based on predefined objectives, such as achieving grid independence, reducing costs, and minimizing emissions. One of most used algorithms that is belong to the DRB strategy is the state machine approach (SMA) [141]. This method models the energy management process as a finite state machine (FSM), in which every state stands for a particular operating condition or mode of the system. Based on pre-defined criteria or rules, the system moves between various modes, hence optimizing energy consumption while preserving system performance. As well, there are many power supervisor techniques under DRB subcategory are mentioned in literature among them Thermostat control strategy and Electric assist control. On the other hand, Fuzzy Rule-Based Control (FRBC) is the second subcategory EMS that belong to the rule-based algorithms. The latter includes three different forms are: conventional FRBC[142], Adaptive FRBC[143], and predictive FRBC[144]. Hence, the truth of every assertion in fuzzy logic is defined as a matter of degree. Fuzzy control is characterized by its simplicity, ease of implementation, and high resilience. It can immediately translate the insights of a designer into control rules. Moreover, expert knowledge may be mathematically represented as a set of rules and used to the process of making decisions. One primary benefit of fuzzy logic is its ability to be adjusted and modified as needed, hence increasing the level of control flexibility [145].

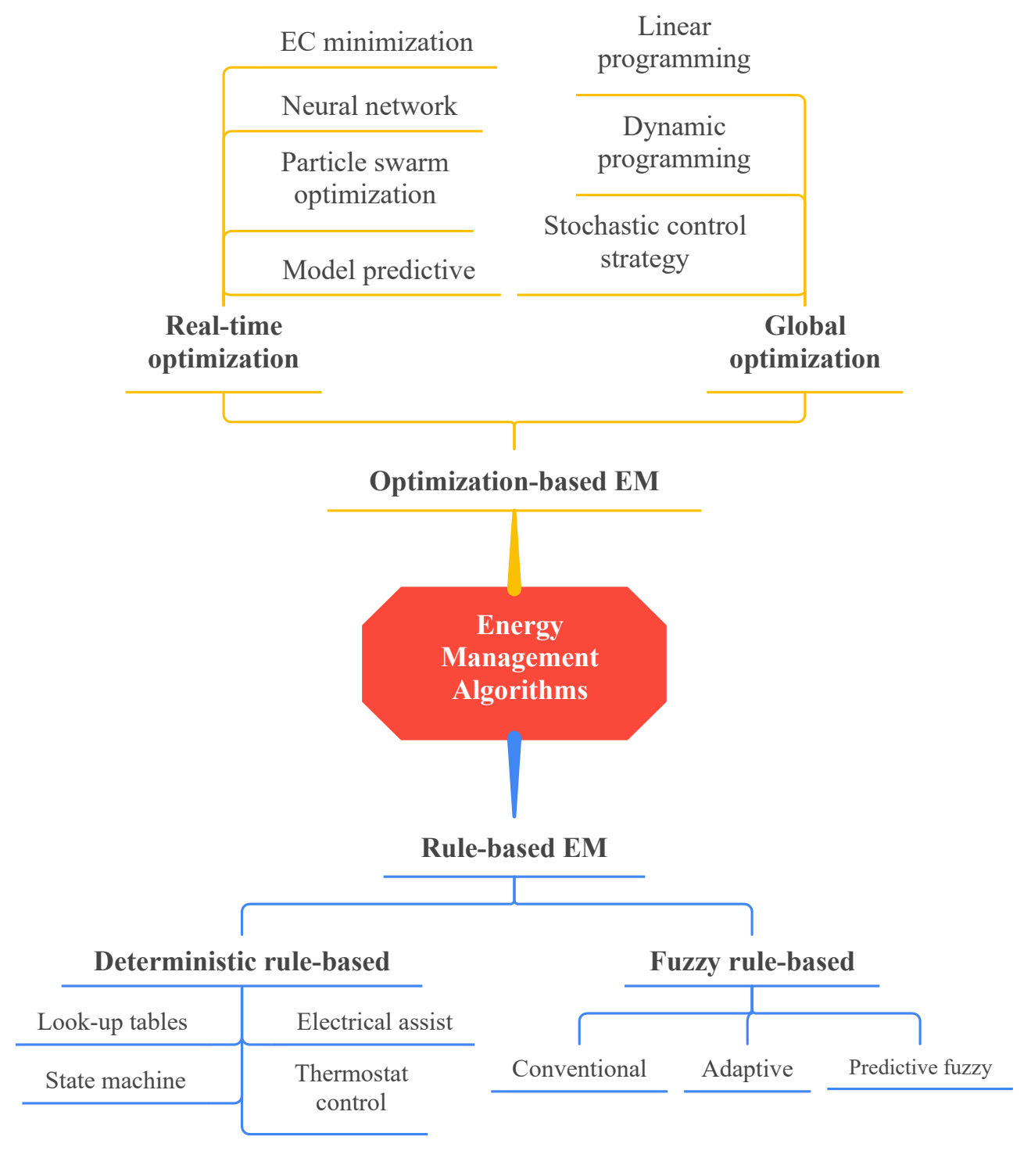


Figure 3.21: Management Strategies Categories.

Nevertheless, in the rule-based management the process of formulating rules is highly intricate, necessitating extensive understanding of the systems while lacking flexibility. Regrettably, the lack of adequate consideration of overall operating circumstances and the heavy reliance on engineering knowledge make rule-based energy management challenging to achieve optimal performance[146].

3.8.2 Optimization-Based Algorithms

In optimization-based control strategies, the primary aim of the controller is to minimize the cost function. Depending on the particular application, a hybrid power system's cost function could include elements like power flow, hydrogen consumption, and energy expenses. Although real-time energy management is not directly achieved by these control approaches, it is possible to derive a real-time control strategy by utilizing an instantaneous cost function. Accordingly, two main groups define optimization-based tactics: real-time or online methods and global optimization or known also as offline optimization techniques. The Global Optimization Strategies plan and maximize energy consumption depending on thorough awareness of the operational traits and restrictions of the system. These techniques are known as "offline" as the optimization process uses previous data or projections instead of real-time data and is done beforehand. Global optimization is the search for the greatest feasible solution to improve efficiency, lower energy costs, or fulfill other particular goals over a certain period. The predominant techniques employed in this context are Linear Programming, Dynamic Programming, Stochastic Control Strategy, and Genetic Algorithm. Dynamic programming (DP) is a crucial technique used to address optimum control problems having control variables constrained to a certain closed set. An essential concept of this approach is to convert the optimum control issue into a multilayer decision-making problem [146]. Among the most often applied techniques in the literature is stochastic dynamic programming (SDP). Solving an infinite horizon optimization problem offline generates a time-invariant state feedback controller, thereby determining the control law offline[147]. The genetic algorithm (GA) is a heuristic method well regarded for its superior optimization performance. By using its inherent features, it may readily select acceptable solutions based on the optimization goals and compensate for these limitations. The aforementioned features render genetic algorithms highly advantageous in the reiterative optimization of a power system[148].

On the other hand, based on real-time data, the Online Optimization Strategies are methods for constantly monitoring, adjusting, and optimizing energy use. Online optimization

constantly changes to fit new circumstances as they arise, unlike offline (global) optimization which depends on pre-computed plans utilizing previous data and projections. This method works especially well in settings where supply, energy demand, and other operational factors are somewhat erratic. The most famous techniques included in this context are Equivalent Consumption (EE) Minimization Strategy[149], Model Predictive Control [150], and Neural Networks based EMS [151] as well as metaheuristics algorithms such as grey wolf optimizer (GWO), salp swarm algorithm (SSA) and particle swarm optimization (PSO).. etc. In fact MPC technique is an effective approach for handling dynamic process models derived from system identification. An essential characteristic of the MPC is its ability to maximize the present timeslot while considering future timeslots. Equivalent Consumption Minimization Strategy (ECMS) is also reported widely in research papers. The main objective of this approach according to [152] is to reduce the equivalent fuel consumption while maintaining the battery and supercapacitor State of Charge (SOC) within their optimized working range, during the complete load profile. Computational correctness of the equivalent fuel usage is crucial for the performance of the ECMS. Artificial neural network (ANN) is a robust computing technique that acquires knowledge and extends its application from training data. Due to its inherent high level of parallelism, the neural network technique may resolve optimization problems in execution time substantially quicker than the most common optimization algorithms.

3.9 Conclusion

This chapter provides a comprehensive survey and general background on the control techniques strategies of the hybrid power systems including the different Maximum power point tracking (MPPT) methods for photovoltaic generator systems, power optimization algorithms for wind energy conversion systems in addition to machine drive control specifically the permanent magnet synchronous generator (PMSG) as well as fuel cell performance control. Moreover, a state of the art about dc-link voltage stabilization and grid current control strategies in addition to grid synchronization methods were incorporated in this chapter. Furthermore, the final subsection discusses energy management strategies and power flow supervision.

Chapter 4

Intelligent Control Design of a grid connected hybrid wind/photovoltaic/fuel cell system

4.1 Introduction

The rapid growth of renewable energy integration into modern power systems necessitates innovative control strategies that ensure optimal performance, stability, and efficiency. This chapter introduces a set of advanced control approaches designed to manage and enhance the operation of various renewable energy sources, including photovoltaic systems, fuel cells, and wind energy converters, as well as their integration into grid-connected hybrid systems. The target of these solutions is to maximize energy extraction under different environmental conditions while maintaining system stability and power quality. The aim for photovoltaic applications is to create robust ways to track the maximum power point and increase energy harvest despite solar irradiance variations. Similarly, wind energy systems require controllers capable of adapting to rapid changes in wind speeds to consistently capture optimal energy output. On the other side for fuel cell systems, the challenge lies in managing dynamic responses and ensuring stable operation despite inherent nonlinearities and variable operating conditions.

In the following sections, detailed discussions on the design principles, implementation, and performance evaluations of these control strategies are presented, providing valuable insights into their practical applications and benefits in modern renewable energy systems.

4.2 MPPT Control Design for Solar PV Systems

4.2.1 High Order Sliding Mode Control

Sliding mode control (SMC) is rooted in relay feedback control. Its key phases include reaching mode, where the system is drawn towards a sliding manifold, and sliding mode, where it moves along this manifold towards the equilibrium point. Finally, in steady-state (Desired value), the system remains at the equilibrium as shown in Figure (4.1). Designing an SMC law necessitates a precise mathematical model. A switching component is often employed to maintain the system on the sliding manifold, ensuring it reaches the desired state. Once in

sliding mode, the system's behavior is determined by the manifold's dynamics, making it resilient to certain uncertainties[153]. Due to its ease of use, resilience, and strong performance, SMC has become a popular choice for designing nonlinear control systems. SMC has been applied to various fields, including robotics, motor control, and inverter control, to address uncertainties arising from varying parameters and unknown external or internal disturbances. Given that the PV system demonstrates nonlinear behavior; hence, it is advisable to utilize a nonlinear control mechanism to track the MPP. Sliding mode control has proven to be a particularly effective and robust approach for this task, as demonstrated in numerous studies[154], [155]. Indeed, two primary control paradigms, namely single-loop and cascadeloop, are commonly employed for MPPT in photovoltaic systems. The single-loop approach eschews a reference point, relying instead on a switching surface designed to converge asymptotically to zero as the system approaches the optimal operating point. In contrast, the cascade-loop architecture incorporates an external loop for MPPT search and an internal loop for tracking the identified optimal operating condition [154]. Nonetheless, SMC is recognized for generating chattering in the control input signal, characterized by high-frequency oscillations around the target value[156]. Generally, the chattering phenomenon is often attributed to the high-frequency switching of discontinuous terms arising from imperfections in the switching function. To mitigate this issue, several extended SMC-based strategies have been introduced in the literature. Terminal sliding mode control is one of the suggested approaches that has been introduced to deal with this issue [157]. A novel MPPT based on adaptive integral derivative sliding mode (AIDSM) has been proposed in [158]; hence, the adaptive mechanism able to adjust automatically the SMC controller parameter according to dynamic performance while the integral effect aims to alleviate steady-state error. Another approach to mitigate the chattering phenomenon in SMC which is introduced in the literature, involves integrating it with intelligent control technologies, such as fuzzy logic or neural networks, to generate smoother control signals[159], [160]. However, the latter makes the control process more complex and needs processing power.

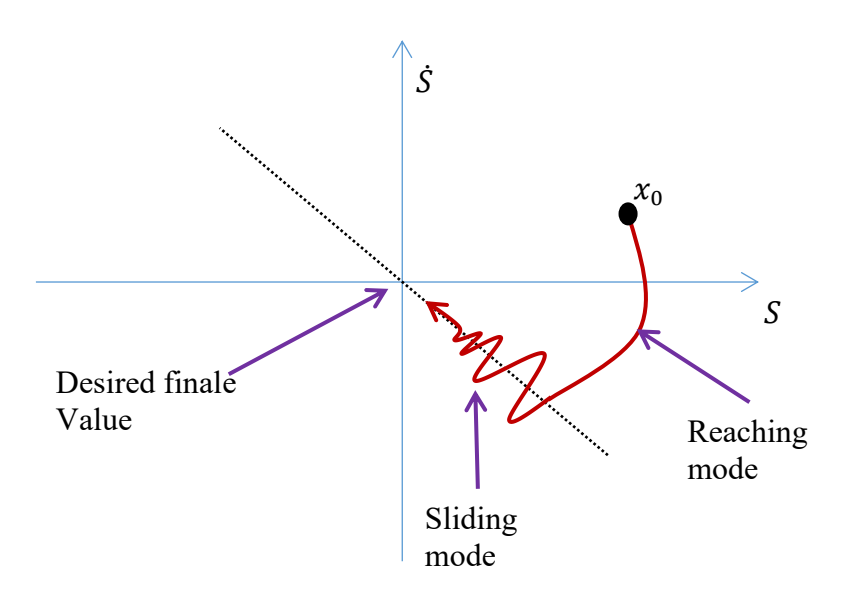


Figure 4.1: phase plane representation of SMC method.

Second-order sliding mode control (SOSMC) has emerged as a prominent technique for mitigating chattering in SMC theory. SOSMC not only effectively addresses the limitations of conventional SMC but also preserves its key advantages, including robust performance and convergence in a finite-time. Common SOSMC algorithms include the twisting algorithm, super-twisting algorithm, drift algorithm, and prescribed convergence law algorithm. Among the SOSMC techniques, the super-twisting algorithm, regarded as a nonlinear proportional-integral control, it has proven particularly effective in handling systems with significant nonlinear characteristics. Accordingly, super-twisting algorithm-based MPPT is introduced in this work.

4.2.1.1 Robust MPPT Controller Based on Super-Twisting for PV Systems

This study presents the super-twisting controller, an enhanced modification of classic SMC, aimed at optimizing the output power of photovoltaic (PV) systems. The super-twisting technique is specifically engineered to address higher-order dynamics and effectively mitigate significant perturbations resulting from model uncertainties and external disturbances common in photovoltaic systems. The super-twisting controller offers a primary advantage over traditional sliding mode control by substantially mitigating, if not completely eradicating, the adverse phenomena referred to as chattering as illustrated in Figure (4.2). Chattering not only causes mechanical degradation but also diminishes the overall efficiency and dependability of the energy harvesting process in photovoltaic systems. The super-twisting method utilizes a non-linear control law that continually modifies the control action, thus optimizing the control effort and improving response time. Moreover, the super-twisting controller demonstrates

superior performance in situations marked by variable conditions, commonly associated with solar energy applications. It rapidly and effectively adjusts to variations in irradiance and temperature, guaranteeing that the maximum power point tracking (MPPT) remains consistently precise and dependable. The exceptional versatility of the super-twisting process renders it an indispensable asset in the field of renewable energy, where environmental fluctuation is a continual challenge. The incorporation of this technology into photovoltaic system control frameworks ensures substantial enhancements in solar energy capture and utilization, optimizing power output while preserving stability and minimizing system degradation over time. Next, we will delineate the precise architecture of the proposed super-twisting controller.

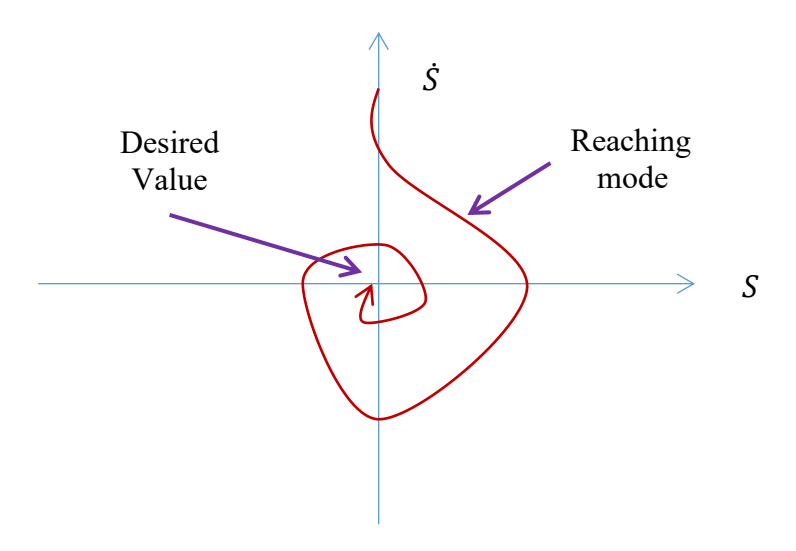


Figure 4.2: phase plane representation of the Super-Twisting algorithm.

Indeed, two primary steps must be adhered to establish sliding mode control. The initial phase in creating an effective sliding mode control system is identifying a suitable sliding surface. This surface serves as a critical benchmark, dictating the trajectory the system must follow to ensure maximum efficiency. In a photovoltaic system employing a boost converter, the sliding surface is determined according to the intended dynamic performance of the system. This entails formulating a mathematical equation that characterizes a surface within the state space where the system's state should ideally reside. The selected sliding surface significantly affects the system's capacity to swiftly attain and sustain the maximum power point, even amidst fluctuating external conditions. The design of the sliding surface must include system parameters and operational conditions, ensuring rapid convergence to the MPP. Equation (4.1) describes the sliding surface 's used in this work

$$S(x,t) = \frac{\partial P_{pv}}{\partial V_{mv}} = V_{pv} \left(\frac{\partial I_{pv}}{\partial V_{mv}} + \frac{I_{pv}}{V_{pv}} \right) = 0$$
(4.1)

The subsequent phase entails formulating a control law capable of efficiently steering the system's state toward the designated sliding surface and sustaining it therein. This control law is essential for the stability and precision of the MPPT process. The control low in SMC generally consists of two components: the equivalent control (u_{eq}) and the switching control. The equivalent control guarantees that once the system attains the sliding surface, it remains on it without deviation. The switching control is tasked with effectively rectifying any deviations from the sliding surface caused by external disturbances or flaws in the model. In super-twisting sliding mode control, the control rule is formulated to be resilient to variations in system dynamics and external perturbations, hence reducing the chattering phenomenon commonly associated with conventional sliding mode controllers. Equation (4.2) outlines the governing principle of the ST-SMC method.

$$u = u_{STA} + u_{eq} \tag{4.2}$$

Consider a state vector as

$$X = \begin{bmatrix} I_L & V_O \end{bmatrix}^T \tag{4.3}$$

Where: I_L denotes the inductor current of the boost converter. Vo represents the output voltage.

The model of a time invariant nonlinear system is given by

$$\dot{X} = f(X) + h(X)u \tag{4.4}$$

Where 'l' is the control input, while 'f' and 'h' are described as follows

$$f(X) = \begin{bmatrix} \frac{V_{PV} - V_o}{L} \\ -\frac{V_o}{RC_{dc}} + \frac{I_L}{C_{dc}} \end{bmatrix} \quad \text{and} \quad h(X) = \begin{bmatrix} \frac{V_o}{L} \\ -\frac{I_L}{C_{dc}} \end{bmatrix}$$
(4.5)

The system's behavior during sliding mode can be represented by the following equation

$$\dot{S} = \left[\frac{\partial S}{\partial X}\right]^{T} \cdot \dot{X} = \left[\frac{\partial S}{\partial X}\right]^{T} \left(f(X) + h(X)u_{eq}\right) \tag{4.6}$$

By formally solving the aforementioned equation (eq. 4.6) for the control input, we derive an expression for \mathcal{U} known as the equivalent control, (u_{eq}) . Consequently, we obtain:

$$u_{eq} = 1 - \frac{V_{pV}}{V_{o}} \tag{4.7}$$

The control switching mechanism for STA design is defined as:

$$u_{STA} = -\lambda' . |S|^{\frac{1}{2}} . sign(S) - \gamma \int sign(S)$$
(4.8)

Where γ and λ' are constant gains.

4.2.2 Double-Stage Control Based MPPT Using Neural Network and Model Reference Adaptive Control

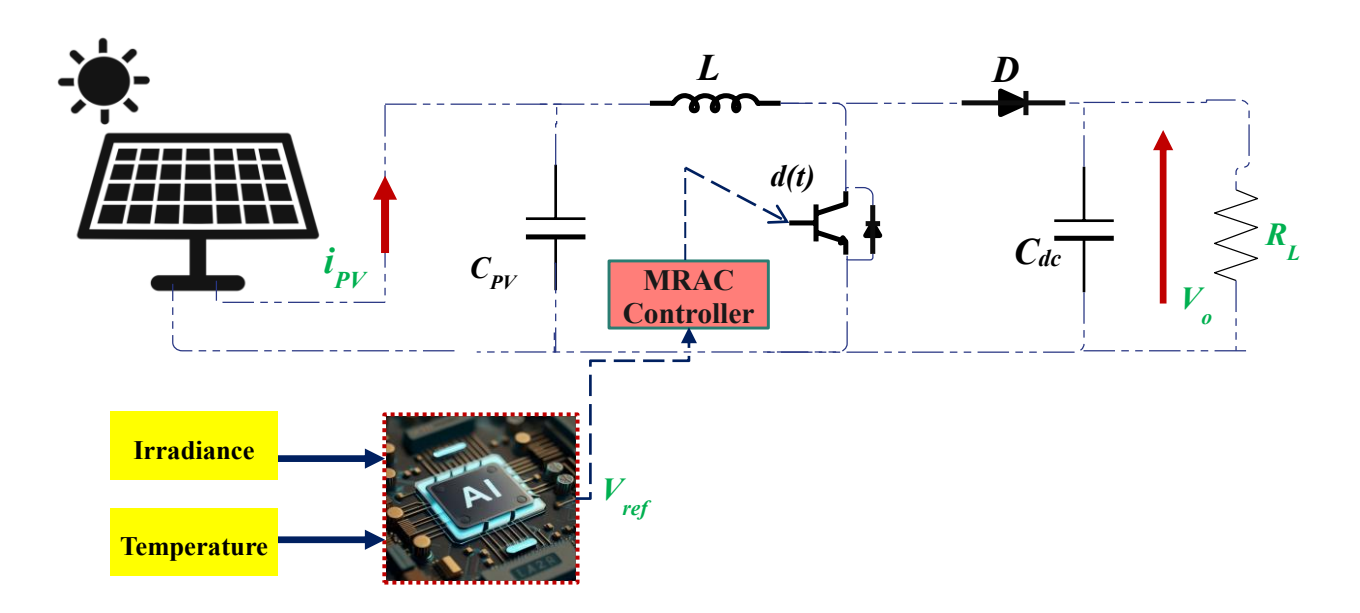


Figure 4.3: Bloc Diagram of the proposed NN-MRAC MPPT.

This section presents an adaptive control framework for maximum power point tracking (MPPT) in photovoltaic (PV) systems, designed to optimize power delivery to the load under varying solar irradiance and ambient temperature conditions. To enhance MPPT performance, we propose a two-tier adaptive control architecture that effectively addresses system uncertainties and disturbances. The first control layer employs artificial neural networks (ANNs), while the second utilizes model reference adaptive control (MRAC). This decoupled approach ensures system stability while achieving highly efficient power[161]. Figure (4.3) depicts the overall control scheme of the suggested MPPT design.

4.2.2.1 Neural-Network Approach for Generating Reference Voltage

For every temperature and irradiance level, a specific reference voltage must be tracked to ensure optimal power extraction from the photovoltaic (PV) array [101]. The PV array's

performance curve is influenced by changes in temperature and irradiance as shown in Figures (2.4) and (2.5). Even minor fluctuations in these parameters can modify the characteristic curve and, consequently, the maximum power point. Various methodologies have been employed for determining the reference peak power voltage of photovoltaic arrays, including Fuzzy Logic, ANFIS approach [162], and Gaussian Process Regression (GPR)[163]. In this research, we utilized a three-layer neural network architecture for Voltage reference estimation as presented in Figure (4.4). This architecture comprises an input layer, a hidden layer, and an output layer, enabling the neural network to effectively learn and adapt to the complex relationship between temperature, irradiance, and the optimal operating point of the photovoltaic system. Moreover, the input and output data for the ANN training are acquired through various measurements as outlined in Table (III).

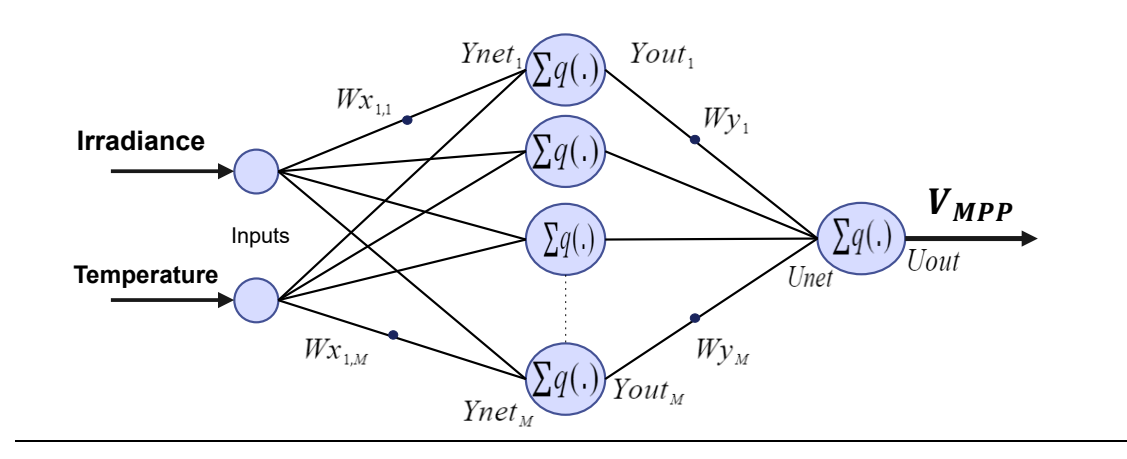


Figure 4.4: ANN Scheme for Voltage reference estimation.

The ANN instantaneous output, which serves as the reference voltage (Uout = Vref), can be mathematically represented as follows:

$$U_{Out} = q(U_{net}) \tag{4.9}$$

351

Where q(.) denoted to the activation function, while U_{net} presents the output layer's input which may be expressed as

| Irradiance (W/m2) | Temperature (C) | V_{MPP} |
|-------------------|-----------------|-----------|
| 1000 | 25 | 348 |
| 900 | 25 | 347.56 |
| 800 | 25 | 350 |

25

Table I: The used data set for ANN training.

700

| 600 | 25 | 352 |
|------|----|--------|
| 500 | 25 | 352 |
| 400 | 25 | 351 |
| 300 | 25 | 349.35 |
| 200 | 25 | 345 |
| 100 | 25 | 346 |
| 1000 | 30 | 349.8 |
| 1000 | 35 | 331.87 |
| 1000 | 40 | 323.95 |
| 1000 | 45 | 316 |
| 1000 | 50 | 308 |
| 1000 | 55 | 300 |
| 1000 | 60 | 292.3 |
| | | |

$$U_{net} = \sum_{j=1}^{M} W_{y_j} . Y_{out_j}$$
 (4.10)

$$Y_{out_j} = q\left(Y_{net_j}\right) \tag{4.11}$$

$$Y_{net_j} = \sum_{i=1}^{N} W_{X_{i,j}} . x_i$$
 (4.12)

Where the following notation applies:

- Y_{net} and Y_{out} represent the input and output of the hidden layer, respectively.
- W_{ν} denotes the weights connecting the hidden layer to the output layer.
- W_x represents the weights connecting the input layer to the hidden layer.
- N signifies the number of input nodes (in this case, N = 2, corresponding to irradiance G and temperature T, denoted as xi, where i = 1, 2).
- M signifies the number of hidden layer nodes (in our study, M = 10).

More details may be found in the Appendix.

4.2.2.2 Proposed MRAC Approach

The previous subsection presented the use of the neural network to determine the reference voltage necessary for maximizing power output under steady-state conditions and facilitating rapid convergence to the MPP during fluctuations in solar irradiance and temperature. As the operating point of a PV system fluctuates with changing solar irradiance, it cannot be guaranteed that the array voltage will exhibit critically damped behavior.

Accordingly, the implementation of an adaptive control strategy is required. However, in order to design an adaptive controller for the PV system we need firstly to model the dynamics between the PV voltage which corresponds directly to solar insolation, and the converter duty cycle variation with respect to time. Basically, this behavior has been approximatively illustrated in Figure (4.5); where the solar array is modeled as a resistor R_I in addition to a small signal PV voltage \hat{V}_{PV} and a small signal PV current $\hat{\iota}_{PV}$. For more detail see [164].

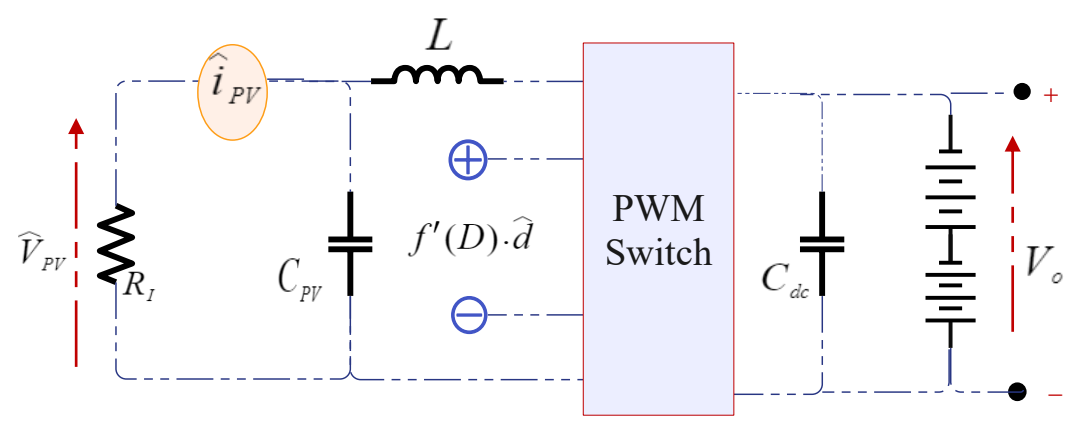


Figure 4.5: small-signal model of a PV power system[161].

We will now derive the transfer function that relates the control signal (duty cycle) to the PV array voltage within a small-signal operating region around a specific operating point. Noteworthily the used battery in the dynamic behavior representation refers to a common configuration in real-world applications. It reflects the common practice of using batteries to store excess energy solar panels generate. Nevertheless, we assumed that the output capacity C_{dc} of the converter large enough to remain V_o constant and stable. Consequently, the analysis is confined to the influence of the output capacitor on the output impedance, implying that parasitic components associated with the elements of the boost converter are neglected. Additionally, the dynamic behavior of the battery is disregarded in this evaluation [164], [165]. Thus, the transfer function that summarizes this analysis can be given in the following relationship

$$\frac{\hat{V}_{PV}(s)}{\hat{d}(s)} = \frac{-\frac{V_o}{LC_{PV}}}{S^2 + \frac{1}{R_I C_{PV}} S + \frac{1}{LC_{PV}}}$$
(4.13)

Which is basically a second-order linear system; therefore, it can be rewritten in the following canonical form:

$$\frac{\hat{V}_{PV}(s)}{\hat{d}(s)} = \frac{-V_o \omega_n^2}{S^2 + 2.\xi . \omega_n S + \omega_n^2}$$
Where $\omega_n = 1/\sqrt{L.C_{PV}}$, and $\xi = \frac{1}{2R_I} \sqrt{\frac{L}{C_{PV}}}$. (4.14)

Moreover, the equivalent resistor of the converter's input R_I can be estimated at an operational point of the system as $\frac{1}{R_I} \approx \frac{\Delta V_{PV}}{\Delta I_{PV}}$. And as such, this parameter will vary with the operating condition variation, which leads to present oscillations in the step response, especially if the damping ratio ξ is less than 1 because the changes in R_I effect directly on the damping ratio ξ . Applying an MRAC controller is advisable to alleviate and deal with such challenges. The MRAC structure is depicted below in Figure (4.6).

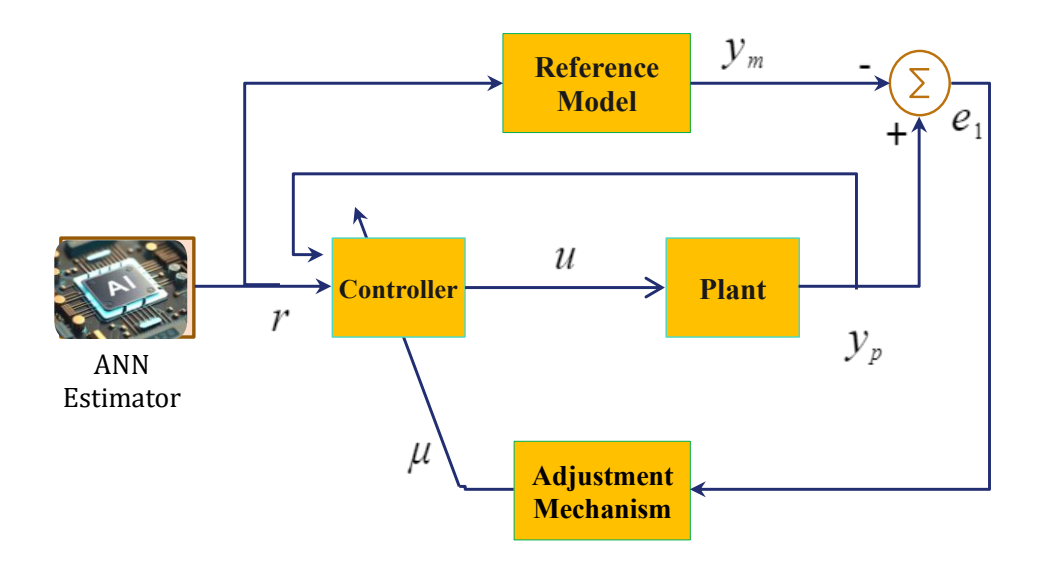


Figure 4.6: The MRAC architecture.

The fundamental principle of MRAC involves designing an adaptive controller that ensures the controlled plant's response closely tracks the desired dynamics of a reference model, even in the presence of uncertainties or variations in plant parameters. The proposed MRAC architecture is depicted in Figure (4.6). The input to the overall system, r(t), represents the change in duty cycle calculated in the preceding section using the ANN. The plant model illustrated in Figure (4.6) corresponds to the transfer function defined in Equation (4.14). The plant input and output are denoted as u(t) and $y_p(t)$, respectively. The plant model can be reexpressed as follows:

$$G_p(s) = \frac{y_p(s)}{u(s)} = \frac{\mathbf{K}_p}{\mathbf{s}^2 + \mathbf{a}_p \mathbf{s} + \mathbf{b}_p}$$
(4.15)

Where
$$k_p = \frac{-V_o}{LC_{PV}}$$
, $a_p = \frac{1}{R_I C_{PV}}$ and $b_p = \frac{1}{LC_{PV}}$.

On the other hand, the transfer function that represents the reference model is given by

$$G_m(s) = \frac{y_m(S)}{r(S)} = \frac{K_m}{s^2 + a_m s + b_m}$$
(4.16)

In the above equation, k_m represents a positive gain, while a_m and b_m are selected to ensure that the reference model exhibits the desired and acceptable response.

Now, let the controller which leads us to the desired be given by

$$u = \mu_1 r - \mu_2 y_p = \mu^T \Theta \tag{4.17}$$

Where $\begin{bmatrix} \mu_1 & \mu_2 \end{bmatrix}^T = \mu$, while $\Theta = \begin{bmatrix} r & y_p \end{bmatrix}$.

However, the vector μ is unknown and must be selected through the adaptation mechanism. Thus, the well-known MIT mechanism will be applied in this context to estimate these vector parameters [166]. Accordingly, this rule adjusts the parameters in such a way a given loss function is minimized. The aforementioned function is defined as

$$J(\mu) = \frac{1}{2}e_1^2 \tag{4.18}$$

Therefore, in order to make 'J' smaller, it is required to vary the parameters in the negative gradient direction of 'J', and as such,

$$\frac{d\mu}{dt} = -\phi \frac{\partial J}{\partial \mu} = -\phi e_1 \frac{\partial e_1}{\partial \mu} \tag{4.19}$$

Where ϕ and $\frac{\partial e_1}{\partial \theta}$ are denoted to the adaptation gain and sensitivity derivative of the system, respectively. Wherein the error e_1 expressed as

$$e_1 = y_p - y_m \tag{4.20}$$

The relation that combines the plant's output y_p and the desired reference 'r' can be formulated by:

$$\frac{y_p}{r} = \frac{k_p \mu_1}{s^2 + a_p s + (b_p + k_p \mu_2)}$$
(4.21)

Therefore, by substituting (4.21) in (4.20) we obtain

$$e_{1} = \left(\frac{k_{p}\mu_{1}}{s^{2} + a_{p}s + (b_{p} + k_{p}\mu_{2})} - \frac{k_{m}}{s^{2} + a_{m}s + b_{m}}\right).r$$
(4.22)

Thus, the sensitivity derivatives are obtained as follows:

$$\begin{cases} \frac{\partial e_{1}}{\partial \mu_{1}} = \frac{k_{p}}{s^{2} + a_{p}s + (b_{p} + k_{p}\mu_{2})} r \\ \frac{\partial e_{1}}{\partial \mu_{2}} = -\frac{k_{p}}{s^{2} + a_{p}s + (b_{p} + k_{p}\mu_{2})} y \end{cases}$$
(4.23)

Afterwards, to guarantee minimal tracking error in this closed-loop system, we assume that the time-domain behavior of the actual system closely matches that of the reference model, as expressed below:

$$s^{2} + a_{n}s + (b_{n} + k_{n}\mu_{2}) = s^{2} + a_{m}s + b_{m}$$
(4.24)

Consequently, the control parameters are updated as follows:

$$\begin{cases} \frac{d\mu_1}{dt} = -\phi \left(\frac{1}{s^2 + a_m s + b_m} . r(t) \right) e_1(t) \\ \frac{d\mu_2}{dt} = \phi \left(\frac{1}{s^2 + a_m s + b_m} y_p(t) \right) e_1(t) \end{cases}$$

$$(4.25)$$

The overall architecture of the suggested MPPT control method is shown in Figure (4.7).

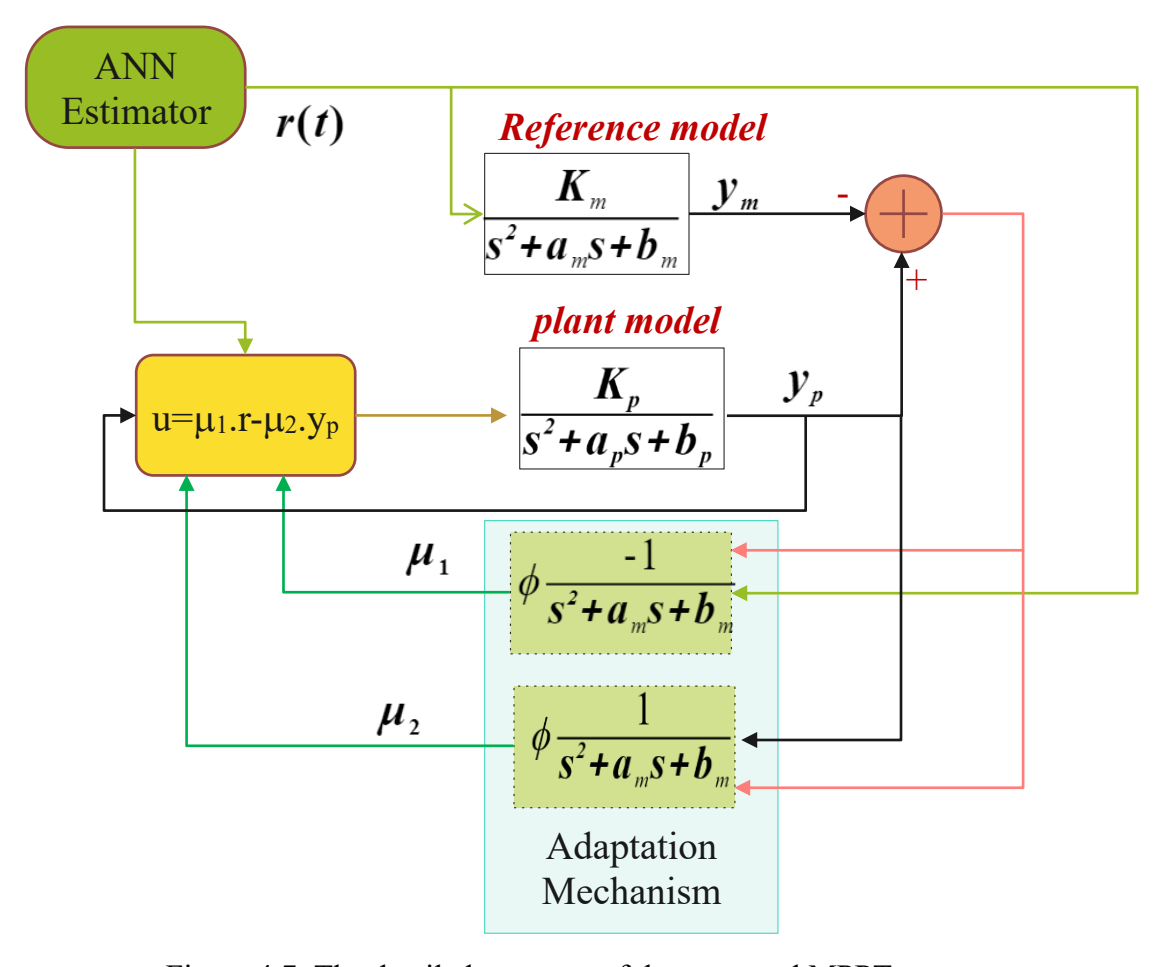


Figure 4.7: The detailed structure of the proposed MPPT.

4.2.3 Double-Stage Control-Based MPPT Using NN and Model Predictive Control

In the previous control scheme, we utilized the ANN approach to generate the voltage reference, while in the following control technique, we aim to employ the ANN method to calculate the optimal reference current $I_{MPP} = I_{PV}^*$. Also, the same training steps that were mentioned earlier will be used in this part (Collecting data, training, and then implementation).

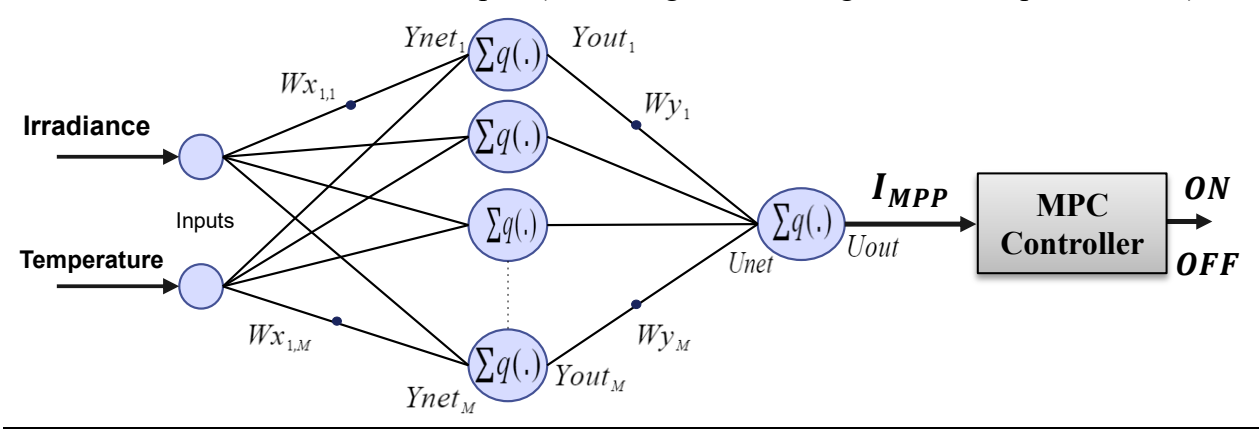


Figure 4.8: ANN-MPC control-based MPPT.

MPC controller Design for Boost Converter:

A mathematical model of a system constitutes a fundamental element in MPC formulation. MPC relies on this model to project the system's behavior over a specified future time horizon, beginning from the current state[167]. The mathematical model necessary for the boost converter that will be used for controller design is established in Subsection (2.4.1). Subsequently, MPC requires the discretization of the continuous model of the system. The discretized prediction model can be represented in the following general form:

$$I_{L}(k+1) = \left(\frac{T_{S}}{L}\right) \left(V_{PV}(k) - V_{o}(k)\left(1 - S'\right)\right) + I_{L}(k)$$
 (4.26)

Where; K presents the number of iterations. Ts denotes the Sampling time. (K+1) is the predicted value. Subsequently, these predictions are assessed against a cost function, which compares them to the predefined reference trajectories. The standard representation of the cost function, g, intended for minimization can be expressed as:

$$g(k+1) = g_I(k+1) + g_{sw}(k+1)$$
(4.27)

Such that:

$$\begin{cases} g_{I}(k+1) = |I_{ref} - I_{L}(k+1)| \\ g_{sw}(k+1) = |S'(k) - S'(k+1)| \end{cases}$$
(4.28)

The global cost function is calculated for all possible switching states during each sample period. The flowchart that summarizes the control process is illustrated in Figure (4.9).

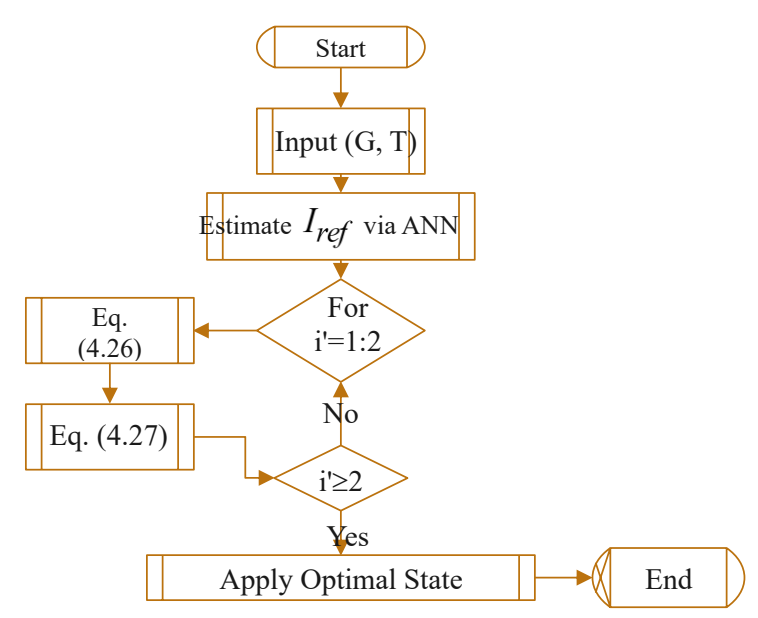


Figure 4.9: ANN-MPC-based MPPT Flowchart.

4.2.4 Results Evaluation

In order to evaluate the performance of the developed algorithms, the investigated photovoltaic system was simulated in MATLAB Simulink as shown in Figure 4.10. The used system parameters are delineated as follows: a solar array of 10 kw type "1Soltech 1STH-215-P" with 4 modules parallel x 12 modules Series-connected; $C_{PV} = 100 \mu F$, $C_{dc} = 1100 \mu F$, $R=80\Omega$. The performance has been examined under varying solar irradiation across five distinct states, as illustrated in Figure 4.11. The comparative analysis between the suggested MPPT algorithms has been conducted with taken into consideration the following terms:

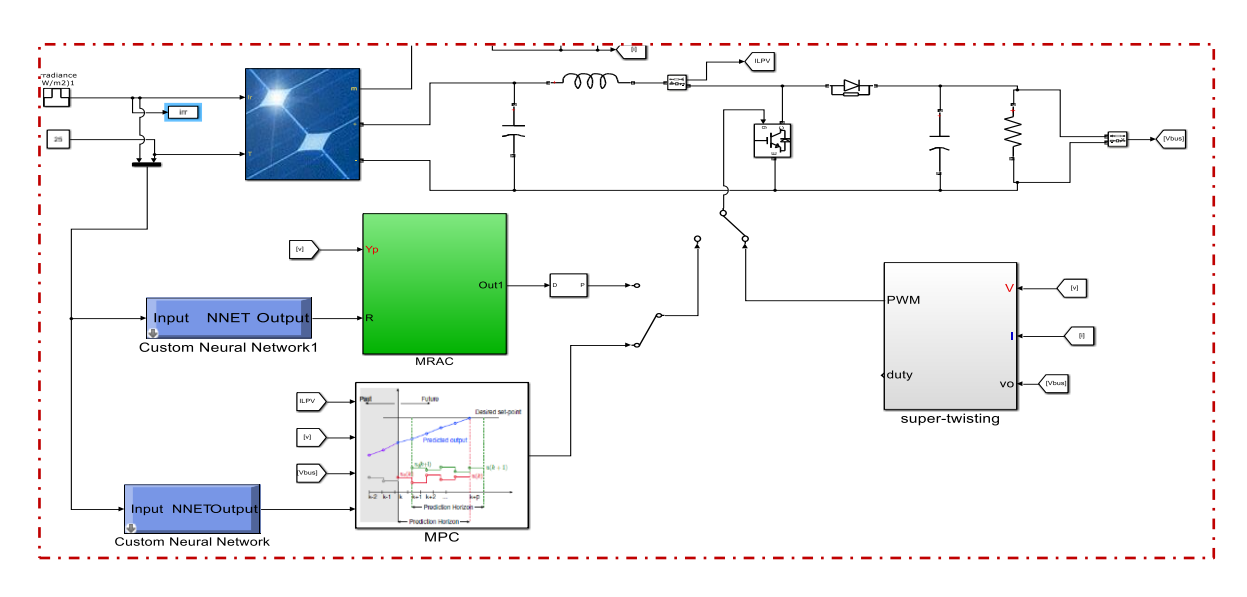


Figure 4.10: MATLAB Simulation of the Proposed MPPT Schemes.

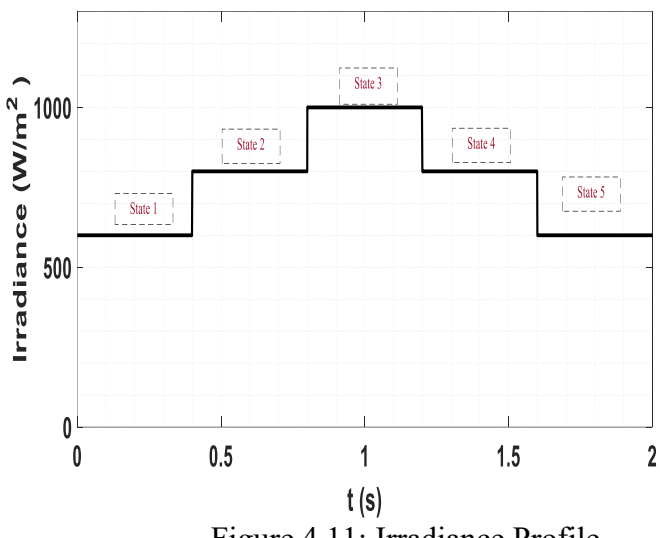


Figure 4.11: Irradiance Profile

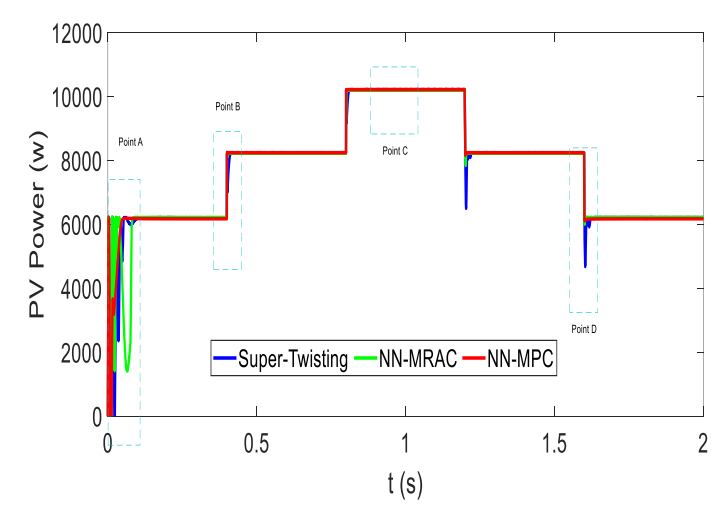


Figure 4.12: Dynamic Performance of the PV Power output.

The tracking efficiency, the overall efficiency and power loss; in addition to error metrics such as RMSE (Root Mean Square Error) and MAE (Mean Absolute Error). Figure 4.12 depicts the dynamic response of the PV power under stochastic irradiance using the developed MPPT methods. It can be seen that NN-MPC exhibits smoother tracking and minimal oscillations compared to NN-MRAC and STA. Furthermore, we specified different points from the power response and we zoomed-in on it, as shown in Figure 4.13. Accordingly, based on the zoom in point "A", both STA and NN-MRAC display significant fluctuations and slower convergence, whereas NN-MPC quickly stabilizes near the MPP. Moreover, STA exhibits a deep undershoot before settling, while NN-MPC maintains a more stable transition, as depicted at Point "B". Likewise, point "C" highlights the superior steady-state response of NN-MPC, which exhibits minimal oscillations compared to NN-MRAC and STA, where they showed noticeable fluctuations. Additionally, Point D reinforces this trend, where STA exhibits a large deviation before stabilization, while NN-MPC and NN-MRAC ensure a faster response. The PV voltage response is illustrated in Figure 4.16. the latter certainly confirms the previous observations. During transient conditions, STA exhibits sharp voltage deviations, indicating less robust performance under rapid irradiance changes. In contrast, NN-MPC and NN-MRAC maintain more stable voltage levels, with NN-MPC demonstrating the least deviation. In addition, the PV current output, as illustrated in Figure 4.17, further reflects these trends. Meanwhile, the P–V characteristics as shown in Figure 4.18 provide a clear visual comparison of how each algorithm achieves the MPP. And as such, STA's trajectory, obviously deviates more significantly around the MPP, while NN-MRAC and NN-MPC remain closer to the theoretical peak, with NN-MPC nearly overlapping the optimal point. Moreover, in terms of total efficiency as shown if Figure 4.14, NN-MPC accomplishes the highest value at 98.734%, followed by STA at 98.61%, and then NN-MRAC at 98.12%. The three MPPT algorithms have significantly varied performances regarding power loss under varying irradiation conditions. NN-MRAC records the highest power loss (Average) at 118.48W, then STA has a power loss at approximately 89.79 W, whereas NN-MPC incurs the lowest value of 79.16 W, as illustrated in Figure 4.15. The aforementioned details have been summarized in Table IV.

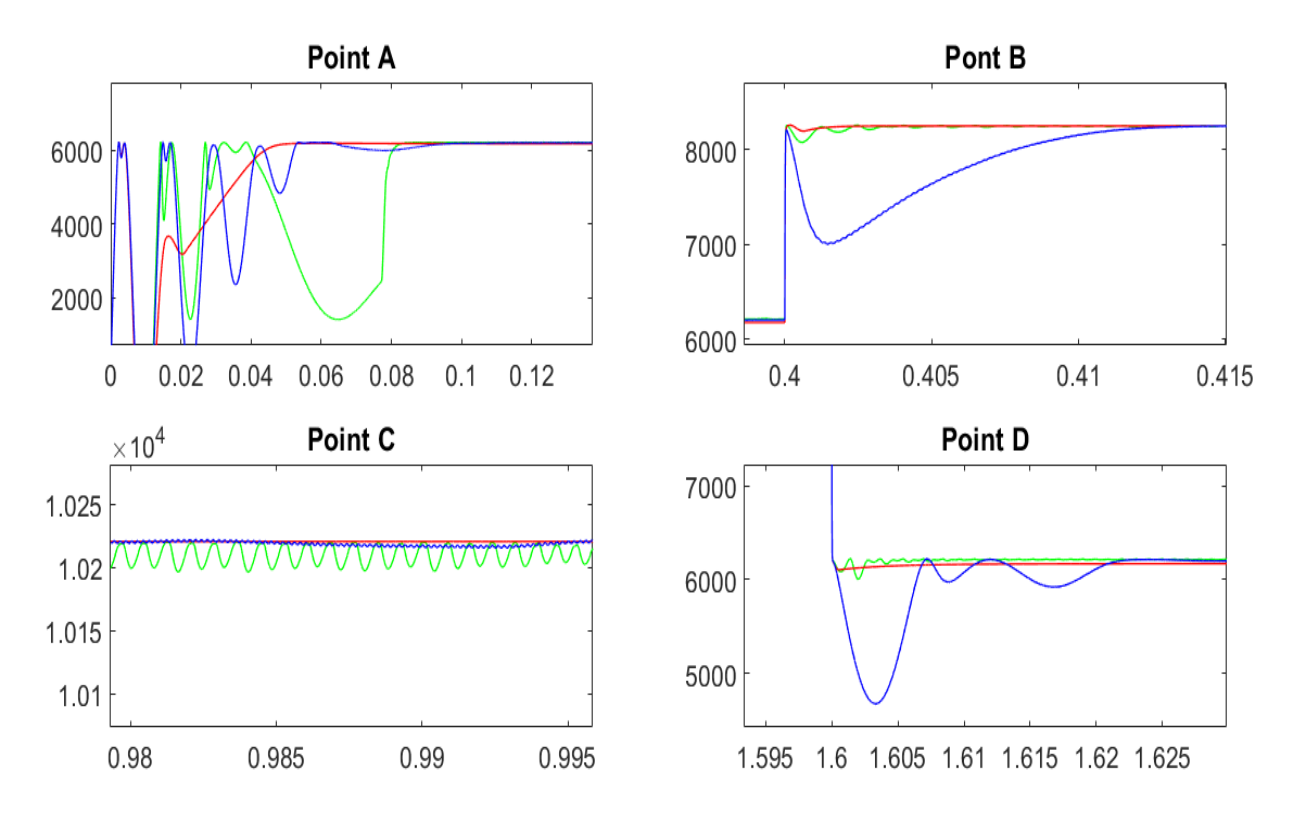


Figure 4.13: Zoom-in of the Power response.

Table II: In-depth comparative examination.

| MPPT Algorithm | | | Metrices | | |
|-------------------|---------|----------------|-------------------|----------|----------|
| Aigorithin | State | Efficiency (%) | Power Loss (W) | RMSE | MAE |
| STA - | State 1 | 94.13 | 364.82 | 1352.4 | 364.8387 |
| | State 2 | 99.80 | 16.33 | 112.1739 | 16.8915 |
| | State 3 | 99.75 | 25.16 | 93.4313 | 25.1687 |
| | State 4 | 99.75 | 20.49 | 153.5802 | 21.2408 |
| | State 5 | 99.64 | 22.16 | 141.3978 | 22.4328 |
| NN-MRAC | State 1 | 90.91 | 564 | 1633.7 | 565.2582 |
| | State 2 | 99.97 | 2.30 | 13.7385 | 3.6558 |
| | State 3 | 99.79 | 21.40 | 25.3271 | 21.4091 |
| | State 4 | 99.96 | 2.95 | 20.5725 | 4.5136 |
| | State 5 | 99.97 | 1.76 | 14.9367 | 2.8626 |
| NN-MPC | State 1 | 94.45 | 344 | 1272.8 | 344.6851 |
| | State 2 | 99.99 | 0.108 | 11.9953 | 0.2990 |
| | State 3 | 99.89 | 11.11 | 17.1796 | 11.1118 |
| | State 4 | 99.99 | 0.36 | 11.8895 | 0.5331 |
| | State 5 | 99.35 | 40.22 | 42.3606 | 40.4017 |

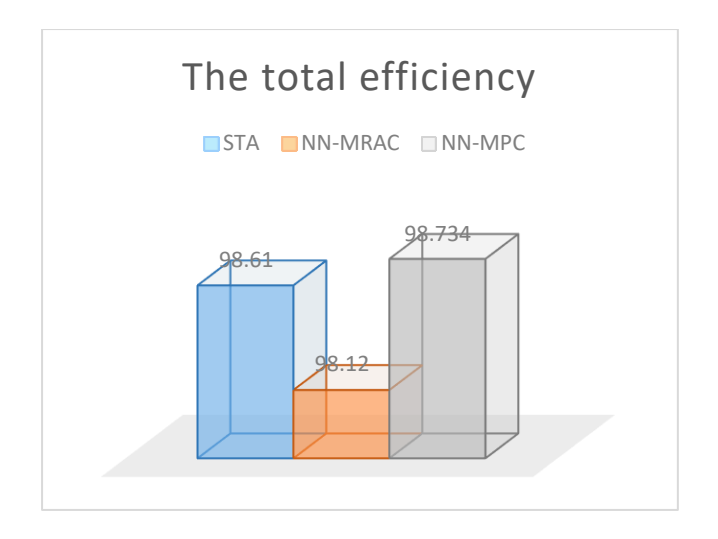


Figure 4.14: Graphical representation of the total efficiency.

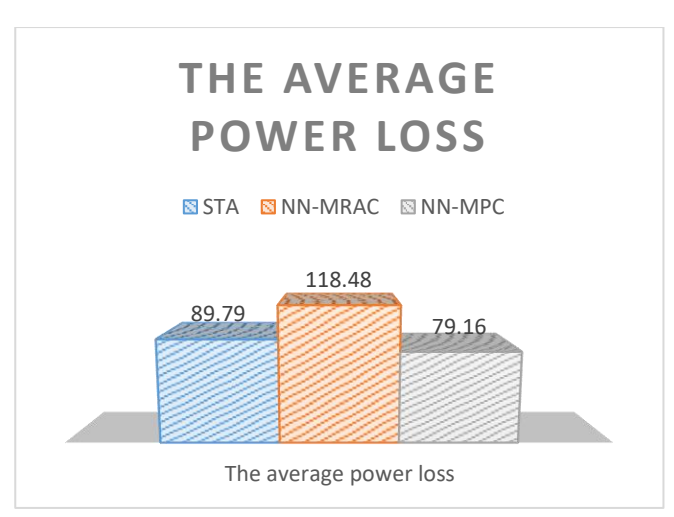


Figure 4.15: Graphical representation of the power loss.

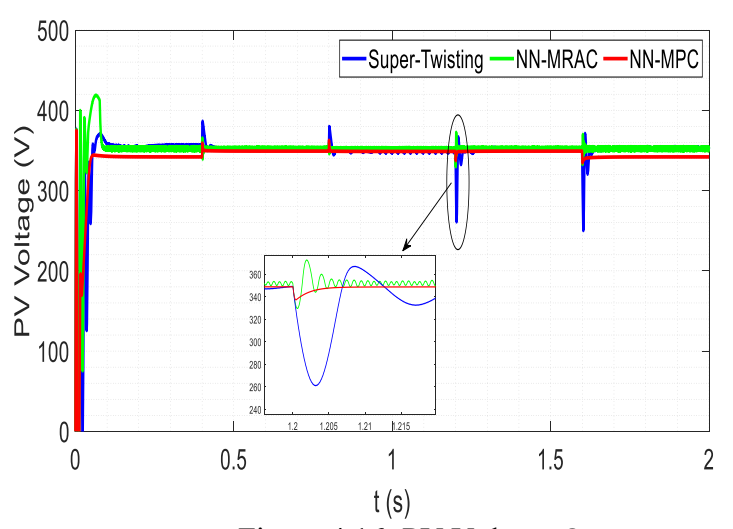


Figure 4.16: PV Voltage Output.

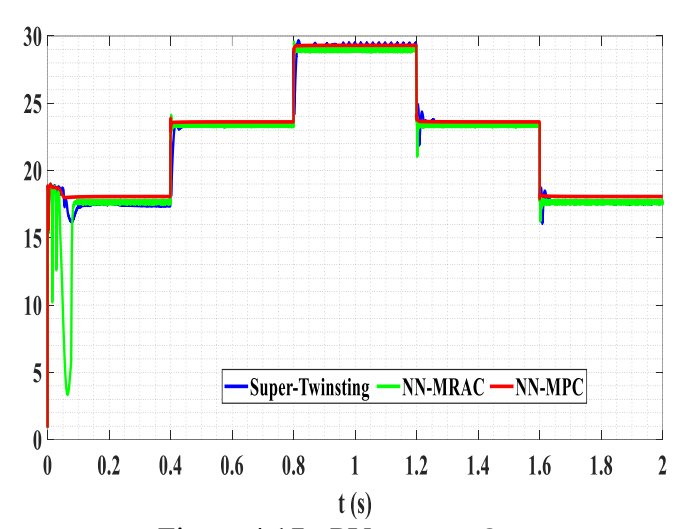


Figure 4.17: PV current Output.

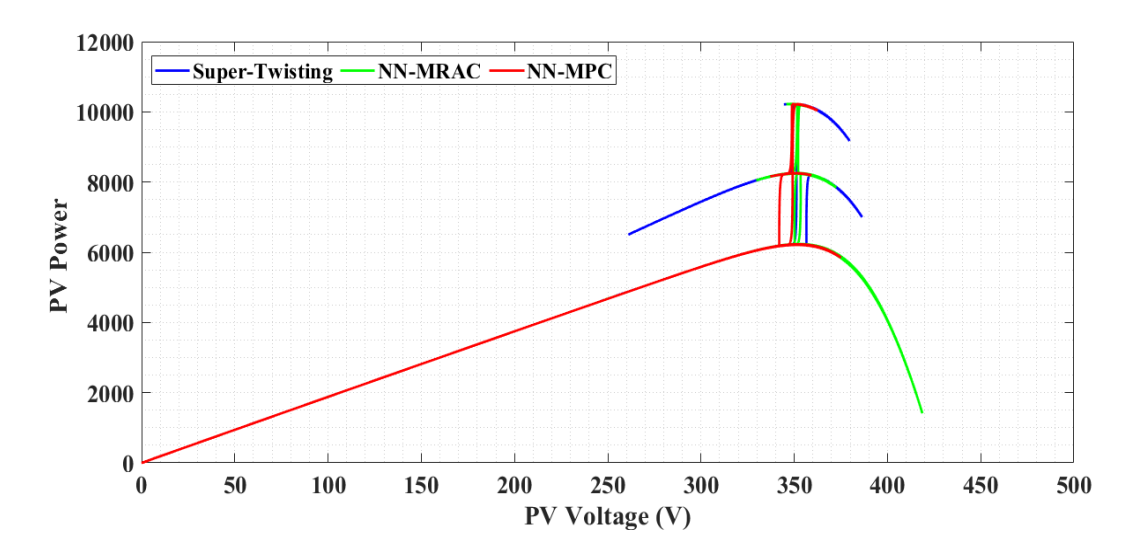


Figure 4.18: P-V characteristics under the proposed MPPT control.

4.3 Control Design for PMSG -Based-WECS

This section will delve into the control strategies employed for (PMSG-WT). The inherent uncertainties associated with PMSG-based WECS can limit the effectiveness of traditional control methods, which may struggle to meet the stringent performance requirements. Therefore, robust and efficient control strategies are imperative for wind energy conversion systems to maximize their performance. As mentioned in [168], the control structure of WT systems divided into two main control loops. The inner control loop which deals with the electric generator part through the power converter. While the outer control loop focusses on the aeroturbine which includes the MPPT bloc. The latter mainly generates the reference input to the inner loop.

4.3.1 MPPT Control

To address the unpredictable nature of wind, it is crucial to optimize power extraction from wind energy using an MPPT controller. The latter allows for the adjustment of the wind turbine's velocity to the optimal value that aligns with the MPP. Therefore, the power coefficient $C_p(\lambda,\beta)$ should approach its maximum value by adjusting either the tip speed ratio or the pitch angle. A practical approach is to fix the pitch angle at its optimal value and track the tip speed ratio to achieve λ_{opt} , where $C_p(\lambda_{opt},\beta_{opt})=C_p^{\max}$ reaches its maximum.

Consequently, the speed reference Ω_t^* expressed in the following manner

$$\Omega_t^* = \frac{\lambda_{opt} \cdot V_v}{R} \tag{4.29}$$

Subsequently, to provide a reference electromagnetic torque, an appropriate speed control must be employed:

$$T_{em}^* = G_{reg} \cdot \left(\Omega_t^* - \Omega_t\right) \tag{4.30}$$

where G_{reg} refers to the speed controller. Figure (4.19) depicts the schematic of the speed control loop

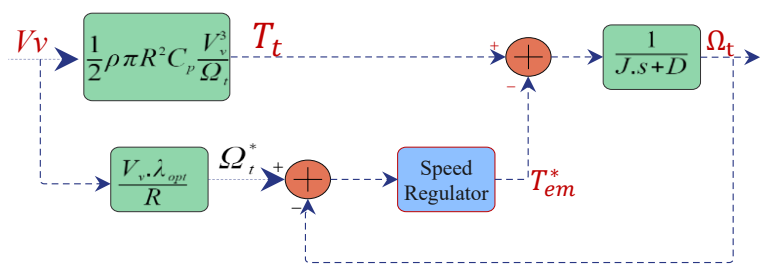


Figure 4.19: Mechanical speed control.

4.3.1.1 Proportional Integral (PI) Controller

This section focuses on an MPPT strategy utilizing a PI controller. The controller generates the control signal based on the error in rotor angular speed, as expressed by:

$$e_{\rm s} = \Omega_t^* - \Omega_t \tag{4.31}$$

Thus, the electromagnetic torque reference obtained as

$$T_{em}^* = K_{ps}.e_s + \int K_{is}e_s dt (4.32)$$

Here, k_{ps} and K_{is} represent the proportional and integral gains of the PI controller, respectively.

4.3.1.2 Super-Twisting Algorithm

Various factors within the studied system, such as oscillations in air density due to variations in altitude, humidity, and temperature, contribute to system uncertainty. The supertwisting control design algorithm effectively addresses these uncertainties and ensures a rapid response. The philosophy of this algorithm has been discussed previously. In this context, the STA relies solely on the information of the sliding surface S_{s} to produce the reference signal for the electromagnetic torque. Wherein the tracking error has been considered as the sliding surface for the STA, thus

$$\begin{cases}
S_S = e_S(\Omega_t) \\
T_{em}^* = \lambda'' \sqrt{|S_S|} . sign(S_S) - \gamma' \int sign(S_S)
\end{cases}$$
(4.33)

whereas, λ'' and γ' are constants gains.

This control strategy is composed of an algebraic term in addition to an integral term. Thus, this algorithm can be regarded as a nonlinear form of a PI controller.

4.3.2 PMSG Control

In this work, we employed the Field Oriented Control (FOC) strategy for the control of the PMSG. This approach offers a straightforward topology and represents a cost-effective solution for small-scale WT applications. The FOC operates within the synchronous reference frame and consists of an outer-loop speed controller accompanied by two inner-loop current controllers[169]. The q-axis reference current I_q^* is defined by the MPPT controller, while the d-axis reference current I_d^* is typically set to zero or determined as a function of I_q^* , contingent upon the specific control strategy employed; nevertheless, the ZDC (zero d-axis current) is the commonly used approach, therefore it was preferred in this work. Thus, the torque equation in (2.32) becomes as

$$T_{em} = \frac{3}{2} p \phi_f I_q \tag{4.34}$$

For the design of the controllers, selected as PI controllers, it is necessary to derive the transfer functions relating I_d to V_d to, and I_q to V_q . To begin, the equations for the Parktransformed voltages in Eq. (2.31), can be reformulated as follows:

$$\begin{cases} V_d = V_{d1} - emf_d \\ V_q = V_{q1} - emf_q \end{cases} \tag{4.35}$$

$$\begin{cases} emf_d = \omega_e L_d I_q \\ emf_q = -\omega_e \phi_f - \omega_e L_d I_q \end{cases}$$
(4.36)

Noteworthily, the variables emf_d and emf_q are treated as disturbances. While V_{d1}, V_{q1} represent the voltage components along the d-q axes, which regulate their respective current components.

$$\begin{cases} V_{d1} = R_s I_d + L_d \frac{dI_d}{dt} \\ V_{q1} = R_s I_q + L_q \frac{dI_q}{dt} \end{cases}$$

$$(4.37)$$

By applying Laplace transformation on Eq. (4.37), we get

$$\begin{cases}
V_{d1} = (R_s + sL_d)I_d \\
V_{q1} = (R_s + sLq)I_q
\end{cases}$$
(4.38)

Thus, based on equation (4.38), the transfers functions between the stator components I_d , I_q and V_{d1} , V_{q1} are defined as follows:

$$\begin{cases} \frac{I_d}{V_{d1}} = \frac{1}{R_s + + sL_d} \\ \frac{I_q}{V_{q1}} = \frac{1}{R_s + sL_q} \end{cases}$$
(4.39)

The overall structure of the PMSG based WECS control is illustrated in Figure (4.20).

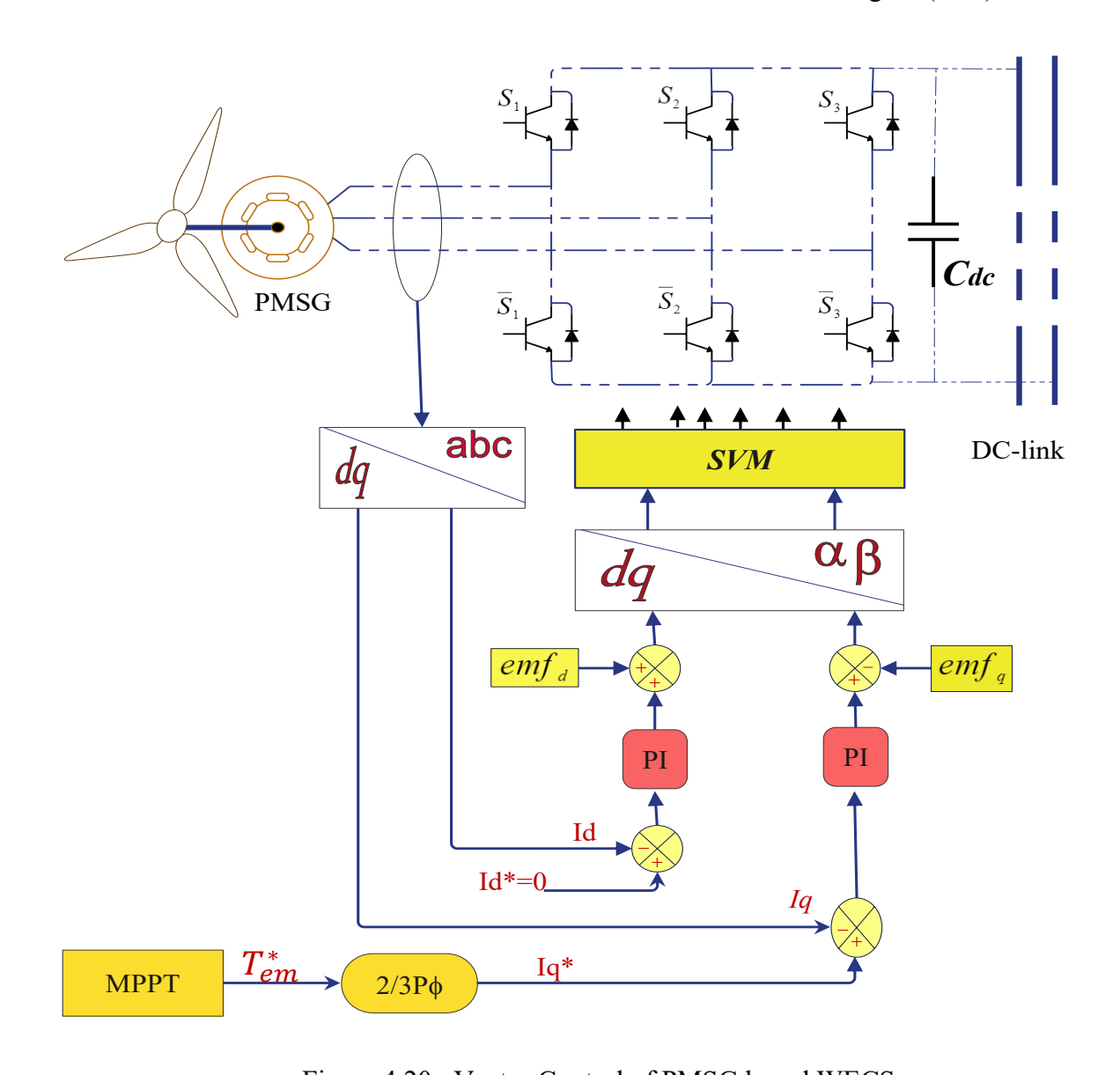


Figure 4.20: Vector Control of PMSG based WECS.

4.3.3 Performance Assessment via MATLAB environment

Numerical simulations were conducted using MATLAB/Simulink software as shown in Figure 4.21, to evaluate the robustness and efficacity of the proposed Super-twisting algorithm based-MPPT for WECS. The specifications of the WECS used in this simulation are as follows: a wind turbine of 8.5kw rated power with base wind speed of 14 m/s whereas its optimal tip speed ratio λ_{opt} and optimal Power Coefficient C_p^{max} are 8.144 and 0.48, respectively. For the PMSG: 2p=10; Stator phase resistance Rsr=0.425 Ω , Armature Inductance = 8.35mH, Friction Factor and Inertia constant are given as 0.001189 *N.m.s* and 0.01197 $kg.m^2$, respectively. The wind inflow used for in this simulation is given in Figure 4.22.

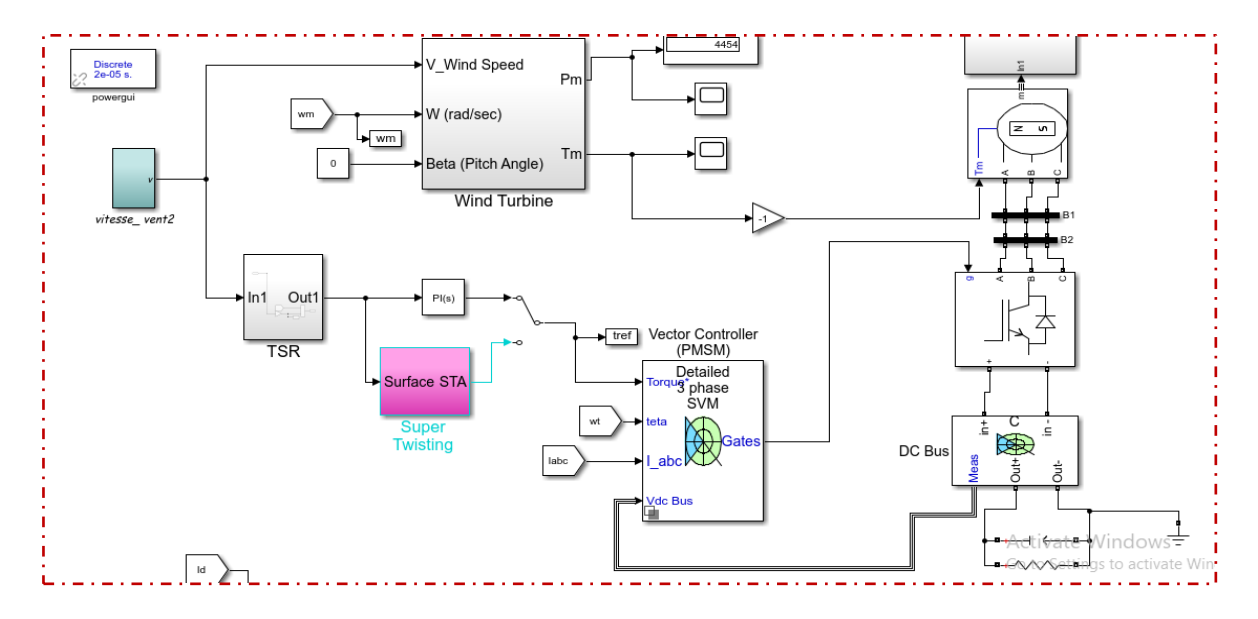


Figure 4.21 : Simulink Implementation of the proposed WECS along with the control scheme.

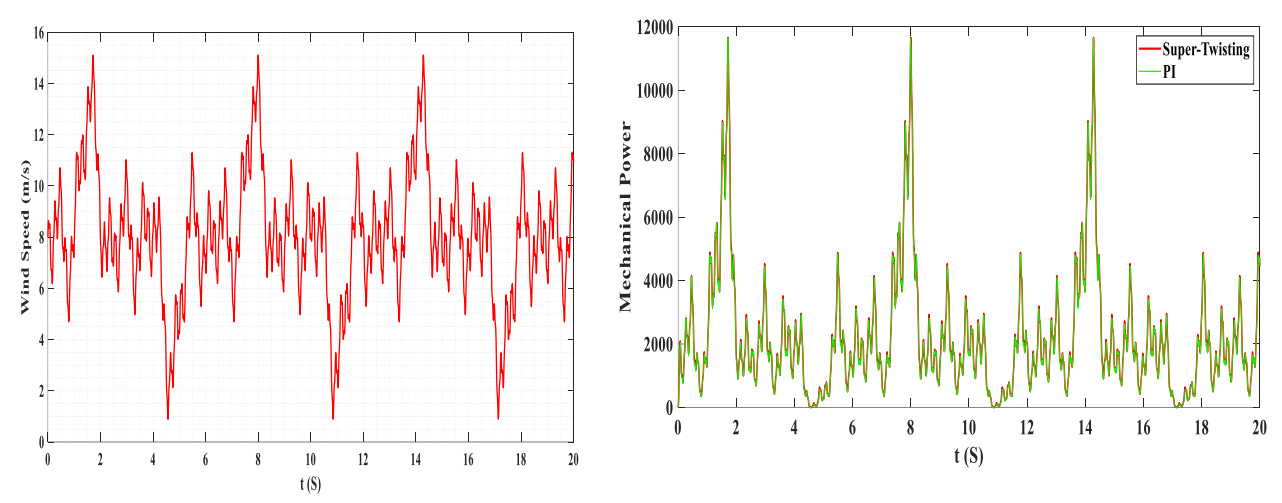


Figure 4.22: Wind Velocity.

Figure 4.23: Mechanical power response

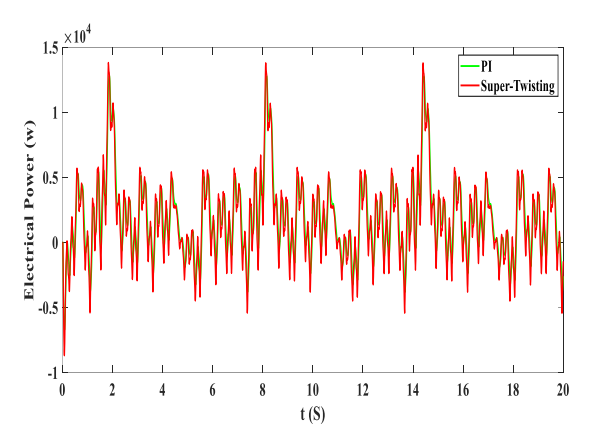


Figure 4.24: Electrical Power response.

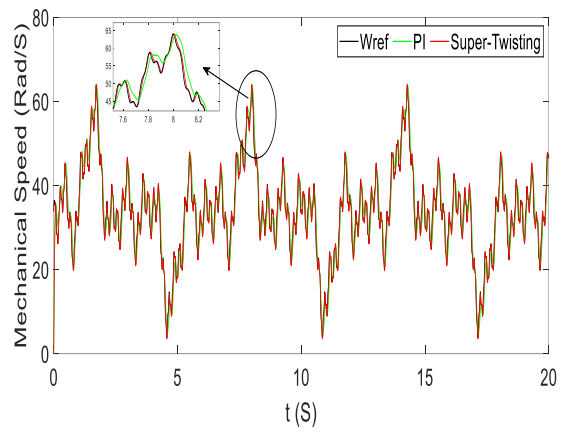


Figure 4.25 : Mechanical speed performance of the WT.

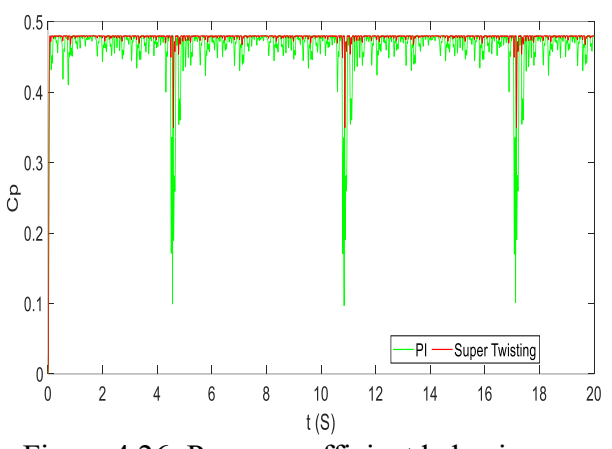


Figure 4.26: Power coefficient behavior.

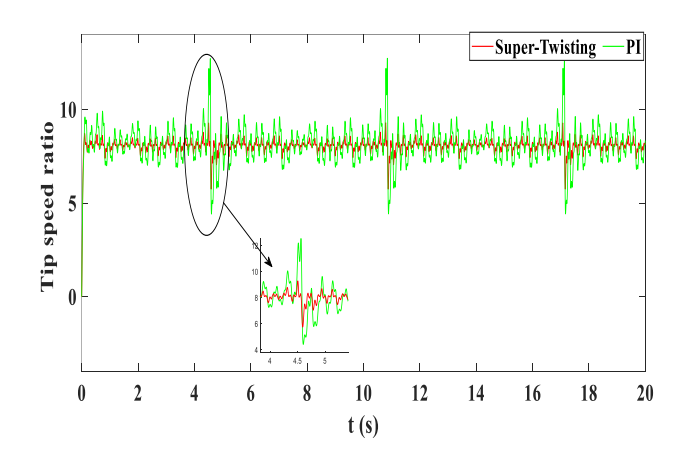


Figure 4.27: Tip Speed Ratio behavior.

In order to conduct an accurate comparison between the conventional MPPT control and the proposed MPPT scheme, several metrices have been chosen. The mechanical and electrical power responses are illustrated in Figures 4.23 and 4.24, respectively. Accordingly,

Table III:Performance Comparison.

| | MPPT | Efficiency (P) | | Performance Indices (Speed tracking error) | | | | |
|--|------|---|---------|--|----------|--------|--------|--|
| | | $\left(\frac{P_{actual}}{P_{max}}\right)$ | IAE | ITAE | ISE | RMSE | MAE | |
| | PI | 96.33 % | 46.4969 | 453.8576 | 171.8431 | 2.9313 | 2.3249 | |

| STA | 99.46 % | 13.0451 | 120.6838 | 36.3301 | 1.3480 | 0.6523 |
|-----|---------|---------|----------|---------|--------|--------|
| | | | | | | |

it may appear that the proposed controller archived results close to the conventional controller. However, finer observation suggests that STA reduces oscillations and has a smoother tracking behavior meaning less power fluctuation compared to the PI-based MPPT; in addition, the peaks in the response power are sharper for PI. Mechanical Speed Performance is depicted in Figure 4.25, it can be seen that reference speed (*Wref*) is closely tracked by both controllers. Nevertheless, STA provides better tracking precision, which is clearly shown in the zoomedin region, where it maintains a closer match to *Wref* than the PI controller. As well as the traditional controller exhibits higher deviations around transient points.

For more specifically, under varying wind speeds, optimal power extraction from the WECS is ensured by maintaining the power coefficient near its maximum value C_p^{max} and the tip-speed ratio close to its ideal value λ_{opt} . It is evident from Figures 4.26 and 4.27 that, within a stochastic wind environment, the tip speed ratio and the power coefficient Cp are readily sustained at their respective ideal values using the proposed MPPT. Consequently, the generator operates at an optimal velocity, enabling the Wind Energy Conversion System to harness maximum power from the wind. However, the PI-based MPPT exhibits obviously deeper drops in Cp, meaning it fails to maintain optimal conditions during transient disturbances. Furthermore, since TSR stability is crucial for efficient wind power extraction, STA proves to be superior.

For more details, Table V Summarizes additionally performance indices that confirm the superiority of the proposed algorithm. Quantitatively, the STA approach achieves higher efficiency (99.46% versus 96.33% for the PI controller) and markedly lower error indices across various metrics such as Integral of Absolute Error (IAE), Integral Time Absolute Error (ITAE), Integral of Squared Error (ISE), RMSE, and MAE, indicating its enhanced accuracy and responsiveness; where STA outperforms PI in all error metrics.

4.4 PEMFC Control Design

In this work, the PEMFC serves as a secondary energy source. Therefore, the primary objective of the control system is to ensure that the system consistently tracks the reference currents supplied by the energy management algorithm, regardless of the specific controller employed. The proposed closed-loop PEMFC system including the used DC-DC converter and its controller is depicted in Figure (4.28). It is noted that the MPC controller has been preferred

to track the desired reference generated through the EMS bloc. Hence, the design of an MPC controller for a boost converter was discussed in Subsection (4.2.3).

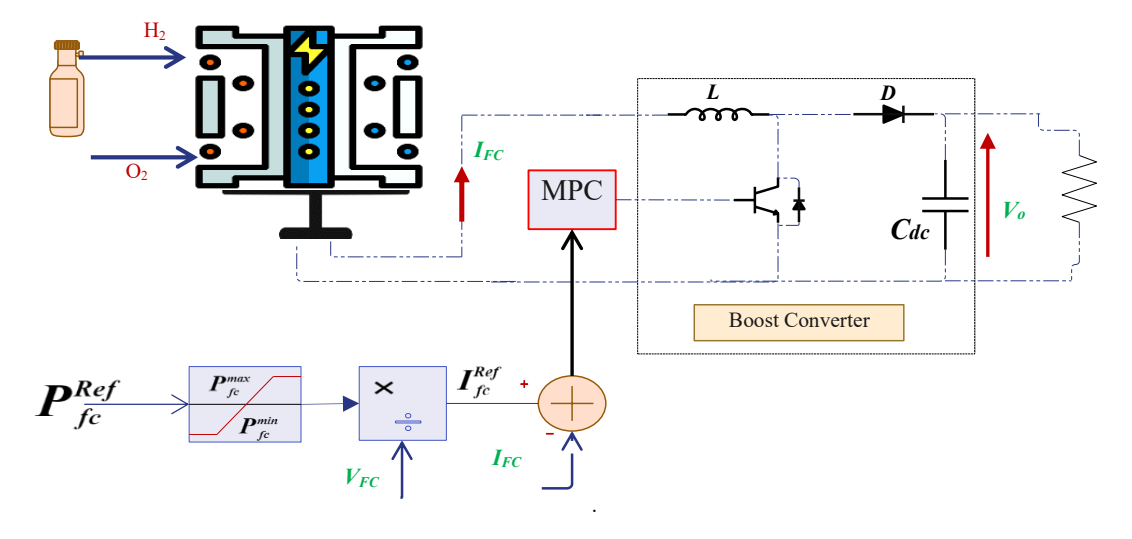


Figure 4.28: The proposed FC system control.

Indeed, different constraints must be taken into consideration in the control design; including that the FC power or current should be maintained within a specified range, such that: $P_{fc}^{ref} \in \left\{10\%P_{fc}^{\max} - -90\%P_{fc}^{\max}\right\}$ [170]. The latter procedure must be conducted in order to prevent the fuel starvation phenomenon in addition to excessive load.

4.4.1 Performance Assessment

The entire system illustrated in figure 4.28 has been simulated in MATLAB/Simulink environment. The power tracking performance is presented in Figure 4.29. Hence, the black dashed curve represents the power reference, and the red solid line is the actual power output of the PEMFC. As depicted, it is clearly that the actual power tracks accurately the reference levels during each step change with a settling of 6.1 ms. In addition, during each transition, the system demonstrates only slight variances from the desired power. Furthermore, once settled, the actual power aligns almost exactly with the reference, implying negligible steady-state error. Accordingly, the FCS-MPC demonstrates strong closed-loop performance, which provides accurate reference tracking, maintains low transient times, and exhibits negligible steady-state error.

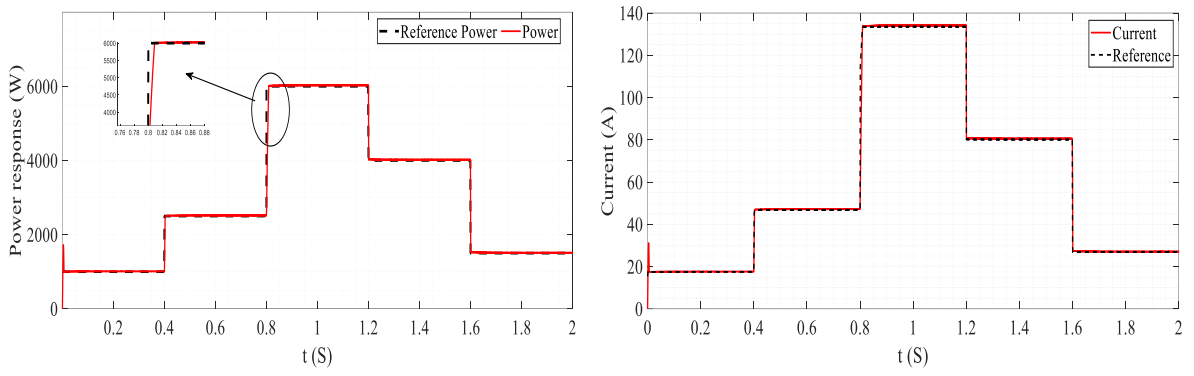


Figure 4.29: Power tracking behavior.

Figure 4.30: Response of the FC current.

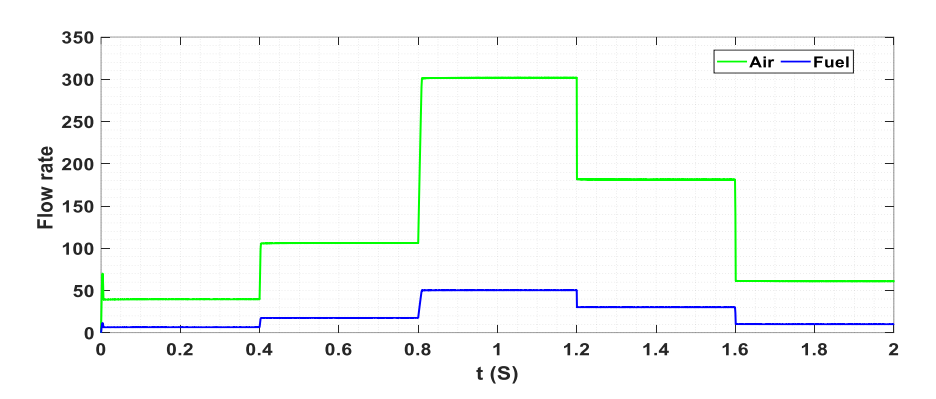


Figure 4.31: Fuel consumption.

4.5 FCS-MPC for Three-Phase Grid-Tied 3-Level NPC Inverter

For grid integration, the employing of a simple conventional inverter with two levels generates a square wave, which is inadequate for most complex applications. It is preferred to have a pure sinusoidal waveform in such applications[171]. Furthermore, the power rating of conventional converters is constrained by the rated power capacity of the semiconductor devices employed and the permissible switching frequencies. According to the literature, as the number of levels in an inverter increases, the output waveform approaches a pure sinusoidal form. Additionally, the Total Harmonic Distortion (THD) is significantly reduced with a higher inverter level. However, increasing the number of levels in the inverter also results in a more complex and costly overall system[172].

Recently, the rapid advancement of renewable energy technologies has brought significant attention to Neutral-Point Clamped (NPC) three-level inverters. These inverters are favored for their enhanced harmonic performance, capability to operate at higher voltages, reduced power losses, and minimized switching stress[173]. As discussed previously, several control strategies have been adopted in this context, nevertheless, in the past few years, MPC

control especially Finite Control Set (FCS-MPC) approach has gained prominence as an effective control strategy, widely advocated for achieving robust control of grid tied inverters due to its flexibility in handling nonlinearities, constraints, and various intricate demands[174].

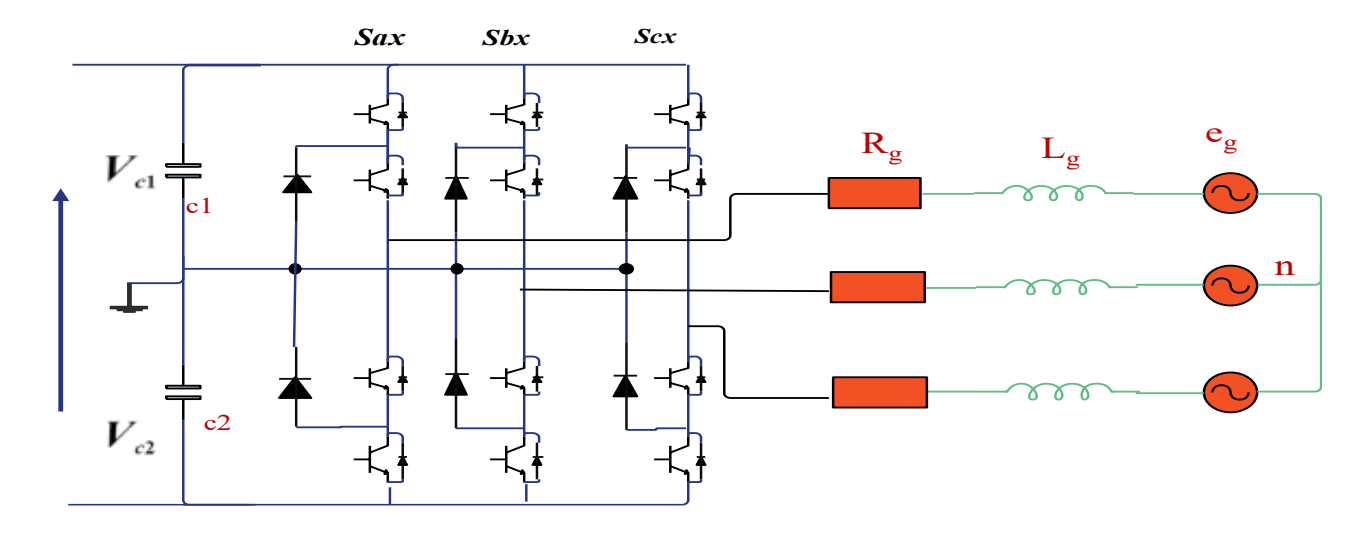


Figure 4.32: Schematic of a grid-tied NPC inverter.

The circuit of an NPC inverter in grid connected mode is depicted in Figure (4.32). This configuration includes four single-directional power switches per arm, along with two Clamping diodes (CD). Two input capacitors to divide the blocking voltage (BV). Clamping diodes (CD) are arranged in series due to the variable voltage stresses on these clamping diodes[172]. Where, V_{dc} represents the DC-link voltage; C_1 and C_2 denote the DC-link capacitors; R_g and L_g correspond to the equivalent resistance and filter inductance, respectively.

4.5.1 Mathematical Model

The inverter generates three voltage levels $\left(-\frac{V_{dc}}{2},0,\frac{V_{dc}}{2}\right)$. When the upper two switches S_{a1} and S_{a2} are activated, phase A output become $\binom{V_{dc}}{2}$. When the lower two switches S_{a3} and S_{a4} are activated, phase A output is $-\frac{V_{dc}}{2}$. If the middle switches S_{a2} and S_{a3} are activated, the voltage of phase A is zero. The aforementioned states are denoted as (+,-, and 0) respectively. Table (VI) below summarizes the possible switching states of a 3-L NPC inverter. Considering the valid switching states generated by the three legs of the NPC converter, a total of $m=3^3=27$ switching states are produced for the entire power converter. In the α β reference frame, this results in 19 nonredundant vectors and eight redundant vectors.

Table IV: NPC-Inverter switching states.

| Sx | Sx_1 | Sx_2 | Sx_3 | Sx_4 | Output |
|----|--------|--------|--------|--------|---------------------|
| + | 1 | 1 | 0 | 0 | $\binom{V_{dc}}{2}$ |
| 0 | 0 | 1 | 1 | 0 | 0 |
| - | 0 | 0 | 1 | 1 | $-V_{dc}/2$ |

Consequently, the dynamic model of the grid-tied inverter is derived as follows:

$$\begin{cases} V_a = L_g \frac{d(I_a)}{dt} + e_{ga} + R_g I_a \\ V_b = L_g \frac{d(I_b)}{dt} + e_{gb} + R_g I_b \\ V_c = L_g \frac{d(I_c)}{dt} + e_{gc} + R_g I_c \end{cases}$$

$$(4.40)$$

Using the Clarke transformation on Eq. (4.40), the grid currents can be represented in the α β two-phase reference frame as:

$$\begin{cases} \frac{d(I_{\alpha})}{dt} = \frac{1}{L_g} \left[-R_g I_{\beta} - e_{g\alpha} + V_{\alpha} \right] \\ \frac{d(I_{\beta})}{dt} = \frac{1}{L_g} \left[-R_g I_{\beta} - e_{g\beta} + V_{\beta} \right] \end{cases}$$
(4.41)

4.5.2 FCS-MPC Design

To implement FCS-MPC for regulating the current in a three-phase inverter, it is essential to apply discrete-time techniques to derive the time-discretized form of Eq. (4.41). Given the one-step prediction horizon, the Euler method is particularly suitable for estimating the future values of controlled variables with a high degree of accuracy. This approach yields the following forward Euler approximation for the derivative:

$$\frac{dI(t)}{dt} = \frac{I(k+1) - I(k)}{T_{s}}$$
 (4.42)

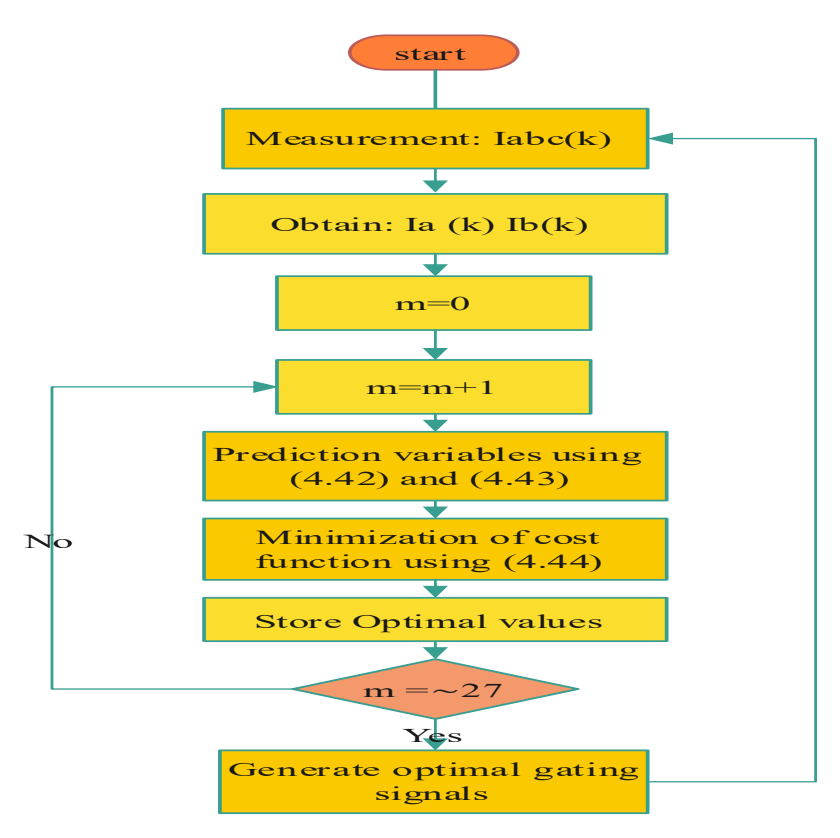


Figure 4.33: FCS-MPC Flowchart for 3-level inverter.

The dynamics of the grid current can be represented through the application of Euler's discretization method as follows:

$$\begin{bmatrix} I_{\alpha}(k+1) \\ I_{\beta}(k+1) \end{bmatrix} = (1 - \frac{RT_s}{L_g}) \begin{bmatrix} I_{\alpha}(k) \\ I_{\beta}(k) \end{bmatrix} + \frac{T_s}{L_g} \begin{bmatrix} V_{\alpha}(k) - e_{g\alpha}(k) \\ V_{\beta}(k) - e_{g\beta}(k) \end{bmatrix}$$
(4.43)

In the final stage, the predicted variables are evaluated against their reference values through a cost function, \widehat{g} , defined as follows:

$$\hat{g} = \|I_{\alpha}(k+1) - I_{\alpha}^{*}\| + \|I_{\beta}(k+1) - I_{\beta}^{*}\|$$
(4.44)

The objective of optimizing the cost function is to bring the value of \widehat{g} as close to zero as possible. The switching state that minimizes this cost function is selected and applied in the subsequent sampling interval. Figure (4.33) illustrates the flowchart diagram of this control algorithm.

4.5.3 Performance Assessment of the Grid Connected Mode

Numerical simulation results have been undertaken to evaluate the performance of the suggested control method for the hybrid system. The models of wind, photovoltaic, fuel cell, bidirectional 3-Level NPC Inverter in addition to Utility grid system are implemented in

MATLAB/Simulink, as shown in Figure 4.34. In the subsequent sections, the presented wind-PV-FC cogeneration system is evaluated under highly demanding operational conditions that might hardly ever arise in reality, such as abrupt changes in wind velocity and significant fluctuations in solar irradiance. These extreme conditions are deliberately imposed to test system stability and validate the performance of the implemented control strategies. The performance evaluation was divided into two distinct scenarios to assess the system's stability and control response effectiveness.

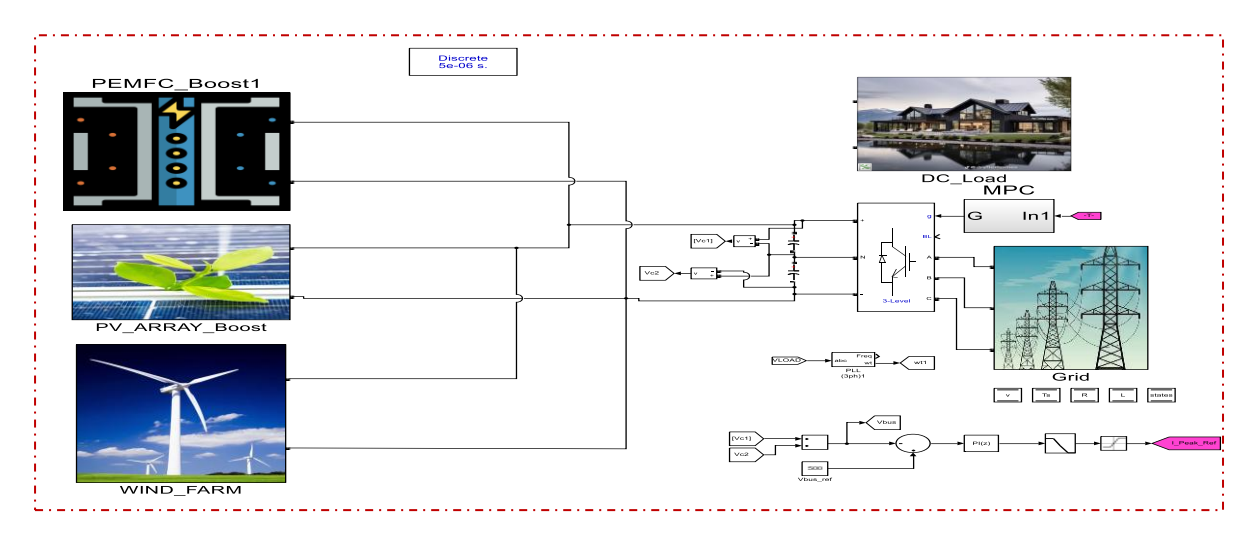


Figure 4.34: Simulink model of the proposed hybrid system integrated to the network.

Case Study 1: Wind-PV-PEMFC cogeneration under varying irradiance and constant wind speed

In order to investigate the influence of solar irradiance fluctuation on the grid-connected system and the robustness of the proposed control shame against this challenge, the PV generator is operated under variable irradiance, as illustrated in Figure 4.35 while the wind generator is operated at constant wind speed. The sun irradiation increases from 500 W/m^2 to 1000 W/m^2 at t=1 s, then decreases from 1000 W/m^2 to 500 W/m^2 at t=2 s. These variations are used to assess how the system adapts to changes in PV input.

Figure 4.36 presents the offered power from the hybrid RE sources. The PV power shows a sudden increase at t=1s and sudden decrease at t= 2 s, while the WT and FC power remains nearly constant. The DC bus voltage behavior during the studied case given in Figure 4.38. It can be seen even with the change in solar irradiance; the DC-link voltage remains close to the reference (500 V) during the whole simulation with small oscillations. Zoomed-in sections highlight minor deviations at approximately 1.02s and 2.02s, which corresponding to changes in PV power. Subsequently, the proposed control scheme effectively regulates the

voltage, ensuring that the inverter has a reliable input under Stable DC Bus. The injected power into the grid which presented as active and reactive power shown in Figure 4.37. The system successfully supplies active power while maintaining a near unity power factor, which is beneficial for grid stability. Furthermore, it is evident from this figure that the grid inverter

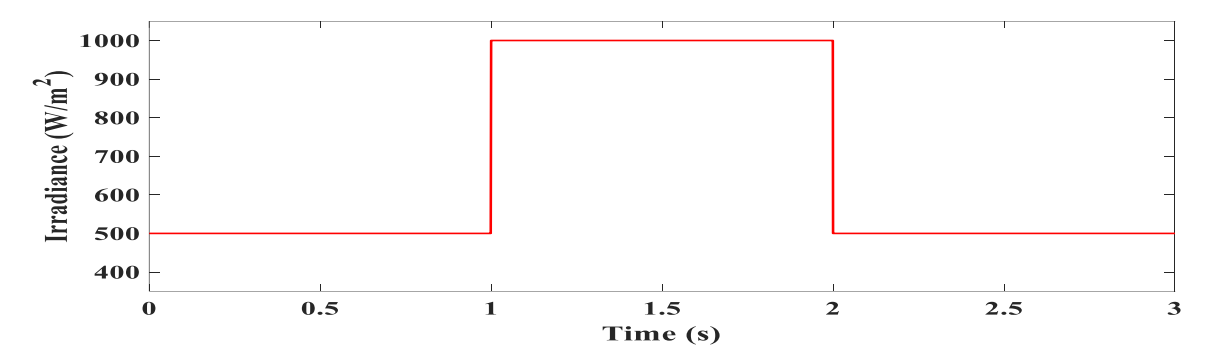


Figure 4.35 : Solar Irradiance.

passed into the distribution grid all the power from the renewable energy sources. Hence, the output power from these sources is similar to Active power in the grid side. This can confirm that the suggested control strategy (FCS-MPC) can balance the dynamic power contributions while meeting grid requirements. The grid current waveforms are illustrated in Figure 4.39. The results show balanced three-phase currents with periodic variations corresponding to changes in power generation. A zoom-in view (Figure 4.40) confirms that the transient responses are well-managed, indicating low distortion and effective synchronization with the grid. This, demonstrates the effectiveness of the FCS-MPC in mitigating switching and dynamic disturbances.

FFT Analysis under Different Irradiation States is depicted in Figure 4.41. The Total Harmonic Distortion (THD) values for different solar irradiation conditions marked as follows: 0.91 % for State 1, State 2 (1.19 %), and 0.91 % for State 3. FFT analysis shows that, even with varying irradiance levels, the harmonic content remains controlled. The system maintains THD below 1.2 %, which is well within IEEE 519 standards for grid-connected inverters (typically requiring THD < 5 %). This reinforces that the converter design and control scheme are successful in minimizing unwanted spectral components.

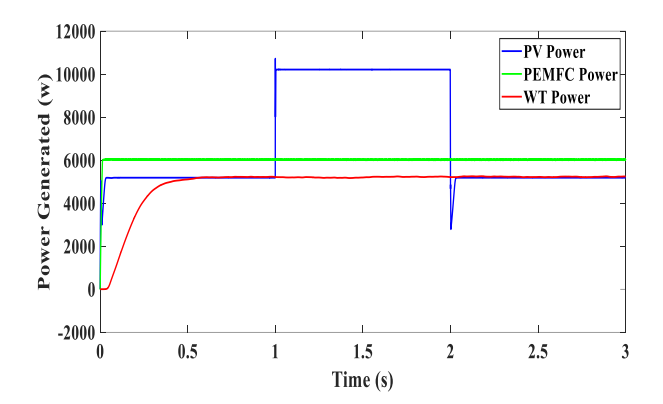


Figure 4.36 : Power response of the different sources.

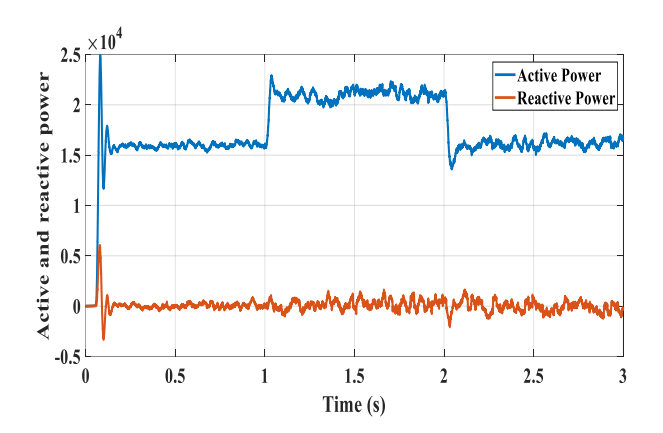


Figure 4.37: Active and Reactive power injected into the grid.

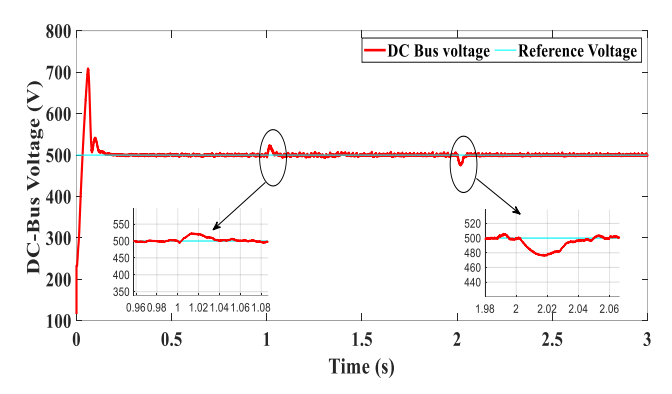


Figure 4.38: DC-Link Voltage performance.

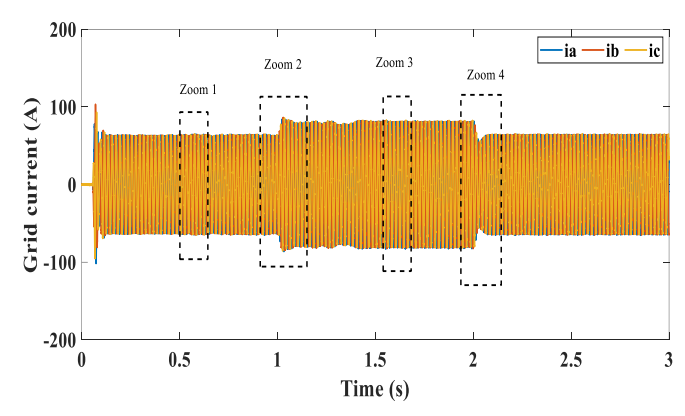


Figure 4.39: Grid Current performance.

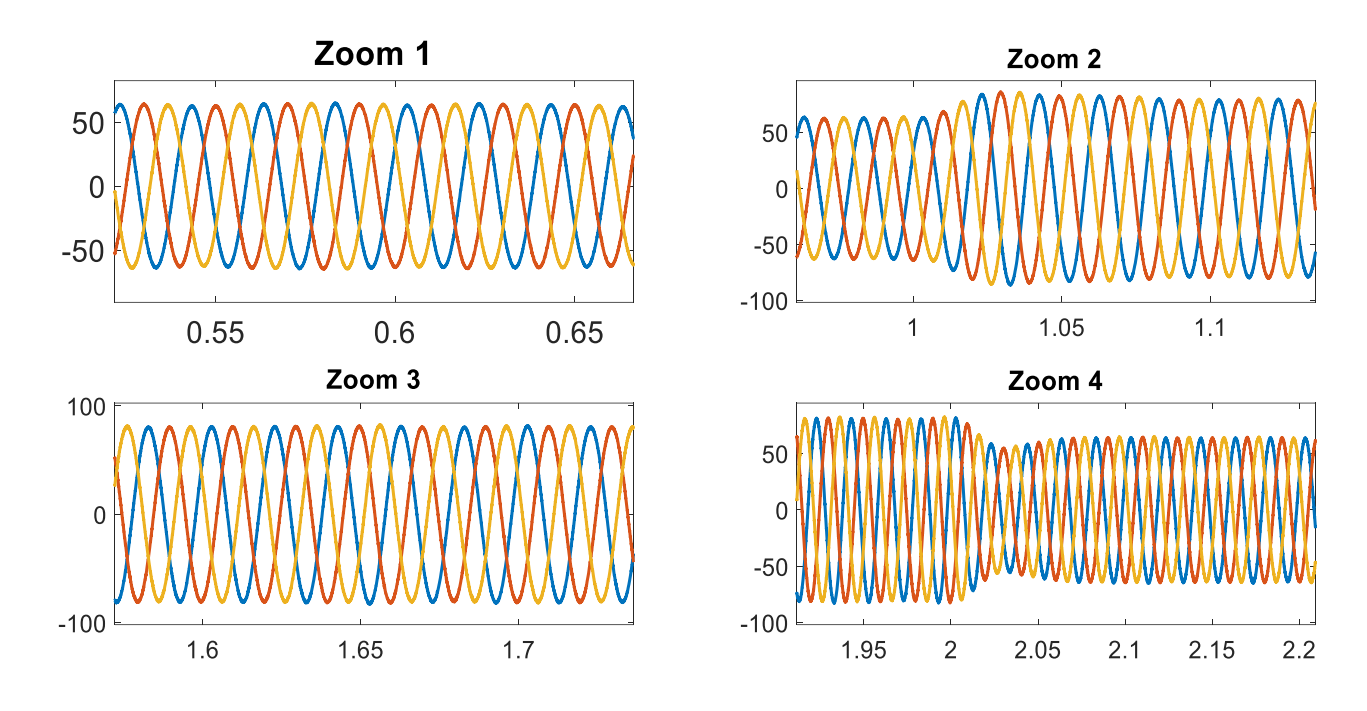


Figure 4.40: Zoom-in of the grid current response.

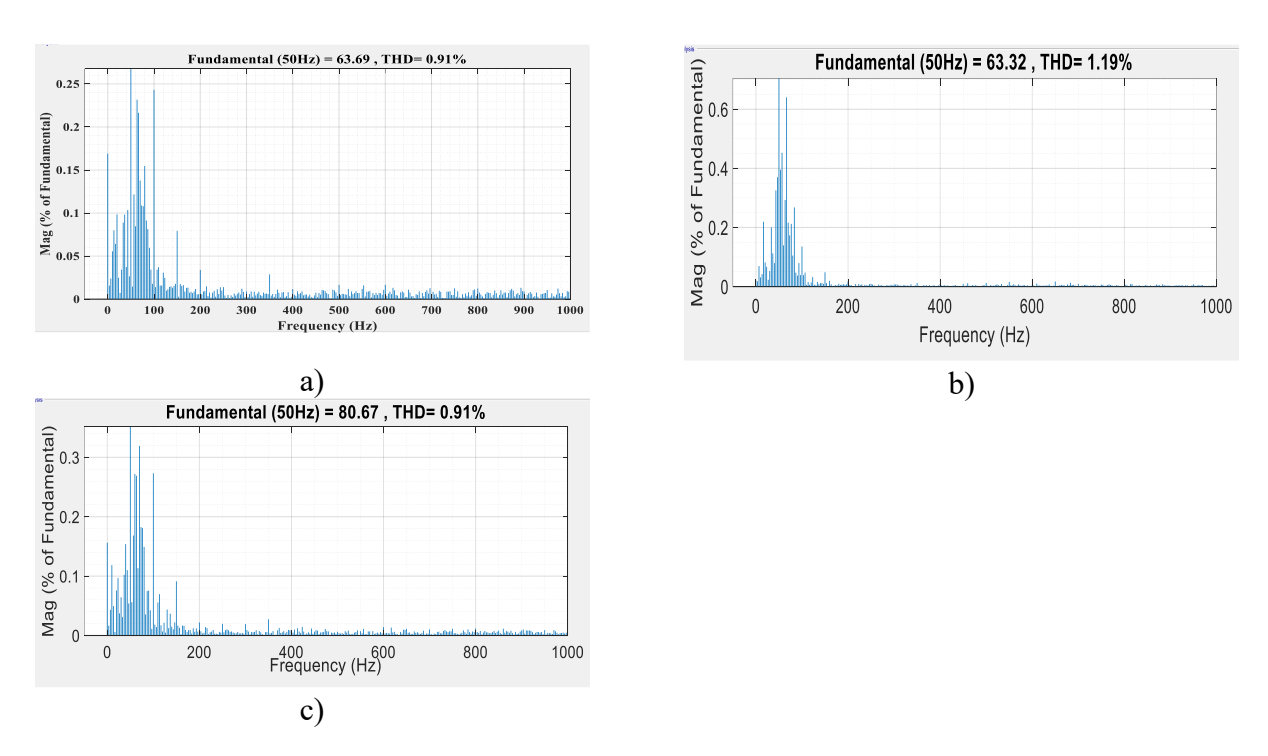


Figure 4.41: FFT Analysis for different irradiation states. a) State 1 (500 w/m 2), b) State 2 2(1000 w/m 2), State 3 (500 w/m 2).

Case Study 2: Wind-PV-PEMFC cogeneration under varying wind speed and constant irradiance

The purpose of this case is to evaluate the system's ability to handle fluctuations in wind power while maintaining stable operation. Since wind speed is inherently variable and can change rapidly, it is crucial to assess how the hybrid system balances power contributions. Where, the wind generator is supplying power under varying wind speed as shown in Figure 4.42. At start, the wind speed is 12 m/s and then drops to 8 m/s at t = 1 s, after that the wind speed jumps to 15 m/s at t = 2 s. on the other hand, we kept the irradiance at a fixed level $(1000w/m^2)$.

The provided powers from the hybrid RES are depicted in Figure 4.44. As wind speed changes, the wind turbine's power output varies accordingly, while the PV and PEMFC units maintain their contributions constant. Figure 4.43 demonstrates satisfactory performance in regulating the DC bus voltage. Even with variable wind input, the DC-link voltage remains stable, indicating a robust energy sharing and powerful regulation within the system. The injected Active and Reactive power are presented in Figure 4.44. This figure clearly indicates that the active power is nearly equivalent to the power supplied by the hybrid sources. Conversely, the reactive power exchange from the grid is sustained at nearly zero in this scenario. Notwithstanding variations in wind speed input, ensuring stability and efficient power supply to the grid highlights the efficacy of the control systems. The grid current waveforms can be seen in Figure 4.46, while Figure 4.47 provides four zoomed-in snapshots at different intervals. These waveforms illustrate how the system responds to changes in wind speed while maintaining a stable, sinusoidal current output. Despite existing distinct transitions in current magnitude, however, these transitions are corresponded to the system adjusting its output as wind speed varies. This means the proposed control technique (FCS-MPC) effectively maintained sinusoidal currents, as well as it ensured smooth transitions, devoid of significant noise or oscillations. The total harmonic distortion was calculated with MATLAB Simulink FFT analysis. The current THD at the grid side, as depicted in Figure 4.48, are 1.74%, 1.92%, and 0.78%, all of which are below the permissible THD of 5% as stipulated by IEEE standards for grid-connected renewable systems. These FFT analyses confirm that the proposed hybrid system, under varying wind speeds, delivers low-distortion current to the grid. The proposed control scheme adeptly adjusts to different power levels, keeping harmonics at a minimum. Notably, the highest wind speed (15 m/s) corresponds to the lowest THD (0.78%), showcasing the inverter's efficiency and stability in high-power scenarios.

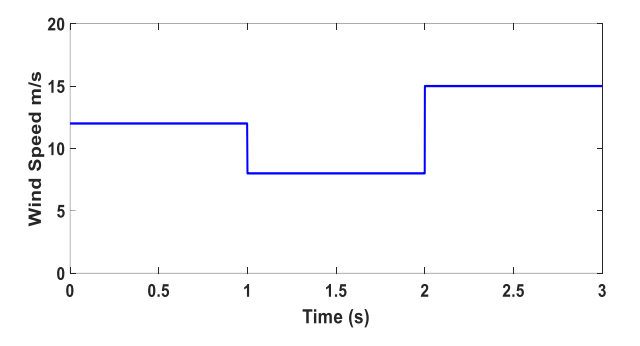


Figure 4.42: Wind Velocity.

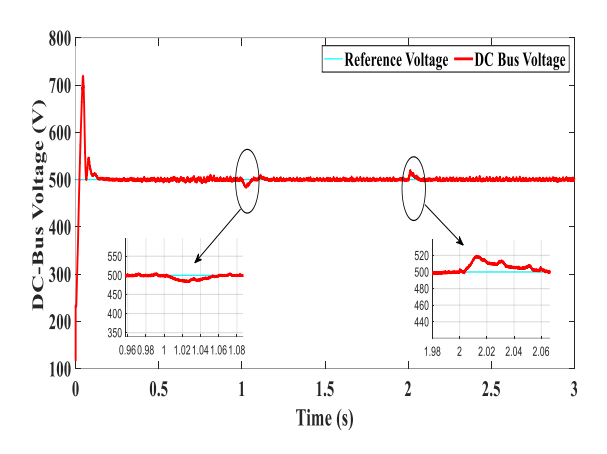


Figure 4.43: DC-Link Voltage.

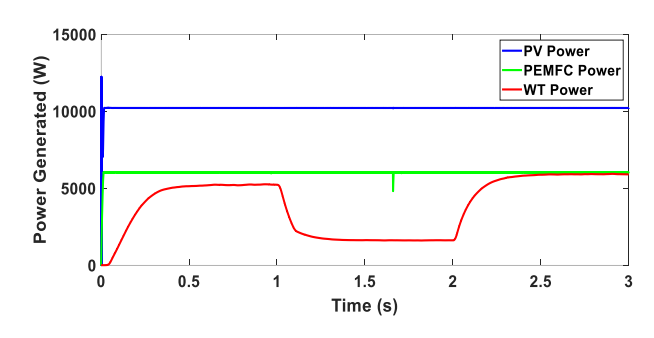


Figure 4.44 : Power Performance of the different sources.

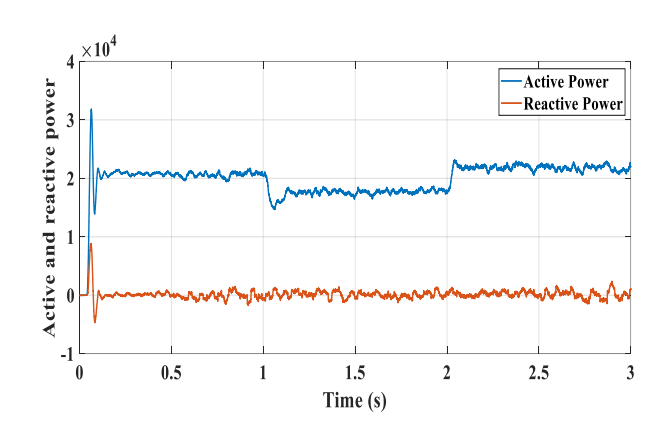


Figure 4.45: Active and Reactive power injected into the grid.

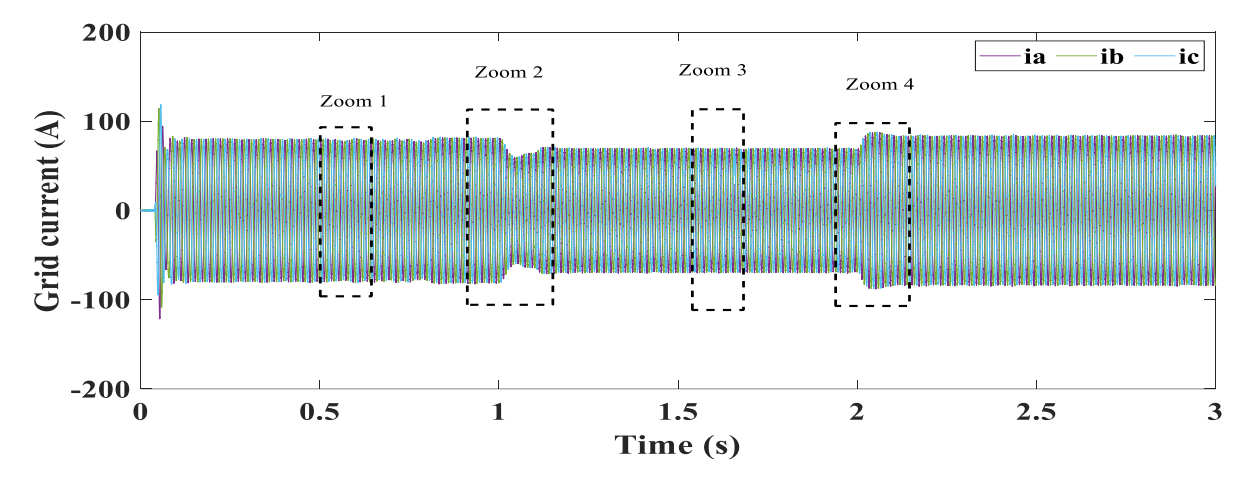


Figure 4.46: The Grid Current.

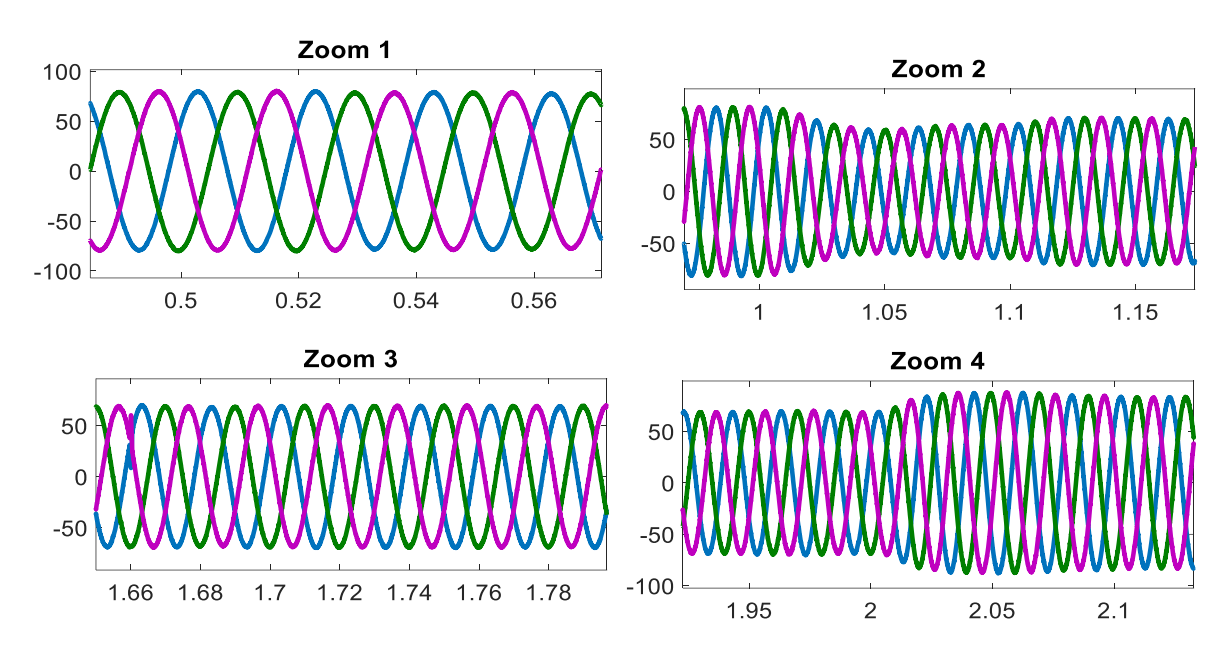


Figure 4.47: Zoom-in of the grid current.

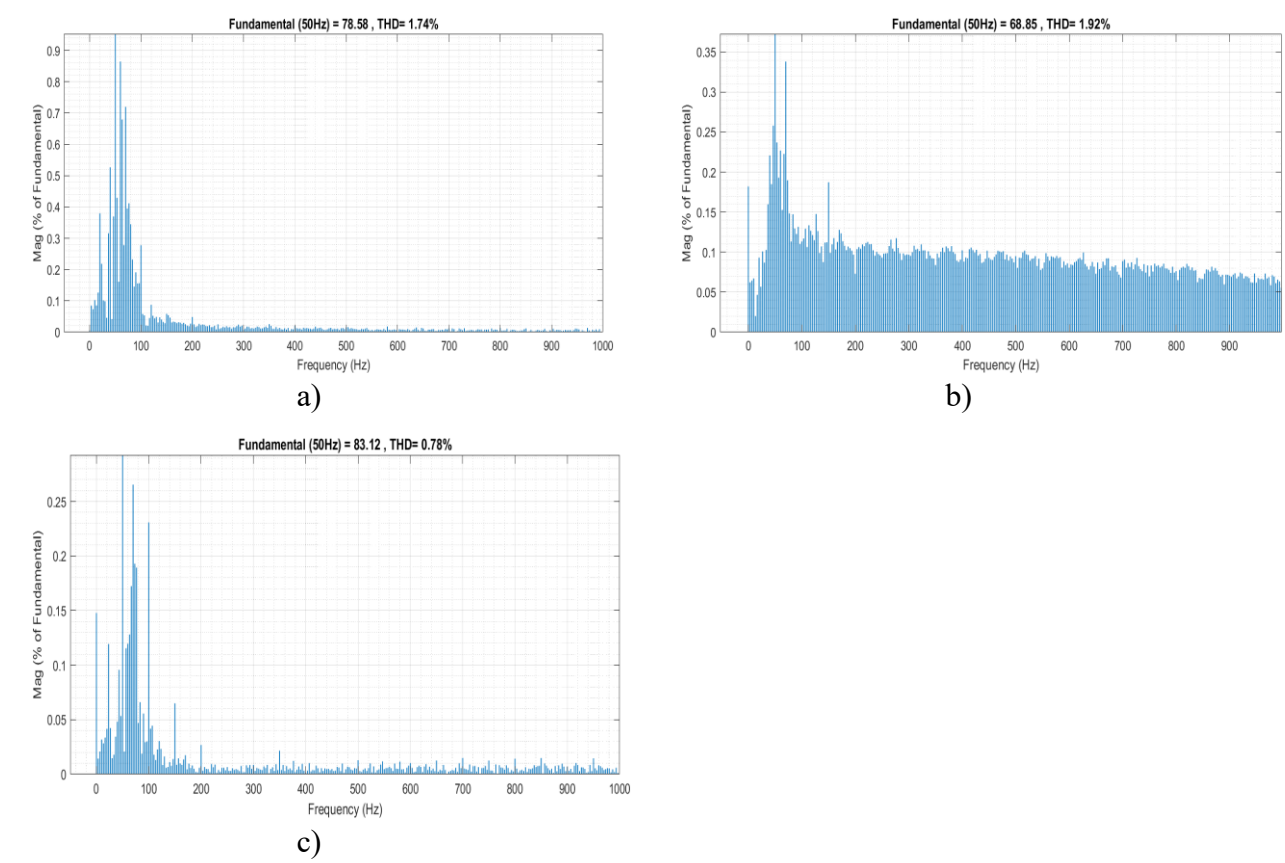


Figure 4.48: FFT Analysis for different wind velocity states. a) State 1 (12 m/s), b) State 2 (8 m/s), c) State 3 (15 m/s).

4.6 Conclusion

This chapter provides novel control strategies for the different renewable energy sources which have been discussed in this thesis. First, we have been dealing with the extracting of MPP in PV systems by suggestion three intelligent MPPT algorithms are: high order sliding mode based Super-Twisting, two levels control based ANN-MRAC, and a double stage MPPT based ANN-FSC-MPC. For the PEMFC control scheme the FSC-MPC has been suggested designed and implemented. On the other hand, a combination between the TSR control and super twisting algorithm have been utilized for the WECS, where, this latter has been compared with the classical MPPT control in the presence of high wind velocity fluctuation. The collected findings support the superiority of the suggested approaches for the different uses. Furthermore, proving the efficiency of the hybrid ANN-MPC MPPT in PV system applications, it provided improved performance above other suggested MPPT techniques. The STA also effectively reduced the chattering phenomena inherent in conventional sliding mode control. Parameters adjustment may help the ANN-MRAC-based MPPT to perform even better. Additionally, this chapter introduced an enhanced control scheme for the grid-connected mode of the hybrid system, utilizing a multi-level NPC inverter based on an FCS-MPC controller. The primary objectives of the developed controllers are to balance the DC-link capacitor voltage regardless of variations in power extracted from each source, ensure the delivery of high-quality power to the grid, and minimize the switching frequency to maintain an acceptable THD level. The results obtained indicate the effectiveness of the proposed approach in achieving the desired balance and improving system performance. The results validate the effectiveness of the developed strategy in enhancing the quality of power injected into the grid, minimizing total harmonic distortion (THD), and ensuring voltage stability across the DC-link capacitors, irrespective of fluctuations in the power drawn from each source.

Chapter 5 Energy Management and Power Flow Schemes Design

5.1 Introduction

To ensure that the hybrid renewable energy system, which combine primary renewable sources, (such as PV arrays and WECS) with supplementary power sources like fuel cells and battery storage systems (Figure 5.1), operate in harmony with the utility grid while adhering to their unique operational limits, an energy management framework is indispensable. Challenges arising from the dynamic nature of energy flows; such as the stochastic variability of renewable generation, fluctuating demand profiles, and the need for grid stability, underscore the importance of an energy management strategy (EMS) capable of real-time optimization and multi-objective decision-making. This chapter details the formulation and simulation of various energy management strategies designed to optimize the overall system performance. Emphasis is placed on developing a strategy that balance power sharing, manage storage cycles, ensure the stability of the DC-Link voltage, and maintain grid compliance.

The performance of each EMS is evaluated under identical conditions, focusing on key comparison criteria such as hydrogen consumption, battery storage system state of charge (SOC), and overall system efficiency.

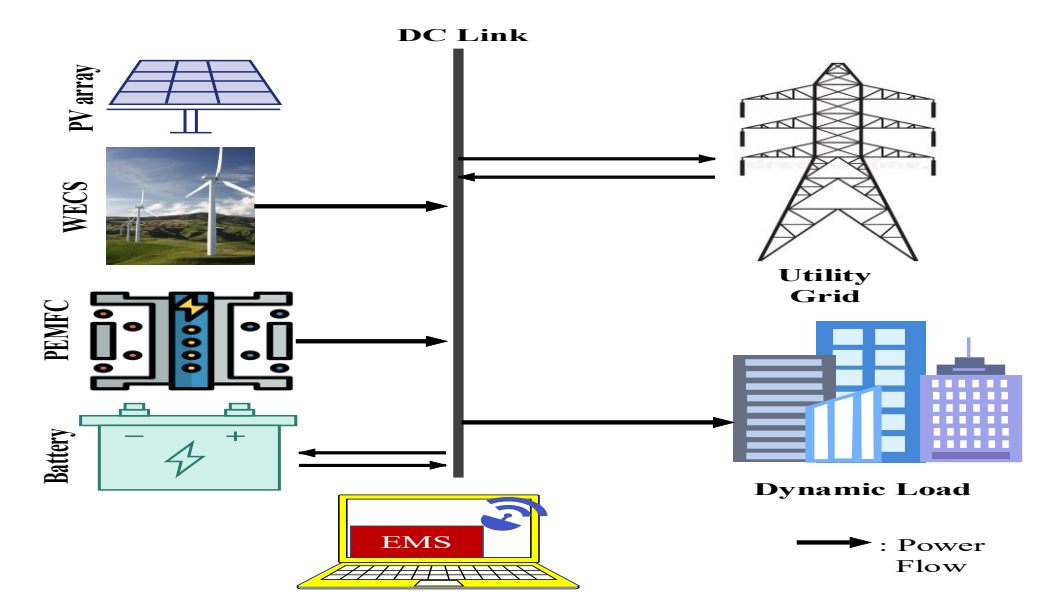


Figure 5.1: Power Flow of the proposed hybrid system.

5.2 Design and Implementation of Energy Management Approaches

The primary aims of an energy management system are to ensure: minimal hydrogen consumption; optimal overall system efficiency; a restricted range of battery state of charge (SOC); and an extended lifespan.

This is accomplished by regulating the power output of each energy source in accordance with load demand via their respective converters, employing a specified energy management strategy (EMS) [175]. The energy management approaches discussed are advanced and represent the most prevalent techniques utilized in hybrid power systems applications, including: State Machine Control (STMC) Strategy [176], conventional PI controller [177], Equivalent Consumption Minimization strategy (ECMS) [178], and External Energy Maximization Strategy (EEMS) [179].

5.2.1 Classical PI Control Strategy

In this method, the battery's state-of-charge (SOC) is regulated by means of a proportional-integral (PI) controller, as illustrated in Figure 5.2 (a). The controller's output, which indicates the battery's power contribution, is deducted from the overall load requirement (ΔP) to determine the fuel cell's target power. When the battery SOC remains above the set minimum threshold, the fuel cell operates at reduced power while the battery delivers its full capacity. Conversely, if the SOC falls below this benchmark, the fuel cell is responsible for providing nearly the entire load demand. This approach is relatively straightforward and easy to implement it compared to alternative strategies, and the PI controller's parameters are refined through iterative adjustments to achieve optimal system performance [175].

$$\Delta P = P_{Load} - (P_{PV} + P_{WT}) \tag{5.1}$$

5.2.2 The State Machine Control Strategy (STMC)

STMC's method is among the most utilized EMS for managing microgrids and hybrid power systems. The aforementioned approach is based on a state machine that comprises eight decisions (States) modes, as detailed in the table below. The fuel cell's output is calculated according to the battery's state-of-charge range and the power load required (ΔP). Figure 5.2(b) illustrates the architecture of this energy management system, which primarily depends on the system's operational condition and predefined roles. Nevertheless, achieving precise measurements is a critical challenge for this method; unexpected fluctuations in renewable

energy production and load variations can diminish overall system performance [140]. Moreover, this technique requires the use of hysteresis control during mode transitions, a factor that may compromise the system's responsiveness to changes in load demand. Finally, as depicted, the algorithm produces a reference power for the fuel cell that is then normalized by dividing it by both the fuel cell voltage and the efficiency of the DC/DC converter, yielding the corresponding reference current [175].

Table V: State Machine Decisions

| State | SOC | Power | Output | |
|---------|---------------|---|-------------------------------|--|
| state=1 | SOC High | $\Delta P < \mathrm{Pfc}_{\mathrm{min}}$ | $Pfc^* = Pfc_{min}$ | |
| state=2 | SOC High | $\Delta P \in [\operatorname{Pfc}_{\min}, \operatorname{Pfc}_{\max}]$ | $Pfc^* = P_{load}$ | |
| state=3 | SOC High | $\Delta P \ge \mathrm{Pfc}_{\mathrm{max}}$ | $Pfc^* = Pfc_{max}$ | |
| State=4 | SOC Normal | $\Delta P < \mathrm{Pfc}_{\mathrm{opt}}$ | $Pfc^* = Pfc_{opt}$ | |
| State=5 | SOC Normal | $\Delta P \in \left[Pfc_{opt} , Pfc_{max} \right]$ | $Pfc^* = P_{load}$ | |
| State=6 | SOC Normal | $\Delta P \ge \mathrm{Pfc}_{\mathrm{max}}$ | $Pfc^* = Pfc_{max}$ | |
| state=7 | SOC Low | $\Delta P < Pfc_{max}$ | $Pfc^* = P_{load} + P_{char}$ | |
| state=8 | SOC Low | $\Delta P \ge \mathrm{Pfc}_{\mathrm{max}}$ | $Pfc^* = Pfc_{max}$ | |

Where: Pfc_{min}, Pfc_{opt}, and Pfc_{max} represent the minimum, optimal, and maximum power of the FC, respectively. while Pfc* denotes the reference power for the FC.

5.2.3 Equivalent Consumption Minimization Strategy (ECMS)

The Equivalent Consumption Minimization Strategy (ECMS) is a widely recognized optimization method based on instantaneous cost functions (Figure 5.2 (c)). The objective is to attain minimal fuel consumption by reducing the fuel used by the fuel cell and the corresponding fuel necessary to maintain the battery's state of charge (SOC). In this method, a dynamic equivalence factor that varies with the battery's SOC is employed. Furthermore, by integrating this factor directly into the objective function for optimization, the approach

becomes less sensitive to variations in the SOC balancing coefficient (μ) [140]. Consequently, the objective function for the optimization problem can be expressed as follows [175]:

$$F = (P_{fc} + \alpha_p P_{batt}) \times \Delta T \tag{5.2}$$

Along with the equality constraint given by:

$$\Delta P = P_{fc} + P_{\text{batt}} \tag{5.3}$$

$$\alpha_p = 1 - 2\mu \frac{(\text{SOC} - 0.5(\text{SOC}_{\text{max}} + \text{SOC}_{\text{min}}))}{\text{SOC}_{\text{max}} + \text{SOC}_{\text{min}}}$$
(5.4)

Under the decision variables boundaries described as:

$$\begin{cases} P_{fc}^{\min} \le P_{fc} \le P_{fc}^{\max} \\ P_{\text{Batt}}^{\min} \le P_{\text{Batt}} \le P_{\text{Batt}}^{\max} \\ 0 \le \alpha_p \le 2 \end{cases}$$
 (5.6)

where P_{batt} is the battery power. α_p represent penalty coefficient. ΔT denote the time sampling. $P_{\text{Batt}}^{\text{min}}$ and $P_{\text{Batt}}^{\text{max}}$ symbolize min and max battery power, respectively. SOC_{min} and SOC_{max} are the min and max battery SOC, respectively. μ is the SOC balance coefficient.

5.2.4 External Energy Maximization Strategy (EEMS)

The traditional ECMS operates by balancing hydrogen fuel cell consumption with an equivalent energy consumption from the battery. This equivalence is defined by a penalty factor, which ensures the battery remains within its state of charge (SOC) limits over a driving cycle. The issue with this approach is its dependence on the load profile, which can be highly stochastic in real-world applications. Therefore, the External Energy Maximization Strategy (EEMS) introduces a fundamental shift in approach. Instead of computing an equivalence factor for fuel minimization, it maximizes battery energy utilization at any given instant. This ensures the system remains within SOC and voltage constraints without requiring predictive modeling of future energy demands. The primary aim of this function is to augment the energy output supplied by both the battery and the DC bus [143] [175] [179]. This is mathematically formulated as follows:

$$J = -(\Delta T \cdot P_{\text{Batt}} + 0.5 \cdot C_{\text{dc}} \cdot (\Delta v)^2)$$
 (5.7)

where Δv represents the DC-bus voltage perturbation.

Note that the negative sign in eq. (5.7) is used to switch between minimization and maximization problem in the optimization techniques theory.

This equation is subjected to the inequality constraint described as follows:

$$\begin{cases} P_{\text{Batt}} \cdot \Delta T \leq (SoC - SoC_{\min}) V_{\text{Batt}} \cdot Q_{\text{Batt}} \\ V_{\text{dc}}^{\min} - V_{dc} \leq \Delta v \leq V_{\text{dc}}^{\max} - V_{\text{dc}} \\ P_{\text{Batt}}^{\min} \leq P_{\text{Batt}} \leq P_{\text{Batt}}^{\max} \end{cases}$$

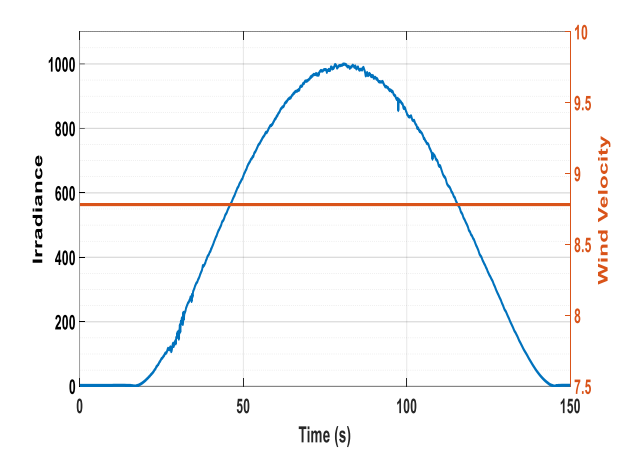
$$SoC^* \longrightarrow PI \longrightarrow P_{k}^{\uparrow} \longrightarrow P_{k}$$

Figure 5.2 : Energy Management Configurations: a) Classical PI. b) State Machine Control. c) Equivalent Consumption Minimization Strategy. d) External energy maximization strategy.

5.3 Simulation Results

In order to investigate and validate the operational efficacy of the proposed energy management strategies (EMS) for the hybrid PV/WT/FC/Battery grid-tied system, a comparative analysis of the evaluated EMSs is conducted using MATLAB/Simulink environment. The simulated model characterized by the following: two main sources represented by a solar PV generator of 10 kw and WT of 8.5 kw (we consider that they work on MPPT mode); a PEMFC with a terminal voltage of 30-60 V and a rated power of 10 kW; 48 V_40Ah Li-ion battery system. Noteworthily that a protective resistor is utilized to mitigate the risk of overvoltage in the input voltage of the inverter. The specification variables have

been chosen as $P_{FC}^{\min} = 850$, $P_{FC}^{\max} = 8800$, $P_{\text{batt}}^{\min} = 1500$, $P_{\text{batt}}^{\max} = 3400$, $SOC^{\min} = 60$, $SOC_0 = 65$, and $SOC^{\max} = 90$. The SOC reference for the traditional PI control system is



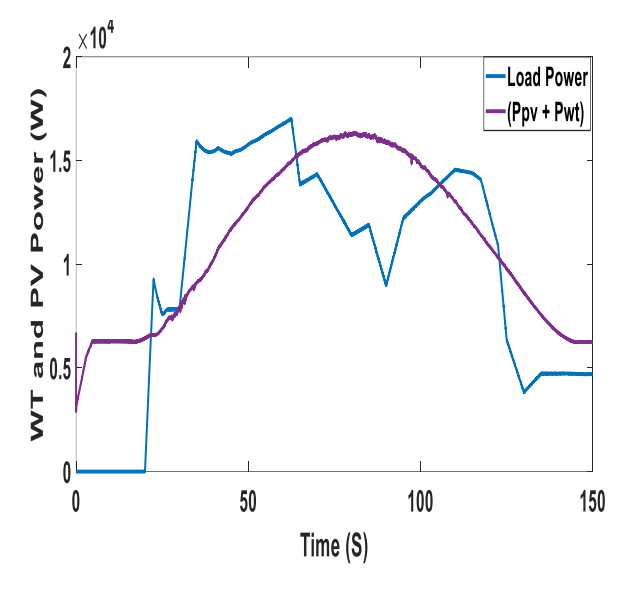
2 × 10⁴

No. 1

No. 2

Figure 5.3 : Irradiance and Wind Velocity Behavior.

Figure 5.4: Load Power.



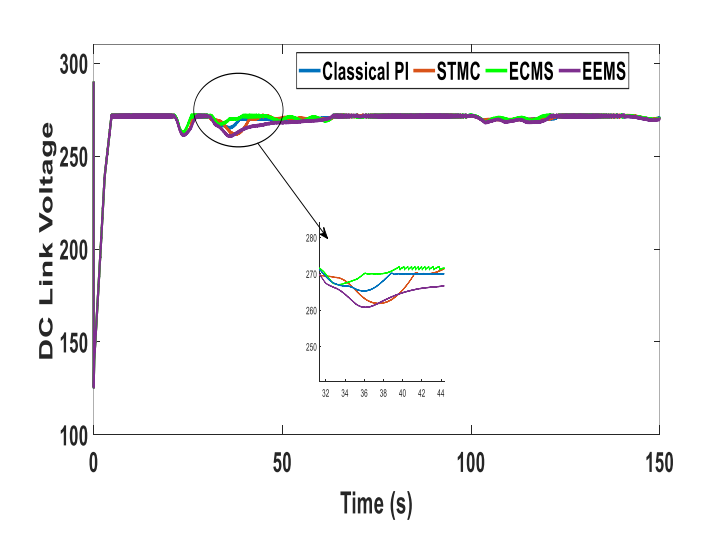
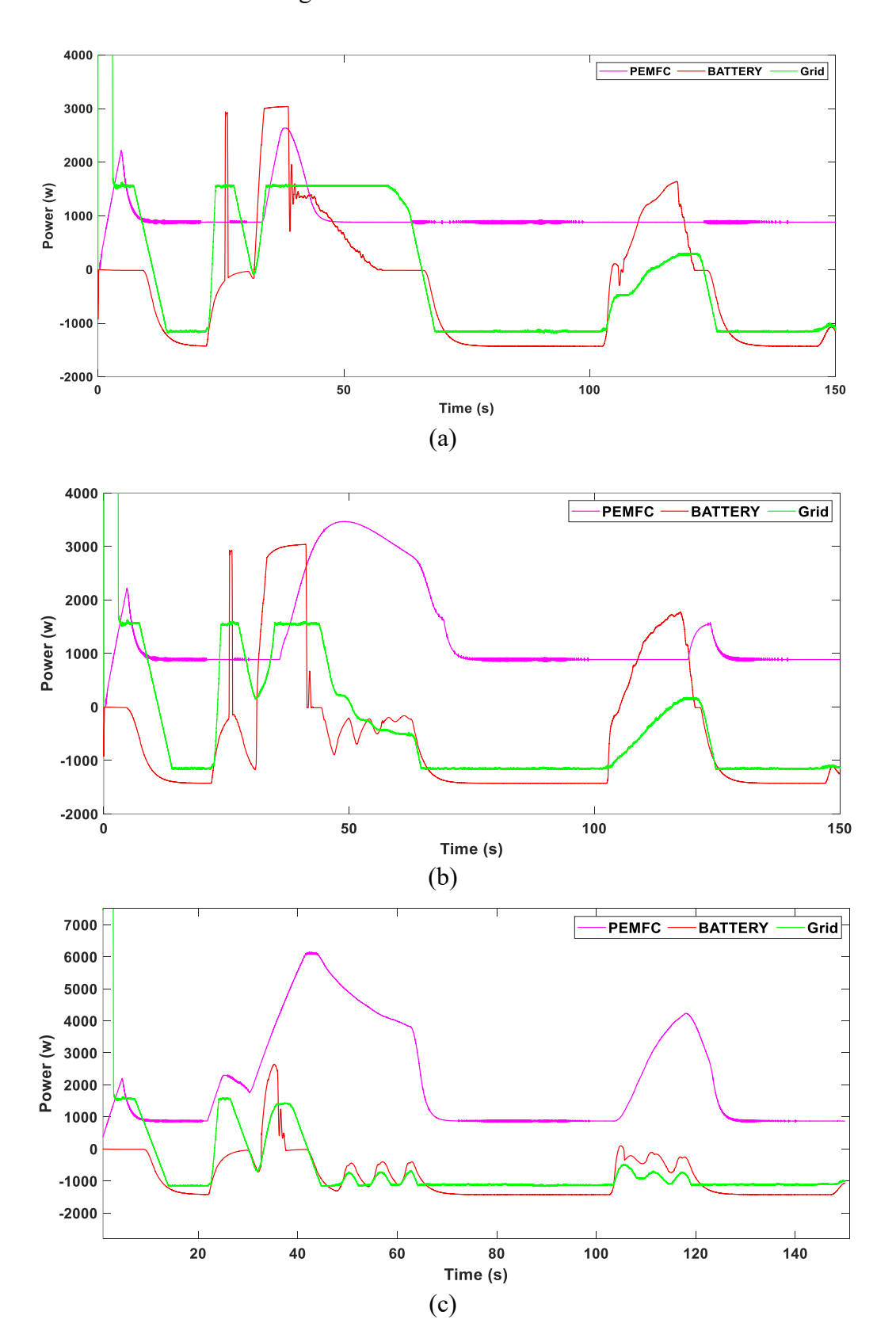


Figure 5.5: (PV+WT) Power generation versus power required.

Figure 5.6 :DC-Bus Voltage.

established at SOC^{\min} to ensure a valid comparison with other methods. The used solar irradiation and wind velocity profiles are illustrated in Figure 5.3; while the variable load profile is given in Figure 5.4. The system underwent simulation for 150 seconds. The dynamic response of the main sources depicted in Figure 5.5. Figure 5.6 shows the DC Link Voltage response over time for the considered EMS. The initial voltage rise is observed in all strategies, a zoomed-in highlights fluctuations in the voltage response between 30–45s, where different

strategies show varying levels of overshoot and oscillations. Classical PI and STMC exhibit slight discrepancies but quickly return to stability; while ECMS has the greatest fluctuation, indicating a delayed reaction to load fluctuations. Nonetheless, EEMS provides the smoothest stabilization of the DC link voltage.



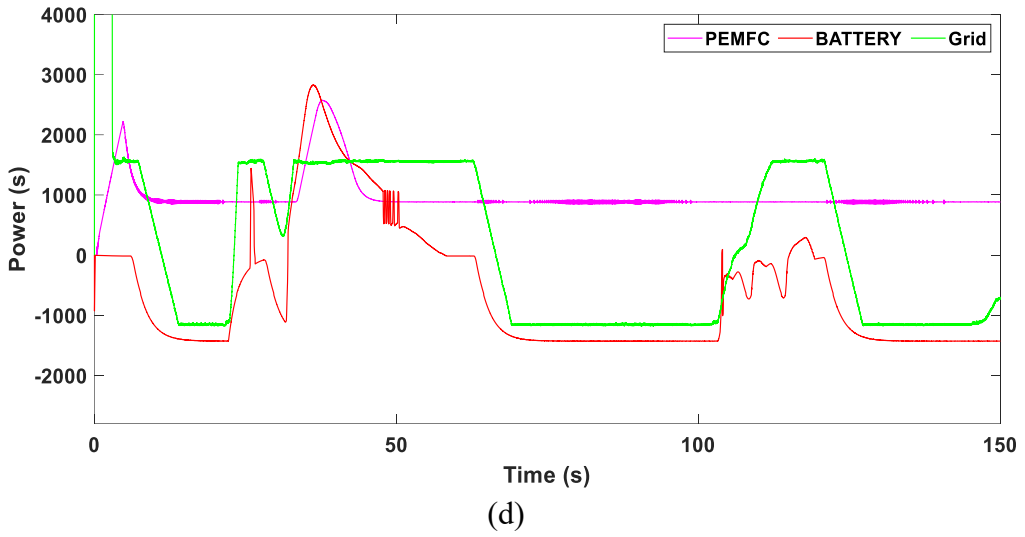


Figure 5.7: PEMFC, Battery, and Grid power response using: (a) classical PI (b) STMC (c) ECMS (d) EEMS.

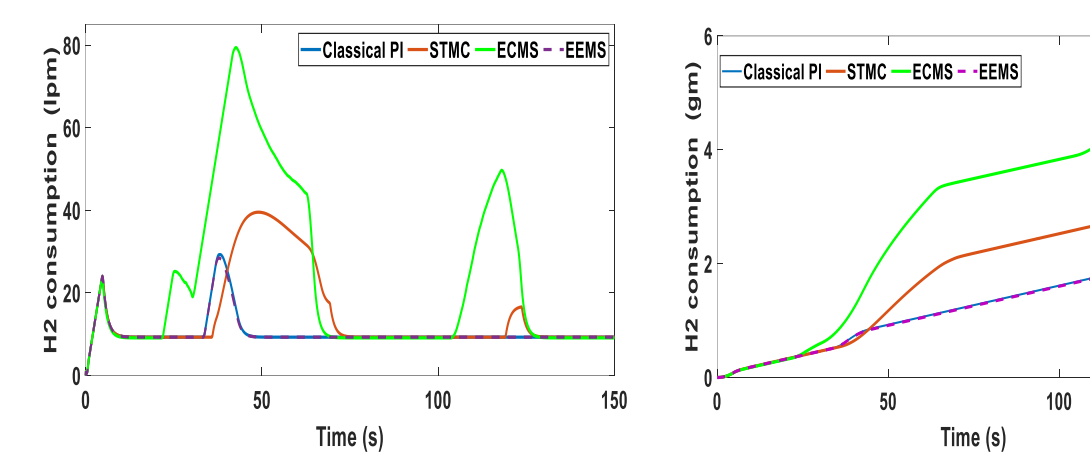


Figure 5.8: H2 consumption in lpm for the examined EMS techniques.

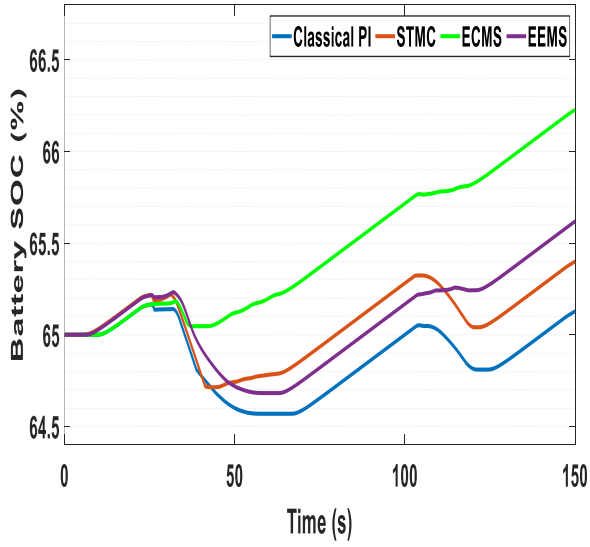
Figure 5.9: H2 consumption in gm for the examined EMS techniques

150

Indicating its efficacy in mitigating transient oscillations while preserving system stability.

Figure 5.7 illustrates the power response of the secondary sources PEMFC, Battery, in addition to the utility Grid under the different EMS approaches. Figure 5.7 (a) presents the power response via Classical PI. It has been noted that the battery experiences large fluctuations, indicating frequent charging/discharging cycles. Whereas the PEMFC exhibits sharp peaks, which indicate sudden increases and decreases in power output rather than behaving smoothly. On the other side, the grid contribution varies significantly, indicating instability in power management. The power response under STMC approach illustrated in

Figure 5.7 (b). it can be seen that the PEMFC operates more smoothly than the earlier strategy; however, fluctuations are still present. Moreover, Grid power exchange is more balanced, reducing sudden variations. The power response under the ECMS is presented in Figure 5.7 (c). Accordingly, ECMS demonstrates a more balanced and optimized power distribution between the PEMFC, battery, and grid compared to the other approaches, which dynamically regulates power distribution between the battery and fuel cell to optimize hydrogen use while providing the necessary power; as well, it is notable that Grid dependence is minimized. Figure 5.7 (d) depicts dynamic response of the power using EEMS strategy. Obviously EEMS provides the most stable and efficient power response, prioritizing external energy sources to minimize internal fuel consumption. In contrast to ECMS, which balances energy distribution based on efficiency, EEMS actively maximizes the contribution of external sources while strategically managing the fuel cell and battery operation.



§ 100 Classical Pl STMC —ECMS -EEMS Average efficiency 84.8 84.6 84.4 84.2 84 83.8 The 83.6 149.99999 50 0 100 150 Time

Figure 5.10: The SOC response for the examined EMS techniques.

Figure 5.11: system efficiency for each evaluated method.

A comparative on the H2 consumption between the evaluated EMS is shown in figures 5.8 and 5.9. The battery SOC and the average efficiency in (%) are also presented in figure 5.10 and 5.11, respectively. According to the obtained results, in terms of hydrogen consumption, EEMS exhibits the lowest value (2.2892 g), which outperforming ECMS (5.2386 g), where the latter consumes the highest amount. Similarly, STMC consumes more hydrogen than EEMS with (3.2639 g). with the Classical PI method, it has been consumed about 2.301 g of hydrogen. In terms of SOC, ECMS achieves the highest final SOC (66.2271%), followed

by EEMS (65.6197%) and STMC (65.4010%), whereas classical PI method has the lowest final SOC (65.1665%). In contrast, based on system efficiency STMC achieves the highest value (84.95%), followed closely by EEMS (84.826%) and the classical PI by (84.404), while ECMS records the lowest efficiency (84.32%). The table below provides a clear and concise analytical comparison of the dynamic performance across the studied EMS techniques.

Efficiency =
$$\frac{\int P_{\text{load}} dt}{\int (P_{PV} + P_{WT} + P_{\text{fc}} + P_{\text{Bat}} + P_{\text{grid}}) dt}$$
 (5.9)

Table VI: Analysis of various management approaches.

| Criteria | Energy Management Strategy | | | | |
|------------------------|----------------------------|---------|---------|---------|--|
| | Classical | STMC | ECMS | EEMS | |
| | PI control | | | | |
| Lowest SOC | 64.71 | 64.71 | 65 | 64.81 | |
| (%) | | | | | |
| Final SOC (%) | 65.1665 | 65.4010 | 66.2271 | 65.6197 | |
| Consumed H2 (gram) | 2.301 | 3.2639 | 5.2386 | 2.2892 | |
| Overall efficiency (%) | 84.404 | 84.95 | 84.32 | 84.826 | |

5.4 Conclusion

This chapter presents a comprehensive comparison among four famous energy management strategies which handle the energy flow in the studied hybrid grid connected power system. These strategies are known as: Classical PI Control, State Machine control (STMC), Equivalent Consumption Minimization Strategy (ECMS), and External Energy Maximization Strategy (EEMS). The comparison has been conducted based on key metrics such as hydrogen consumption, battery state of charge (SOC), and overall system efficiency. According to the obtained in this chapter, we can conclude the following:

- EEMS is optimal for minimizing hydrogen consumption while maintaining competitive efficiency.
- STMC has the highest efficiency but consumes more hydrogen than EEMS.
- ECMS prioritizes battery SOC retention but at the cost of higher hydrogen consumption.
- Classical PI demonstrates good performance, nevertheless it couldn't excel in any criterion.

Chapter 6 : General Conclusion

6.1 A Summary of the Research Work

The research work presented in this dissertation is aims to the optimization of hybrid renewable energy production systems connected to the public network. The main objective of this work is to enhance the control of a hybrid PV/wind/fuel cell (FC) system designed to operate in an on-grid mode.

Chapter 2 comprehensively presents and discusses the hybrid system, including its renewable energy sources and associated power converters. A single-diode model-based PV cell is mathematically modeled, with its properties thoroughly examined. Additionally, the proton exchange membrane fuel cell (PEMFC) is introduced as the second DC source, with both its chemical and electrical characteristics clearly outlined. The wind energy conversion system (WECS), comprising the wind turbine, a two-mass drive-train model, and the permanent magnet synchronous generator (PMSG), is also extensively detailed. For the DC renewable energy sources (PV and FC), a boost converter is selected and modeled, while a three-phase PWM rectifier is chosen for the WECS, with both converters described in depth.

Chapter 3 offers a detailed overview of control techniques for hybrid power systems, including Maximum Power Point Tracking (MPPT) methods for photovoltaic systems, power optimization algorithms for wind energy conversion systems as well control strategies for permanent magnet synchronous generators (PMSGs), and fuel cells control schemes. It also reviews dc-link voltage stabilization, grid integration in addition to inverter current control, and synchronization methods, concluding with a discussion on energy management and power flow supervision strategies.

Chapter 4 introduces novel control strategies for the renewable energy sources discussed in this thesis. For PV systems, three intelligent MPPT algorithms are proposed: a high-order sliding mode-based Super-Twisting (STA) method, a two-level control combining ANN and MRAC (ANN-MRAC), and a double-stage MPPT integrating ANN and MPC (ANN-FSC-MPC). For the PEMFC, an FSC-MPC-based control scheme is designed and implemented. In the case of the WECS, a hybrid approach combining TSR control and the Super-Twisting algorithm is employed and compared with classical MPPT under high wind velocity fluctuations.

The results demonstrate the superiority of the proposed strategies. The hybrid ANN-MPC MPPT for PV system outperforms other techniques, offering enhanced efficiency and performance. The STA effectively mitigates chattering phenomena associated with conventional sliding mode control, while the ANN-MRAC-based MPPT shows great robustness against irradiance fluctuation along with fast response time and high efficiency. Additionally, an advanced control scheme for grid-connected operation is introduced, utilizing a multi-level NPC inverter controlled by an FCS-MPC approach. This scheme ensures DC-link voltage stability despite power variations, delivers high-quality power to the grid, and minimizes switching frequency to maintain acceptable THD levels. The findings validate the effectiveness of the proposed strategies in improving power quality, reducing THD, and maintaining voltage stability across the DC-link capacitors under dynamic power conditions.

Chapter 05 offers a thorough evaluation of four recognized energy management systems that guide energy flow in the analyzed hybrid grid-connected power system. The strategies are identified as: Classical PI Control, State Machine Control (STMC), Equivalent Consumption Minimization Strategy (ECMS), and External Energy Maximization Strategy (EEMS).

6.2 Perspectives and Future Works

In this thesis different contributions are provided. However, notwithstanding existing research, there are still novel insights to be uncovered and some other issues must be in future work, like:

- The proposed MPPT strategies in this study covered only the case of uniform irradiance change. Nonetheless, Partial Shading Condition (PSC) considered also one of the most challenges faced PV systems applications. The reason is that it creates multiple MPPs, only one of them represents the global MPP while the other points called Local MPP.
- 2. The proposed control scheme for WECS depend totally on the wind velocity which require a wind speed senor. Developing an estimation bloc instead of the sensor make the design less expensive.
- 3. For the fuel cell we take into consideration a hydrogen tank for fuel feeding. However, utilizing a Hydrogen Electrolyzer instead will be more effective.
- 4. Experimental implementation and Verification of the suggested strategies in real time.

Appendix A

A.1 Li-ion Battery Model

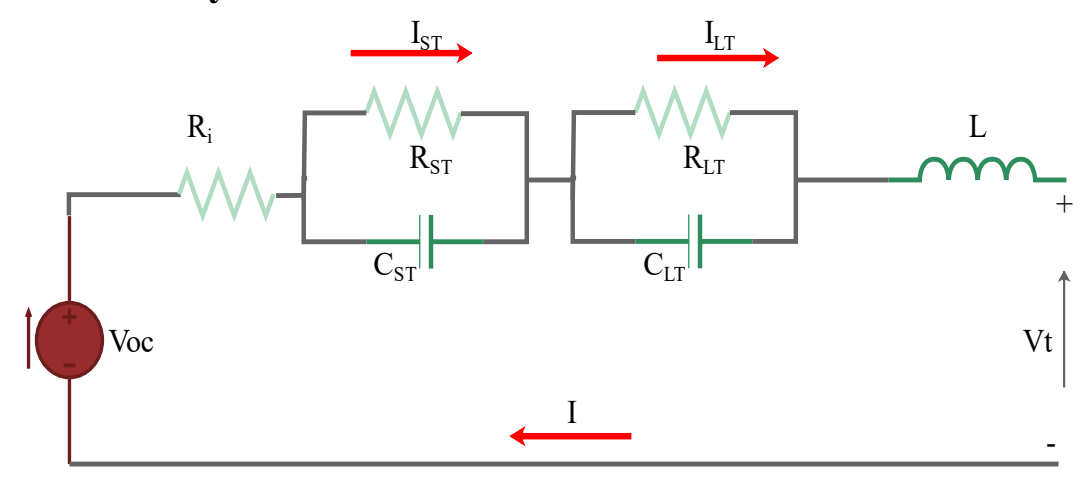


Figure. A1. Battery Equivalent Circuit.

$$\begin{split} V_{t} &= V_{OC} - IR_{i} - \frac{1}{C_{ST}} \int_{0}^{t} (I - I_{ST}) dt - \frac{1}{C_{LT}} \int_{0}^{t} (I - I_{LT}) dt - L \frac{di}{dt} \\ A_{S}I &= (I - I_{loss}), I_{ST} = \frac{V_{ST}}{R_{ST}}, I_{LT} = \frac{V_{LT}}{R_{LT}} \\ V_{t} &= V_{OC} - (I - I_{Loss})R_{i} - \frac{1}{C_{ST}} \int_{0}^{t} (I - I_{loss} - \frac{V_{ST}}{R_{ST}}) dt - \frac{1}{C_{LT}} \int_{0}^{t} \left(I - I_{Loss} - \frac{V_{LT}}{R_{LT}}\right) dt \\ - L \frac{d(I - I_{loss})}{dt} \\ I_{loss} &= I_{0} \exp\left(\frac{V_{t} - V_{N}}{K1} + K2 \frac{T_{b} - T_{N}}{T_{b}T_{N}}\right) \\ SOC &= \frac{\left(SOC_{0}Q_{\max} - \frac{1}{3600} \int_{0}^{t} (I - I_{Loss}) dt\right)}{Q_{\max}} \\ P_{Loss} &= P_{foule} + P_{\min reaction} \\ P_{Loss} &= R_{i}(I - I_{Loss})^{2} + (C_{MR} + V_{Loss})(I - I_{Loss}) \\ T_{b} &= T_{i} + \frac{1}{C_{pm}} \int_{0}^{t} P_{Loss} dt \end{split}$$

Where: V_t denotes the terminal voltage; Voc represents open-circuit voltage; Ri denotes the internal resistance; C_{LT} and R_{LT} represent the capacitance and the resistance for the diffusion; C_{ST} and R_{ST} represent the capacitance and resistance for double layer; I_{LT} and I_{ST} represent the current at long and short mass effect; SOC_o is the initial battery state of charge; Q_{max} denotes the maximum charge capacity; I_{losses} is the current lost according to the coulombs effect; V_{losses} denotes the voltage drop due to the double layer; Io is the initial current; V_N denote the cell nominal voltage; K1 and K2 are the clamps and temperature constants. T_b and T_i are the battery and initial temperatures; P_{joule} is the internal resistance heat generated power; C_{MR} is the battery constant.

A2. Performance Metrices

The tracking efficiency for PV systems (η):

$$\eta = \frac{\int_{t_1}^{t_2} P_{\text{pv}} dt}{\int_{t_1}^{t_2} p_{\text{max}} dt}$$

Root Mean Square Error

$$RMSE = \sqrt{\frac{\sum (Actual Value - Estimated Value)^2}{n}}$$

MAE (Mean absolute error)

$$MAE = \frac{\sum | \text{EstimtedValue} - \text{ActualValue}|}{n}$$

The power loss:

$$P_{\text{loss}} = \sum p_{\text{max}}(t) - \sum p_{actual}(t)$$

Integral Time Absolut Error

$$ITAE = \int t |e| dt$$

Integral Absolute Error

$$IAE = \int |e| dt$$

References

- [1] "The world's energy problem Our World in Data." Accessed: Sep. 10, 2024. [Online]. Available: https://ourworldindata.org/worlds-energy-problem
- [2] "Fossil fuels Our World in Data." Accessed: Sep. 10, 2024. [Online]. Available: https://ourworldindata.org/fossil-fuels
- [3] J. O. Petinrin and M. Shaaban, "Renewable energy for continuous energy sustainability in Malaysia," Renew. Sustain. Energy Rev., vol. 50, pp. 967–981, 2015, doi: 10.1016/j.rser.2015.04.146.
- [4] A. D. A. Bin Abu Sofian, H. R. Lim, H. Siti Halimatul Munawaroh, Z. Ma, K. W. Chew, and P. L. Show, "Machine learning and the renewable energy revolution: Exploring solar and wind energy solutions for a sustainable future including innovations in energy storage," Sustain. Dev., no. July 2023, pp. 3953–3978, 2024, doi: 10.1002/sd.2885.
- [5] T. Falope, L. Lao, D. Hanak, and D. Huo, "Hybrid energy system integration and management for solar energy: A review," Energy Convers. Manag. X, vol. 21, no. August 2023, p. 100527, 2024, doi: 10.1016/j.ecmx.2024.100527.
- [6] M. Tawalbeh, A. Al-Othman, F. Kafiah, E. Abdelsalam, F. Almomani, and M. Alkasrawi, "Environmental impacts of solar photovoltaic systems: A critical review of recent progress and future outlook," Sci. Total Environ., vol. 759, p. 143528, 2021.
- [7] "Installed solar energy capacity." Accessed: Sep. 11, 2024. [Online]. Available: https://ourworldindata.org/grapher/installed-solar-pv-capacity?country=OWID_WRL~CHN~IND~ESP~BRA~MEX~CHL~DZA
- [8] D. Milborrow, "Wind energy development," age Wind energy Prog. Futur. Dir. from a Glob. Perspect., pp. 3–22, 2020.
- [9] "WWEA Annual Report 2023: Record Year for Windpower." Accessed: Sep. 12, 2024. [Online]. Available: https://wwindea.org/AnnualReport2023
- [10] P. Roy, J. He, T. Zhao, and Y. V. Singh, "Recent Advances of Wind-Solar Hybrid Renewable Energy Systems for Power Generation: A Review," IEEE Open J. Ind. Electron. Soc., vol. 3, no. December 2021, pp. 81–104, 2022, doi: 10.1109/OJIES.2022.3144093.
- [11] M. K. Deshmukh and S. S. Deshmukh, "Modeling of hybrid renewable energy systems," Renew. Sustain. Energy Rev., vol. 12, no. 1, pp. 235–249, 2008, doi: 10.1016/j.rser.2006.07.011.
- [12] Y. Yuan, J. Wang, X. Yan, B. Shen, and T. Long, "A review of multi-energy hybrid power system for ships," Renew. Sustain. Energy Rev., vol. 132, p. 110081, 2020.
- [13] F. J. Vivas, A. De las Heras, F. Segura, and J. M. Andújar, "A review of energy management strategies for renewable hybrid energy systems with hydrogen backup," Renew. Sustain. Energy Rev., vol. 82, pp. 126–155, 2018.
- [14] C. Ceylan and Y. Devrim, "Design and simulation of the PV/PEM fuel cell based hybrid energy

- system using MATLAB/Simulink for greenhouse application," Int. J. Hydrogen Energy, vol. 46, no. 42, pp. 22092–22106, Jun. 2021, doi: 10.1016/j.ijhydene.2021.04.034.
- [15] A. F. Bendary and M. M. Ismail, "Battery charge management for hybrid PV/wind/fuel cell with storage battery," in Energy Procedia, Elsevier Ltd, 2019, pp. 107–116. doi: 10.1016/j.egypro.2019.04.012.
- [16] N. A. Ahmed, S. Abdul Rahman, and B. N. Alajmi, "Optimal controller tuning for P&O maximum power point tracking of PV systems using genetic and cuckoo search algorithms," Int. Trans. Electr. Energy Syst., vol. 31, no. 10, pp. 1–21, 2021, doi: 10.1002/2050-7038.12624.
- [17] Y. Sawle, S. C. Gupta, and A. K. Bohre, "Review of hybrid renewable energy systems with comparative analysis of off-grid hybrid system," Renew. Sustain. Energy Rev., vol. 81, pp. 2217–2235, 2018.
- [18] P. Belkhode et al., "Nanomaterials applications in solar energy: Exploring future prospects and challenges," Mater. Today Proc., 2024.
- [19] D. Rekioua and D. Rekioua, "Hybrid renewable energy systems overview," Hybrid Renew. Energy Syst. Optim. Power Manag. Control, pp. 1–37, 2020.
- [20] M. E. M. Soudagar et al., "An overview of the existing and future state of the art advancement of hybrid energy systems based on PV-solar and wind," Int. J. Low-Carbon Technol., vol. 19, pp. 207–216, 2024.
- [21] M. Morey, N. Gupta, M. M. Garg, and A. Kumar, "A comprehensive review of grid-connected solar photovoltaic system: Architecture, control, and ancillary services," Renew. Energy Focus, vol. 45, pp. 307–330, 2023.
- [22] M. Yessef et al., "Experimental validation of feedback PI controllers for multi-rotor wind energy conversion systems," IEEE Access, 2024.
- [23] A. Palani et al., "A novel design and development of multilevel inverters for parallel operated PMSG-based standalone wind energy conversion systems," Iran. J. Sci. Technol. Trans. Electr. Eng., vol. 48, no. 1, pp. 277–287, 2024.
- [24] C. Yan, Y. Zou, Z. Wu, and A. Maleki, "Effect of various design configurations and operating conditions for optimization of a wind/solar/hydrogen/fuel cell hybrid microgrid system by a bioinspired algorithm," Int. J. Hydrogen Energy, vol. 60, pp. 378–391, 2024.
- [25] B. Madaci, R. Chenni, E. Kurt, and K. E. Hemsas, "Design and control of a stand-alone hybrid power system," Int. J. Hydrogen Energy, vol. 41, no. 29, pp. 12485–12496, 2016, doi: 10.1016/j.ijhydene.2016.01.117.
- [26] A. Labouret and M. Villoz, Solar photovoltaic energy. 2010. doi: 10.1049/pbrn009e.
- [27] T. S. L. V. Ayyarao, "Parameter estimation of solar PV models with quantum-based avian navigation optimizer and Newton–Raphson method," J. Comput. Electron., vol. 21, no. 6, pp. 1338–1356, 2022, doi: 10.1007/s10825-022-01931-8.
- [28] A. Harrag and S. Messalti, "Three, Five and Seven PV Model Parameters Extraction using

- PSO," Energy Procedia, vol. 119, pp. 767–774, 2017, doi: 10.1016/j.egypro.2017.07.104.
- [29] T. Ma, H. Yang, and L. Lu, "Solar photovoltaic system modeling and performance prediction," Renew. Sustain. Energy Rev., vol. 36, pp. 304–315, 2014, doi: 10.1016/j.rser.2014.04.057.
- [30] T. S. L. V. Ayyarao and G. I. Kishore, "Parameter estimation of solar PV models with artificial humming bird optimization algorithm using various objective functions," Soft Comput., vol. 0123456789, 2023, doi: 10.1007/s00500-023-08630-x.
- [31] A. Kihal, "Approche avancée pour l'optimisation d'une installation photovoltaïque interconnectée au réseau," UNIVERSITE FERHAT ABBAS SETIF1, 2019.
- [32] S. Sumathi, L. Ashok Kumar, P.Surekha, Solar Photovoltaic & Wind Energy Conversion Systems. 2015. [Online]. Available: internal-pdf://0380800788/Solar PV & Wind E Conversion Systems 2015.pdf
- [33] N. Femia, G. Petrone, G. Spagnuolo, and M. Vitelli, Power Electronics and Control Techniques for Maximum Energy Harvesting in Photovoltaic Systems. 2013. doi: 10.1201/b14303-3.
- [34] C. Kunusch, P. Puleston, and M. Mayosky, Sliding-Mode Control of PEM Fuel Cells. 2012. doi: 10.1007/978-1-4471-2431-3.
- [35] M. Derbeli, "Control of Proton Exchange Membrane Fuel Cell System," 2022. [Online]. Available: http://hdl.handle.net/10810/57099
- [36] S. George, N. Sehgal, K. P. S. Rana, and V. Kumar, "A comprehensive review on modelling and maximum power point tracking of PEMFC," Cleaner Energy Systems, vol. 3. Elsevier B.V., Dec. 01, 2022. doi: 10.1016/j.cles.2022.100031.
- [37] B. Kanouni, A. E. Badoud, and S. Mekhilef, "A multi-objective model predictive current control with two-step horizon for double-stage grid-connected inverter PEMFC system," Int. J. Hydrogen Energy, vol. 47, no. 4, pp. 2685–2707, Jan. 2022, doi: 10.1016/j.ijhydene.2021.10.182.
- [38] M. Derbeli, A. Charaabi, O. Barambones, and C. Napole, "High-performance tracking for proton exchange membrane fuel cell system pemfc using model predictive control," Mathematics, vol. 9, no. 11, pp. 1–17, 2021, doi: 10.3390/math9111158.
- [39] "Université Mohamed Boudiaf-M'sila Thèse Contribution à l'optimisation de la gestion de l'énergie d'un micro-réseau continu Présentée Par FERAHTIA Seydali."
- [40] S. El Aabid et al., "A global approach for a consistent identification of static and dynamic phenomena in a PEM Fuel Cell," Math. Comput. Simul., vol. 158, pp. 432–452, 2019, doi: 10.1016/j.matcom.2018.10.008.
- [41] N. Benchouia, A. E. Hadjadj, A. Derghal, L. Khochemane, and B. Mahmah, "Modeling and validation of fuel cell PEMFC," J. Renew. Energies, vol. 16, no. 2, pp. 365–377, 2023, doi: 10.54966/jreen.v16i2.386.
- [42] H. Bahri and A. Harrag, "Modelling and Analysis of Hybrid PV-PEM Fuel Cell Power System," Prog. Sol. Energy Eng. Syst., vol. 4, no. 1, pp. 29–33, Dec. 2020, doi: 10.18280/psees.040104.

- [43] A. Harrag and S. Messalti, "Variable Step Size IC MPPT Controller for PEMFC Power System Improving Static and Dynamic Performances," Fuel Cells, vol. 17, no. 6, pp. 816–824, Dec. 2017, doi: 10.1002/fuce.201700047.
- [44] M. Derbeli, M. Farhat, O. Barambones, and L. Sbita, "Control of PEM fuel cell power system using sliding mode and super-twisting algorithms," Int. J. Hydrogen Energy, vol. 42, no. 13, pp. 8833–8844, 2017, doi: 10.1016/j.ijhydene.2016.06.103.
- [45] R. F. Mann, J. C. Amphlett, M. A. I. Hooper, H. M. Jensen, B. A. Peppley, and P. R. Roberge, "Development and application of a generalized steady-state electrochemical model for a PEM fuel cell," J. Power Sources, vol. 86, no. 1, pp. 173–180, 2000, doi: 10.1016/S0378-7753(99)00484-X.
- [46] M. Y. Silaa, A. Bencherif, and O. Barambones, "A novel robust adaptive sliding mode control using stochastic gradient descent for PEMFC power system," Int. J. Hydrogen Energy, vol. 48, no. 45, pp. 17277–17292, May 2023, doi: 10.1016/j.ijhydene.2023.01.200.
- [47] A. L. Dicks and D. A. J. Rand, Fuel cell systems explained. John Wiley & Sons, 2018.
- [48] A. Zaidi, "Dynamic Modeling and Simulation of A PEM Fuel Cell: MATLAB and Lab VIEW Modeling Approach," no. Iconce, pp. 272–276, 2014.
- [49] J. T. Pukrushpan, A. G. Stefanopoulou, H. Peng, J. T. Pukrushpan, A. G. Stefanopoulou, and H. Peng, "Fuel cell system model: fuel cell stack," Control fuel cell power Syst. Princ. Model. Anal. Feed. Des., pp. 31–56, 2004.
- [50] J. Zhang, H. Zhang, J. Wu, and J. Zhang, "The Effects of Temperature on PEM Fuel Cell Kinetics and Performance," Pem Fuel Cell Test. Diagnosis, pp. 121–141, 2013, doi: 10.1016/b978-0-444-53688-4.00004-8.
- [51] M. A. Salam et al., "Effect of Temperature on the Performance Factors and Durability of Proton Exchange Membrane of Hydrogen Fuel Cell: A Narrative Review," Mater. Sci. Res. India, vol. 17, no. 2, pp. 179–191, 2020, doi: 10.13005/msri/170210.
- [52] N. Ahmadi, A. Dadvand, S. Rezazadeh, and I. Mirzaee, "Analysis of the operating pressure and GDL geometrical configuration effect on PEM fuel cell performance," J. Brazilian Soc. Mech. Sci. Eng., vol. 38, no. 8, pp. 2311–2325, 2016, doi: 10.1007/s40430-016-0548-0.
- [53] H. Askaripour, "Effect of operating conditions on the performance of a PEM fuel cell," Int. J. Heat Mass Transf., vol. 144, p. 118705, 2019.
- [54] B. Wu, Y. Lang, N. Zargari, and S. Kouro, Power conversion and control of wind energy systems, vol. 74. John Wiley & Sons, 2011.
- [55] B. Boukhezzar and H. Siguerdidjane, "Nonlinear control of a variable-speed wind turbine using a two-mass model," IEEE Trans. Energy Convers., vol. 26, no. 1, pp. 149–162, 2011, doi: 10.1109/TEC.2010.2090155.
- [56] D. Sáez et al., Optimal Control of Wind Energy Systems. 1965. doi: 10.1016/b978-1-4832-1328-6.50024-9.

- [57] G. Abad, J. López, M. A. Rodríguez, L. Marroyo, and G. Iwanski, Doubly Fed Induction Machine: Modeling and Control for Wind Energy Generation. 2011. doi: 10.1002/9781118104965.
- [58] A. Bektache and B. Boukhezzar, "Nonlinear predictive control of a DFIG-based wind turbine for power capture optimization," Int. J. Electr. Power Energy Syst., vol. 101, no. March, pp. 92–102, 2018, doi: 10.1016/j.ijepes.2018.03.012.
- [59] K. Liao, D. Lu, M. Wang, and J. Yang, "A low-pass virtual filter for output power smoothing of wind energy conversion systems," IEEE Trans. Ind. Electron., vol. 69, no. 12, pp. 12874–12885, 2022.
- [60] J. Chen et al., "Nonlinear maximum power point tracking control of wind turbine based on two-mass model without anemometer," Front. Energy Res., vol. 9, p. 753718, 2021.
- [61] A. Safaeinejad, M. Rahimi, D. Zhou, and F. Blaabjerg, "An efficient power control strategy for active mitigation of blade in-plane fatigue loading in PMSG-based wind turbines," IET Renew. Power Gener., vol. 18, no. 2, pp. 261–282, 2024, doi: 10.1049/rpg2.12923.
- [62] N. Attik, "Contribution to the modeling and control of renewable energy systems, application to a hybrid PV/wind/storage system." 2023.
- [63] M. M. Chowdhury, "Modelling and control of direct drive variable speed wind turbine with Interior Permanent Magnet Synchronous Generator." University of Tasmania, 2014.
- [64] B. Majout et al., "Improvement of PMSG-Based Wind Energy Conversion System Using Developed Sliding Mode Control," Energies, vol. 15, no. 5, pp. 1–17, 2022, doi: 10.3390/en15051625.
- [65] A. Raj, S. R. Arya, and J. Gupta, "Solar PV array-based DC–DC converter with MPPT for low power applications," Renew. Energy Focus, vol. 34, pp. 109–119, 2020.
- [66] A. Rajavel and N. Rathina Prabha, "Fuzzy logic controller-based boost and buck-boost converter for maximum power point tracking in solar system," Trans. Inst. Meas. Control, vol. 43, no. 4, pp. 945–957, 2021.
- [67] A. Kirubakaran, S. Jain, and R. K. Nema, "A review on fuel cell technologies and power electronic interface," Renew. Sustain. Energy Rev., vol. 13, no. 9, pp. 2430–2440, 2009, doi: 10.1016/j.rser.2009.04.004.
- [68] A. Kolli, A. Gaillard, A. De Bernardinis, O. Bethoux, D. Hissel, and Z. Khatir, "A review on DC/DC converter architectures for power fuel cell applications," Energy Convers. Manag., vol. 105, pp. 716–730, 2015.
- [69] M. Derbeli, O. Barambones, M. Y. Silaa, and C. Napole, "Real-time implementation of a new MPPT control method for a DC-DC boost converter used in a PEM fuel cell power system," in Actuators, MDPI, 2020, p. 105.
- [70] R. Ma, Y. Wu, E. Breaz, Y. Huangfu, P. Briois, and F. Gao, "High-order sliding mode control of DC-DC converter for PEM fuel cell applications," in 2018 IEEE Industry Applications

- Society Annual Meeting (IAS), IEEE, 2018, pp. 1–7.
- [71] A. Belkheir, B. Amar, B. Ouahid, B. Rabhi, Z. Laid, and B. M. Fouad, "Modeling and control of an interleaved boost DC-DC converter applied for PEM fuel cell," in 2021 IEEE 1st International Maghreb Meeting of the Conference on Sciences and Techniques of Automatic Control and Computer Engineering MI-STA, IEEE, 2021, pp. 80–85.
- [72] M. Koundi et al., "State-feedback control of interleaved buck-boost DC-DC power converter with continuous input current for fuel cell energy sources: theoretical design and experimental validation," World Electr. Veh. J., vol. 13, no. 7, p. 124, 2022.
- [73] R. Saadi, M. Y. Hammoudi, O. Kraa, M. Y. Ayad, and M. Bahri, "A robust control of a 4-leg floating interleaved boost converter for fuel cell electric vehicle application," Math. Comput. Simul., vol. 167, pp. 32–47, 2020.
- [74] N. Subhani, R. Kannan, A. Mahmud, and F. Blaabjerg, "Z-source inverter topologies with switched Z-impedance networks: A review," IET Power Electron., vol. 14, no. 4, pp. 727–750, 2021.
- [75] Y. Huangfu et al., "A novel robust smooth control of input parallel output series quasi-Z-source DC–DC converter for fuel cell electrical vehicle applications," IEEE Trans. Ind. Appl., vol. 57, no. 4, pp. 4207–4221, 2021.
- [76] Y. Lembeye, V. D. Bang, G. Lefevre, and J.-P. Ferrieux, "Novel half-bridge inductive DC–DC isolated converters for fuel cell applications," IEEE Trans. energy Convers., vol. 24, no. 1, pp. 203–210, 2009.
- [77] M. İnci, M. Büyük, M. H. Demir, and G. İlbey, "A review and research on fuel cell electric vehicles: Topologies, power electronic converters, energy management methods, technical challenges, marketing and future aspects," Renew. Sustain. Energy Rev., vol. 137, p. 110648, 2021.
- [78] F. Dai, X. Wang, and W. Kang, "Design and simulation of current-fed dual-active full-bridge DC/DC converter control system applied to proton exchange membrane fuel cell," in E3S Web of Conferences, EDP Sciences, 2021, p. 1008.
- [79] J. A. Baroudi, V. Dinavahi, and A. M. Knight, "A review of power converter topologies for wind generators," Renew. energy, vol. 32, no. 14, pp. 2369–2385, 2007.
- [80] R. Syahputra, K. Purwanto, and I. Soesanti, "Performance investigation of standalone wind power system equipped with sinusoidal PWM power inverter for household consumer in rural areas of Indonesia," Energy Reports, vol. 8, no. 2022, pp. 4553–4569, 2022, doi: 10.1016/j.egyr.2022.03.145.
- [81] I. Yazici and E. K. Yaylaci, "Maximum power point tracking for the permanent magnet synchronous generator-based WECS by using the discrete-time integral sliding mode controller with a chattering-free reaching law," IET Power Electron., vol. 10, no. 13, pp. 1751–1758, 2017, doi: 10.1049/iet-pel.2017.0232.

- [82] P. S. Babu, C. K. Sundarabalan, C. Balasundar, and T. S. Krishnan, "Fuzzy logic based optimal tip speed ratio MPPT controller for grid connected WECS," Mater. Today Proc., vol. 45, pp. 2544–2550, 2021.
- [83] G. Energy, Wind Power Electric Systems: Modeling, Simulation and Control. 2014.
- [84] A. Mahesh and K. S. Sandhu, "Hybrid wind/photovoltaic energy system developments: Critical review and findings," Renew. Sustain. Energy Rev., vol. 52, pp. 1135–1147, 2015, doi: 10.1016/j.rser.2015.08.008.
- [85] R. Al Badwawi, M. Abusara, and T. Mallick, "A Review of Hybrid Solar PV and Wind Energy System," Smart Sci., vol. 3, no. 3, pp. 127–138, 2015, doi: 10.1080/23080477.2015.11665647.
- [86] K. Zeb et al., "A comprehensive review on inverter topologies and control strategies for grid connected photovoltaic system," Renew. Sustain. Energy Rev., vol. 94, pp. 1120–1141, 2018.
- [87] Y. Li and F. Nejabatkhah, "Overview of control, integration and energy management of microgrids," vol. 2, pp. 212–222, 2014, doi: 10.1007/s40565-014-0063-1.
- [88] R. B. Bollipo, S. Mikkili, S. Member, and P. K. Bonthagorla, "Hybrid, Optimal, Intelligent and Classical PV MPPT Techniques: A Review," vol. 7, no. 1, pp. 9–33, 2021, doi: 10.17775/CSEEJPES.2019.02720.
- [89] J. Dadkhah and M. Niroomand, "Optimization methods of MPPT parameters for PV systems: Review, classification, and comparison," J. Mod. Power Syst. Clean Energy, vol. 9, no. 2, pp. 225–236, 2021.
- [90] N. Karami, N. Moubayed, and R. Outbib, "General review and classification of different MPPT Techniques," Renew. Sustain. Energy Rev., vol. 68, pp. 1–18, 2017.
- [91] H. H. H. Mousa, A. R. Youssef, and E. E. M. Mohamed, "Adaptive P&O MPPT algorithm based wind generation system using realistic wind fluctuations," Int. J. Electr. Power Energy Syst., vol. 112, no. May, pp. 294–308, 2019, doi: 10.1016/j.ijepes.2019.04.038.
- [92] D. Baimel, S. Tapuchi, Y. Levron, and J. Belikov, "Improved fractional open circuit voltage MPPT methods for PV systems," Electronics, vol. 8, no. 3, p. 321, 2019.
- [93] M. Lasheen, A. K. A. Rahman, M. Abdel-Salam, and S. Ookawara, "Performance enhancement of constant voltage based MPPT for photovoltaic applications using genetic algorithm," Energy Procedia, vol. 100, pp. 217–222, 2016.
- [94] A. Belhadj Djilali, A. Yahdou, H. Benbouhenni, and I. Colak, "Improved Incremental Conductance MPPT Technique Designed to Addressing Drift Problem in a Photovoltaic System," Electr. Power Components Syst., pp. 1–14, 2024.
- [95] S. Khadidja, M. Mountassar, and B. M'hamed, "Comparative study of incremental conductance and perturb & observe MPPT methods for photovoltaic system," in 2017 International Conference on Green Energy Conversion Systems (GECS), IEEE, 2017, pp. 1–6.
- [96] M. Aly and H. Rezk, "An improved fuzzy logic control-based MPPT method to enhance the performance of PEM fuel cell system," Neural Comput. Appl., vol. 34, no. 6, pp. 4555–4566,

- Mar. 2022, doi: 10.1007/s00521-021-06611-5.
- [97] A. E. Badoud, "Real-Time Experimental Analysis of Hybrid BG-FL Based MPPT Controller for a Photovoltaic System Under Partial Shading Conditions," 2022 19th IEEE Int. Multi-Conference Syst. Signals Devices, SSD 2022, no. May, pp. 1409–1414, 2022, doi: 10.1109/SSD54932.2022.9955848.
- [98] S. Jalali Zand, S. Mobayen, H. Z. Gul, H. Molashahi, M. Nasiri, and A. Fekih, "Optimized Fuzzy Controller Based on Cuckoo Optimization Algorithm for Maximum Power-Point Tracking of Photovoltaic Systems," IEEE Access, vol. 10, no. May, pp. 71699–71716, 2022, doi: 10.1109/ACCESS.2022.3184815.
- [99] L. Zhao and L. Yin, "Multi-step depth model predictive control for photovoltaic maximum power point tracking under partial shading conditions," Int. J. Electr. Power Energy Syst., vol. 151, no. October 2022, p. 109196, 2023, doi: 10.1016/j.ijepes.2023.109196.
- [100] J. P. Ram, N. Rajasekar, and M. Miyatake, "Design and overview of maximum power point tracking techniques in wind and solar photovoltaic systems: A review," Renew. Sustain. Energy Rev., vol. 73, no. February, pp. 1138–1159, 2017, doi: 10.1016/j.rser.2017.02.009.
- [101] S. Ahmed, H. M. M. Adil, I. Ahmad, M. K. Azeem, Z. E. Huma, and S. A. Khan, "Supertwisting sliding mode algorithm based nonlinear MPPT control for a solar PV system with artificial neural networks based reference generation," Energies, vol. 13, no. 14, 2020, doi: 10.3390/en13143695.
- [102] M. H. Ibrahim, S. P. Ang, M. N. Dani, M. I. Rahman, R. Petra, and S. M. Sulthan, "Optimizing Step-Size of Perturb & Observe and Incremental Conductance MPPT Techniques Using PSO for Grid-Tied PV System," IEEE Access, vol. 11, no. February, pp. 13079–13090, 2023, doi: 10.1109/ACCESS.2023.3242979.
- [103] S. Chtita, A. Derouich, S. Motahhir, and A. EL Ghzizal, "A new MPPT design using arithmetic optimization algorithm for PV energy storage systems operating under partial shading conditions," Energy Convers. Manag., vol. 289, no. April, p. 117197, 2023, doi: 10.1016/j.enconman.2023.117197.
- [104] I. Naruei and F. Keynia, "A new optimization method based on COOT bird natural life model," Expert Syst. Appl., vol. 183, p. 115352, 2021.
- [105] A. Harrison, N. H. Alombah, and J. de Dieu Nguimfack Ndongmo, "A New Hybrid MPPT Based on Incremental Conductance-Integral Backstepping Controller Applied to a PV System under Fast-Changing Operating Conditions," Int. J. Photoenergy, vol. 2023, 2023, doi: 10.1155/2023/9931481.
- [106] K. Xia, Y. Li, and B. Zhu, "Improved Photovoltaic MPPT Algorithm Based on Ant Colony Optimization and Fuzzy Logic Under Conditions of Partial Shading," IEEE Access, vol. 12, no. March, pp. 44817–44825, 2024, doi: 10.1109/ACCESS.2024.3381345.
- [107] D. Kumar, Y. K. Chauhan, A. S. Pandey, A. K. Srivastava, and V. Kumar, "A Novel Hybrid

- MPPT Approach for Solar PV Systems Using Particle-Swarm-Optimization-Trained Machine Learning and Flying Squirrel Search Optimization," 2023.
- [108] D. K. Singh, A. K. Akella, and S. Manna, "Adjustable variable step-based MRAC MPPT for solar PV system in highly fluctuating and cloudy atmospheric conditions," Electr. Eng., 2023, doi: 10.1007/s00202-023-01922-3.
- [109] M. A. Hannan et al., "Wind Energy Conversions, Controls, and Applications: A Review for Sustainable Technologies and Directions," Sustain., vol. 15, no. 5, 2023, doi: 10.3390/su15053986.
- [110] S. Azzouz, S. Messalti, and A. Harrag, "Innovative PID-GA MPPT controller for extraction of maximum power from variable wind turbine," Prz. Elektrotechniczny, vol. 95, no. 8, pp. 115– 120, 2019, doi: 10.15199/48.2019.08.26.
- [111] X. Zhang, J. Jia, L. Zheng, W. Yi, and Z. Zhang, "Maximum power point tracking algorithms for wind power generation system: Review, comparison and analysis," Energy Sci. Eng., vol. 11, no. 1, pp. 430–444, 2023, doi: 10.1002/ese3.1313.
- [112] H. H. H. Mousa, A. R. Youssef, and E. E. M. Mohamed, "State of the art perturb and observe MPPT algorithms based wind energy conversion systems: A technology review," Int. J. Electr. Power Energy Syst., vol. 126, no. PA, p. 106598, 2021, doi: 10.1016/j.ijepes.2020.106598.
- [113] D. Kumar and K. Chatterjee, "A review of conventional and advanced MPPT algorithms for wind energy systems," Renew. Sustain. Energy Rev., vol. 55, pp. 957–970, 2016, doi: 10.1016/j.rser.2015.11.013.
- [114] A. Eskandari, R. Vatankhah, and E. Azadi, "Optimization of wind energy extraction for variable speed wind turbines using fuzzy backstepping sliding mode control based on multi objective PSO," Ocean Eng., vol. 285, no. P2, p. 115378, 2023, doi: 10.1016/j.oceaneng.2023.115378.
- [115] H. Chojaa, A. Derouich, S. E. Chehaidia, O. Zamzoum, M. Taoussi, and H. Elouatouat, "Integral sliding mode control for DFIG based WECS with MPPT based on artificial neural network under a real wind profile," Energy Reports, vol. 7, pp. 4809–4824, 2021.
- [116] S. Azzouz, S. Messalti, and A. Harrag, "A Novel Hybrid MPPT Controller Using (P&O)-neural Networks for Variable Speed Wind Turbine Based on DFIG," Model. Meas. Control A, vol. 92, no. 1, pp. 23–29, 2019, doi: 10.18280/mmc a.920104.
- [117] N. Deghfel, "An Enhanced Robust Super-Twisting Sliding Mode Control MPPT Approach for a Stand-Alone Wind Energy Conversion System Equipped with PMSG," in 2024 2nd International Conference on Electrical Engineering and Automatic Control (ICEEAC), IEEE, 2024, pp. 1–6.
- [118] R. Tiwari and N. R. Babu, "Recent developments of control strategies for wind energy conversion system," Renew. Sustain. Energy Rev., vol. 66, pp. 268–285, 2016, doi: 10.1016/j.rser.2016.08.005.
- [119] S. Manna, D. K. Singh, and A. K. Akella, "A Review of Control Techniques for Wind Energy

- Conversion System," Int. J. Eng. Technol. Innov., vol. 13, no. 1, pp. 40–69, 2023, doi: 10.46604/ijeti.2023.9051.
- [120] I. M. Alsofyani and N. R. N. Idris, "A review on sensorless techniques for sustainable reliablity and efficient variable frequency drives of induction motors," Renew. Sustain. energy Rev., vol. 24, pp. 111–121, 2013.
- [121] V. Yaramasu, "Predictive control of multilevel converters for megawatt wind energy conversion systems," Ryerson Univ., 2014.
- [122] D. Wu, C. Peng, C. Yin, and H. Tang, "Review of System Integration and Control of Proton Exchange Membrane Fuel Cells," Electrochemical Energy Reviews, vol. 3, no. 3. Springer Science and Business Media B.V., pp. 466–505, Sep. 01, 2020. doi: 10.1007/s41918-020-00068-1.
- [123] K. B. Samal, S. Pati, and R. Sharma, "A review of FCs integration with microgrid and their control strategies," International Journal of Hydrogen Energy, vol. 48, no. 91. Elsevier Ltd, pp. 35661–35684, Nov. 15, 2023. doi: 10.1016/j.ijhydene.2023.05.287.
- [124] M. Derbeli, M. Farhat, O. Barambones, and L. Sbita, "Control of Proton Exchange Membrane Fuel Cell (PEMFC) power system using PI controller," Int. Conf. Green Energy Convers. Syst. GECS 2017, 2017, doi: 10.1109/GECS.2017.8066175.
- [125] I. Kocaarslan, S. Kart, Y. Altun, and N. Genc, "Lyapunov based PI controller for PEM fuel cell based boost converter," Int. J. Renew. Energy Res., vol. 10, no. 1, pp. 275–280, 2020, doi: 10.20508/ijrer.v10i1.10487.g7867.
- [126] M. Habib, F. Khoucha, and A. Harrag, "GA-based robust LQR controller for interleaved boost DC–DC converter improving fuel cell voltage regulation," Electr. Power Syst. Res., vol. 152, pp. 438–456, Nov. 2017, doi: 10.1016/j.epsr.2017.08.004.
- [127] A. K. Singh, I. Hussain, and B. Singh, "Double-Stage Three-Phase Grid-Integrated Solar PV System With Fast Zero Attracting Normalized Least Mean Fourth Based Adaptive Control," IEEE Trans. Ind. Electron., vol. 65, no. 5, pp. 3921–3931, 2018, doi: 10.1109/TIE.2017.2758750.
- [128] M. T. Benchouia, I. Ghadbane, A. Golea, K. Srairi, and M. E. H. Benbouzid, "Implementation of adaptive fuzzy logic and PI controllers to regulate the DC bus voltage of shunt active power filter," Appl. Soft Comput., vol. 28, pp. 125–131, 2015.
- [129] T. He, D. D.-C. Lu, L. Li, J. Zhang, L. Zheng, and J. Zhu, "Model-predictive sliding-mode control for three-phase AC/DC converters," IEEE Trans. Power Electron., vol. 33, no. 10, pp. 8982–8993, 2017.
- [130] A. S. Soliman, M. M. Amin, F. F. M. El-Sousy, and O. A. Mohammad, "Experimental validation for artificial data-driven tracking control for enhanced three-phase grid-connected boost rectifier in DC microgrids," IEEE Trans. Ind. Appl., vol. 59, no. 2, pp. 2563–2580, 2022.
- [131] N. Ramesh Babu, "Smart grid systems: modeling and control," Taylor Fr. eBooks DRM Free

- Collect., 2019.
- [132] S. Tahir, J. Wang, M. H. Baloch, and G. S. Kaloi, "Digital control techniques based on voltage source inverters in renewable energy applications: A review," Electron., vol. 7, no. 2, 2018, doi: 10.3390/electronics7020018.
- [133] S. A. Larrinaga, M. A. R. Vidal, E. Oyarbide, and J. R. T. Apraiz, "Predictive control strategy for DC/AC converters based on direct power control," IEEE Trans. Ind. Electron., vol. 54, no. 3, pp. 1261–1271, 2007.
- [134] J. Hu, J. Zhu, and D. G. Dorrell, "Model predictive control of grid-connected inverters for PV systems with flexible power regulation and switching frequency reduction," IEEE Trans. Ind. Appl., vol. 51, no. 1, pp. 587–594, 2014.
- [135] Z. Zheng, T. Zhang, and J. Xue, "Application of Fuzzy Control in a Photovoltaic Grid-Connected Inverter," J. Electr. Comput. Eng., vol. 2018, no. 1, p. 3806372, 2018.
- [136] N. Barr, S. Li, and X. Fu, "Control of grid-connected inverters for circulating current suppression using artificial neural network and conventional control methods," Int. Trans. Electr. Energy Syst., vol. 31, no. 8, p. e12972, 2021.
- [137] B. Jain, S. Jain, and R. K. Nema, "Control strategies of grid interfaced wind energy conversion system: An overview," Renew. Sustain. Energy Rev., vol. 47, pp. 983–996, 2015, doi: 10.1016/j.rser.2015.03.063.
- [138] F. Blaabjerg, R. Teodorescu, M. Liserre, and A. V Timbus, "Overview of control and grid synchronization for distributed power generation systems," IEEE Trans. Ind. Electron., vol. 53, no. 5, pp. 1398–1409, 2006.
- [139] R. Aljarrah, B. B. Fawaz, Q. Salem, M. Karimi, H. Marzooghi, and R. Azizipanah-Abarghooee, "Issues and Challenges of Grid-Following Converters Interfacing Renewable Energy Sources in Low Inertia Systems: A Review," IEEE Access, vol. 12, no. December 2023, pp. 5534–5561, 2024, doi: 10.1109/ACCESS.2024.3349630.
- [140] A. G. Alharbi, A. G. Olabi, H. Rezk, A. Fathy, and M. A. Abdelkareem, "Optimized energy management and control strategy of photovoltaic/PEM fuel cell/batteries/supercapacitors DC microgrid system," Energy, vol. 290, no. December 2023, p. 130121, 2024, doi: 10.1016/j.energy.2023.130121.
- [141] A. M. Fernandez, M. Kandidayeni, L. Boulon, and H. Chaoui, "An adaptive state machine based energy management strategy for a multi-stack fuel cell hybrid electric vehicle," IEEE Trans. Veh. Technol., vol. 69, no. 1, pp. 220–234, 2019.
- [142] Y. Ayat, A. E. Badoud, S. Mekhilef, and S. Gassab, "Energy management based on a fuzzy controller of a photovoltaic/fuel cell/Li-ion battery/supercapacitor for unpredictable, fluctuating, high-dynamic three-phase AC load," Electr. Eng. Electromechanics, vol. 2023, no. 3, pp. 66–75, 2023, doi: 10.20998/2074-272X.2023.3.10.
- [143] A. Fathy, S. Ferahtia, H. Rezk, D. Yousri, M. A. Abdelkareem, and A. G. Olabi, "Optimal

- adaptive fuzzy management strategy for fuel cell-based DC microgrid," Energy, vol. 247, p. 123447, 2022, doi: 10.1016/j.energy.2022.123447.
- [144] M. Jafari, Z. Malekjamshidi, J. Zhu, and M.-H. Khooban, "A novel predictive fuzzy logic-based energy management system for grid-connected and off-grid operation of residential smart microgrids," IEEE J. Emerg. Sel. Top. Power Electron., vol. 8, no. 2, pp. 1391–1404, 2018.
- [145] A. Panday and H. O. Bansal, "A review of optimal energy management strategies for hybrid electric vehicle," Int. J. Veh. Technol., vol. 2014, 2014, doi: 10.1155/2014/160510.
- [146] X. Wang, Y. Huang, F. Guo, and W. Zhao, "Energy management strategy based on dynamic programming considering engine dynamic operating conditions optimization," in 2020 39th Chinese Control Conference (CCC), IEEE, 2020, pp. 5485–5492.
- [147] T. Leroy, F. Vidal-Naquet, and P. Tona, "Stochastic dynamic programming based energy management of hev's: an experimental validation," IFAC Proc. Vol., vol. 47, no. 3, pp. 4813–4818, 2014.
- [148] X. Lü et al., "Energy management of hybrid electric vehicles: A review of energy optimization of fuel cell hybrid power system based on genetic algorithm," Energy Convers. Manag., vol. 205, no. January, p. 112474, 2020, doi: 10.1016/j.enconman.2020.112474.
- [149] H. Zhang, Q. Li, H. Wang, Q. Li, G. Qin, and Q. Wu, "A review of energy management optimization based on the equivalent consumption minimization strategy for fuel cell hybrid power systems," Fuel Cells, vol. 22, no. 4, pp. 116–130, 2022.
- [150] K. Song, X. Huang, Z. Cai, P. Huang, and F. Li, "Research on energy management strategy of fuel-cell vehicles based on nonlinear model predictive control," Int. J. Hydrogen Energy, vol. 50, pp. 1604–1621, 2024.
- [151] P. Kalaivani and C. S. Joice, "Design and modelling of a neural network-based energy management system for solar PV, fuel cell, battery and ultracapacitor-based hybrid electric vehicle," Electr. Eng., vol. 106, no. 1, pp. 689–709, 2024.
- [152] S. N. Motapon, L.-A. Dessaint, and K. Al-Haddad, "A Robust H2-Consumption-Minimization-Based Energy Management Strategy for a Fuel Cell Hybrid Emergency Power System of More Electric Aircraft," IEEE Trans. Ind. Electron., vol. 61, no. 11, pp. 6148–6156, 2014.
- [153] A. Mehta and B. Naik, Sliding Mode Controllers for Power Electronic Converters, vol. 534.
 Springer, 2019.
- [154] F. F. Ahmad, C. Ghenai, A. K. Hamid, and M. Bettayeb, "Application of sliding mode control for maximum power point tracking of solar photovoltaic systems: A comprehensive review," Annu. Rev. Control, vol. 49, pp. 173–196, 2020.
- [155] A. Mughees and I. Ahmad, "Multi-Optimization of Novel Conditioned Adaptive Barrier Function Integral Terminal SMC for Trajectory Tracking of a Quadcopter System," IEEE Access, vol. 11, no. July, pp. 88359–88377, 2023, doi: 10.1109/ACCESS.2023.3304760.
- [156] N. Deghfel and B. Kanouni, "A Comparative Analysis Study Between Sliding Mode control and

- Back-Stepping Control For Maximum Power Point Tracking in Photovoltaic Systems," in 2024 2nd International Conference on Electrical Engineering and Automatic Control (ICEEAC), IEEE, 2024, pp. 1–6.
- [157] W. Saad, A. Sellami, and G. Garcia, "Terminal sliding mode control-based MPPT for a photovoltaic system with uncertainties," Int. J. Model. Identif. Control, vol. 29, no. 2, pp. 118– 126, 2018, doi: 10.1504/IJMIC.2018.090478.
- [158] A. Kihal, F. Krim, A. Laib, B. Talbi, and H. Afghoul, "An improved MPPT scheme employing adaptive integral derivative sliding mode control for photovoltaic systems under fast irradiation changes," ISA Trans., vol. 87, pp. 297–306, 2019.
- [159] L. Zaghba et al., "Enhancing grid-connected photovoltaic system performance with novel hybrid MPPT technique in variable atmospheric conditions," Sci. Rep., vol. 14, no. 1, p. 8205, Apr. 2024, doi: 10.1038/s41598-024-59024-4.
- [160] I. U. Haq et al., "Neural network-based adaptive global sliding mode MPPT controller design for stand-alone photovoltaic systems," PLoS One, vol. 17, no. 1, p. e0260480, 2022.
- [161] R. Khanna, Q. Zhang, W. E. Stanchina, G. F. Reed, and Z.-H. Mao, "Maximum power point tracking using model reference adaptive control," IEEE Trans. power Electron., vol. 29, no. 3, pp. 1490–1499, 2013.
- [162] N. Deghfel, A. E. Badoud, F. Merahi, M. Bajaj, and I. Zaitsev, "A new intelligently optimized model reference adaptive controller using GA and WOA-based MPPT techniques for photovoltaic systems," Sci. Rep., vol. 14, no. 1, p. 6827, 2024.
- [163] R. Khan, L. Khan, S. Ullah, I. Sami, and J. S. Ro, "Backstepping based super-twisting sliding mode mppt control with differential flatness oriented observer design for photovoltaic system," Electron., vol. 9, no. 9, pp. 1–30, 2020, doi: 10.3390/electronics9091543.
- [164] N. Femia, G. Petrone, G. Spagnuolo, and M. Vitelli, "Optimization of perturb and observe maximum power point tracking method," IEEE Trans. Power Electron., vol. 20, no. 4, pp. 963– 973, 2005, doi: 10.1109/TPEL.2005.850975.
- [165] R. Dadkhah Tehrani and F. Shabani, "Performance Improvement of Fuel Cells Using Perturbation-Based Extremum Seeking and Model Reference Adaptive Control," Asian J. Control, vol. 19, no. 6, pp. 2178–2191, 2017, doi: 10.1002/asjc.1519.
- [166] K. J. Åström and B. Wittenmark, Adaptive control. Courier Corporation, 2013.
- [167] P. Vidyasagar and K. Shanti Swarup, Design and Development of Model Predictive Primary Control of Micro Grids. 2023. [Online]. Available: https://link.springer.com/10.1007/978-981-19-5852-6
- [168] B. Boukhezzar and H. Siguerdidjane, "Nonlinear control with wind estimation of a DFIG variable speed wind turbine for power capture optimization," Energy Convers. Manag., vol. 50, no. 4, pp. 885–892, 2009, doi: 10.1016/j.enconman.2009.01.011.
- [169] N. D. Dao, D. C. Lee, and S. Lee, "A simple and robust sensorless control based on stator current

- vector for PMSG wind power systems," IEEE Access, vol. 7, pp. 8070-8080, 2019, doi: 10.1109/ACCESS.2018.2889083.
- [170] S. Ferahtia, A. Djeroui, H. Rezk, A. Houari, S. Zeghlache, and M. Machmoum, "Optimal control and implementation of energy management strategy for a DC microgrid," Energy, vol. 238, p. 121777, 2022, doi: 10.1016/j.energy.2021.121777.
- [171] S.-A. Amamra, K. Meghriche, A. Cherifi, and B. Francois, "Multilevel inverter topology for renewable energy grid integration," IEEE Trans. Ind. Electron., vol. 64, no. 11, pp. 8855–8866, 2016.
- [172] S. Mehta and V. Puri, "A review of different multi-level inverter topologies for grid integration of solar photovoltaic system," Renew. energy Focus, vol. 43, pp. 263–276, 2022.
- [173] N. Jin, D. Dai, H. Xie, J. Wu, and L. Guo, "Virtual vector-based FCS-MPC for NPC three-level grid-tied inverter without weighting factor of neutral-point voltage balancing," IEEE access, vol. 10, pp. 72806–72814, 2022.
- [174] F. Donoso, A. Mora, R. Cardenas, A. Angulo, D. Saez, and M. Rivera, "Finite-Set Model-Predictive Control Strategies for a 3L-NPC Inverter Operating with Fixed Switching Frequency," IEEE Trans. Ind. Electron., vol. 65, no. 5, pp. 3954–3965, 2018, doi: 10.1109/TIE.2017.2760840.
- [175] Njoya Motapon, S. Design and Simulation of a Fuel Cell Hybrid Emergency Power System for A More Electric Aircraft: Evaluation of Energy Management Schemes. Ph.D. Thesis, École de technologie supérieure, Montréal, QC, Canada, 2013.
- [176] F. Peng et al., "Development of master-slave energy management strategy based on fuzzy logic hysteresis state machine and differential power processing compensation for a PEMFC-LIB-SC hybrid tramway," Applied Energy, vol. 206, pp. 346–363, Sep. 2017, doi: 10.1016/j.apenergy.2017.08.128. Available: https://doi.org/10.1016/j.apenergy.2017.08.128
- [177] Thounthong, P., V. Chunkag, P. Sethakul, S. Sikkabut, S. Pierfederici, and B. Davat. 2011." Energy management of fuel cell/solar cell/supercapacitor hybrid power source". *Journal of Power Sources*, vol. 196, n. 1, p. 313-324.
- [178] K. Choi, J. Byun, S. Lee, and I. G. Jang, "Adaptive Equivalent Consumption Minimization Strategy (A-ECMS) for the HEVs with a Near-Optimal Equivalent Factor considering driving conditions," *IEEE Transactions on Vehicular Technology*, vol. 71, no. 3, pp. 2538–2549, Nov. 2021, doi: 10.1109/tvt.2021.3127691. Available: https://doi.org/10.1109/tvt.2021.3127691
- [179] S. N. Motapon, L. Dessaint, and K. Al-haddad, "A robust H2 -consumption-minimization-based energy management strategy for a fuel cell hybrid emergency power system of more electric aircraft," IEEE Trans. Ind. Electron., vol. 61, no. 11, pp. 6148–6156, 2014.